Contributors to This Volume

J. Bohsung
R. W. Haase
Andre Katz
P. Kramer
R. Penrose
Marjorie Senechal
H.-R. Trebin

APERIODICITY AND ORDER

Volume 2

Introduction to the Mathematics of Quasicrystals

Edited by

Marko V. Jarić
Center for Theoretical Physics
Texas A&M University
College Station, Texas

ACADEMIC PRESS, INC.
Harcourt Brace Jovanovich, Publishers
Boston San Diego New York
Berkeley London Sydney
Tokyo Toronto

Copyright © 1989 by Academic Press, Inc.
All rights reserved.
No part of this publication may be reproduced or transmitted in any form or by any means, electronic or mechanical, including photocopy, recording, or any information storage and retrieval system, without permission in writing from the publisher.

ACADEMIC PRESS, INC.
1250 Sixth Avenue, San Diego, CA 92101

United Kingdom Edition published by
ACADEMIC PRESS INC. (LONDON) LTD.
24–28 Oval Road, London NW1 7DX

Library of Congress Cataloging-in-Publication Data

Aperiodicity and order.

Vol. 3 edited by Marko V. Jarić and Denis Gratias.
Includes bibliographies and indexes.
Contents: v. 1. Introduction to quasicrystals—
v. 2. Introduction to the mathematics of quasi-
crystals— v. 3. Icosahedral structures.
1. Metal crystals. I. Jarić, Marko V.,
Date- . II. Gratias, Denis.
QD921.A67 1987 530.4'1 87-11527
ISBN 0-12-040602-0 (v. 2)

Printed in the United States of America
89 90 91 92 9 8 7 6 5 4 3 2 1

Contributors

Numbers in parentheses indicate the pages on which the authors' contributions begin.

J. Bohsung (183), *Institut für Theoretische und Angewandte Physik, Universität Stuttgart, Pfaffenwaldring 57, D-7000 Stuttgart 80, Federal Republic of Germany*

R. W. Haase (81), *Institut für Theoretische Physik, Universität Tübingen, Auf der Morgenstelle 14, 74 Tübingen 1, Federal Republic of Germany*

Andre Katz (147), *Centre de Physique Théoretique, Ecole Polytechnique, 91128 Palaiseau, France*

P. Kramer (81), *Institut für Theoretische Physik, Universität Tübingen, Auf der Morgenstelle 14, 74 Tübingen 1, Federal Republic of Germany*

Roger Penrose (53), *Mathematical Institute, Oxford University, Oxford OX1 3LB, England*

Marjorie Senechal (1), *Department of Mathematics, Smith College, Northampton, Massachusetts 01063*

H.-R. Trebin (183), *Institut für Theoretische und Angewandte Physik, Universität Stuttgart, Pfaffenwaldring 57, D-7000 Stuttgart 80, Federal Republic of Germany*

Preface

Quasicrystals, whose diffraction patterns have non-crystallographic symmetries but, nonetheless, consist of sharp peaks, brought a dramatic change to our way of thinking about the structure of solids. This revolution required not only the development of new physical concepts, but it also demanded new mathematical tools. While the first volume of this series offered an introduction to the physics of quasicrystals, this companion volume is intended to provide mathematical concepts and results necessary for a quantitative description or analysis of quasicrystals. An effort has been made not to remain purely mathematical, but rather to emphasize the subjects of interest to physicists, crystallographers and metallurgists, focusing on the results and their possible ramifications, thus occasionally sacrificing the rigor of the proof.

The three mathematical areas most relevant to quasicrystals are the theory of almost periodic functions, the theory of aperiodic tilings, and group theory.

The theory of almost periodic functions, developed in the twenties and described in the classic book by Besicowich, is as important in the field of quasicrystals as the theory of periodic functions is in the field of crystals: It is its cornerstone. A practical dimension of this theory was recognised in the 1970s by theorists like DeWolf, Janner and Janssen who realized that an incommensurate crystal can be always identified with a cut through a higher

dimensional crystal. For example, it is very easy to understand diffraction from incommensurate crystals in terms of the associated hypercrystals. This extremely useful point of view, equally applicable to quasicrystals (which can be considered as a special case of incommensurate crystals), was described in a chapter by Per Bak and Alan Goldman in the first volume of this series and is not extensively elaborated here.

Although at the time of the discovery of quasicrystals the theory of quasiperiodic functions had been known for nearly sixty years, it was the mathematics of aperiodic Penrose tilings, mostly developed by Nicolaas de Bruijn, that provided the major influence on the new field. For example, de Bruijn's "strip-projection" and "multigrid" methods, although not as general as the above mentioned "cut method," are widely used for quasicrystal description. Although quasicrystals, even if truly quasiperiodic, are generically not tilings, a reason for the importance of quasiperiodic tilings lies in the simplicity of the geometric "atomic" models they provide. Even before the discovery of quasicrystals, such geometric models were explored by Paul Steinhardt in connection with icosahedral and pentagonal order in metallic glasses and supercooled liquids. The tiling picture of quasicrystals, while approximate, is proving to be valuable in conceptual understanding of quasicrystal properties such as growth, low temperature excitations, and structural relationship with large unit-cell crystals.

Group theory, which traditionally provides an indispensible tool in studies of ordered structures and their defects, should also be of great importance in quasicrystals with high symmetry. Indeed, several years before the discovery of icosahedral quasicrystals, Peter Kramer invented a group theoretical method for constructing quasiperiodic tilings, like the Penrose tiling, and he used this method to construct a three-dimensional icosahedral tiling, which now provides a geometric conceptual model of icosahedral quasicrystals. Undoubtedly, group theory, which has already been used in the theories of elasticity, phase transitions, and defects in quasicrystals, will continue to play an important role in studies of quasicrystals.

In conclusion, let me emphasize that this volume is intended as a pedagogical introduction for the beginners in the field of quasicrystals. However, with its extensive collection of the results and bibliography, it can also serve as a reference for already experienced researchers working in this field. In particular, the material contained in this and the previous volume of the series provides an easy access to the next volume, devoted to various models of structures with icosahedral symmetry.

Chapter 1

A Brief Introduction to Tilings

MARJORIE SENECHAL

Department of Mathematics
Smith College
Northampton, Massachusetts

Contents

1 Tilings and Crystals 2
1.1 Introduction 2
1.2 Analogies and Models 5
2 Basic Concepts 7
2.1 Tiles and Tilings 7
2.2 Symmetry 11
2.3 Lattices and the Crystallographic Restriction 13
2.4 Duality 15
2.5 Order 17
3 Construction Techniques 22
3.1 "Filling the Whole" 22
3.2 Dirichlet Tilings 24
3.3 Dissection Tilings 28
3.4 Duals of Multigrids 29
3.5 Tilings Obtained by Projection 31
4 Forcing Transitivity 33
4.1 Regular Polyhedra and Polytopes 33
4.2 A Local Criterion for Transitivity 35
4.3 Isohedral Polyhedra and Isohedral Tilings 36

APERIODICITY AND ORDER 2
Introduction to the
Mathematics of Quasicrystals

Copyright © 1989 by Academic Press, Inc.
All rights of reproduction in any form reserved.
ISBN 0-12-040602-0

5 Forcing Nonperiodicity 42
5.1 General Principles 42
5.2 Two Dimensional Penrose Tiles 45
5.3 Three Dimensional Ammann Tiles 47
5.4 Two Dimensional Ammann Tiles and Wang Tiles 48
5.5 Conclusion 50
References 50

1 Tilings and Crystals

1.1 Introduction

No one knows when and where clay tiles were first designed for floors, stoves, and walls; probably they were developed in very ancient times, together with bowls, jugs and other earthenware. Equally ancient—perhaps more so—are the first three dimensional tiles, the familiar bricks. Their designers must have been the first to consider the problem of filling the plane, or a region of space, with congruent objects, a problem which continues to challenge designers today.

Also lost in the mists of time are the earliest musings of natural philosophers on the existence of atoms, a question which leads directly to the problem of designing tiles: if the universe is built from indivisible atomic units (and if there is no vacuum), then in order to fit together to fill space without gaps, these units have to have definite shapes.

In his dialogue *Timaeus*, Plato designated four of the five regular solids (Fig. 1), the regular hexahedron (the cube), octahedron, tetrahedron and

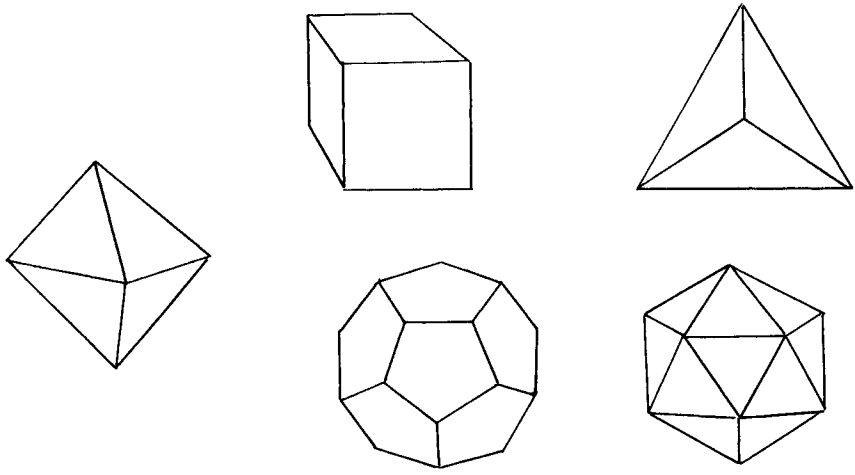

Figure 1. The five regular solids played a key role in Plato's cosmology.

icosahedron, to be the shapes of the ultimate particles of earth, air, fire and water, an association which captured the imaginations of artists and natural philosophers through the Renaissance, despite Aristotle's cogent refutation of this theory. Aristotle argued that "In general it is incorrect to give a form to each of the singular bodies, in the first place, because they will not succeed in filling the whole." It is clear that, although he did no calculations and made no models, Aristotle realized that some of the regular solids do not fill space. In fact, only the cube does; the others do not[1].

Eventually of course the vacuum was shown to exist, and today few people propose rigid tiling models for air, fire, or water. But tilings continues to be a useful way to study the solid state (Senechal, to appear). For over 150 years, since Haüy showed how various crystyal forms can be built from congruent bricks (Fig. 2), tilings have been used to illustrate geometrical properties of crystals such as the relation between internal crystal structure and external polyhedral form. Today the image of a pattern partitioned into congruent blocks is so central to our concept of crystal structure that it is difficult to imagine how it might be otherwise.

Thus tiling theory emerges from the confluence of two rich sources—the practical problem of designing useful and decorative tiles and bricks, and the scientific problem of modeling the internal structure of crystals. A third source—mathematical creativity—also plays a crucial role, that of organizing, simplifying, and generalizing basic concepts, devising classification schemes, and posing (and sometimes solving) new questions. For example, as the tiling model for crystal structures has been refined, challenging geometrical problems have arisen. Which polyhedra fill space? If a polyhedron does fill space, in how many different ways can it do so and what properties will the tilings have? What conditions can one place on a set of tiles to force nonperiodicity? Although we have partial answers to these questions, in many respects they remain unsolved.

The literature on tilings is voluminous, but until recently it has been almost inaccessible, spread among the journals of many fields (design, mathematics, crystallography, biology, etc.) and written in many languages. Moreover, it is often imprecise and frequently contains serious errors. Fortunately, 1987 saw the publication of a definitive treatment of tilings and patterns in the plane, *Tilings and Patterns*, by Branko Grünbaum and Geoffrey Shephard. (Hereafter we will refer to this book simply as G&S.) This 700 page monograph-textbook is a richly illustrated, rigorous yet very readable account of the state of the theory today. There is no comparable treatment of tilings and patterns in three dimensional space; indeed, there is no comparable theory! However a great deal of useful information about

[1] Aristotle thought that the regular tetrahedron was also a space filler.

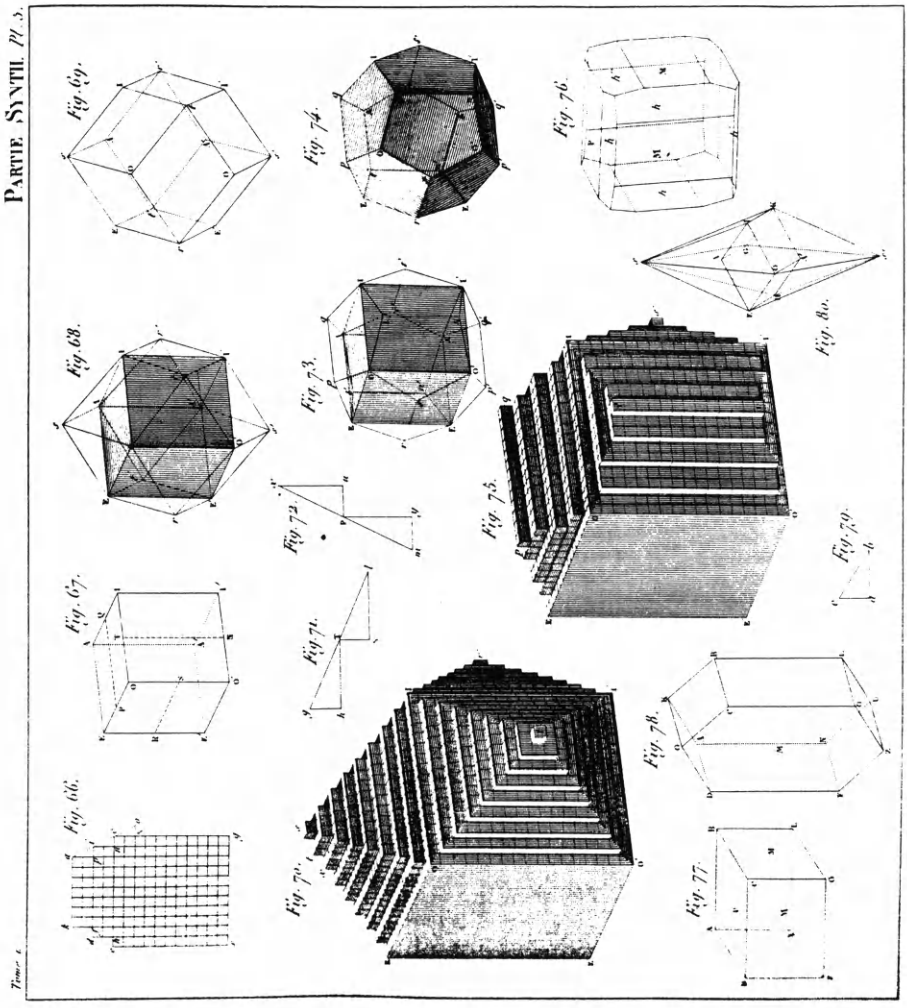

Figure 2. Hauy's concept of the relation between structure and form.

crystallographically significant tilings in n dimensions ($n \geq 2$) can be found in *Geometrical Crystallography* by Engel (1986). H. S. M. Coxeter's *Regular Polytopes* (1973) is also required reading.

The purpose of this chapter is to sketch those aspects of the theory of tilings in two and three dimensional space that are important for understanding some of the ways in which "classical" mathematical crystallography is being generalized to include possible models for aperiodic crystals. Although the aesthetic attractiveness of tilings suggests that the theory is accessible, it is not as easy as it looks. Unfortunately, the recent literature shows that many of its subtleties continue to be ignored. If the theory is to develop in a satisfactory way, investigators must be aware of what is and is not known about tilings, and why.

1.2 *Analogies and Models*

In Figs. 3, 4 and 5 we see some of the ways in which tilings are used today to illustrate particular aspects of crystal structure: patterns of crystal growth, twinning and structural defects. Underlying these and similar analogies is the concept of the structure of an ideal crystal as a periodic tiling of space by parallelopipedal "unit cells" which contain the translational repeat units of the atomic pattern of the crystal. Deviations from strict periodicity in these tilings are thought to be analogous to deviations from the ideal crystalline state.

In addition to providing visual analogies, tilings are also used as working

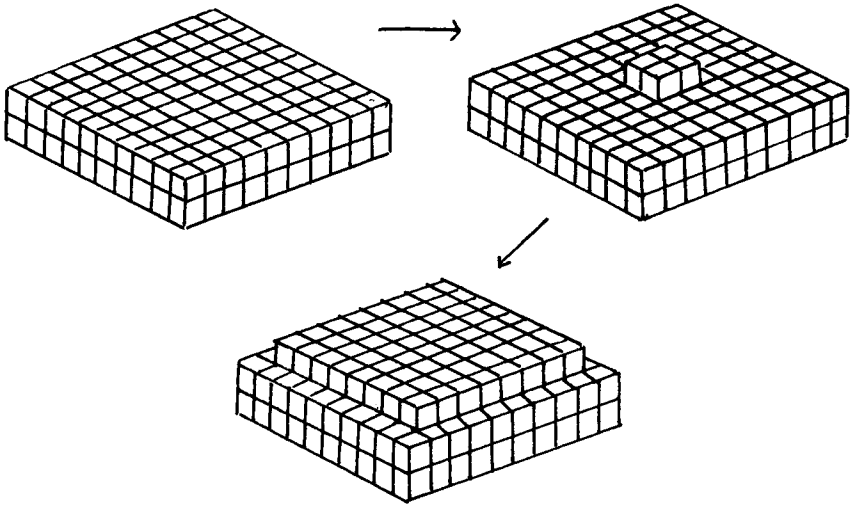

Figure 3. A model for crystal growth.

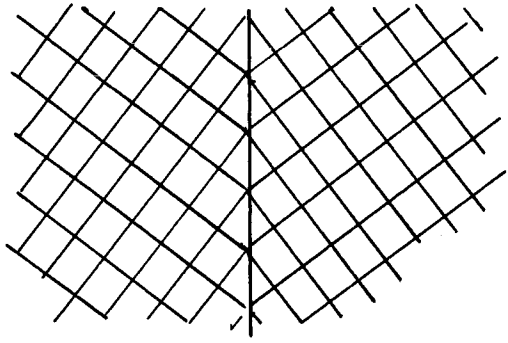

Figure 4. A tiling model for a twin boundary.

models for the exploration of crystallographic problems. In these cases the tiling is not only an illustration of a crystallographic idea; it is an alternative formulation of the idea. It is hoped that the solution of the tiling problem (if it can be solved), properly reinterpreted, will provide the solution to the crystallographic problem. For example, the Russian crystallographer E. S. Fedorov (1885), erroneously believing that crystal structures could be unambiguously partitioned into polyhedral cells, interpeted the problem of classifying crystals as the problem of determining which polyhedra fill space. Defining a *parallelohedron* to be a convex polyhedron which fills space when arranged face to face, in parallel position (all of these terms are defined in Section 2.1), Fedorov proved that there are exactly five parallelohedra (Fig. 23) and used them as the basis for his classification of crystals.

One hundred years later, tilings are again being used to model important crystallographic phenomena, but now we are in a new period in which the

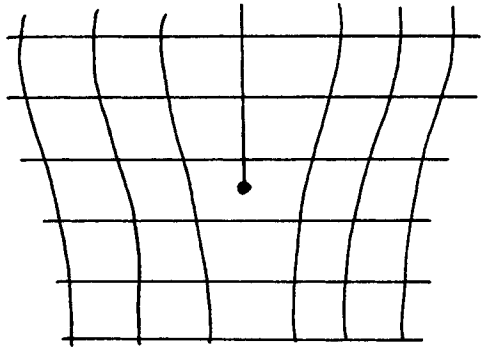

Figure 5. Model of a crystal dislocation.

necessity of the laws of periodicity associated with classical crystallography is being challenged. The announcement in 1984 of the discovery of "quasicrystals" was startling because the diffraction pattern of these crystals, with its five-fold symmetry, breaks the "crystallographic restriction" (Section 2.3) and thus challenges the crystallographic paradigm that the structure of a crystal is a repeating pattern like that envisioned by Haüy and Fedorov. Because certain nonperiodic tilings appear to have diffraction properties analogous to those of the quasicrystals, the discovery of quasicrystals has generated new research in tiling theory. A closely related problem has been discussed by C. Radin (to appear), who argues that "the crystal problem" (why are solids crystalline?) is equivalent to what he calls "the tiling problem": how is the periodicity of a tiling forced by matching rules?

2 Basic Concepts

2.1 Tiles and Tilings

A *tiling* is a partition of the plane or space by copies of objects which we call *tiles*. By "partition" we mean that every point belongs to at least one tile, and if a point belongs to more than one tile, then it must lie on the tiles' shared boundary.

This definition is widely accepted but subtleties arise when we try to define the word "tile." In fact, the word "tile" cannot be defined independently of "tiling" since there is, in general, no criterion for determining whether or not copies of a given set of objects fill the plane or space. On the other hand, although most shapes do not tile (here we are using the word as a verb) there are surprisingly many space-filling shapes besides the standard brick. Some are infinite, some are even toroidal (Fig. 6)! Thus when we are dealing with tiles in a specific context it is necessary to place restrictions on their sizes and shapes in order to make the problem of analyzing them more tractable. In most cases—and in this chapter unless stated otherwise—a *tile* is defined to be a finite region of the plane or space with a polygonal or polyhedral boundary that can be (continuously) deformed into a disk or a ball (accordingly as the tile is two or three dimensional)[2].

Let us recall some of the basic properties of finite polygons and polyhedra. A *polygon* is a finite sequence of line segments or *edges*, joined end to end to form a closed circuit which does not intersect itself. Each edge

[2] A disk (ball) is a circle (sphere) together with its interior.

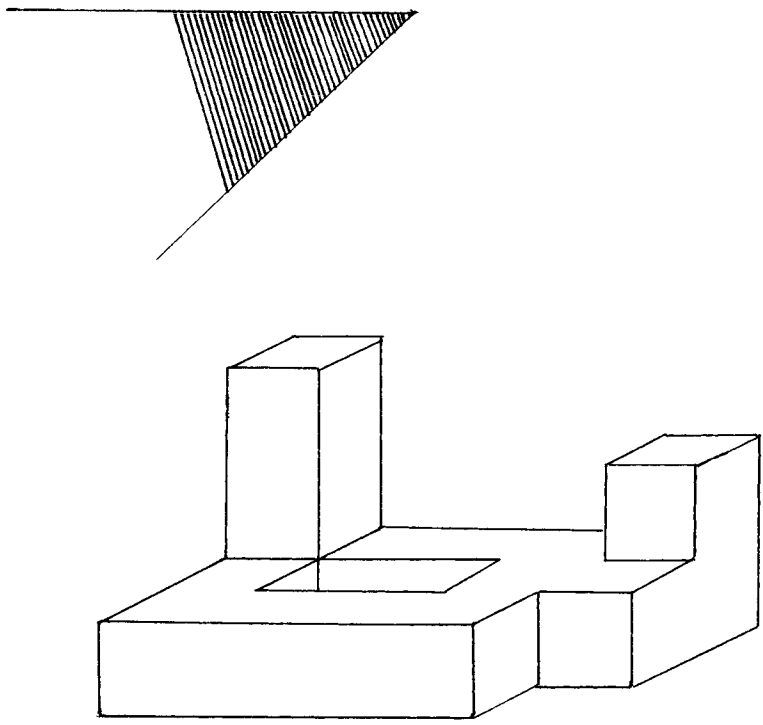

Figure 6. An object which tiles space need not be bounded or convex.

has two endpoints, which in turn belong to exactly two edges. The endpoints are the *vertices* of the polygon. The interior angle formed by two adjacent edges is called a polygonal angle. A *polyhedron* is the union of a finite number of plane polygonal regions, which are called the *faces* of the polyhedron. We require that the faces share whole edges (exactly two faces share each edge) and that it is possible to trace a path from any face to any other which does not pass through any vertex. We will assume that adjacent faces are not coplanar. Obviously, the edges and vertices of a polyhedron coincide with the edges and vertices of its faces. The number of edges meeting at a vertex v is called the *valence* of v. The convex hull of the midpoints of these edges is called the *vertex figure* of v. The interior angle formed by two faces is called a dihedral angle of the polyhedron. For example, a cube has six faces, all of which are squares. Adjacent faces always meet at right angles; thus all the dihedral angles of the cube are 90° Three faces meet at each of its eight vertices, which are thus 3-valent.

A region is *convex* if any two of its points can be joined by a line segment which lies entirely within it (the wedge in Fig. 6 is convex, the toroid is not).

Most of the tilings one encounters in crystallographic problems have convex tiles, but it should not be assumed that all important tilings have this property. Indeed, it is sometimes useful to deform convex tiles into non-convex ones in order to restrict the ways in which they can fit together. We will sometimes refer to the *convex hull* of a set of points; this is the smallest convex region containing them. For example, a convex polygon or polyhedron is the convex hull of its vertices.

The terms vertex, edge and face are also used in the description of tilings, but in a somewhat more subtle way. We define a vertex of a plane tiling to be a point where three or more tiles meet. The vertices and edges of the tiling may or may not be identical with those of the tiles: for example, in Fig. 7 the vertices of the tiling are not vertices of all of the tiles to which they belong. Similarly, a vertex of a three dimensional tiling is a point at which at least four tiles, not all sharing an edge, meet; such a point need not be a vertex of all of the tiles. Nor need the edges and faces of a three dimensional tiling always coincide with those of the constituent tiles. In the special case in which the tiles in a plane tiling share whole edges, the tiling is said to be *edge-to-edge*; similarly, if the tiles in a three dimensional tiling meet along whole faces, then the tiling is said to be *face-to-face*.

In most tilings of crystallographic interest, the tiles are all congruent copies of, or combinatorially equivalent to, a finite set of tiles, called *prototiles*. A tiling is said to be *k-hedral* if the number of prototiles is k. When $k = 1$, the tiling is *monohedral*.

A tiling is *normal* if the sizes of the tiles are uniformly bounded from above and below; by this we mean that there are circles or spheres of fixed radii d and D which can be, respectively, inscribed in and circumscribed

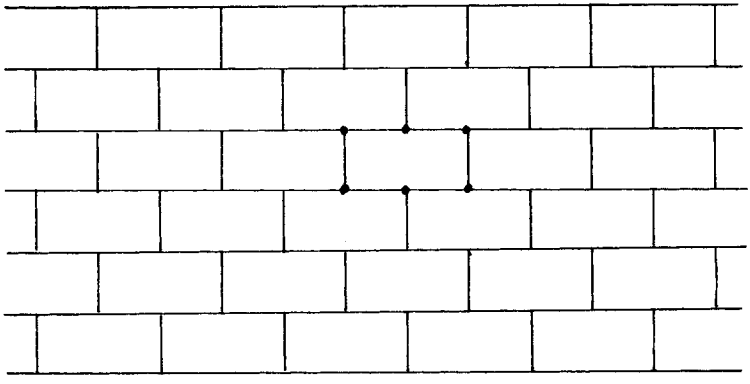

Figure 7. In this common tiling by rectangular bricks, six vertices *of the tiling* belong to each tile, although each tile, taken alone, has only four vertices.

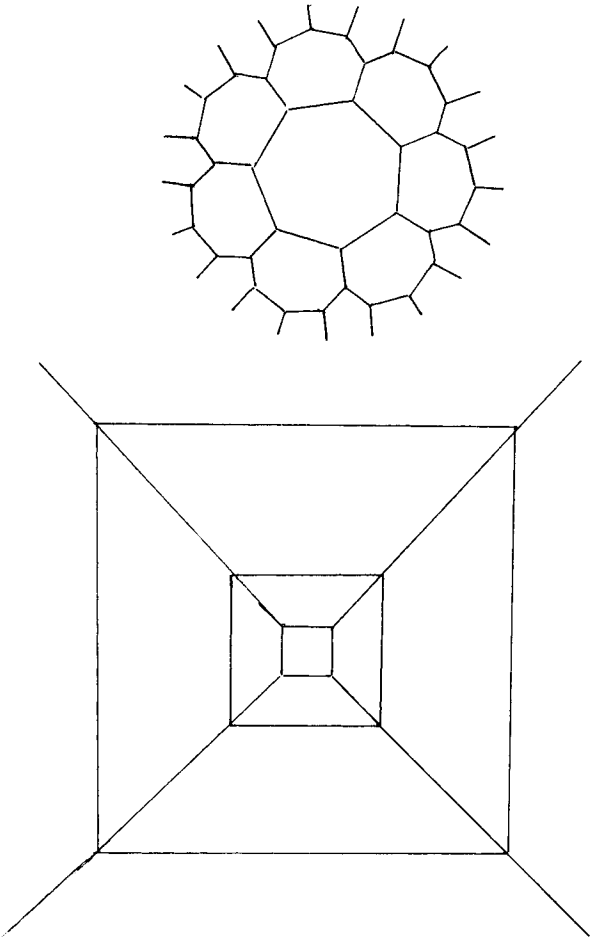

Figure 8. Two tilings which are not normal. In one, the heptagonal tiles become arbitrarily small; in the other, the quadrilateral tiles become arbitrarily large.

about each tile[3]. k-hedral tilings are necessarily normal if congruent copies are used. Two nonnormal tilings ae shown in Fig. 8.

Finally, following G&S we will say that two tilings are *congruent* if one can be brought into coincidence with the other (matching edges to edges and vertices to vertices) by a rigid motion (Section 2.2), while if coincidence

[3] In the literature, an edge-to-edge or face-to-face tiling is sometimes called a normal tiling, but we will always use "normal" as we have defined it here.

requires a change of scale, the tilings will be said to be *equal*. If coincidence requires any other kind of (continuous) deformation, then the tilings are *combinatorially equivalent*[4]. Congruent tilings are of course equal, and equal tilings are also combinatorially equivalent.

2.2 *Symmetry*

While we all have intuitive ideas of the meaning of terms like "highly symmetrical," "asymmetrical," and so forth, the mathematical study of symmetry is based on careful definitions.

The symmetry of an object is characterized by the symmetry operations that can be performed on it. A symmetry operation or, briefly, a *symmetry*, is a rigid motion, one which does not alter the distances between any pair of points in the plane or in space. Rotations and reflections are examples of symmetries.

In any dimension, the number of different kinds of rigid motions is finite. A simple fixed-point argument shows that in the plane, if three noncolinear points are fixed then all points are fixed and hence the motion is the identity (no motion at all); if two points are fixed so are all points of the line on which they lie and the motion is reflection cross that line; if exactly one point is fixed then the motion is a rotation; and translation and glide reflection are the isometries which have no fixed points. In space, three coplanar, noncolinear fixed points imply that the motion is a reflection in a plane; two, that it is a rotation about an axis; and one, inversion or rotary inversion. In addition to translation and glide reflection, screw rotation (a motion combining rotation and translation parallel to the rotation axis) also has no fixed points. Only the identity has four fixed points which are not coplanar.

An object is said to have a given symmetry if the corresponding operation brings the object into self-confidence. Notice that if we can perform a symmetry operation on an object we can also reverse it; thus for each symmetry we also have an inverse symmetry. The set of all symmetries of a given object form a group in the technical mathematical sense if we include the identity, because then the composition (successive application) of two symmetries is always again a symmetry. Not surprisingly, this group is called the symmetry group of the object. It is a very instructive exercise to find the symmetries of the regular solids (Fig. 1) and of the regular tilings of the plane (Fig. 31), and to determine the results of various compositions.

[4] Combinatorially equivalent tilings are sometimes said to be isomorphic.

The subunits of a pattern (faces of a polyhedron, tiles of a tiling, points of a point set) which can be brought into coincidence with one another by the operations of a symmetry group are said to be *symmetrically equivalent.* Equivalence in this sense is stronger than congruence: the faces of a cube are equivalent not only because they are congruent squares, but also because any one of them can be moved, by a symmetry operation of the cube, to the position of any other in such a way that the cube appears not to have been moved at all. The symmetry group is said to *act transitively* on the equivalent subunits; we also say that the subunits are a transitive set.

A polyhedron or tiling on whose faces or tiles a symmetry group acts transitively is said to be *isohedral.* If group acts transitively on the vertices of a polyhedron or tiling, then it is *isogonal,* and if its edges are equivalent it is *isotoxal.* (Apparently no word has been coined yet for equivalent two dimensional faces in a three dimensional tiling!)

The regular polyhedra are isohedral, isotoxal and isogonal. Their face centers, edge midpoints and vertices lie on three concentric spheres. These polyhedra are the convex hulls of their vertices, which lie on the outermost sphere. The convex hulls of their face centers, which lie on the innermost sphere, are also regular polyhedra. The convex hull of the edge midpoints of a regular polyhedron is not necessarily regular, but it is interesting nevertheless, since it is always isogonal and has the same symmetry group as regular polyhedron from which it is derived. For example, the convex hull of the edge midpoints of the cube (and of the octahedron) is a cuboctahedron, an isogonal polyhedron with six square and eight triangular faces, while the convex hull of the edge midpoints of the icosahedron (and dodecahedron) is an isogonal icosidodecahedron, which has twelve pentagonal and twenty triangular faces (Fig. 9).

The symmetry group of any polyhedron is finite. Finite symmetry groups are sometimes called *point groups*; they are subgroups of the symmetry group of the sphere. These finite groups fall into four classes: the symmetry

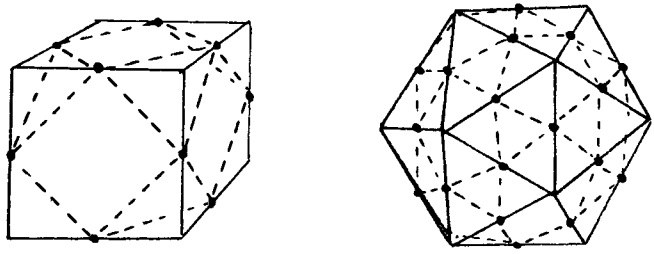

Figure 9. The isogonal cuboctahedron and icosidodecahedron (broken lines) are the convex hulls of the edge midpoints of the cube and the icosahedron.

group of the cube (and regular octahedron) and its subgroups, the symmetry group of the regular icosahedron (and dodecahedron) and its subgroups, and the symmetry groups of right k-gonal prisms and of pyramids with k-gonal bases. There is considerable overlapping of subgroups. The symmetry groups of tilings are more complicated, since they are infinite. A good introductory discussion can be found in G&S.

2.3 *Lattices and the Crystallographic Restriction*

An infinite set of points equally spaced along a line is a *one dimensional lattice*. If all of these points are translated in the plane by a vector which is not parallel to the line, we obtain a copy of the lattice which is parallel to it; if this translation is repeated ad infinitum (in both positive and negative directions) we obtain a *two dimensional lattice*. Similarly, a *three dimensional lattice* is obtained by successive translations of a two dimensional one. Since the time of Haüy, the lattice has been the fundamental concept underlying theories of crystal structure.

It is sometimes useful to think of an n-dimensional lattice (n may be any positive integer, including two or three) as the set of endpoints of sums and differences of n independent translation vectors $x_1, \ldots, x_n$. Then every lattice point is associated with a unique vector $a_1x_1 + \cdots + a_nx_n$, where the coefficients a_i are integers. The vectors x_i are called a basis for the lattice. The basis vectors are not unique; there are infinitely many sets of n vectors which generate the same lattice.

A set is *discrete* if there is a minimum distance between its points. Since the shortest vector in a lattice defines a minimum distance, a lattice is thus a discrete, translation-equivalent set of points. Because the points of a lattice are equally spaced along any lattice row, every lattice point is a center of inversion for the lattice as a whole, and so is the midpoint between any pair of lattice points. The least symmetric lattices have no other symmetries.

Crystallographers classify lattices into families according to the symmetries which fix (any of) their lattice points and according to the way in which this symmetry group acts on the lattice. The symmetry of lattices is governed by geometrical laws. In particular, a lattice can have m-fold rotational symmetry only if $m = 1, 2, 3, 4$ or 6. This result is known as the *crystallographic restriction*.

A simple geometric argument shows why five-fold symmetry is incompatible with a planar or three dimensional lattice. If a lattice had five-fold symmetry, then the set of points about which this rotation takes place must, by translational symmetry, include a lattice. Assume, then, that the points of a plane lattice have five-fold symmetry, and that P is such a point. In any lattice, there is a minimum distance between points; let Q be a lattice point

at minimum distance from P. By hypothesis, P is surrounded by five such Q's and Q is surrounded by five such P's. We see (Fig. 9) that this contradicts the assumption that the distance between P and Q is minimal. The conclusion holds for three dimensional lattices too, since a rotation about an axis effects rotations in the lattice planes normal to the axis.

It follows that if a crystal has a periodic structure, it cannot have five-fold symmetry (Fig. 10). Even its external form cannot be a regular icosahedron (or dodecahedron), since a crystal's form cannot have a symmetry forbidden by its internal structure (notice that the dodecahedron in Fig. 2 is not regular). Equivalently, if a crystal exhibits five-fold symmetry then its structure is not periodic.

It is even easier to show that a two or three dimensional lattice cannot have rotational symmetry of order greater than six. Again we consider a plane lattice whose points are centers of rotation, say of order m. Let P be a lattice point and Q a lattice point at minimum distance d from P. Rotating about P, we come to a lattice point Q', also at distance d from P, such that measure of angle QPQ' is $360/m$. But if $m > 6$, the distance from Q to Q' is less than d. This concludes the proof of the crystallographic restriction. Although the argument does not prove that lattices with two-, three-, four- or six-fold symmetry exist, another simple argument shows that successive m-fold rotations ($m = 3, 4$ or 6) about two points generates a lattice with four- or six-fold (and thus two- or three-fold) symmetry.

The crystallographic restriction is dimension dependent (Pleasants, 1985) because the list of possible symmetry operations is. In four- and all higher

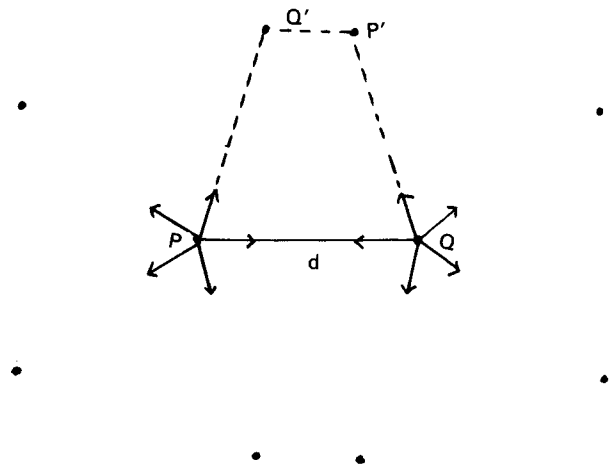

Figure 10. A lattice cannot have points of 5-fold symmetry.

dimensions five-fold symmetry is permitted. Twelve-fold symmetry first occurs in four dimensional lattices, seven-fold in six.

2.4 *Duality*

The concept of duality arises in several crystallographic contexts: there are dual lattices, dual polyhedra, and dual tilings. Even within one of these contexts the word is sometimes used with different meanings. Thus it is important to distinguish them carefully. Perhaps the most important distinction to keep in mind is that some duals are defined by metric conditions, and others are defined by combinatorial ones.

2.4.1 Dual lattices. To every lattice L there is associated another lattice L^*, called it dual or reciprocal lattice. L^* can be most economically defined as the set of endpoints of the vectors whose scalar (dot) products with the vectors of L are integral: y is in L^* if and only if, for every x in L, $x \cdot y$ is an integer.

Thus the points of L^* lie on lines normal to the planes of L, and the spacing of points of L^* along these lines is reciprocal to the spacing between the corresponding planes of L.

If $x_1, \ldots, x_n$ are basis vectors for L, then the vectors $y_1, \ldots, y_n$ defined by $x_i \cdot y_i = 1$ if $i = j$, 0 otherwise, is a basis for L^*.

It follows from the definition that $(L^*)^* = L$, so each lattice is the dual of the other. (Equality is used here in the same sense as in Section 2.1: two lattices are equal if one can be brought into coincidence with the other by a symmetry operation and change of scale.)

If L is contained in L^* (which means that the squared length of every vector of L is an integer) then L is said to be an *integral lattice*. If $L = L^*$, then L is integral and *self-dual*.

The dual lattice is entirely a metric concept. It plays a central role in the determination of crystal structure by x-ray diffraction, and is also important in the analysis of the geometry of quasiperiodic patterns (this is explained in more detail in other chapters of this volume).

2.4.2 Dual polyhedra. To every convex polyhedron P can be associated a family of polyhedra which are dual to P in the sense that they can be obtained from P by reciprocation in a sphere. To carry out this construction, choose a point O inside P and draw a sphere S of radius r about O. For every vertex v of P construct the plane $v \cdot x = r^2$. (In classical terminology, this plane is the polar of the endpoint of v with respect to S, and v in turn is the pole of the plane.) The smallest convex region enclosed by these planes is a polyhedron P^* which is said to be reciprocal or dual to P. Again (if the same sphere S is used), $(P^*)^* = P$.

For example, if P is a cube and S is the sphere on which its vertices lie, then the desired planes are tangent to S. There are eight of them, since the cube has eight vertices, and they enclose a regular octahedron. Conversely, if P is a regular octahedron, the reciprocal polyhedron constructed in this way will be a cube. Similarly, the regular icosahedron and the dodecahedron are dual. The reciprocal of a tetrahedron is another tetrahedron.

If P is isohedral, isogonal or isotoxal then the dual obtained by reciprocation in the sphere on which its face centers, vertices, or edge midpoints lie will be (respectively) isogonal, isohedral, or isotoxal, respectively. Thus the duals of the cuboctahedron and icosidodecahedron are isohedral; the first is the rhombic dodecahedron (Fig. 23, top right) and the second the triacontahedron (Fig. 28).

It is interesting to note that the rhombic dodecahedron fills space (it is one of Fedorov's five parallelohedra) but the cuboctahedron does not, even if distortions are allowed (Schulte, 1984). Thus the property of being a tile is not necessarily shared by pairs of dual polyhedra.

It is important to remember that a polyhedron has uncountably many duals: the point O can be any point inside P and the radius r of the sphere can be any positive real number. The size of P^* depends on r and its symmetry properties depend on the location of O.

For any choice of O and r, however, reciprocation establishes a one-to-one correspondence between the faces, edges and vertices of P and the vertices, edges and faces of P^* (inclusion is reversed). This correspondence defines a weaker form of duality, called *combinatorial duality*. To find an example of a combinatorial dual of a polyhedron P, mark a point in the center of each face of P, and join two points if and only if the faces in which they lie share an edge. We obtain a network of faces, edges and vertices corresponding to the vertices, edges and faces of P. Unlike reciprocation, this procedure does not necessarily preserve convexity or any other metric properties of P (Grünbaum and Shephard, 1988). However it is a useful construction, not only in the theory of polyhedra but also in tiling theory.

2.4.3 Dual tilings. There is no analogue of reciprocation in a sphere for constructing dual tilings, but combinatorial duals can be constructed just as for polyhedra. As in the case of polyhedra, two tilings are said to be *combinatorial duals* if there is a one to one mapping of the faces, edges and vertices of one to the vertices, edges and faces of the other which reverses inclusion.

As in the case of polyhedra, we can obtain examples of combinatorial duals of a given tiling by choosing a point in each tile and joining them if they lie in adjacent faces. But it should be noted that this construction does

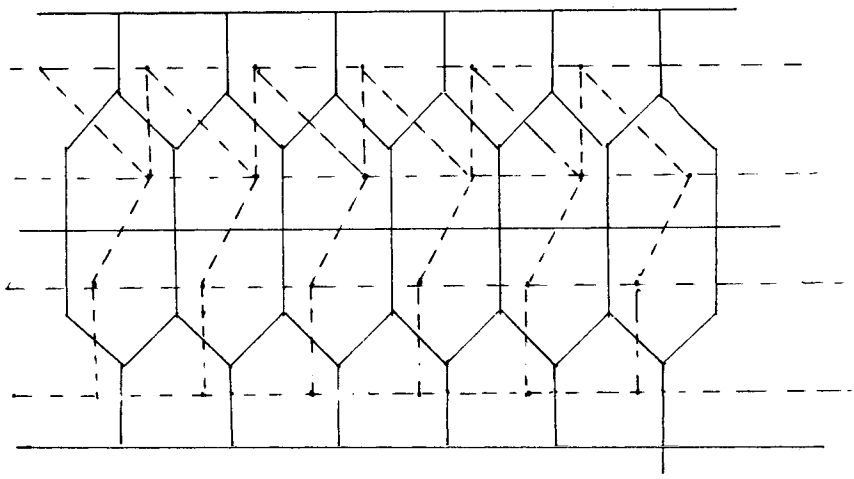

Figure 11. A tiling (solids lines) and a combinatorial dual of that tiling (broken lines).

not give us all possible combinatorial duals (nor does it do so in the case of polyhedra). It gives us only the special class of *dually situated* tilings, those which can be superimposed so that the vertices of one are interior to the faces of the other. The tilings in Fig. 11 are dually situated, but in Section 3.4 we will discuss an important class of dual tilings that are not dually situated.

2.5 *Order*

The literature on quasicrystals abounds with suggestive terminology for the order properties of tilings, such as "long-range (translational, rotational) order," "bond-orientational order," "short-range order," "quasiperiodic order" and so forth. However the definitions of these terms vary from author to author (when they are defined at all). Hopefully, as the theory develops, precise and standard definitions will emerge. In this section we will review some of the order properties of periodic and nonperiodic tilings that appear to be widely accepted today.

2.5.1 Transitivity. This is the strongest type of order. As explained in Section 2.2, a tiling is said to be tile-transitive, or isohedral, if its tiles are equivalent under the symmetry group of the tiling; vertex-transitive

(isogonal) tilings and edge-transitive (isotoxal) tilings are defined similarly. An isohedral and an isogonal tiling (one of which is also isotoxal) are shown in Fig. 12. An isohedral tiling is necessarily monohedral, but the converse of this statement is false (see Fig. 15).

2.5.2 Periodicity. A periodic tiling is one which can be divided into finite cells on which a group of translations acts transitively. In particular, the cells can be chosen to be boxes whose edges are independent translation vectors (Fig. 13). This gives us a superimposed tiling by congruent parallelograms or parallelopipeds which are stacked *in parallel position* edge-to-edge or face-to-face. These boxes are called *unit cells* by

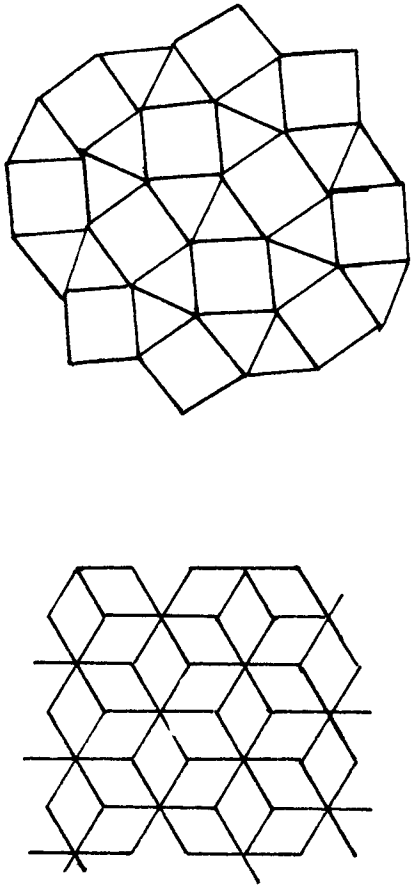

Figure 12. An isohedral and an isogonal tiling. Which of them is also isotoxal?

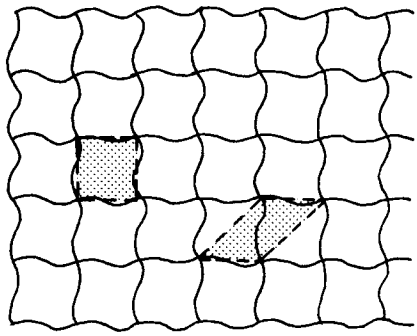

Figure 13. Two choices of a unit cell for a periodic tiling (dotted lines). The cell can be chosen in infinitely many ways.

crystallographers. To avoid confusion, it is important to distinguish between the tiles of a tiling and its unit cells. For example in Fig. 14 the tiles are parallelograms or parallelopipeds, but they are not unit cells of the tiling because they differ in orientation. The vertices of the unit cells of a periodic pattern form a lattice. The lattice is more fundamental than the unit cell because it is independent of the choice of translation vectors.

A transitive tiling of the plane is necessarily periodic because the number of independent translations in a symmetry group of a transitive tiling is always equal to the dimension of the tiled space (Bieberbach, 1910) but a periodic tiling is not necessarily transitive, nor need it be monohedral (Fig. 15).

2.5.3 Nonperiodicity. A tiling is nonperiodic if it is not periodic. There are many kinds of nonperiodic tilings; they include spiral tilings (Fig. 16),

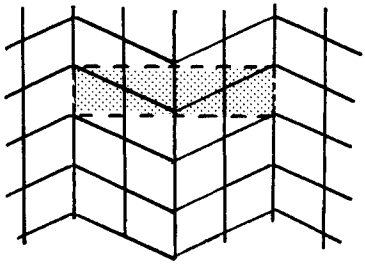

Figure 14. The tiles in this isohedral parallelogram tiling are not unit cells! A true unit cell is shown by dotted lines.

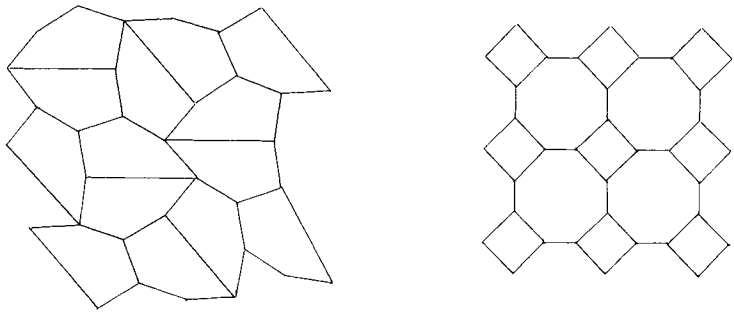

Figure 15. Two intransitive periodic tilings of the plane.

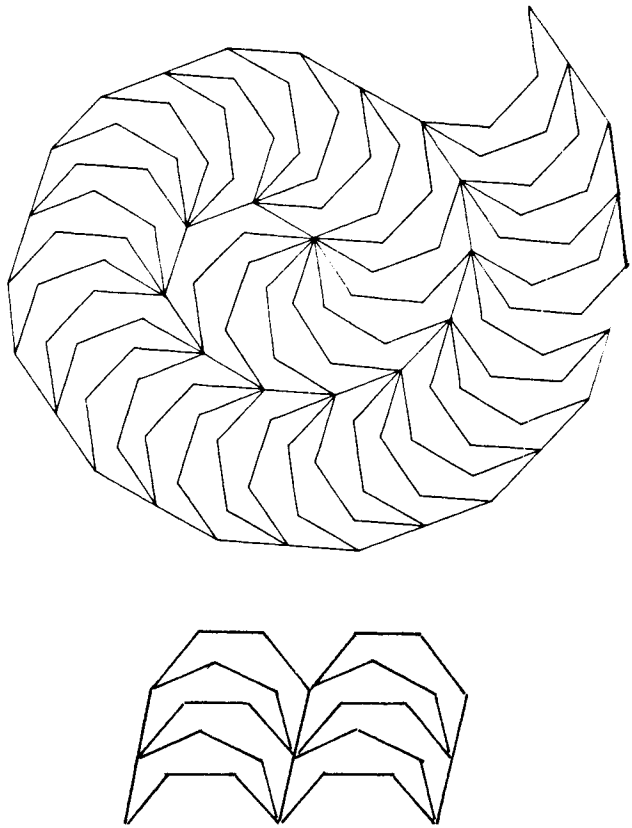

Figure 16. A monohedral spiral tiling. Notice that these tiles can also be arranged in a periodic way.

highly deterministic but nonperiodic tilings such as the Penrose tilings (Fig. 17), and "random" tilings such as that shown in Fig. 18. Thus "nonperiodic" includes a wide range of phenomena. Much recent research in tiling theory is centered on finding criteria for characterizing and distinguishing among them. The title of this series is *Aperiodicity and Order*, but what is aperiodicity?

A great deal of attention is currently being given to "quasiperiodic" tilings. It seems to be generally agreed that a *quasiperiodic tiling* (of a line, a plane or three dimensional space) is one which can be obtained by projecting a section of a tiling that is periodic in a higher dimensional space (Section 3.5). Unfortunately, this definition does not provide us with a local test for quasiperiodicity: how can we tell by inspection whether a given tiling has been obtained in this way? Nevertheless, quasiperiodicity is an important concept, since it can be shown that the diffraction patterns of such tilings have bright spots and thus are formally analogous to crystals (Elser, 1986). In particular, the Penrose tiles are quasiperiodic (Section 5).

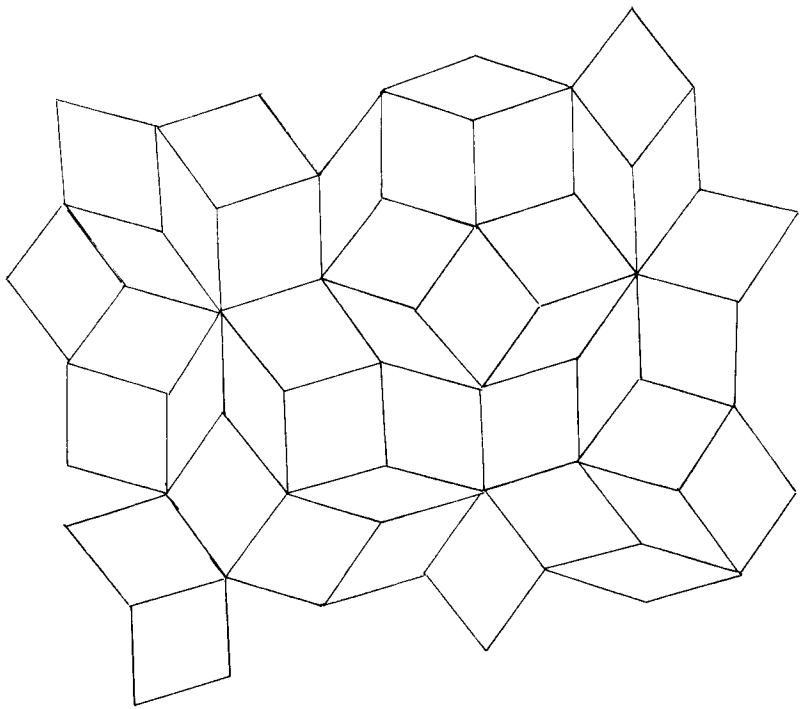

Figure 17. A Penrose tiling of the plane by rhombs. The matching rules (not shown) are prescribed by the colors and orientations of the edges.

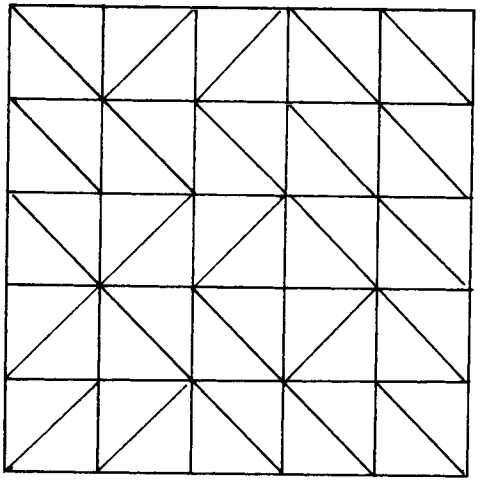

Figure 18. A square tiling divided into congruent triangles; the orientation of the triangles is random.

A warning: In G&S the term "aperiodic" is used to describe a special property of certain sets of prototiles: A set of prototiles is called *aperiodic* if *every* tiling that can be constructed with copies of these prototiles is nonperiodic. (The Penrose tiles and several other examples of aperiodic prototiles will be discussed in Section 5.) Aperiodic prototiles *force* nonperiodicity. Unfortunately, the distinction between prototiles which *can* be arranged nonperiodically and prototiles which *must* be arranged nonperiodically is often blurred in the literature, and "aperiodic" is being used more or less synonymously with "nonperiodic." Some way to distinguish these cases is needed however, since the distinction is important, both mathematically and physically.

3 Construction Techniques

3.1 "Filling the Whole"

As we mentioned earlier, Aristotle pointed out long ago that in order for copies of a polyhedron to fill space without gaps or overlaps, they must "fill the whole"; in particular, it must be possible to fit them together about a common vertex (the same holds of course for polygons in the plane). Aristotle's criterion does not guarantee that the polyhedra really tile all of space; sometimes a patch of tiles (a *patch* is the finite set of tiles contained

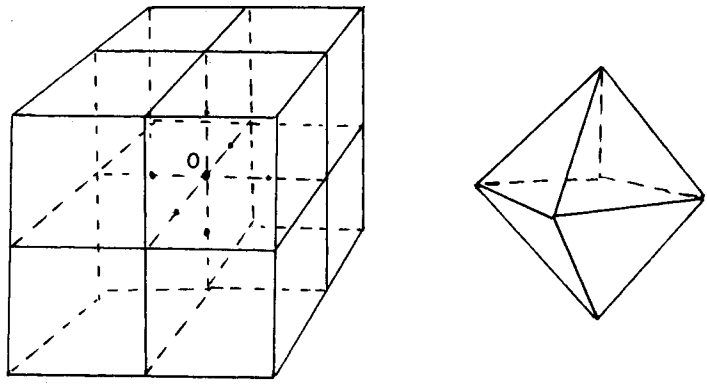

Figure 19. If polyhedra fit together at a point O, we can create a polyhedron about O by taking the convex hull of the points where a small sphere about O intersects their edges.

in and intersecting the boundary of a spherical or circular disk) cannot be extended. But filling the whole is certainly a necessary condition.

It is not very difficult to determine whether copies of a given polygon fill the whole; we are familiar with jig-saw puzzles. It is more difficult if the tiles are polyhedra. How can we determine whether polyhedra fit together at a common vertex to completely fill the immediate neighborhood? In some cases it is obvious but usually it is decidedly not. There is a fairly simple technique, however, for deciding whether a hypothetical configuration is *a priori* impossible. A sufficiently small sphere drawn about the vertex as center will cut the edges of the polyhedra which share that vertex in a finite set of points. The convex hull of this set of points is a polyhedron whose center is the common vertex and whose faces are similar to the vertex figures of the constituent polyhedra. (For example, when eight cubes meet at a point O, then the polyhedron we construct by this method is an octahedron (Fig. 19).) Since such a polyhedron must satisfy Euler's formula ($V - E + F = 2$, where V, E and F are the numbers of vertices, edges and faces of the polyhedron; see Section 4.1), this can be used as a preliminary test. For example, no collection of hexagonal pyramids or dipyramids can fit together at their apices: if they did, we would have a polyhedron all of whose faces are hexagonal. But no polyhedron with only hexagonal faces can exist[5].

[5] If all the faces of a polyhedron are k-gons, then $V \leq kF/3$ and $E = kF/2$ so that $2 = V - E + F \leq kF/3 - kF/2 + F = F(1 - k/6)$. The right hand term would be 0 if $k = 6$ and negative if $k > 6$; therefore $k \leq 5$.

3.2 *Dirichlet Tilings*

Given any discrete set X of points in the plane or in space, finite or infinite, we can use Dirichlet's construction to associate a unique tiling with X. For each point x of X we construct a tile or *Dirichlet domain*, which is the closure of the set of points in the plane or in space which are closer to x than to any other point of X. If x and y are any two points, then points lying on the perpendicular bisector of the line segment joining them are equidistant from both of them, while the points in the half-plane or half-space containing x are closer to x than to y (Fig. 20). To find the Dirichlet domain of x, we join x to all the other points of X by straight line segments and construct their bisectors. The smallest convex region bounded by these bisectors which contains x is the region we are looking for (Fig. 21).

The Dirichlet tiling is uniquely determined by X but the converse is false (the four vertices of a rectangle of any edge lengths determine congruent Dirichlet tilings).

The most important Dirichlet tilings (for crystallography) are those corresponding to discrete, relatively dense point sets. We have already defined discreteness (Section 2.3). X is said to be *relatively dense* in the space in which it lies if there are no arbitrarily large regions which are "empty" of points of X. That is, there is a positive real number R such that every disk

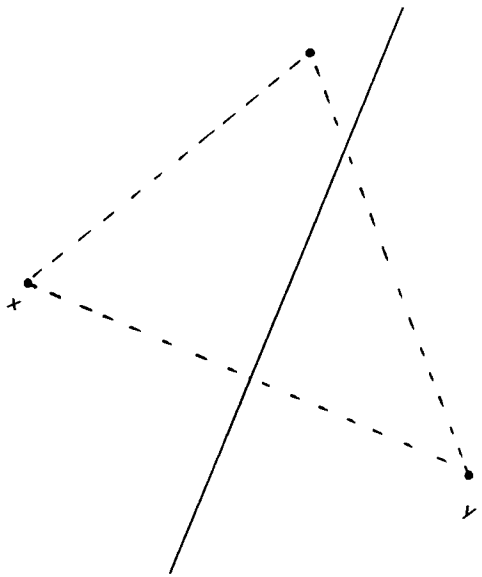

Figure 20. Any point in the plane which does not lie on the bisector is closer to x than to y, or vice versa.

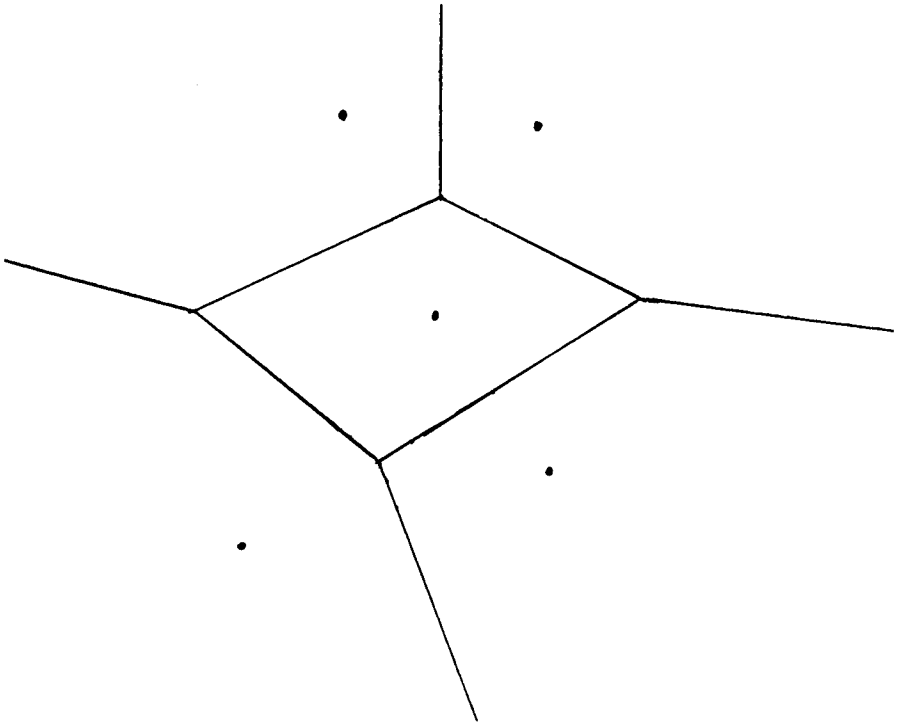

Figure 21. The Dirichlet tiling corresponding to a set of five points.

or ball of radius R in the plane or in space, contains at least one point of X. In particular, X does not lie entirely in a half-plane or half-space, nor are there infinite wedges or cones without points of X in them.

Since the discreteness of X prescribes a real $r > 0$ which is the minimum distance between its points, a discrete relatively dense point set is sometimes called an (r, R) *system*. We will say that a Dirichlet tiling is an (r, R) tiling if it has a defining point set which is an (r, R) system.

All (r, R) Dirichlet tilings are normal, the tiles are convex, and they are matched face-to-face. The tiles which are the domains of points within radius $2R$ of a point x include all those which belong to the *first corona* of the Dirichlet domain about x, i.e., those which share at least one boundary point with this domain. (These assertions are easy to prove; we leave them as an exercise in understanding the Dirichlet construction.)

If an (r, R) system is transitive, then the Dirichlet tiling will be isohedral. This has been exploited by Delaunay and his colleagues to find new space-filling polyhedra. More recently, Engel (1981) has used this fact and the computer to find Dirichlet domains for highly symmetric transitive (r, R)

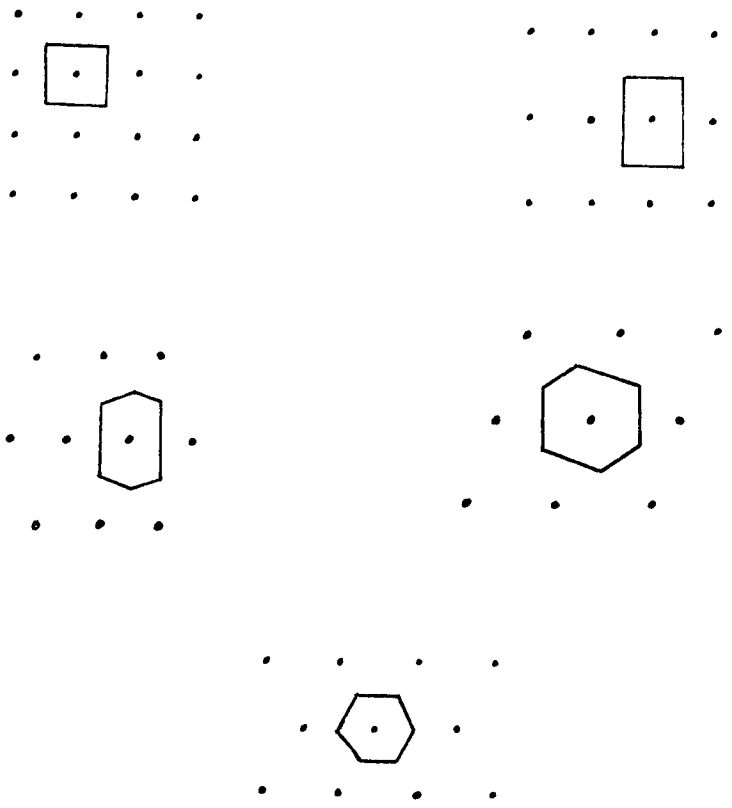

Figure 22. The five symmetry types of Dirichlet domain for plane lattices.

systems. In the process he discovered two different space filling polyhedra with thirty eight faces, the largest number so far known. Delaunay (1961) had proved that if X is a transitive (r, R) system then the number of faces of its Dirichlet domain[6] is less than 390, but Engel's work suggests that the true upper bound is considerably less than this. Determining a "good" upper bound for the number of faces of a space-filling polyhedron is a challenging open problem. (It is not known whether an upper bound of the number of faces of an arbitrary face-to-face normal monohedral tiling even exists.)

In an (r, R) Dirichlet tiling defined by a point set X, a vertex of the tiling is equidistant from the centers of the tiles whch share that vertex and thus these centers lie on a circle or sphere about the vertex. Taking the convex

[6] Since the Dirichlet domains of a transitive (r, R) system are congruent we can speak of *its* domain.

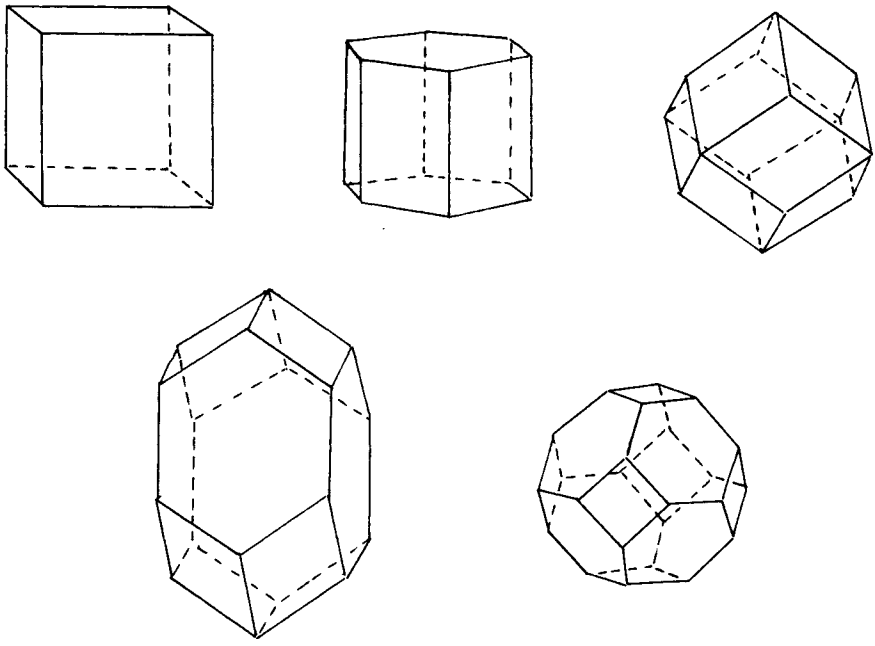

Figure 23. The five combinatorial types of Dirichlet domains for space lattices are Fedorov's five parallelohedra: from clockwise from upper left, they are the cube, the hexagonal prism, the rhombic dodecahedron, the truncated octahedron, and the elongated dodecahedron (discovered by Fedorov).

hulls of these centers, about each vertex of the Dirichlet tiling, we obtain a dually situated tiling whose tiles are polygons or polyhedra which can be inscribed in circles or spheres. This dual tiling was first introduced by Delaunay (1924) and is therefore sometimes called a Delaunay tiling.

If the (r, R) system is a latice, the Dirichlet domains are analogous to the unit cells of a lattice since they too tile the plane in parallel position. In fact, Dirichlet domains are sometimes more useful than unit cells since they give us immediate information about the symmetry of the lattice. For example, the Dirichlet domains of plane lattices are either rectangles or hexagons (Fig. 22), representing five different symmetry groups[7] and thus five different lattices.

The Dirichlet domains of space lattices are Fedorov's five parallelohedra (Fig. 23). By considering the ways in which symmetry groups compatible

[7] Two of these groups are isomorphic to the dihedral group D2, but are considered different because they act on lattices in different ways.

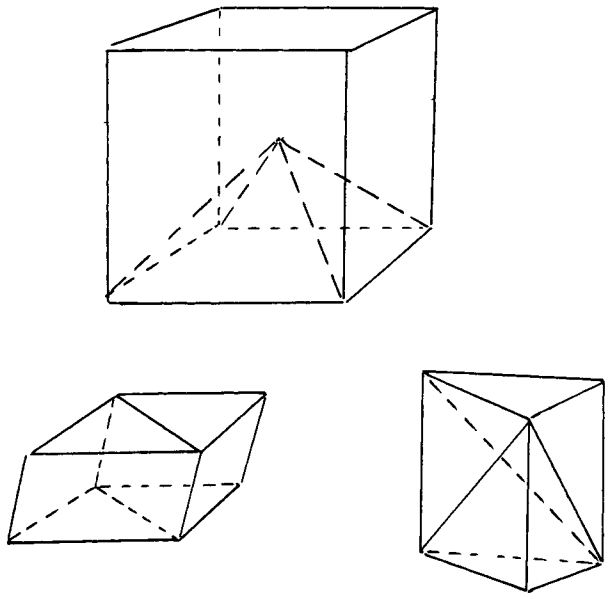

Figure 24. A cube can be partitioned into six congruent pyramids; from this we obtain a new monohedral tiling of space. A parallelopiped can be partitioned into two triangular prisms, which in turn can be partitioned into three tetrahedra. (Under what conditions are the tetrahedra congruent?).

with the lattices can act on them, we conclude that there are fourteen distinct space lattices.

3.3 Dissection Tilings

Like "dual," the word "dissection" is used in tiling theory in at least three different ways:

1. The simplest way to create a new tiling from a given one is to subdivide each tile into a finite number of pieces. The result of this dissection can be called a dissection tiling. The dissection tilings of greatest interest are those which are monohedral; two examples are shown in Fig. 24. There does not seem to be an algorithm for producing monohedral dissection tilings; evidently their discovery requires a great deal of ingenuity. Nevertheless they are of mathematical interest and crystallographic importance: many of the atomic patterns which frequently occur in crystals are closely related to dissections of tilings by cubes and parallelopipeds.

2. When the tiles of the dissection tiling are similar to the original pro-

totiles, and when there is a fixed rule or rules which have been followed in carrying out the dissection, the process of subdividing is sometimes called decomposition. Decomposition plays an important role in the theory of nonperiodic tilings (Section 5.1).

3. There are many intriguing geometric problems which are concerned with the dissection of finite objects into a finite number of pieces, subject to constraints of various kinds. Since most of these have little to do with the problem of infinite tilings, we will mention only the most famous of them, Hilbert's third problem (see Section 5.1). It is a remarkable fact that if two polygons have equal area, then they are equidecomposable: either one can be subdivided into a finite number of pieces which can be reassembled to form a polygon congruent to the other. Hilbert asked whether the same is true for polyhedra. The answer turned out to be no: polyhedra of equal volume are not necessarily equidecomposable (for an elementary discussion of this problem, see Boltianskii, 1978). In particular, a cube and a regular tetrahedron of equal volume are not; this is related to the fact that the regular tetrahedron does not fill space. Not surprisingly, the only polyhedra which are *translation-equidecomposable* with the cube are parallelohedra.

3.4 *Duals of Multigrids*

The work of N. G. de Bruijn (1981) on the two dimensional Penrose tilings (Section 5.2) has led to the discovery of an interesting new class of tilings of the plane by rhombs and of space by rhombohedra. We will discuss the planar case; the three dimensional case is completely analogous.

Following de Bruijn, we define a *grid* to be an infinite family of equispaced parallel lines. To such a grid we associate a unit vector x normal to the grid lines; the vector determines positive and negative directions for the grid (Fig. 25). The superposition of a finite number m of such grids (with the same spacing), is called a multigrid, or an *m-grid*. A regular m-grid is one in which the grids are shifted relative to one another so that at most two lines intersect at any point (Fig. 26).

An m-grid can be interpreted as a tiling M of the plane, since it partitions the plane into polygons. Assume first that the m-grid is regular. We construct a dual tiling M^* by associating to each vertex of M a rhombic tile whose edges are the normals to the grid lines which meet there. More precisely, if the vertex is the intersection of lines from grids i and j, then a small loop around the vertex alternately crosses each of these lines, once in the positive and once in the negative direction (Fig. 26); to this loop we associate the rhombus whose edges are $x_i, x_j, -x_i$ and $-x_j$. The set of all such rhombs is a tiling M^* of the plane. It is dual to M, since each rhomb

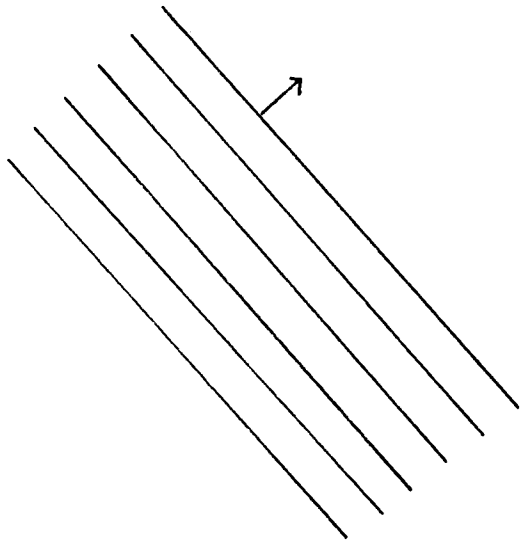

Figure 25. A grid with unit normal vector.

corresponds to a vertex of M and each vertex corresponds to a mesh of M. M and M^* are not dually situated. Notice also that the construction of M^* would be the same no matter how M might be deformed, as long as the same normal vectors continued to be associated with each grid.

Singular m-grids (those which are not regular) can be regarded as limiting cases of regular m-grids; this permits their duals to be constructed in a similar way.

The tilings M^* of greatest interest are those in which the $2m$ normal vectors (counting both directions) of M point to the vertices of a regular $2m$-gon. Then M^* will be composed of $m/2$ different rhombs if m is even, and $[m/2]$ if m is odd. For example, if $m = 2$, then we have the usual tiling of the plane by squares; if $m = 3$, we have a tiling of the plane by congruent rhombs whose angles are 60° and 120°. But since m can be any positive integer, the symmetry of the $2m$-gon need not be crystallographic. Indeed, in the case studied by de Bruijn, $m = 5$ and there are two kinds of rhombs. Their smaller angles are 72° and 36°—they are the thick and thin Penrose tiles.

De Bruijn proved that the M^* tiling constructed in this way is a "true" Penrose tiling—the edges of the tiles can be labeled in such a way that nonperiodicity is forced (Section 5.2). But this appears to be a very special, perhaps unique, case. Evidently none of the other tilings obtained as duals of m-grids have this property.

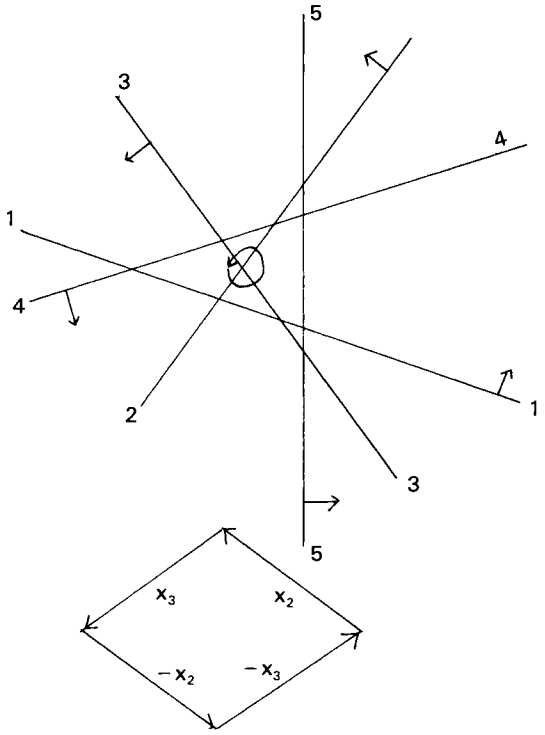

Figure 26. For each vertex of a regular m-grid (here $m=5$) we construct a rhomb whose edges are normal to the grid lines intersecting there.

3.5 *Tilings Obtained by Projection*

In Fig. 27 we see the ordinary tiling of the plane by squares, on which is drawn a line with an irrational slope. The points marked on the line are the orthogonal projections of lower right-hand vertices of the squares through which the line passes. Notice that these points are irregularly spaced. Notice also that there are exactly two different spacings, C and D, between successive points, according as the points from which they are projected are joined by a vertical or horizontal edge of a square.

We can regard the points on the line as the vertices of a tiling of one-dimensional space by C and D tiles. The tiling is not periodic: if it were, there would be a repeating block of, say, x C tiles and y D tiles which in the square tiling would correspond to a path of x horizontal and y vertical steps. But then the slope of the line would be rational. This projected tiling is thus an example of a one dimensional quasiperiodic pattern.

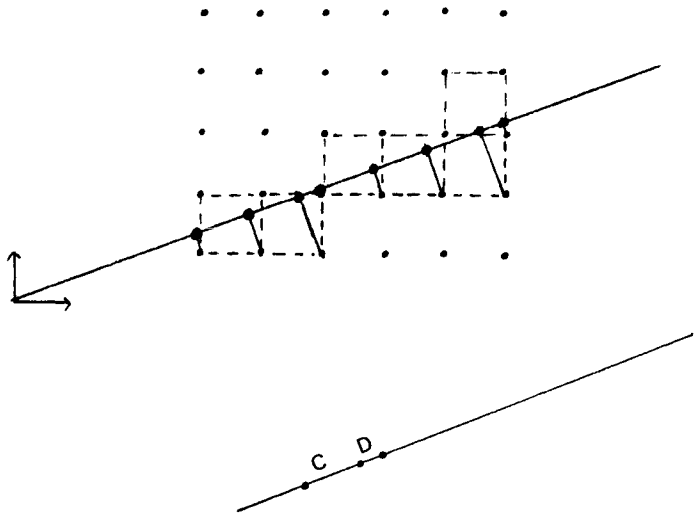

Figure 27. A one dimensional quasiperiodic tiling is obtained from a two dimensional periodic tiling by projection (see text).

This procedure can be generalized in several ways. For example, we can project sections of lattice tilings in higher dimensional spaces onto irrational two or three dimensional subspaces to obtain quasiperiodic tilings of the plane or of space (a subspace is irrational if it contains at most one lattice point). It must of course be shown that this procedure actually leads to a tiling (i.e., that the projected tiles fill space and do not overlap) and that the tiling is nonperiodic (i.e., that the tiling does not admit "accidental" translations).

Quasiperiodic patterns are closely related to the duals of m-grids (see Section 5.2).

Most of the quasiperiodic patterns that have been studied so far are projections from tilings of n-dimensional space by n-dimensional cubes[8]. Coxeter (1973) shows that the orthogonal projections of an n-cube into three dimensional space is an isohedral polyhedron whose faces are parallelograms; it belongs to the class of polyhedra called *zonohedra*. The n-cube, with its n mutually perpendicular edges, contains $n(n-1)(n-2)/6$ three-dimensional cubes within it; these cubes project onto rhombohedra within the zonohedron. The 4-cube projects onto a rhombic dodecahedron

[8] The n-cube, which is sometimes called a hypercube or measure polytope, has 2^n vertices and $2n$ cells. Thus when $n = 3$, the cube has 2^3 vertices and 2×3 faces; the 4-cube has 2^4 vertices and 2×4 three dimensional faces, which are cubes.

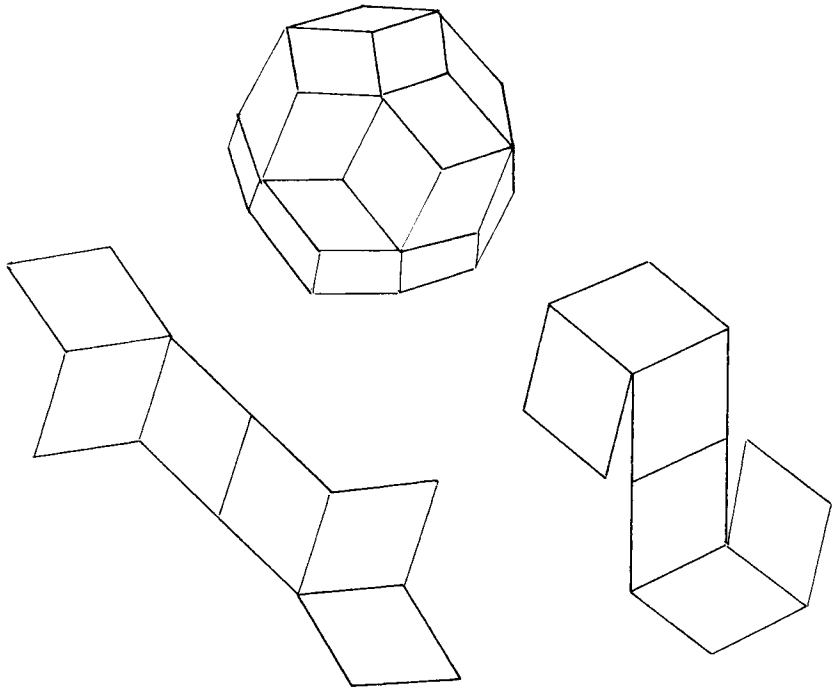

Figure 28. The triacontahedron can be partitioned into ten prolate and ten oblate rhombohedra. Models of these rhombohedra can be made by folding up these nets.

(Fig. 23, top right) and the 6-cube onto a triacontahedron (Fig. 28). The rhombic dodecahedron can be partitioned into four congruent rhombohedra, and the triacontahedron into twenty which fall into two congruence classes. These two rhombohedra are the geometric prototiles for the three dimensional Penrose tilings which we will briefly discuss in Section 5.3.

4 Forcing Transitivity

In this section we will briefly discuss some of the ways in which local order in tilings of the plane (and of three dimensional space) determines the transitivity properties of the tiling. The problem is illuminated by a discussion of the local and global symmetry properties of regular polyhedra.

4.1 Regular Polyhedra and Polytopes

The best known polyhedra are of course the five regular convex "solids" (Fig. 1), which were discovered by the ancient Greeks. Here the word

"regular" means that all the faces of the given polyhedron are congruent, regular, convex polygons and the vertex figures are congruent too. Remarkably, when these local requirements are satisfied the polyhedra are isohedral, isogonal, and isotoxal.

But this should not be taken for granted!

1. It is easy to show—as Euclid did—that there are no other regular polyhedra. In order to fit polygons together to form a polyhedral angle, the sum of their angles at the common point must be less than 360°. If the polygons are convex and regular, this will only be possible if we join three, four, or five equilateral triangles, or three squares, or three regular pentagons together. This argument does not prove that any of the five possible regular polyhedra exist; it must also be shown that the patterns of polygonal angles can be continued at every vertex until a closed figure is formed. Since we know that they can and the results are convex, we know that all five polyhedra do exist. But why are they isohedral, isogonal, and isotoxal?

2. Let us briefly review Euler's formula. Obviously, a polygon has the same number of vertices (V) as it has edges (E). This is clearly not the case for the polyhedra, since for the cube $V = 8$, while $E = 12$ (and the number of faces, F, is 6). However, for any convex polyhedron there is a linear relation among the three numbers V, E, and F. This is Euler's famous formula, $V - E + F = 2$. (If you are unfamiliar with it, find V, E and F for the regular solids and observe that the equation is satisfied.)

Euler's formula can be used to derive the regular polyhedra. Surprisingly, it turns out that the small number of regular polyhedra is a combinatorial limitation, not just a metric one. For, if all the faces of a polyhedron are k-gons and all the vertices are j-valent, then $V = 2E/j$ and $F = 2E/k$. Thus $2E/k - E + 2E/j = 2$. Dividing by $2E$ and rearranging terms, the formula becomes $1/j + 1/k = 1/2 + 1/E$.

Since j and k are integers greater than three, the only solutions are $(j, k) = (3, 3), (3, 4), (4, 3), (3, 5)$ or $(5, 3)$. This means that the corresponding polyhedra must be combinatorially equivalent to one of the five regular solids.

Notice, however, that Euler's formula does not say anything about angles, size or shape; it only prescribes the possible networks of edges and vertices that a polyhedra with k-gonal faces and j-valent vertices can have. We know that these networks can be realized as the "skeletons" of convex polyhedra; this is guaranteed by a theorem of Steinitz (Grünbaum, 1967). But why is it always possible to impose symmetry on the polygonal faces so that the polyhedra are regular?

3. We can derive the regular polyhedra by starting with finite symmetry groups and constructing the convex hulls of sets of points on which these groups act transitively (Weyl, 1952). Consider a finite group of rotations of

the sphere S. Each rotation axis intersects S in two points, called poles; the poles can be divided into sets on which the group acts transitively. The convex hull of any such set is an isogonal polyhedron, and its dual (by reciprocation in S) is isohedral. In fact, we discover by inspection that in some cases the face centers of these isogonal polyhedra lie on the axes through a second equivalence class of poles, and their edge midpoints on a third; thus we recover the regular solids, together with polygons (single- and double-sided) and prisms.

Alternatively, the regular polyhedra can be recovered (as tilings of the sphere) by constructing the (spherical) Dirichlet domains of equivalence classes of poles.

So, local symmetry requirements lead to regular polyhedra, but it is not clear why. Transitivity arguments also produce the regular polyhedra, but some of the local symmetry seems to be fortuitous. A recent result of Delaunay and his colleagues (1976) shows that local symmetry (on a sufficiently large scale) always forces transitivity. In the next section we will sketch their argument (for a more detailed discussion, see Senechal, 1986).

4.2 *A Local Criterion for Transitivity*

Consider an (r, R) system in the plane (or in space of any dimension, or on the sphere). If a symmetry group acts transitively on this set of points, then the "spider" formed by joining any point to all the other points in the set must be congruent to any other such spider. Delaunay and his colleagues asked whether the congruence of small spiders might be enough to ensure transitivity. The answer turned out to be yes.

Briefly, at each point P of the (r, R) system we consider a finite sequence of finite spiders, those formed by joining P to the other points which lie inside spheres about P of radii $2R$, $4R$, $6R$, and so forth (by the definition of R, we are guaranteed that such points exist). The size of the symmetry groups of these spiders cannot increase, since the addition of extra legs to the spider cannot increase the symmetry of the configuration of legs that are already there. Since the system is discrete, there are only a finite number of legs in each sphere and thus the symmetry group is finite. At each step we obtain a larger spider but an equal or even smaller symmetry group. After a certain number of steps, then, the symmetry group of the spider must stabilize (Fig. 29).

Now assume that the stable spiders are congruent for each point in the system. Then a rigid motion which carries the spider about P onto the spider about another point Q also carries the spider of a nearby point ($\leq 2R$) onto another spider, and the same for a point near it, and so forth. By this "continuation" argument, we find that every point of the system has been

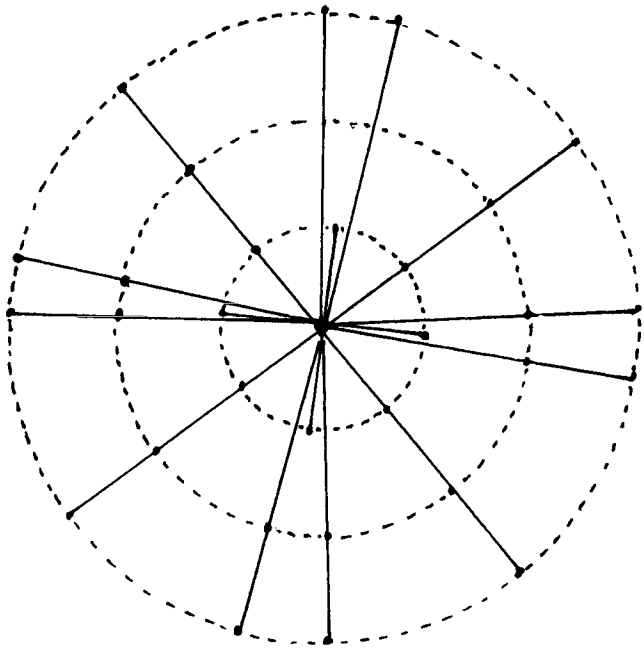

Figure 29. The symmetry of a spider in an (r, R) system stabilizes in a finite number of steps.

carried to another point of the system and so, by definition, the motion is a symmetry operation for the (r, R) system. Since P and Q were chosen arbitrarily, the group of all such symmetries acts transitively on the set. Thus local symmetry implies transitivity. (But the theorem does not tell us how small the stabilizing radius can be, only that it is finite.)

The result can be applied to tilings by taking the Dirichlet domains of the points of an (r, R) system. It turns out that for tilings of the plane the congruence of the tiles together with their first coronas is sufficient to ensure that the tiling is isohedral; moreover, this is true for any tiling, not just for Dirichlet tilings (Moran, to appear). For polyhedra and higher dimensional tilings the situation is not so simple: there are monohedral tilings of the sphere and of space (Engel, 1986) in which the first coronas of the tiles are congruent but which are not isohedral.

4.3 *Isohedral Polyhedra and Isohedral Tilings*

Euler's formula can also be used to find the combinatorial types of isohedral polyhedra. We do not require now that all vertices have the same

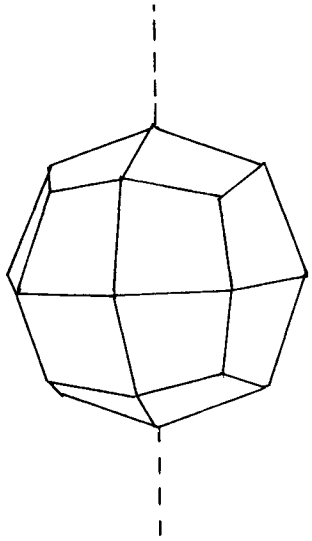

Figure 30. An isohedral realization of the spherical network with uniform vertex cycle [3, 4, 4, 4]. If we rotate the top half 45° about the vertical axis we obtain a second realization which cannot be made isohedral.

valence, only that the cycle of valences be the same for each face so that we can match them when we match faces. If the cycle of valences is $[j_1, \ldots, j_k]$, then Euler's formula becomes, after substitution and rearrangement, $1/j_1 + \cdots + 1/j_k = k/2 - 1 + 2/F$.

Each solution of this equation must be tested to see whether such a network of edges and vertices actually exists; for example, [3, 3, 12] satisfies the equation (with $F = 8$), but there is no such network since a vertex of valence twelve implies that there are at least twelve faces. Then for each network we have to show that it can be realized as a convex isohedral polyhedron.

In fact, the existence of a polyhedron with a given vertex cycle does *not* imply that the corresponding polyhedron is combinatorially equivalent to one which is isohedral! The solution [3, 4, 4, 4], with $F = 24$, can be realized in two ways, one of which is isohedral (Fig. 30) and one of which is not (the second is obtained from the first by rotating the top half of the polyhedron 45° about the vertical axis). It is instructive to make models of these polyhedra (you will need 18 squares and 8 equilateral triangles, all with the same edge lengths, for each polyhedron).

Euler's formula can also be used to find the combinatorial types of isohedral tilings of the plane, but we have to take into account the fact that for a tiling, V, E, and F are infinite. It was first observed by Cauchy in 1811

that if we remove one face of a convex polyhedron and stretch the remaining surface out onto a plane (which we can do since the surface of a convex polyhedron is topologically equivalent to a sphere), we have converted the polyhedron, minus one face, to a finite planar graph. Then Euler's formula becomes $V - E + F = 1$.

To study infinite planar tilings, we begin with a patch of it and use a limiting process. Suppose that every tile in the tilings is a k-gon. For the tiles in the patch, we would have $E = kF/2$ except for the fact that the boundary edges are counted only once. Thus $E = kF/2 + r$, where r, an error term, depends upon the patch, and $V \leq kF/3$. We have $1 = V - E + F \leq kF/3 - kF/2 + F + r = F(1 - kF/6) + r$, or $1/F - r/F \leq 1 - kF/6$.

Now we let the number of tiles grow without bound (this process can be made precise, as shown in G&S). The term $1/F$ approaches 0 and careful analysis shows that, if the tiling is normal, r/F approaches 0 also. We conclude that if every tile of a tiling is a k-gon, $k/6 \leq 1$. Thus $k \leq 6$. In other words, the plane can be tiled with triangles, quadrilaterals, pentagons or hexagons.

Yes, there are pentagons that tile the plane, although of course the regular pentagon does not. In fact there are a great many types (up to similarity) of pentagons which tile. Two are shown in Figs. 11 and 15; others can be found in G&S. Some tilings by pentagons are isohedral, others are not, but all those known so far are periodic. The problem of finding the metric types of *all* pentagons that tile is unsolved, since it has not been proved that the current list is complete. (Each time completeness has been announced, another tessellating pentagon has been discovered—often by an amateur.)

To find the isohedral tilings of the plane by k-gons, we assume the cycle of valences of the k vertices is the same for each tile, $[j_1, \ldots, j_k]$. For any patch of such a tiling, $E = kF/2 + r$; now $V = F(1/j_1 + \cdots + 1/j_k) + s$ —again we must include an error term, s, because of boundary vertices. Fortunately, for normal tilings s too approaches 0 as F gets large. Substituting for E and V in Euler's formula, dividing by F and rearranging terms we have $1/j_1 + \cdots + 1/j_k + r + s = k/2 - 1 + 1/F$. Thus in the limit we have $1/j_1 + \cdots + 1/j_k = k/2 - 1$.

The networks we are looking for are characterized by solutions of this equation.

When $j_1 = \cdots = j_k$, the equation becomes $k/j = k/2 - 1$, or $1/j + 1/k = 1/2$. The only solutions are (3, 6), (4, 4), and (6, 3), which we recognize as the tilings by equilateral triangles, squares, and regular hexagons (Fig. 31).

Not every solution characterizes a network, however. For example, if $k = 3$ and $[j_1, j_2, j_3] = [5, 5, 10]$, the equation is satisfied but there is no such network (Fig. 32).

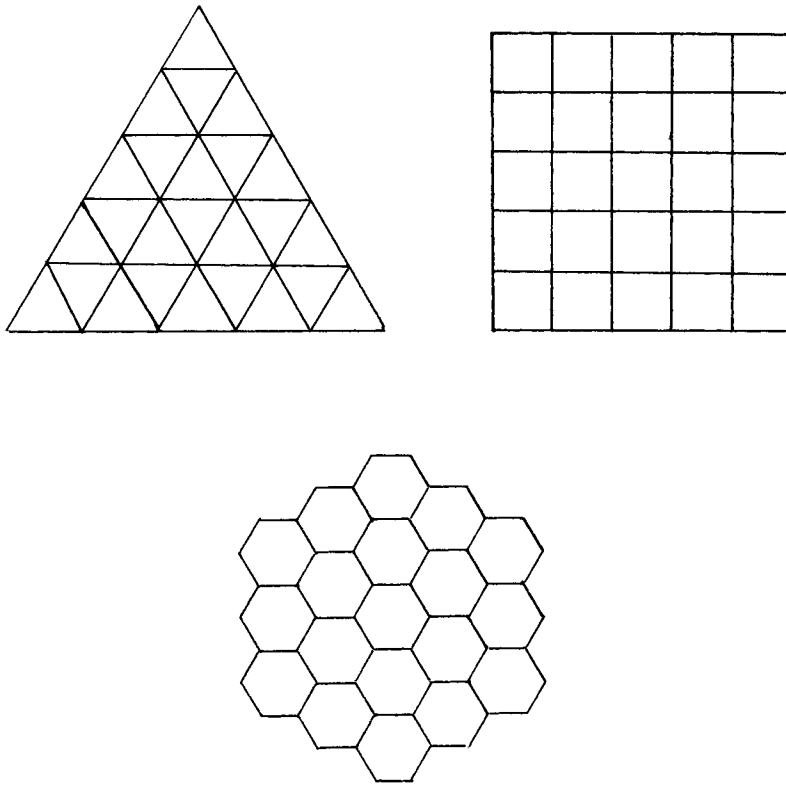

Figure 31. The three tilings of the plane by regular polygons.

In fact, only ten of the seventeen solutions correspond to nets: for $k = 3$, [3, 12, 12], [4, 6, 12], [4, 8, 8] and [6, 6, 6]; for $k = 4$, [3, 4, 6,4], [3, 6, 3, 6] and [4, 4, 4, 4]; for $k = 5$, [3, 3, 3, 4, 4], [3, 3, 4, 3, 4] and [3, 3, 3, 3, 6]; and for $k = 6$, [3, 3, 3, 3, 3, 3]. Notice that one solution can be realized as two distinct vertex cycles. Thus there are eleven nets, called Laves nets, after the German crystallographer F. Laves (Fig. 33).

In order for a tiling of the plane to be isohedral, its network of edges and vertices must be a Laves net. It is shown in G&S that all the Laves nets can be realized as isohedral tilings, in a total of 81 different ways (93 if markings on the tiles are allowed). This classification was determined by enumerating "adjacency symbols" which record the ways in which the symmetries of k-gons can be realized in the eleven nets. In effect, these symbols specify the geometry of the first coronas of the tiles; as we have seen, this is enough to ensure that the tiling is isohedral.

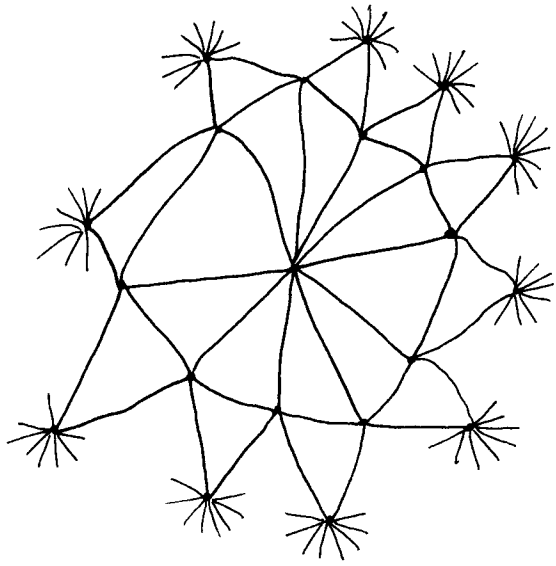

Figure 32. Why can't this network, in which each triangle is to have vertex cycle [5, 5, 10], be continued?

The planar nets in which every vertex is j-valent and the face cycles are uniform, are dual to the Laves nets. They can be obtained as dually situated nets or derived directly from Euler's formula. These nets were actually discovered long before the Laves nets: they were discussed and illustrated by Kepler in 1619, in his enumeration of the isogonal tilings of the plane by regular polygons.

In comparison with the situation in the plane, the study of isohedral tilings in three dimensional space is still unsatisfactory. In addition to the Dirichlet domains of the points of the three dimensional lattices, we know (all) the Dirichlet domains for only one other type of transitive (r, R) system (Stogrin, 1973).

Of course we know many examples of isohedral tilings of space. Part of the difficulty in determining all of them is that we do not have an analogue of the Laves nets for three dimensional tilings. The three dimensional analogue of a finite planar graph is a tiling of a region of space by a finite number C of polyhedra or cells. Regarding this configuration as a projection of a polytope from which one cell has been removed, Euler's formula, as generalized by Schlafli (Coexter, 1973) becomes $V - E + F - C = -1$. Unfortunately, a single linear equation in four unknowns cannot yield sufficient information to classify three dimensional nets, even if we impose

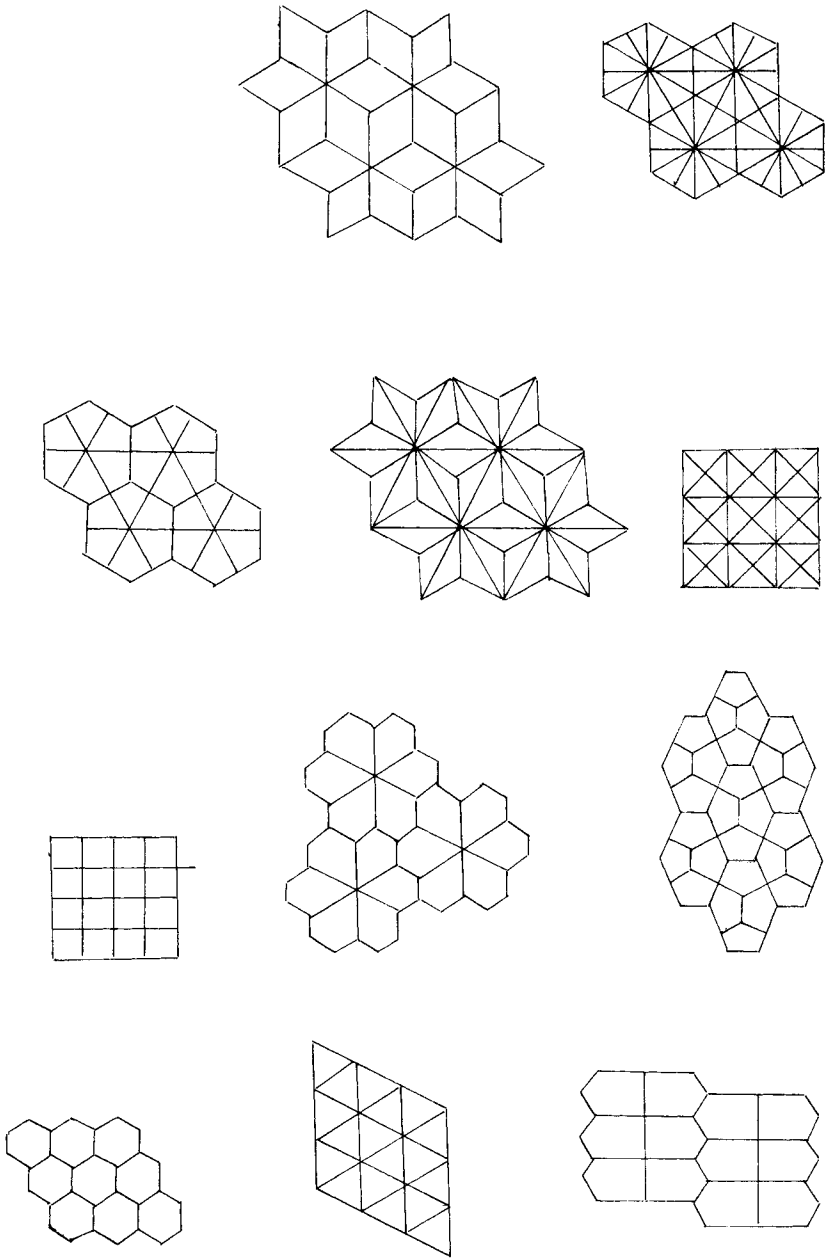

Figure 33. The eleven Laves nets.

uniformity conditions to ensure the combinatorial isomorphism of cells, vertices, or some other feature. At this time, therefore, the list of three dimensional nets must be considered incomplete. However a great many nets which are frequently encountered in crystal structures have been carefully studied, and some methods for generating and classifying them have been described in the literature (see, for example, Wells, 1977).

As noted in Section 3.2, we can obtain isohedral tilings of space by constructing the Dirichlet domains of transitive (r, R) systems. However, the combinatorial properties of these domains are highly unstable; a small displacement of the positions of the points, which need not change the symmetry of the set, may effect a discontinuous transformation of the tiles (something like the way in which soap bubble clusters switch from one configuration to another). This makes it very difficult to determine whether any list of infinite isohedral Dirichlet tilings is complete.

5 Forcing Nonperiodicity

5.1 General Principles

In 1900 the reknowned German mathematician David Hilbert posed twenty-three problems which he hoped would influence the course of mathematical research in the early years of the twentieth century. The eighteenth problem consisted of three parts, all of them influenced by crystallography. The second of these was, "Do polyhedra exist which do not appear as fundamental regions of groups of motions, by means of which nevertheless by a suitable juxtaposition of congruent copies a complete filling up of all space is possible?"

There are many ways to interpret this question (see Grünbaum and Shephard, 1980). The most interesting interpretation, and by far the most difficult, is: does there exist a polyhedron which tiles space, but *only nonperiodically*? This question has not been settled even for polygons tiling the plane. But in recent years it has been found that if we allow tilings which are copies of two or more different prototiles, then the answer is yes.

The first such set of prototiles was discovered by Berger in 1966; it contained 20,426 prototiles. These tiles belong to a class of tiles known as Wang tiles: they are squares with colored edges which must be placed edge-to-edge in parallel position so that colors match (Section 5.4). Berger's tiles are of no apparent use in crystallography, but his discovery helped to settle—in the negative—a major question in decidability theory (a branch of mathematical logic) and in tiling theory: does there exist an algorithm for

deciding whether copies of a given set of prototiles tile the plane? During the last twenty years several other sets of tiles which force nonperiodicity have been discovered; several of these sets consist of only two prototiles. There is still no general theory for constructing them. However, as the study of nonperiodicity becomes more important for crystallography, these tiles and the tilings that can be formed with them are receiving increasing attention.

How can we tell whether a tiling is nonperiodic? Certainly not by visual inspection: any finite portion of a tiling might, for all we know, be part of a larger repeating block. We need either some kind of global information about the tiling (for example, that it was obtained by projection from a periodic tiling onto an irrational plane, or by decorating a periodic tiling in an irregular but deterministic way), or sufficient local information to guarantee that the tiling cannot have translational symmetry.

An example of local information which forces nonperiodicity is a *composition rule*. A tiling is constructed by a composition rule if its tiles can be grouped, *uniquely*, into larger tiles similar to the original ones.

Consider, for example, the monohedral tiling shown in Fig. 34. Its prototile is composed of six equilateral triangles. The tiling has the composition property: any tile can be grouped together with three neighboring tiles to form a larger tile similar to itself. Notice also that, within the tiling, this grouping into larger tiles can be done in only one way.

Thus the original tiling contains within it a unique larger copy of itself. Clearly we can repeat this process, grouping together four large tiles to form even larger tiles, again in a unique way. Since the composition process can be continued indefinitely and since at each stage the tiles are four times larger than at the preceding one, we see that for any real number $d > 0$ there will be some stage at which a circle of radius d can be inscribed in the tiles.

This observation implies that the tiling is nonperiodic. For, suppose that the tiling were periodic. The uniqueness of composition implies that the hierarchical levels of the tiling are intrinsic to the tiling and thus any symmetry of the tiling must carry each level onto itself. If the tiling were periodic, then among the symmetries of the tiling there would be a translation, in some direction, through a finite distance d. But then there would be a level of the hierarchical tiling at which the tiles would not be moved to other tiles by this translation, but would overlap with their original positions. We conclude that the tiling is nonperiodic.

On the other hand, it is easy to see that the prototile of Fig. 34 can also tile the plane in a periodic way: two of them fit together to form a parallelogram, which tiles the plane periodically. This shows that the nonperiodicity of the tiling in Fig. 34 is not forced by the tiles themselves outside the context of that tiling.

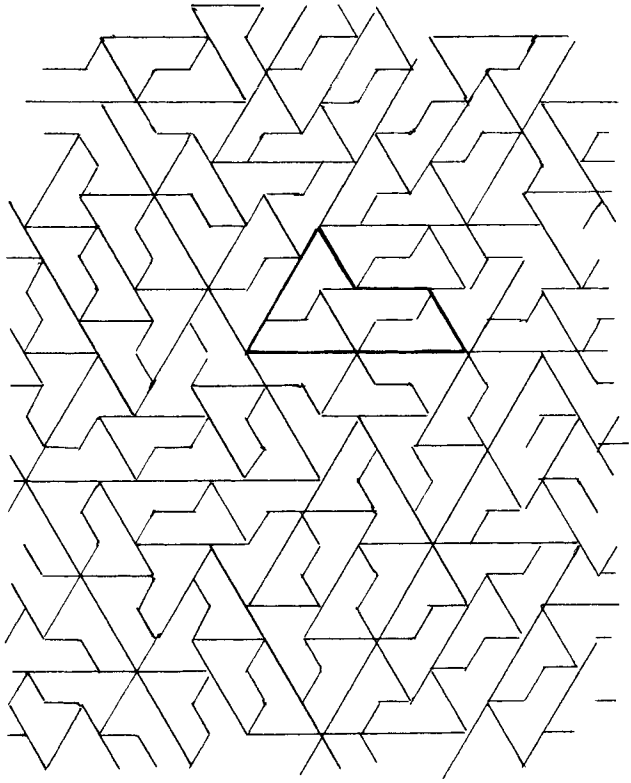

Figure 34. A tiling of the plane which has the composition property. Four tiles can be grouped into a larger tile which is similar to the original prototile.

There are many properties, in addition to nonperiodicity, that are implied by composition. One important property is known as local isomorphism, a term originally intended to designate relations between sets of tilings, but which can also be applied to a single tiling—a tiling can be locally isomorphic to itself. A tiling is said to have the *local isomorphism property* if every patch occurs "relatively everywhere" within it (i.e., there are no arbitrarily large regions in which the patch does not occur). Obviously any periodic tiling has this property; it is remarkable that nonperiodic tilings can have it too.

The composition property guarantees local isomorphism in the following way. Since we can group the tiles together to form larger ones, in a unique way, it follows that there is also a unique way to dissect the tiles into smaller ones. Then we have a tiling which represents a (negative!) hierarchical level of the one we started with. It follows that if we then inflate the smaller tiles

by the appropriate scale factor, any patch of the tiling can be obtained by dissection and inflation from any starting configuration of the tiles, and thus the patch must appear "relatively everywhere." It follows also that any two tilings by copies of the same set of aperiodic prototiles must be locally isomorphic.

Wang tiles, the Penrose tiles, and the various sets of Ammann tiles (one of which we will discuss in Section 5.4) all have the composition property and thus every tiling by copies of these tiles is nonperiodic. The composition property is defined by the rules by which the tiles are put together. These rules can sometimes be expressed by ensuring that the edges of the tiles permit only certain juxtapositions; usually they are described by marking the tiles in some way, such as coloring edges, coloring vertices, or both.

A composition rule is characterized by a substitution matrix, which encodes the number of prototiles of each kind which are contained in the larger ones. The scaling factor of the hierarchical levels of the tiling is an eigenvalue of this matrix. To some extent, then, the properties of composition matrices can be studied independently of tilings. But it is not obvious how to decide whether a given composition matrix can be realized as a hierarchical tiling.

In any case, there exist prototiles which force nonperiodicity for which no composition rule is known (Section 5.3).

5.2 *Two Dimensional Penrose Tiles*

The Penrose tiles are discussed in great detail in G&S, so we will review only a few of their basic properties here. Although these tiles are usually represented as "kites and darts," we will discuss only their alternative representation by thick and thin rhombs (Fig. 17). This formulation allows us to study the tilings from several points of view.

The rhombs themselves do not force nonperiodicity, since two thick rhombs and one thin one can form a hexagon; without restrictions, this hexagon could be used as the prototile of a periodic tiling. Nonperiodicity is guaranteed by marking the edges or vertices of the tiles to make such configurations impossible. This can be done in various ways; we follow de Bruijn (1981) in using colored and orienting the edges (Fig. 35).

The marked rhombs obey a composition rule: the thick and thin rhombs can be grouped into larger thick and thin rhombs in a unique way, although this is far from obvious. The process is illustrated in Fig. 36. Let us denote the thick rhombs by A, the thin ones by B, and the larger rhombs by A' and B'. Then $A' = 2A + B$ and $B' = A + B$. Notice that the large rhombs are not built of whole small rhombs, but of halves of them. This may seem strange until we notice that the real units of these Penrose tilings (and also

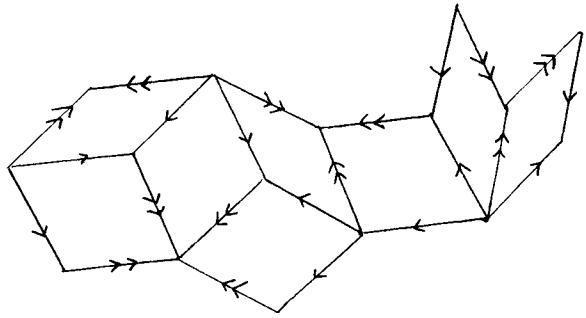

Figure 35. A Penrose tiling of the plane by thick and thin rhombs. Notice that the arrangement of the tiles is dictated by the requirement that the colors and arrows on the edges must be properly matched.

the tilings by kites and darts) are two kinds of triangles of which the thick and thin rhombs are composed and which we find in the regular pentagon. The triangles can be grouped together to form larger triangles similar to the original ones; these are the subunits of the larger rhombs. The larger rhombs inherit their matching rules from the smaller ones: on the edges

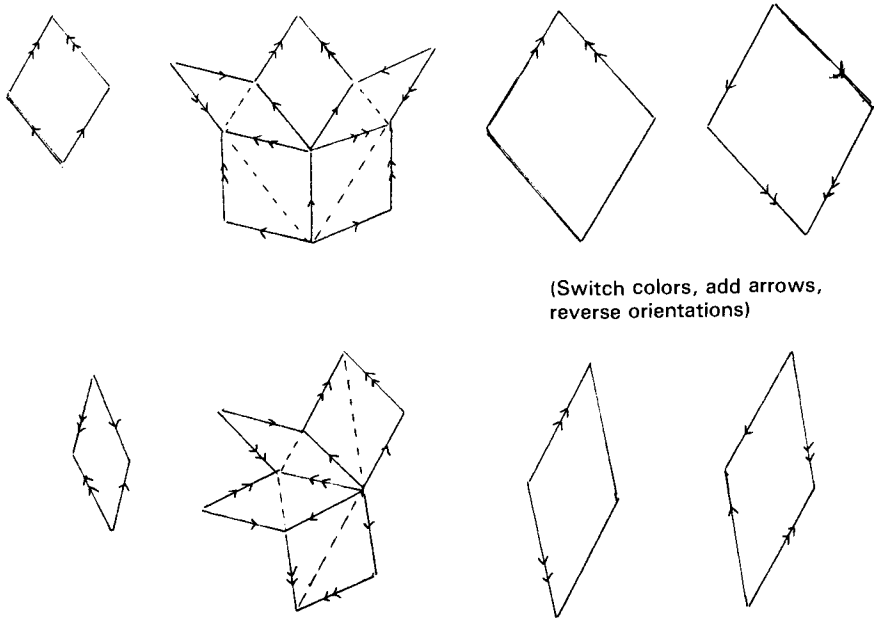

Figure 36. The composition rule for the Penrose rhombs. The tiles are composed of the same triangles as the regular pentagon

which are already marked (double arrows) we reverse the orientation and change the colors; the new edges receive the other color and the appropriate orientation.

The Penrose tiles have many interesting properties which are due to their composition rule. But one of their most important properties does not appear to be related to composition: the Penrose tiles are duals of 5-grids (Section 3.4). This was discovered by N. G. de Bruijn (1981), whose paper has been the stimulus for all further work on quasiperiodicity.

Although the dual m-grid approach does not necessarily guarantee that the resulting tiling will obey a composition rule, de Bruijn was able to reconstruct the matching rules in the case of the Penrose tiles. Using a function defined in terms of the shifts of the grids from the origin that characterizes a regular m-grid, he was able to associate an integer "index," 0, 1, 2, 3 or 4, to each vertex. The patterns of indices allowed a reconstruction of the colored and oriented edges.

Further, de Bruijn showed that the Penrose tiles are quasiperiodic: they can be obtained by projection from five dimensional space. To each mesh of a pentagrid, we can assign an ordered pentuple of five integers which specifies its location with respect to each of the five grid directions. This pentuple can be thought of as the coordinates of a point of a five dimensional integer lattice. Since the meshes of the pentagrids correspond to the vertices of the dual tiling by rhombs, these vertices can be regarded as projections of lattice points in five dimensional space. (Not all lattice points correspond to vertices, only certain of those which lie in a certain slice of the lattice.)

The diffraction pattern of a five dimensional lattice can be calculated in the standard way; to obtain the diffraction pattern for the vertices of Penrose tilings, we restrict the functions involved to the slice. This can also be done for the three dimensional version of the Penrose tiles; the diffraction patterns they produce are intriguingly similar to those of icosahedral quasicrystals. It is this property of the Penrose tiles that has caused such interest among those studying quasicrystals. But it is still not known whether the structures of these tilings and the crystals have any real relation to one another.

5.3 *Three Dimensional Ammann Tiles*

We have already noted that the orthogonal projection of a 6-cube into three dimensional space is a rhombic triacontahedron. The three dimensional faces of the 6-cube project into twenty nonoverlapping rhombohedra, all with the same rhombic faces but of two different shapes, thick and thin (Fig. 28). These rhombohedra, properly marked, can be regarded as the three dimensional version of the Penrose tiles, first suggested by Ammann (unpublished) and discussed in more detail by Katz in Chapter 4 [see also (Katz, 1988)].

Katz discovered matching rules for these tiles which force nonperiodicity. However, there are fourteen different markings for the thick rhombohedra and eight for the thin, giving essentially twenty two different tiles.

The Katz prototiles are the first example of three dimensional tiles which force nonperiodicity. They are also the first example of such tiles which (evidently) do not satisfy a composition rule. (The fact that every tiling with these prototiles is nonperiodic is proved by showing that the tilings can be obtained by projection from a six dimensional lattice.)

5.4 *Two Dimensional Ammann Tiles and Wang Tiles*

The Penrose tiles and Wang tiles are not the only tiles which are known to force aperiodicity. In addition to making fundamental contributions to the theory of Penrose tiles, Robert Ammann has discovered several new sets of prototiles with this property (Ammann, Grünbaum and Shephard, to appear). One of these is shown in Fig. 37. These tiles can be regrouped, in

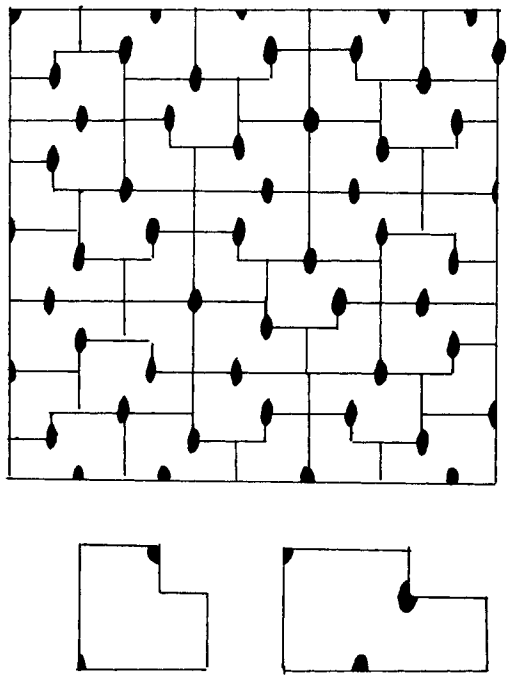

Figure 37. A tiling by Robert Ammann. The two prototiles are shown above; they must be matched to complete the partial ellipses.

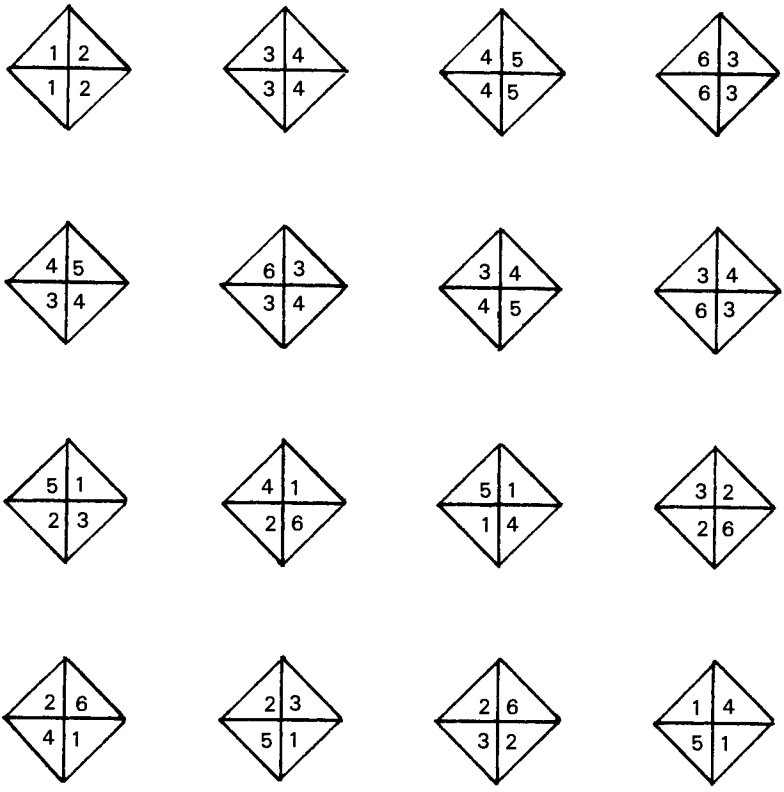

Figure 38. The sixteen aperiodic Wang tiles. The numbers indicate the colors of the edges.

only one way, to form a similar tiling with larger prototiles in which equivalent matching conditions hold[9]. Thus every tiling constructed with these tiles is nonperiodic. It is not known whether they are quasiperiodic (i.e., whether they can be obtained by projection, perhaps after some suitable reformulation).

Berger's 20,426 Wang tiles is a rather large set. Today, the smallest set of Wang tiles has only sixteen prototiles (Fig. 38). This set was also discovered by Ammann (and in fact is closely related to the Penrose tilings). Again, to prove that nonperiodicity is forced one must prove the existence of unique hierarchical levels in any tiling set. This significance of Wang tiles for crystallography has been discussed by Radin in his very interesting paper.

[9] The similarity of the large and small tiles is not crucial; the existence of matching conditions for the larger tiles is.

5.5 Conclusion

It is not an exaggeration to say that we still have no theory of nonperiodic tilings. There are several major questions and many smaller ones:

What properties characterize the different kinds of nonperiodic tilings? What local criteria distinguish tilings obtained by projection from other tilings? Which composition rules can be realized as hierarchical tilings? What are the properties of tiles that force nonperiodicity? What are the properties of the tilings that they form?

Which kinds of nonperiodicity have crystallographic significance? What do we mean by "long range order" in a tiling? Should we define this to be order sufficient for the pattern to produce a diffraction pattern with bright spots! If so, what kinds of order are necessary and sufficient for this to occur? (Is local isomorphism necessary? Is it sufficient?) The existence of hierarchical levels is sufficient for diffraction for a large class of one-dimensional nonperiodic tilings (Bombieri and Taylor, 1986) but it does not appear to be necessary. Other order properties that may turn out to be related to diffraction include the finiteness of the set of prototiles and slow growth (relative to radius) of the number of possible patches. Neither these properties nor the composition property seem to be related in any particular way to symmetry.

Tilings continue to provide a link between mathematics and science, as they have for hundreds of years. Certainly at no time in its interdisciplinary history has the field been as full of open, important and challenging problems as it is today.

References

Ammann, R., Grünbaum, B. and Shephard, G. S. Aperiodic tiles. To appear in *Discrete and Computational Geometry*.

Berger, R. (1966). The undecidability of the domino problem. *Memoirs of the American Mathematical Society* **66**.

Bieberbach, L. (1910). Uber die Bewegungsgruppen der n-dimensionalen Euklidischen Raume mit einem endlichen Fundamentalbereich. *Gottinger Nachrichten*, 75–84.

Bombieri, E. and Taylor, J. (1986). Which distributions of matter diffract? *Journal de Physique, Colloque C#*, supplement to No. 7, **47**, C3-19—C3-28.

de Bruijn, N. G. (1981). Algebraic theory of Penrose's non-periodic tilings. *Nederl. Akad. Wetensch. Proc.*, Ser. A, **84**, 39–66.

Coxeter, H. S. M. (1973). *Regular Polytopes*. Dover, N.Y.

Delaunay, B. N. (1924) Sur la sphere vide. *Proc. Intern. Math. Congress*, Toronto, August 11–16. (Publication: Toronto, 1928, 695–700).

Delaunay, B. N. (1961). A proof of the fundamental theorem of stereohedra. *Reports of the Academy of Sciences of the U.S.S.R.* **138**, 1270–1272 (in Russian).

Delaunay, B. N. and Sandakova, N. N. (1961). Theory of Stereohedra. *Trudy Mat. Inst. Steklov.* **64**, 28–51 (in Russian).

Delaunay, B. N., Dolbilin, M. I., Shtogrin, M. I. and Galiulin, R. V. (1976). A local criterion for regularity of a system of points. *Reports of the Academy of Sciences of the U.S.S.R.* (in Russian) **227**. (English translation: *Soviet Math. Dokl.* **17**, No. 2, 319–322.

Elser, V. (1986). The diffraction pattern of projected structures. *Acta Crystallographica* **A42**, 36–43.

Engel, P. (1981). Uber Wirkungsbereichasteilungen mit kubischer Symmetrie. *Zeitschrift fur Kristallographie* **157**, 259–275.

Engel, P. (1986). *Geometrical Crystallography*. Riedel, Dordrecht.

Fedorov, E. A. (1885). *Introduction to the Theory of Figures*. St. Petersburg, Academy of Sciences (in Russian).

Grünbaum, B. (1967). *Convex Polytopes Interscience*, London.

Grünbaum, B. and Shephard, G. S. (1980). Tiling with congruent tiles. *Bulletin (New Series) of the American Mathematical Society* **3**, No. 3, 951–973.

Grünbaum, B. and Shephard, G. S. (1987). *Tilings and Patterns*. W. Freeman and Co., N.Y.

Grünbaum, B. and Shephard, G. S. (1988). *Duality, in Shaping Space* (M. Senechal and G. Fleck, eds.). Birkhauser Boston.

Katz, A. (1988). Theory of matching rules for the 3-dimensional Penrose tiles. *Com. Math. Phys.* **118**, 263.

Kepler, J. (1619). *Harmonices Mundi*.

Moran, J. Thesis, in preparation.

Pleasants, P. A. B. (1985). Quasicrystallography: some interesting new patterns. *Elementary and Analytic Theory of Numbers* **17**, 439–461. Branch Center Publications, PWN-Polish Scientific Publishers, Warsaw.

Radin, C. Low temperature and the origin of crystalline symmetry, to be published.

Schulte, E. (1984). Nontiles and nonfacets for the Euclidean space, spherical complexes and convex polytopes. *Journal fur die reine und angewandte Mathematik* **352**, 161–183.

Senechal, M. (1986). Geometry and crystal symmetry. *Computers and Mathematics with Applications* **12B**, Nos. 3/4, 565–578; reprinted in *Symmetry: Unifying Human Understanding* (I. Hargittai, ed.). Pergamon Press, New York, 1986.

Senechal, M. A brief history of geometrical crystallograhy. *An Historical Atlas of Crystallography* (edited by J. Lima de Faria), to be published.

Stogrin, M. I. (1973). Regular Dirichlet-Voronoi partitions for the second triclinic group. *Proceedings of the Steklov Institute of Mathematics* **123**; English translation published by the American Mathematical Society, Providence, 1975.

Wells, A. F. (1977). *Three Dimensional Nets and Polyhedra*. John Wiley & Sons, New York.

Weyl, H. (1952). *Symmetry*. Princeton University Press.

Chapter 2

Tilings and Quasi-Crystals; a Non-Local Growth Problem?

R. PENROSE

Mathematical Institute
Oxford University
Oxford, England

Contents

1 Introduction 53
2 The Non-Locality of Mistakes 57
3 Fibonacci Sequences 71
4 Non-Locality of Fibonacci Sequences 76
References 78

1 Introduction

Shechtman and his coworkers announced their discovery of an icosahedral quasi-crystalline phase of aluminium-manganese alloy in 1984, but interest had been expressed a good deal earlier in the theoretical possibility of actual quasi-crystalline substances having icosahedral symmetry—with a structure perhaps similar to that of the tiling patterns that I had previously found (Penrose, 1974, 1979; *cf.* Mackay, 1982). Indeed, in the late 1970s and early 80's I had often been asked to give lectures on these tiling patterns, and a question frequently posed to me after the lecture might be: "Does this not mean that there is a whole new area of crystallography opening up, with pentagonal and icosahedral symmetry allowed?" My normal response

Copyright © 1989 by Academic Press, Inc.
All rights of reproduction in any form reserved.
ISBN 0-12-040602-0

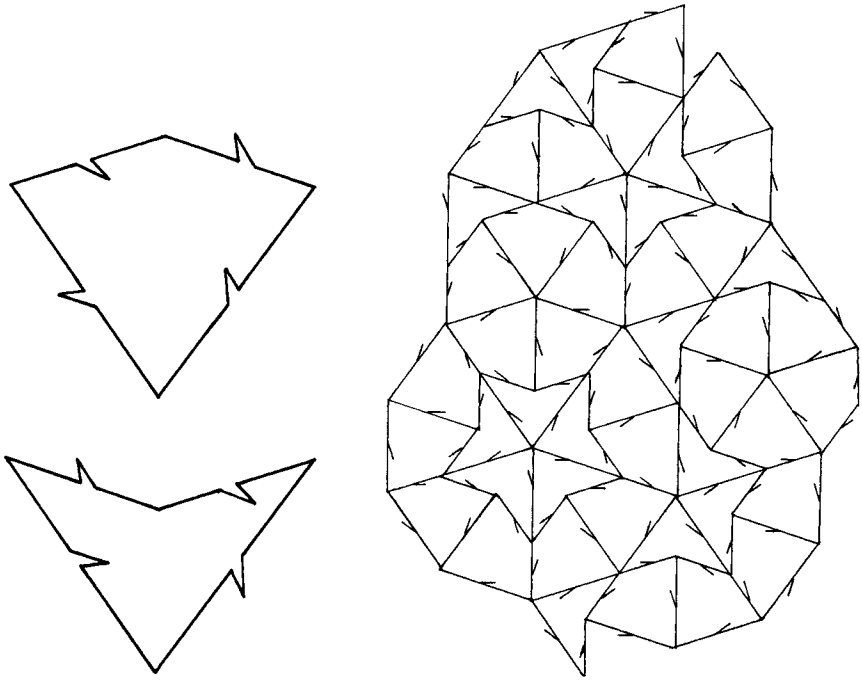

Figure 1. Left: A Kite (above) and a dart (below). Right: A portion of the plane tiled with kites and darts.

would be: "In principle, yes; but how on earth would Nature do it?" I had in mind that such substances might, with great difficulty, be perhaps synthesized artificially, but the problem confronting the *spontaneous* growth of large regions of such quasi-crystalline five-fold-symmetric substances had seemed to me to be virtually insurmountable.

To appreciate the problem that I had envisaged, imagine a plane tiling—say a kite and dart pattern (Penrose, 1979, 1987; *cf.* Gardner, 1977; Grünbaum and Shephard, 1987; see Fig. 1)—to be built up one tile at a time, as a jig-saw puzzle might be assembled. (An equivalent rhombus pattern would also do, but kites and darts are clearer, so most of my discussion will be formulated in terms of kites and darts. The modifications necessary for the rhombus case will be indicated where appropriate.) If the tiles are simply placed one after the other, wherever they will fit (the correct matching rules being assumed), then it will usually not be long before a configuration is reached in which there is some gap which cannot be filled in any way by either a kite or a dart. In order to continue such a pattern further, it would be necessary to remove a number of the tiles already placed, and then put

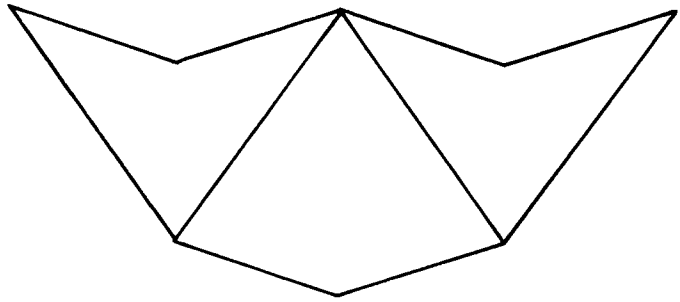

Figure 2. A simple "mistake".

them back in a different arrangement. Now, suppose that, in the assembly, the tiles are not simply placed so blindly—where originally the only criterion used had been whether or not they will fit locally—and, instead, some attention is now paid to the locations of tiles not immediately adjacent to the one being placed. For example, account may be taken of the locations of tiles *two* tiles away from the tile being placed. In this way we may avoid making "mistakes" of the kind illustrated in Fig. 2, where two darts and one kite are placed in a way that provides a "locally legal" pattern, but which cannot be continued to fill the whole plane (as can be readily seen). This enables larger patterns, on the average, to be constructed—until some arrangement is again almost certainly formed which cannot be continued further without gaps. If account is taken of the locations of tiles that are *three* tiles away from the one being placed, then even larger regions than before will be produced, on the average, before trouble tends to arise. But still non-continuable patterns will be almost certain to arise if the assembly merely proceeds in this largely random fashion. The conclusions would be similar if account is now taken of the locations of tiles that are *four* tiles away—or, as we shall see, with any other fixed bound on the distance away.

In my lectures on this topic, I usually illustrated this point with a slide showing the pattern of Fig. 3. I had made this slide from a picture that I had drawn out, without realizing, at the time, that the tiling was incorrectly assembled. The tiles are "bird" versions of the kites and darts, with markings on the back to indicate the relationship between these ("bird") kites and darts and a pentagonal type of quasi-periodic tiling that I had found earlier. The error is within the left-hand part of the figure. When subsequently examining the slide I realized that there were two stars (pentacles), formed from the markings, that should not be as close to one another as they are. This implies that there must be something wrong in the assembly and, indeed, it must be the case that if one attempts to continue the pattern somewhat further on the left, there must come a point where the

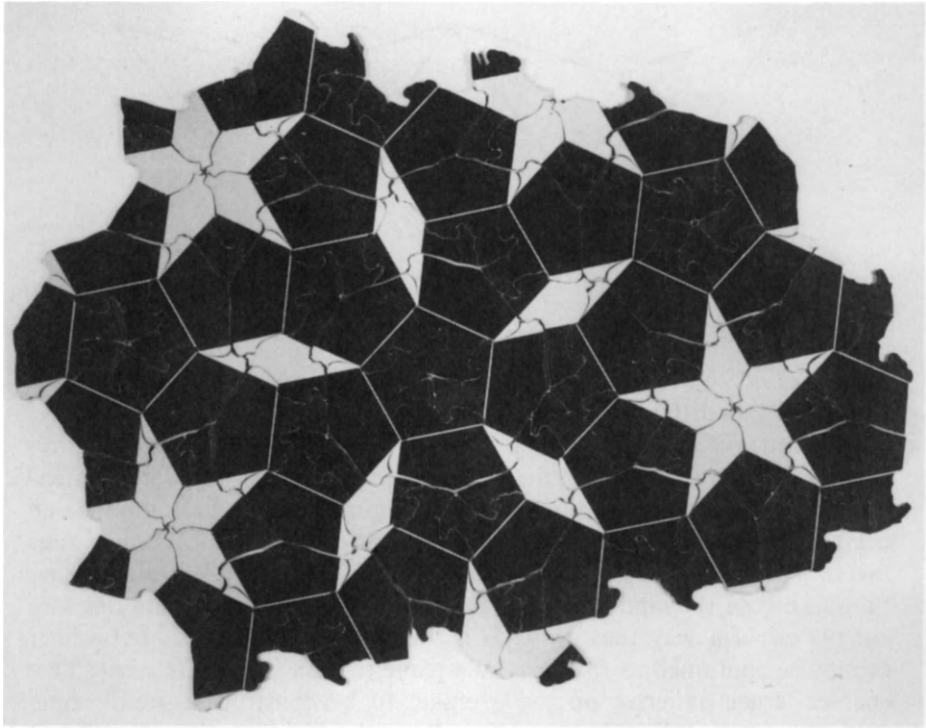

Figure 3. A tiling with (Escher-type) "bird" kites and darts (marked to bring out the relationship with an earlier pentagon tiling) which is "incorrect".

continuation becomes impossible, and one cannot proceed without leaving gaps. (The trouble is not immediately apparent; it becomes so only after various different attempts at continuation are made on the left.) In order to make a continuation which *will* eventually cover the whole plane, it is necessary first to reposition some of the tiles already placed—so that one or other of the stars on the left becomes only a three-pointed one (a "jester's cap"), as in Fig. 4.

How big a region must be examined at each stage in order that we may be sure that the pattern can be continued indefinitely without gaps? I have stated that there is *no limit* on the size of the regions which must be examined, at some stage or other. It is not hard to see why this must be so.

The kite and dart patterns are always based on a hierarchical arrangement. We may recall the *inflation* rules that Martin Gardner referred to in his 1972 Scientific American article (Gardner, 1977; *cf.* also Grünbaum and Shephard, 1987). In order to tile indefinitely large regions in a correct continuable fashion, one must, in effect, construct larger and larger "versions"

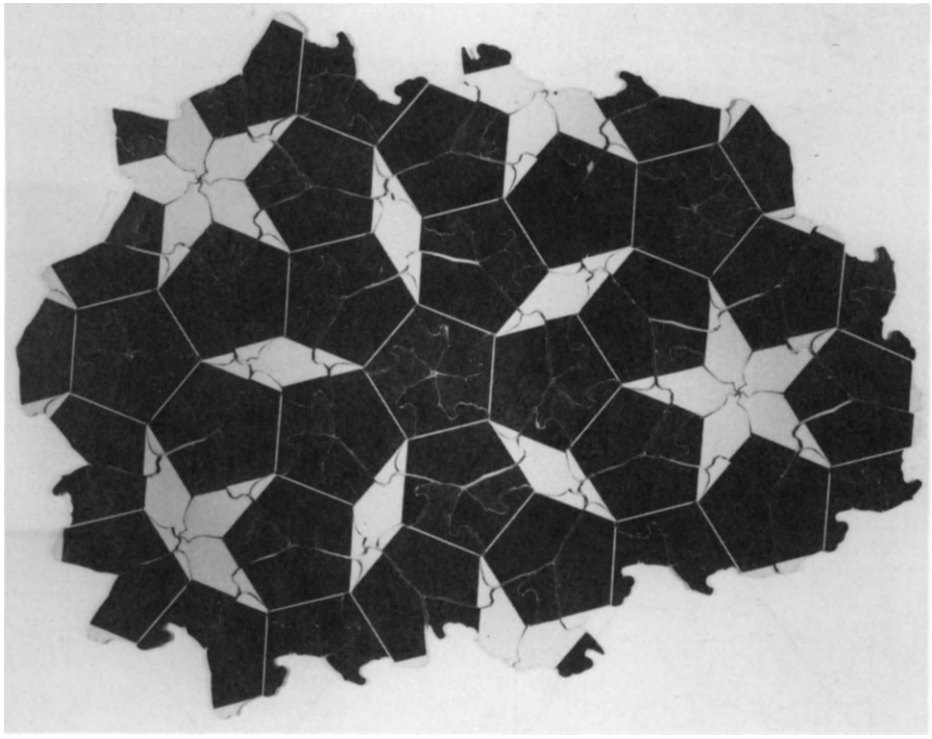

Figure 4. A corrected tiling with "bird" kites and darts.

of the original kite and dart tiles made up by the composition of greater and greater numbers of individual kites and darts (see Fig. 5). The corresponding "mistake" to the one just considered, for example, can be made again at every stage of the hierarchy (see Fig. 6). The larger the version of the "mistake", the harder it will be to see—in the sense of the farther away that one must look in the assembled pattern—that the pattern indeed cannot be continued without gaps.

In this article I shall try to provide some understanding of the non-local nature of such "mistakes." This might have significance in relation to the growth of quasicrystals—and to the question of how closely a physical quasicrystal might be able to approximate a three-dimensional version of these tilings.

2 The Non-Locality of Mistakes

For connected (and simply-connected) finite arrangements of tiles, I shall use the terms "legal" and "correct" in two clearly distinguished senses

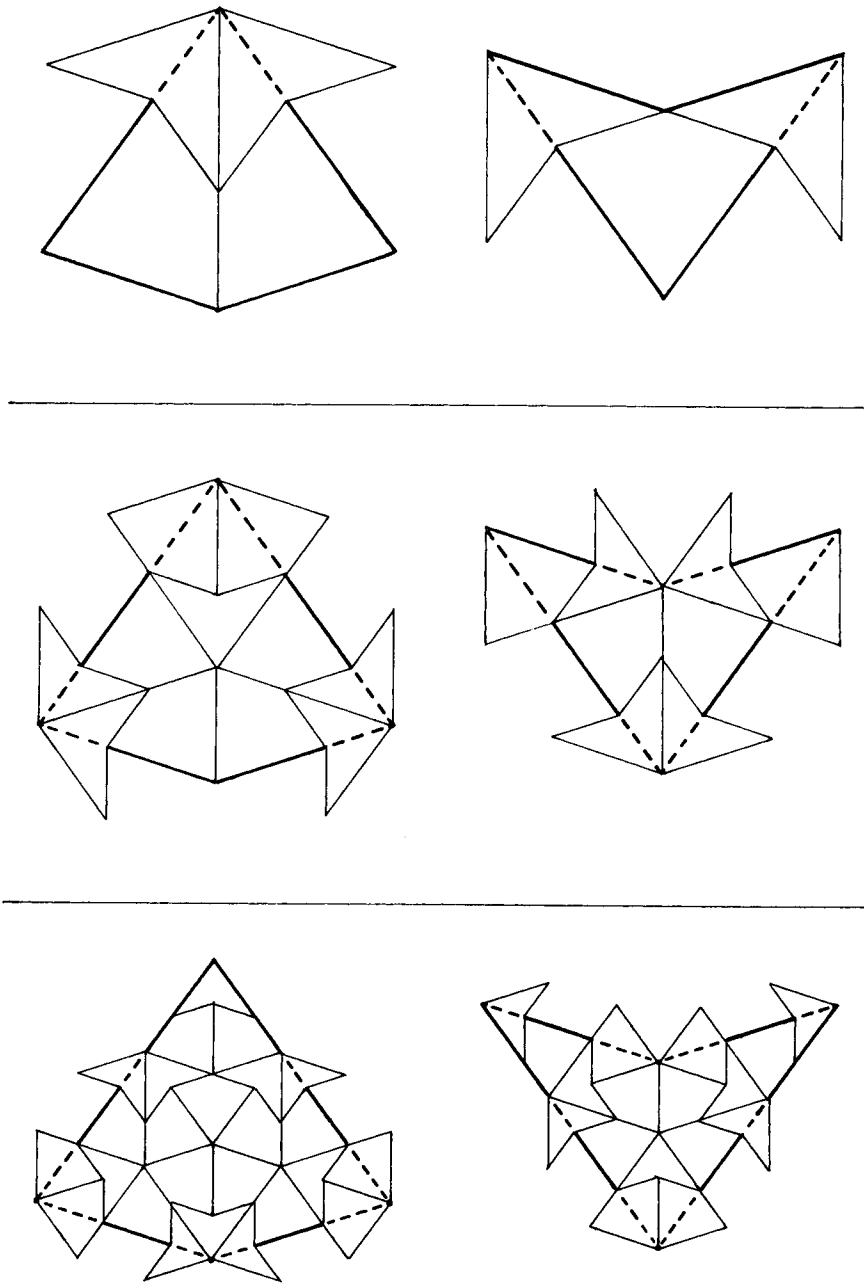

Figure 5. Three stages of hierarchy of kites and darts.

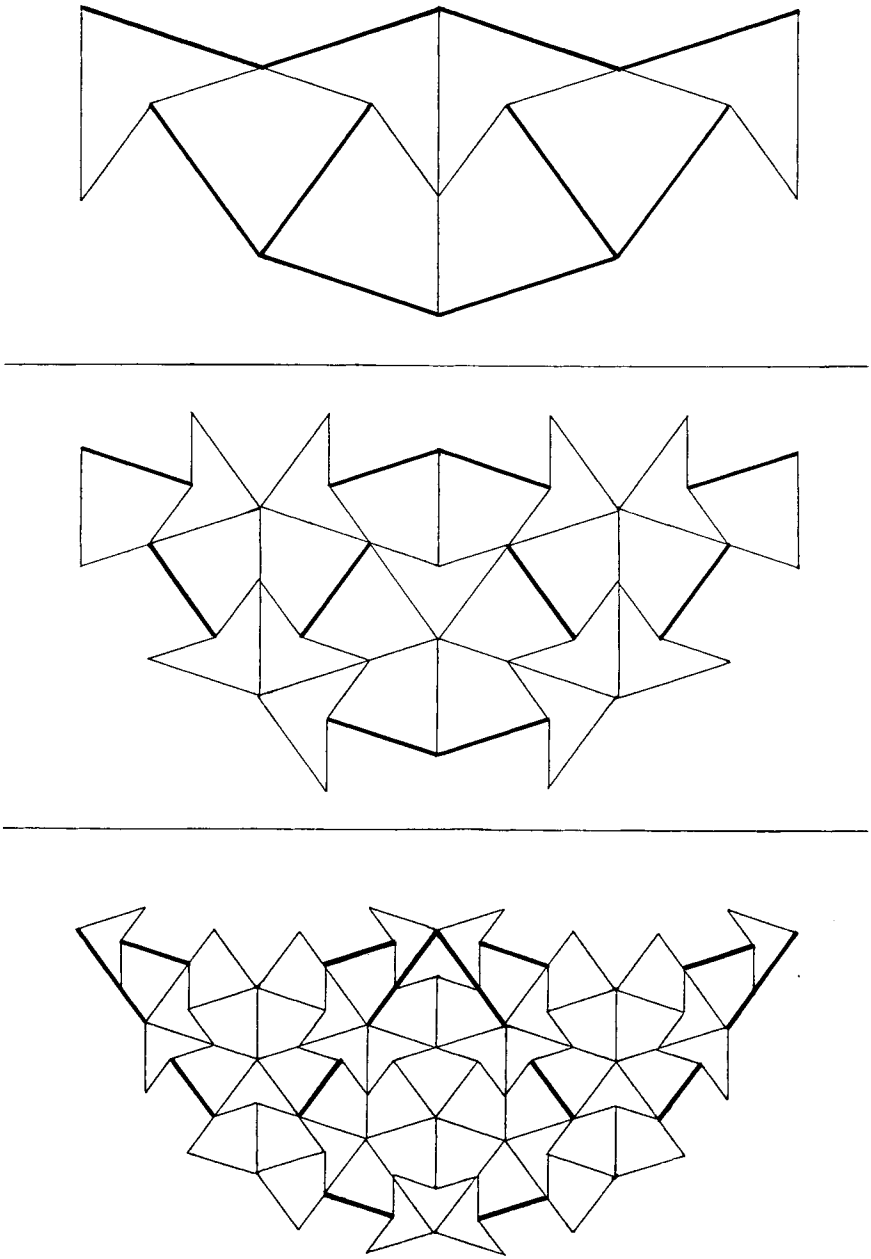

Figure 6. Incorrect tilings which are versions of the mistake of Fig. 2 at three different stages of hierarchy.

A *legal* arrangement is one where the tiles all have been fitted together locally without any gaps or overlaps, the local matching rules being all taken to be satisfied, but where a continuation to an infinite plane tiling is not necessarily possible. A *correct* tiling, on the other hand, is one which is a subset of a legal tiling of the entire plane. Thus, every correct tiling is legal, but some legal tilings are not correct, namely those which cannot ultimately be continued to cover the whole plane. I use the word "mistake," as above, for a placement of a tile which extends a correct tiling to a legal but incorrect tiling. Note that the tilings depicted in Figs. 2, 3, 6 are all legal but not correct.

Mistakes arise because there can be a choice as to whether it is a kite or a dart which must be placed along an unmatched edge at the outside of the growing pattern. Sometimes, because of the positioning of the neighbouring tiles, there is no such choice: just a kite or just a dart would fit as a legal placement. Sometimes, neither would be legal—but such a situation would arise only if a mistake had occurred at some stage earlier in the assembly, i.e., if the previous arrangement is not correct. Let us assume that *no* such mistakes have so far been made, so the previous arrangement is indeed correct. It then may be that *either* a dart *or* a kite can be correctly placed along the chosen unmatched edge, so that *both* placements can be continued to tilings of the entire plane. However, in other circumstances, it will be the case that only *one* of the two placements—either a kite or a dart—will be correct; but the other, though legal, is a mistake, and no continuation to the entire plane will turn out to be possible after that placement has been made.

In some cases, it may not be at all obvious whether or not such a placement is indeed a mistake. However, there is always an algorithm for ensuring correct placements: one can make use of the inflation rules referred to above. All patterns which continue to infinity must accord with these rules. We start with a correct configuration, which therefore has *already* been assembled in a way consistent with the inflation rules. Accordingly, the assembled kites and darts can be grouped together, by composition, to form larger kites and darts—where the darts must be bisected in order that the geometrical form of the kites and darts be preserved at each larger scale. The process is repeated with the larger kites and darts, so that these larger ones compose even larger kites and darts, and so on—until the original pattern, and its intended continuation, fall entirely within *one* large-scale kite or dart (see Fig. 7). There may be some choice as to how these groupings are made, but this does not matter. It merely reflects a choice which may be present in continuing the pattern.) Decomposing back down again we find a pattern of kites and darts on the smallest scale which includes the one we started with, and allows us to continue as we require, without mistakes. Repeating this procedure, we can continue indefinitely and cover as large a region of the plane as we please.

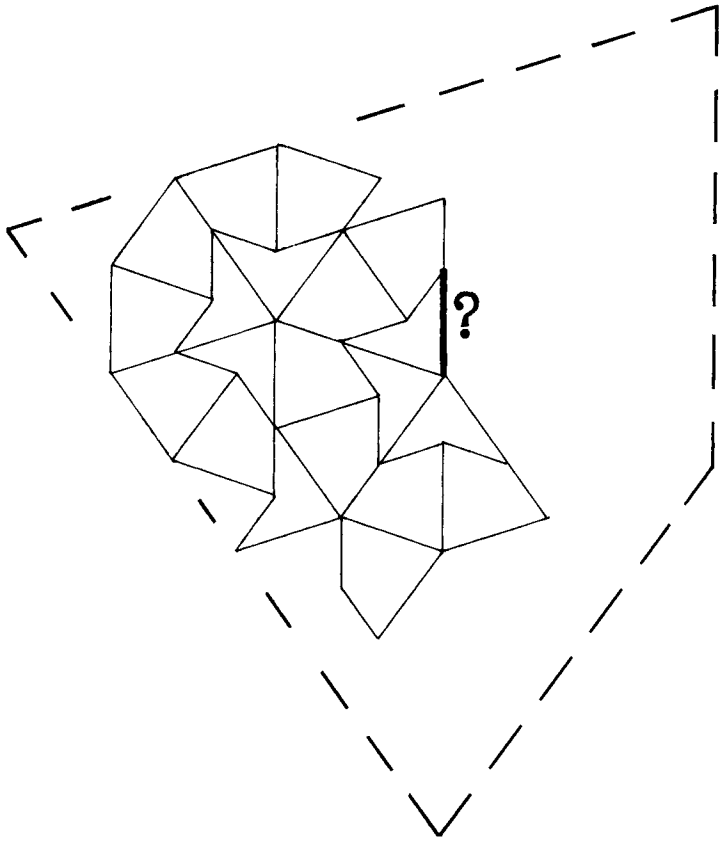

Figure 7. A method for deciding whether to place a kite or a dart at "?" is to proceed backwards along the hierarchy of Fig. 5 until all the tiles fall within one large-scale kite or dart, and then to proceed forward again by subdivision. In this case it turns out that only the dart is correct at "?".

Notice that this procedure is *not a local one*. We may need to examine the entire assembled pattern before we are assured how we may continue. As indicated above, there is *no* local algorithm, and this actually follows from the fact that, at every stage of the hierarchy, there is a version of the mistake of Fig. 2 that may be made (*cf.* Fig. 6). Let us explore this in a little more detail. First imagine that we have one kite and one dart joined together along one of their longer edges. If we wish to place another tile against the remaining longer edge of the kite, then we must make sure that this new tile is a kite and not a dart, otherwise we arrive at the forbidden configuration of Fig. 2. Now suppose that this original kite-dart pair is replaced by a much larger assembly of kites and darts, namely one obtained

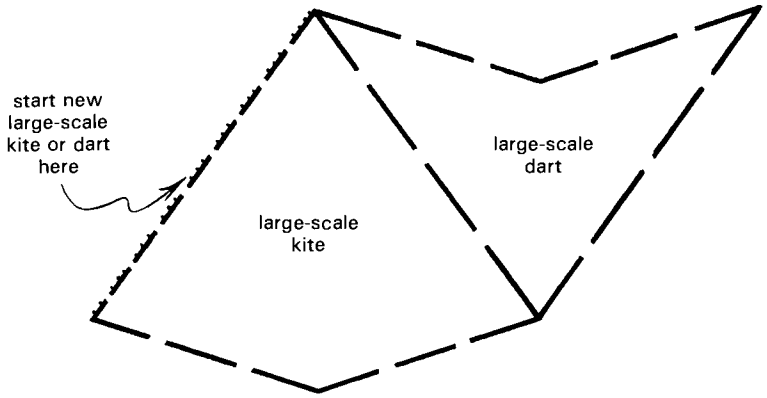

Figure 8. Suppose we wish to continue a correct tiling of a large-scale kite and adjoining large-scale dart by adding small kite and dart tiles along the sloping line at the left. If a new large-scale dart rather than a kite is assembled, this would be incorrect.

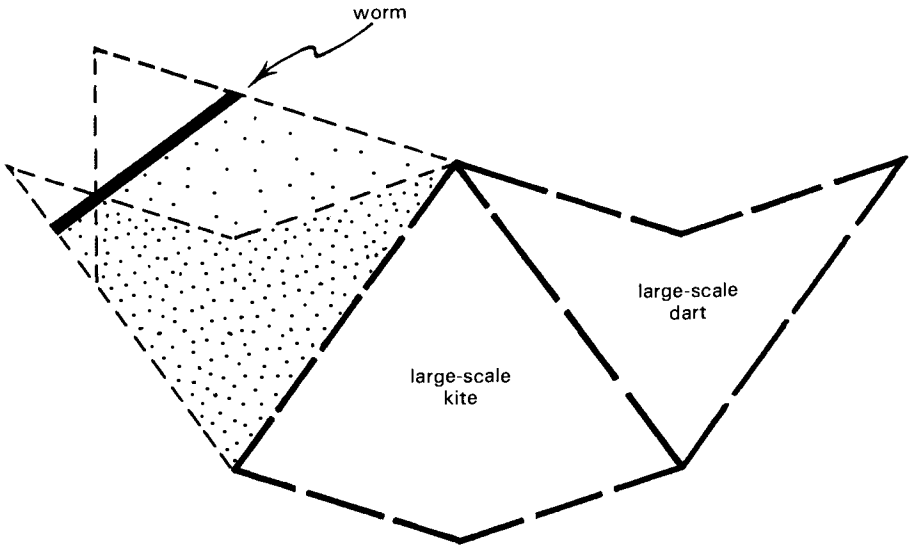

Figure 9. The difference between a new large-scale kite and a new large-scale dart, added on the left of the tiling of Fig. 8, does not arise until the *worm* (centered on the thick black line) is reached.

from the original pair by the above decomposition process repeated a great number of times. We now have a configuration which, on a large scale, resembles a kite and a dart joined along one of their longer edges, but in reality the whole pattern is made up of very many tiny kites and darts. Let us imagine that we are adding some additional tiny kites and darts in order to grow outwards from the unmatched longer edge of the large-scale kite (Fig. 8). We know that we must grow a new large-scale kite and not a large-scale dart. Otherwise we shall be producing a large-scale version of the mistake of Fig. 2 and 6. However, at first, the assembly of a large-scale kite turns out to be completely identical with that of a large-scale dart. If the individual tiny kites and darts are very small compared with the large-scale ones, then the large-scale kite that is being assembled will be practically complete before its detailed construction begins to distinguish it from a large-scale dart. There is a straight line, that I have indicated in Fig. 9, in the neighbourhood of which the differences between the large-scale kite and dart will first appear. The smaller that the tiny kites and darts are, the closer to this line the differences will lie. The line represents an example of what J. H. Conway has termed a "worm" (Fig. 10). The worm has to be turned over across its length in order to get from one large-scale pattern to the other. The way that the worms arise in the large-scale kite-dart pattern that I have just described is indicated in Fig. 11 and in Figs. 9 and 12.

We know that it is only the large-scale kite, in the position of Fig. 9, that allows an indefinite continuation to infinity without gaps; but this is the case only because of the positioning of the original large-scale dart. Had that large-scale dart been a large-scale kite instead, then *both* continuations would have been correct. But in order to *know* that this original large-scale dart was indeed a dart and not a kite, we should have had to examine the pattern as far as the corresponding worm at the *other* end of the pattern. Thus, the arrangement of tiny tiles in the worm at one end of the pattern will determine the correct arrangement in the worm at the other end. The entire arrangement in either worm is completely fixed by any *one* tile in the worm. Thus, the position of a single tile in the worm at one end, say at A in Fig. 13—assuming that it lies within a large-scale *dart*—will determine the positioning, say at B of the correct first tile to be placed in the worm at the opposite side of the pattern, namely that consistent with a large-scale *kite*. The alternative tile, placed at B, would be a mistake.

What will go wrong if we *do* allow ourselves to make this mistake? We can place tiles so as to fill up the entire interior of the triangle ABC, where C is the point at which the extended worms meet. However, at C itself it will not be possible to place either tile. The mistake at B is a mistake because of a tile placed at A, and the fact that it is a mistake becomes apparent only when the continuation has proceeded as far as the point C!

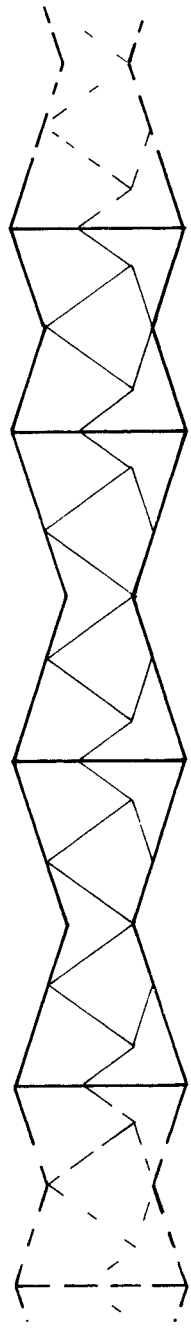

Figure 10. A worm (of kites and darts).

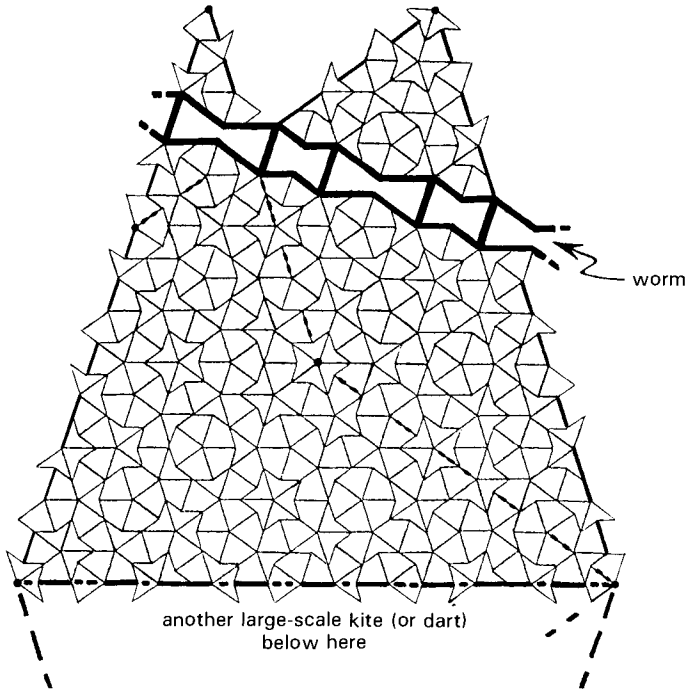

Figure 11. The detailed structure of a large-scale kite or dart, assembled on the long edge of another large-scale kite (or dart). Whether a kite or a dart is assembled, the detailed pattern is the same—except that the worm indicated has the opposite orientation in the two cases.

One can set up situations where the manifestation of a mistake occurs at an even more remote location than this. In Figs. 14a and 14b, I have shown how far one must proceed, when building out from a large-scale kite or a large-scale dart, before there is any choice in the correct placements of individual kites and darts. There is only one correct continuation of individual tiles out as far as the four boundary worms indicated. Each single boundary worm could be placed either way around; but for any pair of adjacent worms, one out of the three possibilities is illegal. For all *four* worms, for a large-scale kite it turns out that only *five* out of the sixteen possibilities will be legal, while for a large-scale dart, *seven* of the sixteen possibilities will be legal. The allowed possibilities are indicated in Figs. 15a and 15b, where the arrows show the direction in which each worm is to be oriented. (It should be noted that the relation between the worm orientation and the arrow reverses at each stage in the hierarchy.) To see how remote the manifestation of a mistake can sometimes turn out to be, consider Fig. 16.

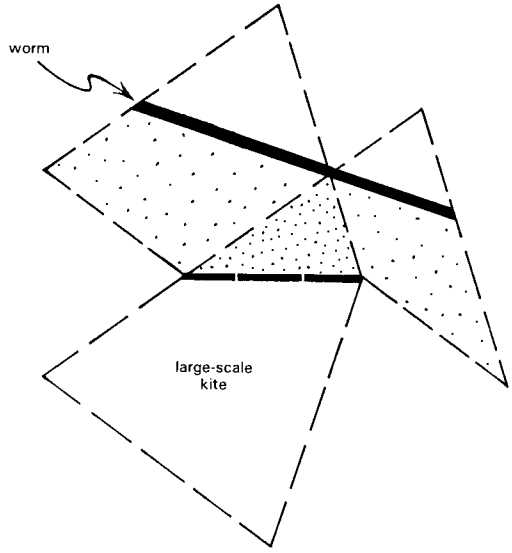

Figure 12. The detailed difference between a large-scale kite and a large-scale dart, when assembled on the *short* edge of another large-scale kite, is again along a worm.

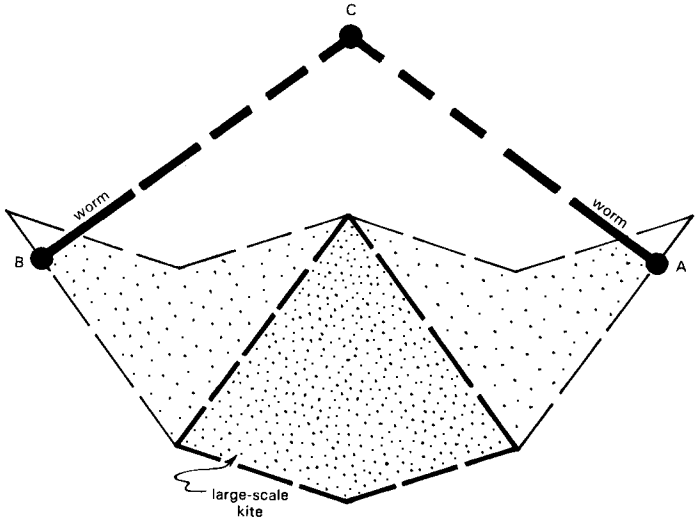

Figure 13. The placing of a tile at A which forces a large-scale dart on the right is incompatible with the placing of a corresponding tile at B forcing a large-scale kite on the left. The incompatibility of A with B does not emerge until C is reached—where the two worms meet.

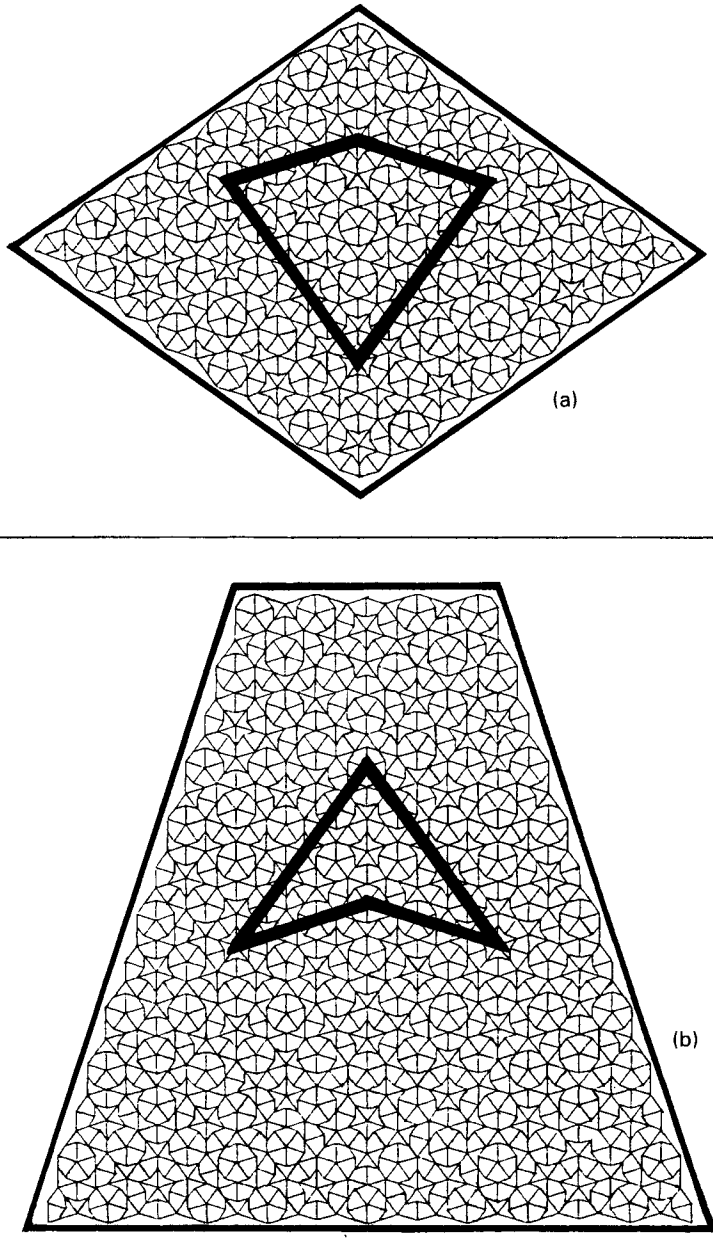

Figure 14. a. The central area is a large-scale kite, and a correct tiling proceeds unambiguously until the external quadrilateral is reached, whose sides are worms; b. the same for a large-scale dart.

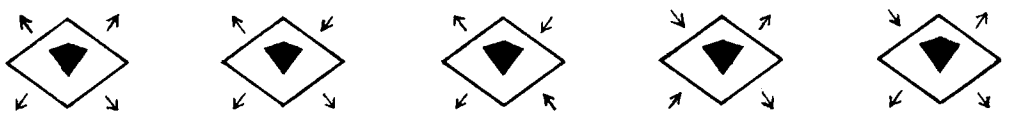

(a)

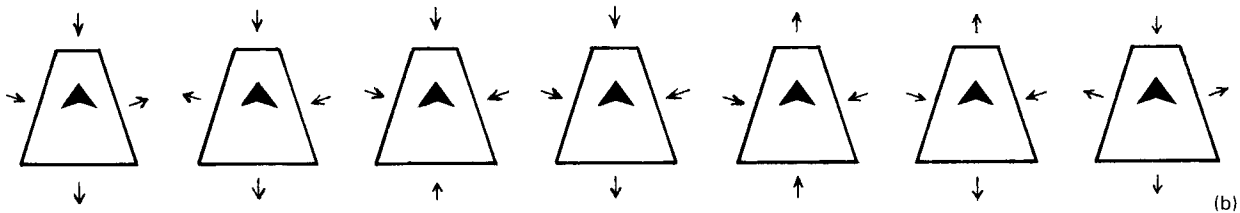

(b)

Figure 15. a. Only five out of the sixteen possible worm orientations are legal for the quadrilateral surrounding a large-scale kite. (The relation between the arrow and worm-orientation reverses at each level of hierarchy.) b. The same for a large-scale dart: just seven out of the sixteen worm orientations are legal.

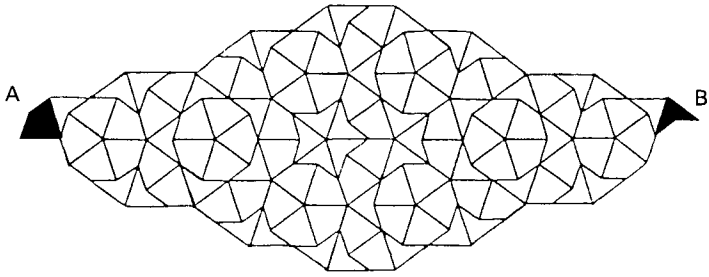

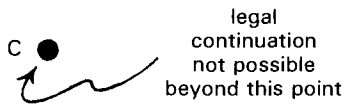

Figure 16. The placing of a kite at A is incompatible with a dart at B, whereas each would be correct without the other. The incompatibility only becomes evident when C is reached

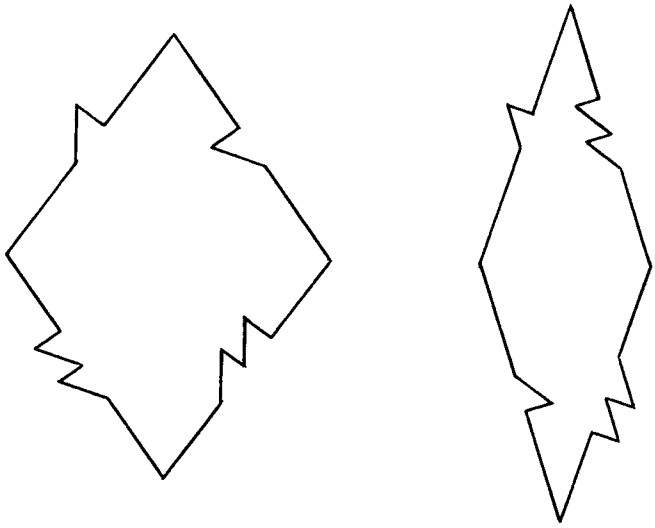

Figure 17. The rhombus tiles.

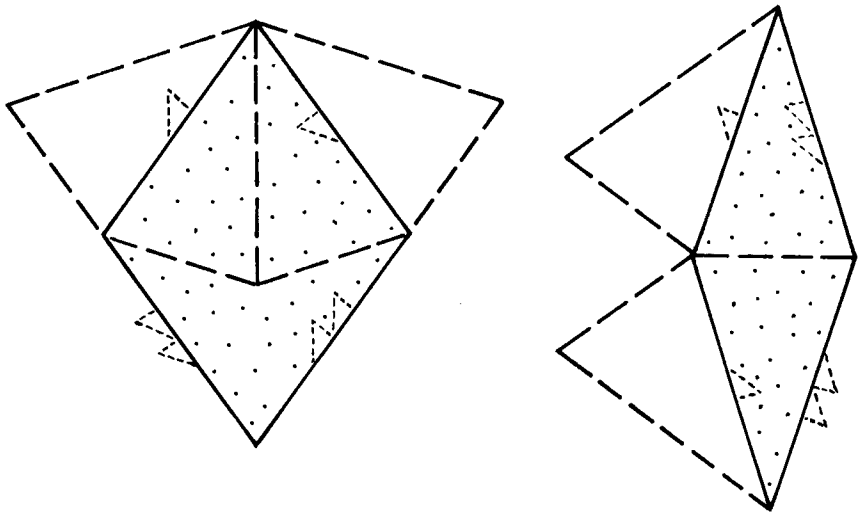

Figure 18. The relation between the rhombus pair and the kites and darts, at a particular stage of hierarchy.

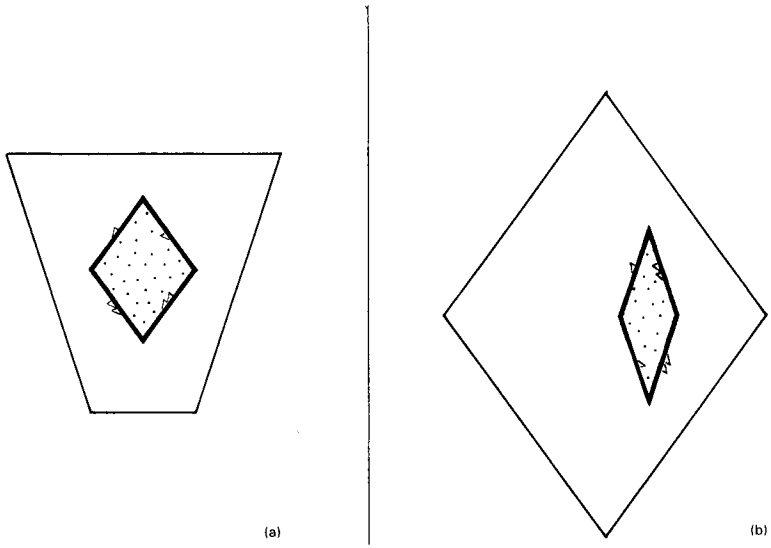

Figure 19. a. The central area is a large-scale fat rhombus, and a correct tiling proceeds unambiguously to the external region bounded by worms; b. the same for a large-scale thin rhombus.

The correct placement of a tile at B depends upon the tile which happens to be at A, and the effect of a mistaken replacement at B does not become manifest until the point C is reached!

Here I have been considering only kites and darts, but the situation with the rhombus tiles (with appropriate matching rules), as depicted in Fig. 17, is similar. The relation to the kite/dart tiles is shown in Fig. 18, at one stage of the kite/dart hierarchy. In Figs. 19a and 19b, I have shown the extent of the regions of forced correct tiling (as with Figs. 14a and 14b), now starting from each large-scale *rhombus* until the boundary worms are reached. The rules telling us which combinations of orientations of the worms are correct are the same as those for the kites and darts, as indicated in Figs. 15a and 15b (except that the relation between the direction of the arrow and the worm orientation is opposite, as between Fig. 15a and 15b.)

It may be remarked that it is always along worms that the differences between closely identical correct tiling patterns will occur. Striking patterns of straight lines can sometimes be seen when a transparency marked finely with either kites and darts or with rhombuses, is moved over another copy of itself until the patterns almost agree with each other. These straight lines are always worms.

3. Fibonacci Sequences

Notice that the worms are made up of two kinds of units, the long and the short. In the case of the kites and darts, these resemble long and short "bow ties" (*cf.* Grünbaum and Shephard, 1987), the long bow tie consisting of four kites and three darts, and the short one consisting of three kites and two darts. In the rhombus case, the worms are made up of two (non-regular) hexagons: a fat (i.e. "long") hexagon, built from two fat rhombuses and one thin one, and a thin (i.e. "short") hexagon, built from two thin rhombuses and one fat one (see Fig. 20). The long unit is, in each case, exactly the *golden ratio* ($= \tau = (1 + \sqrt{5})/2$) times as long as the width of the short unit. The sequence of long and short, for a correct tiling, always follows a strict rule, namely that given by a Fibonacci sequence (referred to as a "musical sequence" by Grünbaum and Shephard).

The rule for generating a Fibonacci sequence is a hierarchical one: start with 1 (representing a short unit) at the first generation; then replace 1 with τ (representing a long unit) at the second generation; then replace τ with 1τ at the third generation; then continue, making exactly these replacements again and again for each 1 or τ occurring in the entire sequence at each

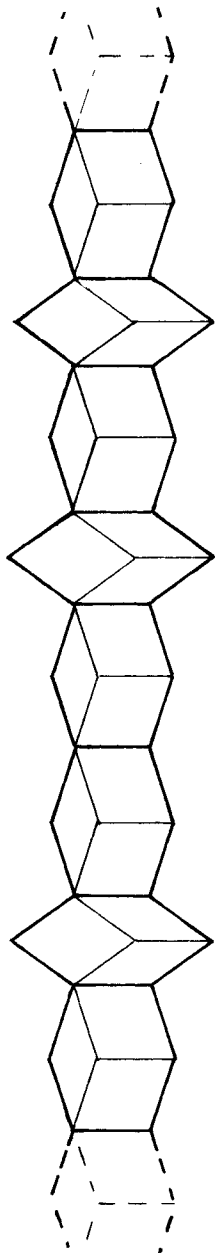

Figure 20. A worm of rhombuses.

generation. Thus we have:

$$1 \to \tau \to 1\tau \to \tau 1\tau \to 1\tau\tau 1\tau \to \tau 1\tau 1\tau\tau 1\tau$$
$$\to 1\tau\tau 1\tau\tau 1\tau 1\tau\tau 1\tau \to \tau 1\tau 1\tau\tau 1\tau 1\tau\tau 1\tau\tau 1\tau 1\tau\tau 1\tau \to \ldots . \tag{1}$$

The sequences that can arise in this way (perhaps infinite, in one or both directions), or any consecutive subsequence of such a sequence, will be referred to as a *Fibonacci sequence*.

To check whether or not a sequence of 1's and τ's constitutes a Fibonacci sequence, one can effectively apply the above procedure in reverse. One first ascertains that the original sequence never has two (or more) 1's in succession, and that the τ's occur either singly or in pairs; then one forms a new sequence in which each 1 is replaced by a τ and each pair of τ's by a 1, single τ's being ignored. Again, one must ascertain that the τ's occur either singly or in pairs in the new sequence (the 1's can now only occur singly), and the procedure to form a new sequence is repeated as before. If (and only if), in the continued application of this procedure, no sequence of more than two τ's ever arises (and no pair of 1's occurred initially) then the sequence is indeed a Fibonacci sequence.

As an example, let us apply this procedure to the sequence $\tau\tau 1\tau\tau 1\tau\tau 1\tau 1\tau\tau 1\tau$. We get

$$\tau\tau 1\tau\tau 1\tau\tau 1\tau 1\tau\tau 1\tau \to 1\tau 1\tau 1\tau\tau 1\tau \to \tau\tau\tau 1\tau, \tag{2}$$

which fails because of the triple τ, showing that the original sequence is not a Fibonacci sequence. But if we replace the first τ in our sequence by a 1, we get

$$1\tau 1\tau\tau 1\tau\tau 1\tau 1\tau\tau 1\tau \to \tau\tau 1\tau 1\tau\tau 1\tau \to 1\tau\tau 1\tau \to \tau 1\tau \to \tau, \tag{3}$$

showing that $1\tau 1\tau\tau 1\tau\tau 1\tau 1\tau\tau 1\tau$ is indeed a Fibonacci sequence.

Any worm which proceeds according to a Fibonacci sequence constitutes a correct tiling. (This is easily seen, because the inflation rule corresponds to the hierarchical rule for generating Fibonacci sequences.) However, a general sequence of 1's and τ's constitutes a tiling which is merely legal. Thus, for example, the worm corresponding to $\tau\tau 1\tau\tau 1\tau\tau 1\tau 1\tau\tau 1\tau$ would be legal but incorrect—so the tiles which build the first τ on to the rest of the sequence must involve a mistake. This mistake would become manifest only if the tiling is continued some way off to one side of the worm. We may note that the incorrect tilings of Fig. 6 arise, in effect, from the non-Fibonacci sequences 11 and $\tau\tau\tau$, respectively. In these cases the mistake would become manifest in the continued tiling some way above (although not below) the worm.

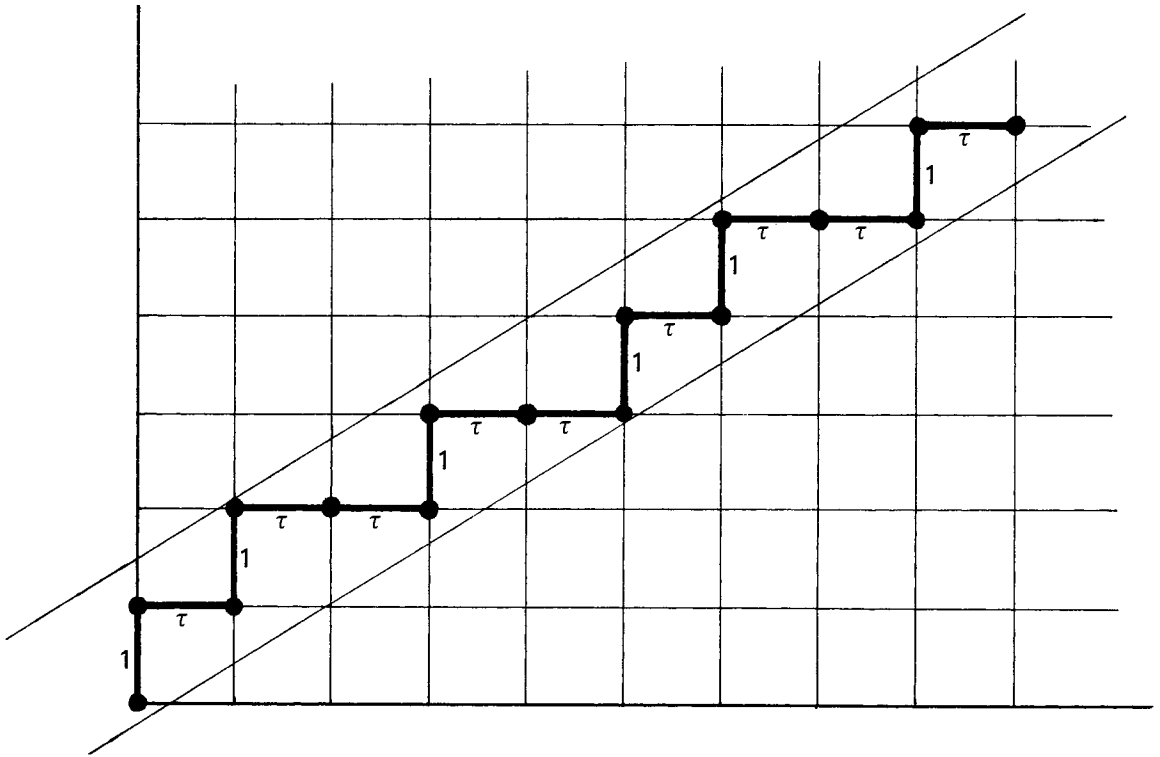

Figure 21. A test for a Fibonacci sequence (after de Bruijn). For each "1" we proceed vertically and for each "τ", horizontally. For a Fibonacci sequence, the points lie within a strip sloping at $1:\tau$ and of such a width that it would just contain a lattice square.

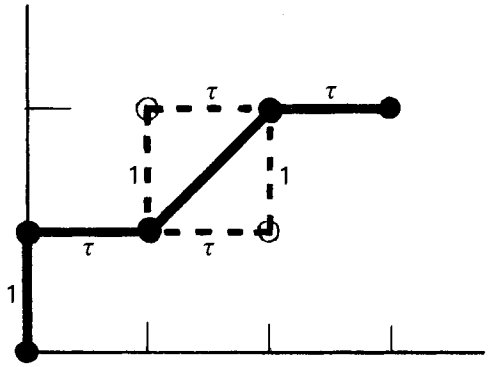

Figure 22. In case of doubt between 1τ and $\tau 1$ we proceed diagonally. This gives the quasicrystal "the benefit of the doubt".

Fibonacci sequences underlie correct kite/dart or rhombus tilings in a very basic way. (In particular, they govern the arrangement of wide and narrow Ammann bars; *cf.* Grünbaum and Shephard, 1987). If one examines such a tiling by viewing it obliquely from appropriate positions, with one's eye close to the plane of the tilings and off to one side, then one will observe such sequences of wide and narrow strips.

Electron micrograph pictures of icosahedral phase aluminium–manganese alloys will also exhibit such patterns of wide and narrow strips. It would seem reasonable to use the closeness with which these patterns accord with Fibonacci sequences as some measure of the closeness with which the atomic positions accord with an ideal icosahedral quasi-crystalline arrangement. A difficulty often arises in practice with this procedure, because it is not always clear whether a pair of adjacent terms in the sequence should be read as 1τ or $\tau 1$. To enable one to proceed nevertheless, one may, in such occasions of doubt, adopt a procedure which gives the quasi-crystal "the benefit of the doubt".

This procedure makes use of an alternative characterization of a Fibonacci sequence which I first learned about some years ago from P. Pleasants, who had adapted an idea of de Bruijn, 1981 to this situation.) Consider a sequence of 1's and τ's, say the one $1\tau 1\tau\tau 1\tau\tau 1\tau 1\tau\tau 1\tau$, considered above. We plot these as a zig-zag line on a square lattice, proceding horizontally by one step to the right for each τ, and vertically by one step upwards for each 1 (see Fig. 21). The condition for the sequence to be a Fibonacci sequence is that the resulting zig-zag line lie within a strip whose slope is $1/\tau$, and whose width is so that the opposite edges of the strip could just pass through the diagonal points of a lattice square. The way that one gives the quasi-crystal "the benefit of the doubt" is simply to plot the doubtful

cases, where one cannot decide whether a pair of adjacent terms is 1τ or $\tau 1$, as a diagonal to a lattice square, sloping upwards to the right (see Fig. 22).

My own conclusions based on a somewhat tentative analysis of various micrograph pictures of icosahedral phase aluminium-manganese alloys is that they tend to correspond remarkably closely to Fibonacci sequences, but the correspondence is by no means always perfect. Surprisingly, the type of "fault" that one tends to encounter is not a "glitch" here or there, but sometimes a slight, but significant, error in the slope of the strip. This is a genuinely *non-local* kind of error which I find to be perhaps as puzzling as an absolutely perfect "correct" assembly might be.

4 Non-Locality of Fibonacci Sequences

Suppose that we imagine a sequence of 1's and τ's growing in length, with one symbol being added at a time. Let us suppose that the growth proceeds randomly, but subject to some constraints. The constraints are to rule out incorrect sequences of symbols up to some prescribed length k—where "incorrect" means that it is incompatible with a Fibonacci sequence. The incorrect sequences are those containing the following:

$$\begin{aligned}
&11,\\
&\tau\tau\tau,\\
&1\tau1\tau1,\\
&\tau\tau1\tau\tau1\tau\tau,\\
&1\tau1\tau\tau1\tau1\tau\tau1\tau1,\\
&\tau\tau1\tau\tau1\tau1\tau\tau1\tau1\tau\tau1\tau\tau,\\
&1\tau1\tau\tau1\tau1\tau\tau1\tau1\tau1\tau\tau1\tau1\tau\tau1\tau1\tau\tau1\tau1,\\
&\ldots\ldots;
\end{aligned} \tag{4}$$

where each is, in effect, obtained from the previous one by the above hierarchical procedure. Table I (opposite) shows how the number $n_{r,k}$ of sequences of length r compatible with the constraints for length up to k depends upon r and k.

The way that this table is constructed is by use of a recurrence relation (which I give without proof) for the entries in each column:

Table I.

r \ k	1	2	3	4	5	6	7	8	9	10	11	12	13	14	...
0	1	1	1	1	1	1	1	1	1	1	1	1	1	1	...
1	2	2	2	2	2	2	2	2	2	2	2	2	2	2	...
2	4	3	3	3	3	3	3	3	3	3	3	3	3	3	...
3	8	5	4	4	4	4	4	4	4	4	4	4	4	4	...
4	16	8	5	5	5	5	5	5	5	5	5	5	5	5	...
5	32	13	7	7	6	6	6	6	6	6	6	6	6	6	...
6	64	21	9	9	7	7	7	7	7	7	7	7	7	7	...
7	128	34	12	12	8	8	8	8	8	8	8	8	8	8	...
8	256	55	16	16	10	10	10	9	9	9	9	9	9	9	...
9	512	89	21	21	12	12	12	10	10	10	10	10	10	10	...
10	1024	144	28	28	14	14	14	11	11	11	11	11	11	11	...
11	2048	233	37	37	17	17	17	12	12	12	12	12	12	12	...
12	4096	377	49	49	20	20	20	13	13	13	13	13	13	13	...
13	8192	610	65	65	24	24	24	15	15	15	15	15	14	14	...
14	16384	987	86	86	29	29	29	17	17	17	17	17	15	15	...
15	32768	1597	114	114	34	34	34	19	19	19	19	19	16	16	...
16	65536	2584	151	151	41	41	41	21	21	21	21	21	17	17	...
17	131072	4181	200	200	49	49	49	23	23	23	23	23	18	18	...
18	262144	6765	265	265	58	58	58	26	26	26	26	26	19	19	...
...	...	...	...	...	...	...	...	...	...	...	...	...	...	...	...

$$
\begin{aligned}
n_{r,k} + n_{r,k} &= n_{r+1,k} \ (k = 1,\ r + 1 \geq 1),\\
n_{r,k} + n_{r+1,k} &= n_{r+2,k} \ (k = 2,\ r + 1 \geq 1),\\
n_{r,k} + n_{r+1,k} &= n_{r+3,k} \ (k = 3,\ 4,\ r + 1 \geq 2),\\
n_{r,k} + n_{r+2,k} &= n_{r+5,k} \ (k = 5, 6, 7,\ r + 1 \geq 3),\\
n_{r,k} + n_{r+3,k} &= n_{r+8,k} \ (k = 8, 9, 10, 11, 12,\ r + 1 \geq 5),\\
n_{r,k} + n_{r+5,k} &= n_{r+13,k} \ (k = 13,\ 14, \ldots, 20,\ r + 1 \geq 8),\\
&\cdots\cdots\cdots\cdots\cdots\cdots\cdots\cdots\cdots\cdots
\end{aligned}
\tag{5}
$$

The numbers 0, 1, 1, 2, 3, 5, 8, 13, 21, ... appearing here are the Fibonacci numbers. Note also that

$$n_{r,k} = r + 1 \quad \text{if} \quad k \geq r, \tag{6}$$

that

$$n_{r,3} = n_{r,4},\ n_{r,5} = n_{r,6} = n_{r,7},\ n_{r,8} = n_{r,9} = \cdots = n_{r,12}, \text{ etc.} \tag{7}$$

and that $n_{r,1}$ and $n_{r,2}$ are the powers of 2 and the Fibonacci numbers, respectively.

It follows from the above recurrence relations that if any bound is placed on k, then $n_{r,k}$ will increase exponentially with r, whereas for the correct Fibonacci sequences (i.e. $k \geq r$), $n_{r,k}$ is just linear in r (and, in fact, is just $r + 1$). Thus, for large r, the chance of avoiding making a mistake, if k is bounded, becomes vanishingly small. It follows, therefore, that for a two-dimensional (or three-dimensional) tiling of this general five-fold (or icosahedral) quasi-periodic type, the assembly must be highly non-local—unless serious mistakes in the resulting structure are to be permitted.

In my opinion, this raises a number of interesting issues. It may, of course, be the case that the quasi-crystalline substances that have been so far produced do not bear any very close relation to the tiling patterns that I have been discussing. Or perhaps they do, but very large numbers of mistakes are continually being made. My impression, however, is that such mistakes would tend to lead to serious trouble in the continuation, rather than just local "glitches." I do, myself, find the regularity of many of the micrograph pictures to be strikingly impressive, and I am inclined to believe that there is indeed some rather close relationship between quasi-crystalline substances and such tiling patterns. If this turns out to be the case, then we may have to face up to the possibility that there could be something remarkable and non-local about the way that they grow (*cf.* Penrose, 1987). There are essentially non-local aspects to quantum theory. Perhaps these aspects are sometimes being exploited in the way that a quasi-crystal—or even an ordinary crystal—might grow.

Added in proof: A recent preprint, "Growing Perfect Quasicrystals," by G. Y. Onoda, P. J. Steinhardt, D. P. Di Vincenzo, and J. E. S. Socolar, proposes a "local" growth procedure for quasicrystals in which tiles would only stick at places where there is a legal choice when all places where there is *no* choice have been exhausted. This is an interesting suggestion—though it is not actually local in the sense intended here.

References

de Bruijn, N. G. (1981). *Proc. Konink. Ned Akad Wetensch* **A84**, 39–53.

Gardner, M. (1977). Extraordinary nonperiodic tiling that enriches the theory of tiles. *Sci. Amer.* **236**, 110–121.

Grünbaum, B. and Shephard (1987). *Tilings and Patterns* (W. H. Freeman).

MacKay, A. L. (1982). Crystallography and the Penrose pattern. *Physica* **114A**, 609.

Penrose, R. (1974). The rôle of aesthetics in pure and applied mathematical research. *Bull. Inst. Math. Applications* **10**, no. 7/8, 266–271,

Penrose, R. (1979). Pentaplexity. *Mathematical Intelligencer* **2**, 32–38 (from *Eureka*, No. 39).

Penrose, R. (1987). Hermann Weyl, space-time and conformal geometry. *Hermann Weyl 1886–1986* (ed. S. Chandrasekharan). E.T.H. Zurich.

Shechtman, D., Blech, I., Gratias, D. and Cahn, J. W. (1984). Metallic phase with long-range orientational order and no translational symmetry. *Phys Rev. Lett.* **53**, 1951–1953.

Chapter 3

Group Theory of Icosahedral Quasicrystals

P. KRAMER and R. W. HAASE

Institut für Theoretische Physik der Universität
Tübingen
Federal Republic of Germany

Contents

1 Introduction 81
2 Some Group Theory Basics 85
3 Representation Theory 92
4 Space Group Concepts 106
5 Stars and Polytopes 110
6 Cells and Quasilattices 117
7 Continuous and Subgroup Relations for the Cubic and Icosahedral Groups 123
8 The Hyperoctahedral Group and Its Representations 130
9 The Hypercubic Lattice in $\mathbb{E}^6$, Its Metrical Dual and Its Epicells* 135
10 Quasicrystal Models and Their Fourier Transform 141
Acknowledgments 143
References 143

1 Introduction

Complex alloy structures, in particular those of transition metals, are usually determined by geometrical requirements for sphere packing and space filling

* Note Added in Proof: In this chapter the term "epicell" has been introduced by the editor of this volume to replace the term "klotz," which was the original term chosen by the author of this chapter and has appeared in several of his other publications.

Copyright © 1989 by Academic Press, Inc.
All rights of reproduction in any form reserved.
ISBN 0-12-040602-0

(Frank and Kasper, 1958, 1959). The former, with some type of description for nearest neighbor atomic interactions, determines the possible local arrangements of the atoms, and hence polyhedra of the domain of an atom and subsequent coordination polyhedra of nearest neighbors. The latter requirement determines the long-range ordering of atoms and atomic clusters. In this context, although icosahedral clustering of atoms is possible and energetically favoured, polyhedra with icosahedral symmetry do not fill space in the sense of face-to-face tesselations without holes and overlaps.

The space-filling requirement implies also that the global structure is based on the periodic repetition of a single polyhedron—the crystallographic unit cell. Conclusive evidence for such an arrangement is obtained through the point symmetry and periodicity of the pattern seen in X-ray diffraction from the materials—conclusive, that is, until the discovery by Shechtman *et al.* (1984) of icosahedral point symmetry in the diffraction from the splat-cooled alloy Al-Mn. This point symmetry definitely excludes periodic order and establishes a new type of orientational order. Since then, many researcher (compare the experimental work in the bibliography given by Mackay (1987)) have discovered numerous other transition metal alloys which display this forbidden symmetry and, in particular, some authors (Dubost *et al.*, 1986) have grown large grains featuring triacontahedral shapes as in Al-Li-Cu and dodecagonal shapes with pentagonal facets as in Al-Mn-Si. These new and different phases require the condensed matter physicist to understand a new type of atomic order both on a local and a global level (Levine and Steinhardt, 1984).

More detailed analysis of the Bragg peaks in the diffraction pattern shows that they are not sharp—some broadening exists. Furthermore the peaks are not quite symmetrically arranged—small shifts occur. In some samples, other anomalies such as arcs or rings of diffuse intensity are observed. As a consequence there is a large leeway for interpolating a growth mechanism particularly in the light of the fact that all these alloy phases are produced by rapid cooling. Defect structures, phason strains and constrained substitutional disorder among clusters of atoms (Steinhardt, 1988) seem to occur and have been incorporated in various dynamical models, such as

(i) the icosahedral glass model (Stephens and Goldman, 1986), where icosahedral clusters are randomly packed,
(ii) the Monte-Carlo simulations (Widom, 1988) with Lennard-Jones potentials between two types of atoms (this is a 2-D analysis),
(iii) the growth simulation models (Elser, 1987) with algorithms for local atomic combinations.

However, despite the experimental evidence for and appeal of some

of these models, there is still a need to investigate geometric modelling which one could associate with an idealization of a quasicrystal. This approach follows more closely the classical crystallographic prescription as outlined in the opening paragraph. Certain notions must be revised and indeed assumptions such as the periodicity of the lattice and the requirement of a single unit cell must be dropped. Happily the mathematical tools for doing just this have already been elucidated, prior to Shechtman's announcement, through the two-dimensional non-periodic patterns introduced by Penrose (1974); the global analysis of these patterns given by de Bruijn (1981); the proposal of Mackay (1982) of rhombohedral building blocks for three-dimensional icosahedral patterns; and the construction of a corresponding global non-periodic icosahedral pattern by Neri and Kramer (1984). As was pointed out by Kramer (1985), Kowalewski (1938) had already constructed the rhombohedral cells and considered their packing into Kepler's triacontahedron. The non-periodic patterns which we shall call quasilattices are projections from hypercubic lattices in $n > 3$ dimensions, as was shown for pentagonal quasilattices with $n = 5$ by de Bruijn (1981) and for icosahedral ones with $n = 6$ by Kramer and Neri (1984).

A considerable amount of theoretical studies of icosahedral structures appeared after the publication of Shechtman *et al.* (compare the bibliography of Mackay (1987)). We mention here only some early contributions. Icosahedral order was discussed by Levine and Steinhardt (1984) and by Bak (1985, 1986). The diffraction from icosahedral quasilattices was studied by Duneau and Katz (1985), Katz and Duneau (1986), Gähler and Rhyner (1985), Elser (1986), and Jarić (1986). Janssen (1985) related the new structures to the theory of incommensurate phases. Atomic models for icosahedral phases were given, for example, by Elser and Henley (1985) and by Audier and Guyot (1986) compare also Mackay (1986). For contributions by the present authors we refer to Kramer (1982), Kramer and Neri (1984), Kramer (1985–1988), Kramer and Mackay (1985), Urban *et al.* (1986), and Haase *et al.* (1987).

In considering these icosahedral constructions, we return to an old problem of finding space-filling polyhedra. The new feature is that we require a set of such polyhedra. The restriction to those tesselations or tilings yielding icosahedral symmetry under Fourier analysis distinguishes the class of icosahedral quasilattices. The task is to provide a coherent account of the algebraic and geometric properties of these quasilattices. The general framework must also envelop naturally the ideas of classical crystallography so that one can describe crystal systems of say cubic symmetry as well as icosahedral or any other symmetry. Although crystals are three-dimensional objects, crystallography of higher ($n > 3$) dimensions is

forced on us, but in a natural way, particularly for the description of icosahedral quasilattices.

The orientational order seen in quasicrystals is best described in terms of point groups. These point groups act as geometric transformations on the Euclidean space $\mathbb{E}^m$ of the (quasi-)lattice. In $\mathbb{E}^3$, one has the tetrahedral, octahedral, and icosahedral groups, and the series of cyclic and dihedral groups. In Section 2, the abstract properties of these groups are given, relations between them are discussed, and linear actions are defined. This enables the construction of representations of the icosahedral group to be found by induction, subduction and coupling. This is performed in Section 3. Transformations decomposing the representations are found for some examples, so that subrepresentations of smaller dimension are produced.

These representations, particularly those of induction, allow one to embed a non-crystallographic group given in $\mathbb{E}^m$, into a crystallographic group in $\mathbb{E}^n$, $n > m$, and this embedding proves to be crucial for the construction of quasilattices. To describe long-range order we require space group theory in $\mathbb{E}^n$ which is briefly outlined in Section 4. Given a space group in $\mathbb{E}^n$ with a point (sub-)group P, a natural decomposition of $\mathbb{E}^n$ is obtained by the subspaces invariant under P. For a given invariant subspace $\mathbb{E}^m$, the question is if there is also a translation subgroup which leaves $\mathbb{E}^m$ invariant. If so, one finds in E^m a periodic structure, if not, one gets at most a quasilattice in $\mathbb{E}^m$. Corresponding criteria are given in Section 4. Point symmetry is employed in Section 5 to interpret stars of vectors in $\mathbb{E}^m$ as projections from a lattice basis in $\mathbb{E}^n$ and to associate polyhedral cells with these stars. These constructions pave the way towards the possible cell structure of quasilattices and space-filling of $\mathbb{E}^n$.

A quasilattice in $\mathbb{E}^m$ cannot be obtained by the projection of a full lattice from $\mathbb{E}^n$ to $\mathbb{E}^m$ since this projection would yield a multiple covering. One must identify m-dimensional objects in $\mathbb{E}^n$ such that their projections to $\mathbb{E}^m$ form a space filling in the sense described above. In Section 6 we give principles for this construction and illustrate them for the dimensions $n = 2$ and $m = 1$. The geometric objects used in $\mathbb{E}^n$ are the boundaries to the cells of the lattice and their duals of complementary dimension. The quasilattice construction is formulated in terms of dualization and intersection of these boundaries. An alternative prescription is given by the construction of new cells in $\mathbb{E}^n$ called epicells. The epicells have their boundaries parallel or perpendicular to the chosen subspace $\mathbb{E}^m$ and replace the unit cell in $\mathbb{E}^n$. The quasilattice then arises as the m-dimensional slice through the epicells.

The main applications are obtained from hypercubic lattices in $\mathbb{E}^n$, and so we discuss the hyperoctahedral point group of this lattice in Section 8. By use of the representation theory given in Section 4, three cubic lattices and the icosahedral quasilattice in $\mathbb{E}^3$ can all be linked together by continuous

rotations in a space $\mathbb{E}^7$ as shown in Section 7. More details on the icosahedral quasilattice obtained from $\mathbb{E}^6$ are examined in Sections 9 and 10. For a quasicrystal model, the rhombohedral cells serve as new units and carry stable atomic densities. The Fourier transform in this model is written in terms of integrals over the densities in these cells.

2 Some Group Theory Basics

Although the subject of group theory and in particular the icosahedral group has been adequately expounded upon in the literature (Coxeter and Moser, 1957; Coxeter, 1963; Hamermesh, 1962), we shall for completeness recall a few of the algebraic structures relevant for our discussion. We present them in general form so as to give a coherent formalism applicable to any group although we have in mind application to the icosahedral and related groups.

An abstract group G is a set of elements closed with respect to an associative multiplication. Every element of G can be expressed as a finite product of a subset of G—the elements of this subset being called the generators. These satisfy a certain number of conditions which together are called the abstract definition of G. We are interested here in particular to the finite groups of rotations of the regular dihedrons, tetrahedron, octahedron and icosahedron. We have tabulated the order, generators, elements and abstract definitions of these groups for later reference (see Table I).

There are various group-subgroup chains interconnecting these finite rotation groups. The connections are depicted in Fig. 1. Note that the octahedral group $\mathcal{O}$ and icosahedral group $\mathcal{I}$ consist of three dihedral subgroups—$\mathcal{D}_4, \mathcal{D}_3, \mathcal{D}_2$ for $\mathcal{O}$ and $\mathcal{D}_5, \mathcal{D}_3, \mathcal{D}_2$ for $\mathcal{I}$. Each of these dihedral groups contains $\mathcal{D}_1$, a group of order 2 isomorphic to $\mathcal{C}_2$ and generated by $\dot{g}_2$. In what follows we have two $\mathcal{D}_1$ subgroups, one is conjugate to the n-fold generators g_n of $\mathcal{D}_n < \mathcal{O}$ ($n = 2, 3, 4$) and the other separately conjugate to the n-fold generators g_n of $\mathcal{D}_n < \mathcal{I}$ ($n = 2, 3, 5$). The relative orientation of all these generators and those of the tetrahedral group are displayed in Figs. 2, 3, 4. We have chosen the g_3 generator of $\mathcal{O}$ and $\mathcal{T}$ coincident. It is more natural not to take the g_3 of $\mathcal{I}$ coincident with g_3 of $\mathcal{T}$ and $\mathcal{O}$, and as a consequence the $\dot{g}_2$ of $\mathcal{O}$ and $\dot{g}_2$ of $\mathcal{I}$ are not aligned.

The notion of group actions is very useful through which various structures on the group can be defined. If G acts on a set X of objects, the set of all bijections forms a group,

$$G : X \to X \tag{1}$$

and the map is called the group action. Given a point $x_o \in X$, the orbit at

Table I. Abstract groups.

Group	Generators	Abstract Definition	Order	Elements	Remarks
$\mathfrak{D}_n$	$\dot{g}_2, g_n$	$(\dot{g}_2)^2 = (g_n)^n = (g_n\dot{g}_2)^2 = e$	$2n$	$g_n^\nu \dot{g}_2^\sigma$ $\nu = 0, 1, \ldots, n-1, \sigma = 0, 1$	$\dot{g}_2 g_n \dot{g}_2 = g_n^{-1}$
$\mathfrak{T}$	g_2, g_3	$(g_2)^2 = (g_3)^3 = (g_2 g_3)^3 = e$	12	$g_3^\tau, g_3^{\tau'} g_2 g_3^\tau$ $\tau', \tau = 0, 1, 2$	
$\mathfrak{O}$	g_2, g_3	$(g_2)^2 = (g_3)^3 = (g_2 g_3)^4 = e$	24	$g_3^\tau g_2^\sigma, g_3^{\tau'} g_2 g_3^\tau g_2^\sigma$ $\tau', \tau = 0, 1, 2, \sigma = 0, 1$	$\dot{g}_2 \equiv g_2 g_3^{-1} g_2 g_3 g_2 g_3^{-1}$ $g_4 \equiv g_3 g_2 g_3$
$\mathfrak{I}$	g_2, g_3	$(g_2)^2 = (g_3)^3 = (g_2 g_3)^5 = e$	60	$g_5^\mu g_2^\sigma, g_5^\mu g_2 g_5 \dot{g}_2^\sigma$ $\mu, \nu = 0, 1 \ldots, 4, \sigma = 0, 1$	$\dot{g}_2 \equiv g_2 g_5^{-1} g_2 g_5 g_2 g_5^{-1}$ $g_5 \equiv g_3 g_2 g_3$ $g_3 = g_5^2 g_2 g_5^3 \dot{g}_2$

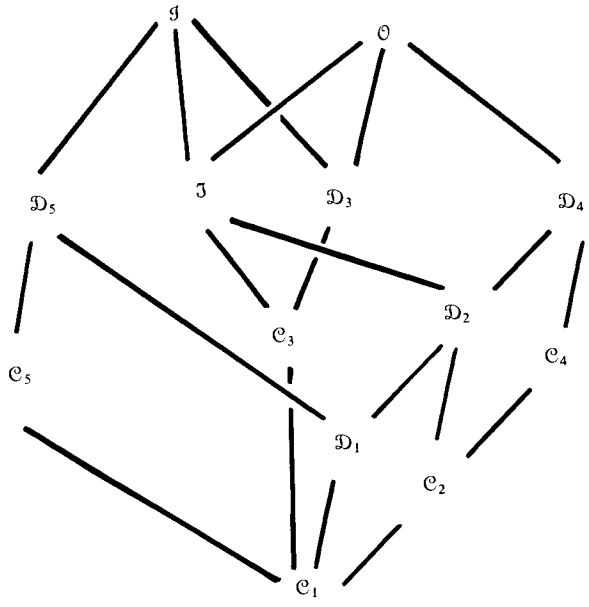

Figure 1. The abstract group embedding. The subgroups $\mathfrak{D}_3$ and $\mathfrak{C}_3$ in $\mathfrak{I}$ and $\mathfrak{O}$ are conjugate.

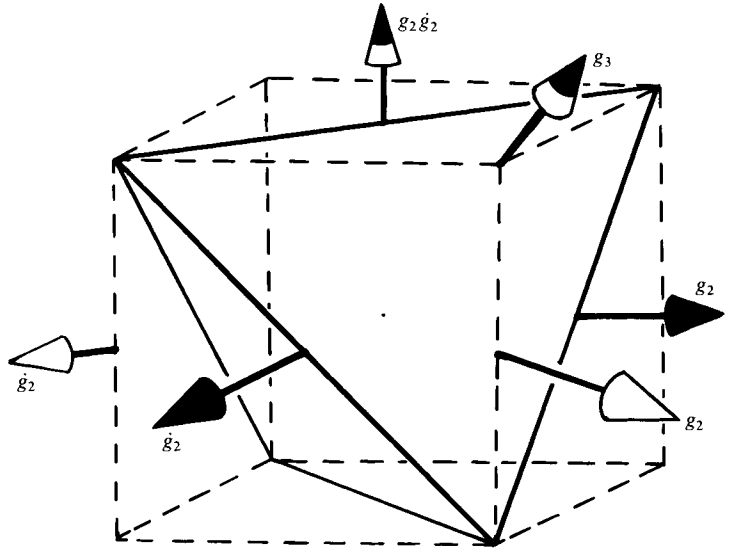

Figure 2. The octahedron–tetrahedron embedding. Open (full) arrows denote $\mathfrak{O}(\mathfrak{J})$ generators.

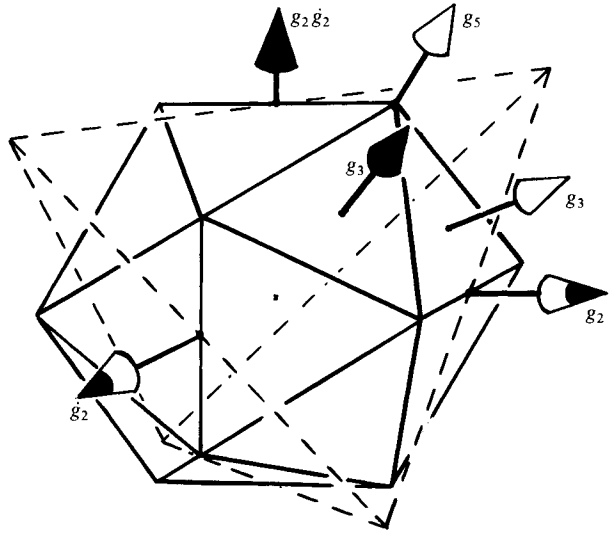

Figure 3. The icosahedron-tetrahedron embedding. Open (full) arrows denote $\mathfrak{I}(\mathfrak{I})$ generators.

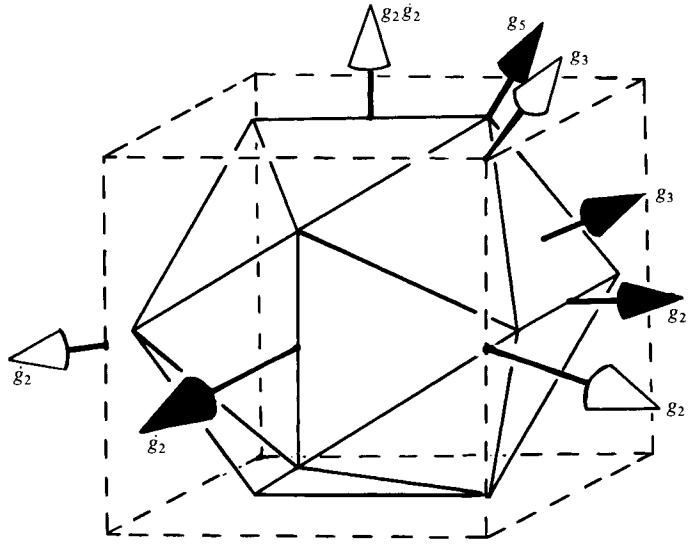

Figure 4. The icosahedron-octahedron embedding. Open (full) arrows denote $\mathfrak{O}(\mathfrak{I})$ generators.

x_o under G is the subset

$$O_G(x_o) \equiv \{x \mid x = gx_o \quad \text{for some} \quad g \in G\}. \tag{2}$$

The property that points are in the same orbit as an equivalence relation on X, and so partitions X into disjoint orbits.

The stability group $\mathcal{S}_G(x_o)$ of a point $x_o \in X$ on the orbit $O_G(x_o)$ is the set

$$\mathcal{S}_G(x_o) = \{g \mid gx_o = x_o \quad \text{for} \quad g \in G\} \tag{3}$$

and is a subgroup of G. The stability groups of different points on the same orbit are conjugate subgroups.

Group actions arise through the group multiplication law. For example the action of G on $g_o \in G$ by

$$g : g_o \to gg_og^{-1} \tag{4}$$

determines an orbit which is the conjugacy class of g_o

$$C(g_o) \equiv \{gg_og^{-1} \quad \text{for all} \quad g \in G\} \tag{5}$$

with stability group

$$\mathcal{S}(g_o) \equiv \{g \mid gg_og^{-1} = g_o \quad \text{for} \quad g \in G\}. \tag{6}$$

The conjugacy map partitions G into disjoint classes, and by varying g_o all classes are obtained. From the presentation of the icosahedral group, one quickly finds the class structure which is given in Table II.

If one considers a subgroup $H < G$, the right action of H on G generates as orbits the left cosets of G with respect to H. These left cosets partition G and so there exists coset representatives such that

$$G = \bigcup_{q=1}^{n} c_qH \qquad n \equiv |G|/|H| \tag{7}$$

and each subset c_qH disjoint. Each element of G can be expressed as $g = c_qh$ with $g \in G$, $h \in H$. The subset c_qH is the left coset of H with

Table II. Icosahedral group.

Order of class	Class	($\mu = 0, 1, \ldots, 4$)
1	$C(e)$	e
12	$C(g_5)$	$g_5, g_5^{-1}, g_5^{\mu}g_2g_5^{\mu-2}\dot{g}_2, g_5^{\mu-2}g_2g_5^{\mu}\dot{g}_2$
12	$C(g_5^2)$	$g_5^2, g_5^{-2}, g_5^{\mu}g_2g_5^{4-\mu}, g_5^{\mu-4}g_2g_5^{-\mu}$
15	$C(g_2)$	$g_5^{\mu}\dot{g}_2, g_5^{\mu}g_2g_2^{-\mu}, g_5^{\mu}g_2g_5^{\mu}\dot{g}_2$
20	$C(g_3)$	$g_5^{\mu}g_2g_5^{2-\mu}, g_5^{\mu-2}g_2g_5^{-\mu}, g_5^{\mu}g_2g_5^{\mu-1}, g_2g_5^{\mu}\dot{g}_2$

Table III. Coset representatives for the various subgroups of the icosahedral group ($q = 0, 1, \ldots, 4$).

$\mathcal{I} > \mathcal{D}_5$:
$[\mathcal{I}/\mathcal{D}_5] = \{g_5^q g_2, e\}$

$\mathcal{I} > \mathcal{D}_3$:
$[\mathcal{I}/\mathcal{D}_3] = \{g_5^q, g_5^q g_2\}$

$\mathcal{I} > \mathcal{D}_2$:
$[\mathcal{I}/\mathcal{D}_2] = \{g_5^q, g_5^q g_2 g_5^4, g_5^q g_2 g_5^3\}$

$\mathcal{I} > \mathfrak{I}$:
$[\mathcal{I}/\mathfrak{I}] = \{g_5^q\} = \mathcal{C}_5$

respect to coset representative c_q. Given G and H, the coset representatives are not unique. However fixing a representative fixes a coset. We denote our chosen set of coset representatives of G and H as

$$[G/H] \equiv \{c_1, \ldots, c_n\} \tag{8}$$

and assume that they remain fixed. For later use, we give our choices of coset representatives for the subgroups $\mathfrak{I}$, $\mathcal{D}_5$, $\mathcal{D}_3$, $\mathcal{D}_2$ of $\mathcal{I}$ (see Table III). Since the g_3 generators of $\mathcal{I}$ and $\mathfrak{I}$ are only conjugate, and that of $\mathcal{D}_3$ a complex expression in terms of the g_2 and g_5 generators, we give also a table of the factorization of the icosahedral group elements into the form $g = c_q h$ (see Tables IV, V).

The importance of the coset factorizations is the following. If the left cosets of H with respect to G are taken as the points of the set $X \equiv G/H$, called the coset space, the left action of G determines a group action

$$G: G/H \to G/H \tag{9}$$

Table IV. Factorization of the icosahedral group $\mathcal{I}$ with respect to the tetrahedral group ($\mu = 0, 1, \ldots, 4$, $\sigma = 0, 1$).

$$\mathcal{I} = [\mathcal{I}/\mathfrak{I}] \cdot \mathfrak{I}$$

$$g_5^\mu g_2^\sigma = g_5^\mu \cdot g_2'^\sigma$$

$$g_5^\mu g_2 g_2^\sigma = g_5^\mu \cdot g_2 g_2'^\sigma$$

$$g_5^\mu g_2 g_5^2 g_2^\sigma = g_5^{\mu-2} \cdot g_3^2 g_2'^{\sigma-1}$$

$$g_5^\mu g_2 g_5^2 g_2^\sigma = g_5^{\mu-1} \cdot g_3 g_2'^{\sigma-1}$$

$$g_5^\mu g_2 g_5^3 g_2^\sigma = g_5^{\mu-4} \cdot g_2' g_3 g_2'^\sigma$$

$$g_5^\mu g_2 g_5^4 g_2^\sigma = g_5^{\mu-3} \cdot g_2' g_3^2 g_2'^\sigma$$

Table V. Factorization of the icosahedral group $\mathcal{I}$ with respect to the dihedral group $\mathcal{D}_3$ ($\mu = 0, 1, \ldots 4$, $\sigma = 0, 1$).

$$\mathcal{I} = [\mathcal{I}/\mathcal{D}_3] \cdot \mathcal{D}_3$$

$$g_5^{\mu} \dot{g}_2^{\sigma} = g_5^{\mu} \cdot \dot{g}_2^{\sigma}$$

$$g_5^{\mu} g_2 \dot{g}_2^{\sigma} = g_5^{\mu} g_2 \cdot \dot{g}_2^{\sigma}$$

$$g_5^{\mu} g_2 g_5 \dot{g}_2^{\sigma} = g_5^{\mu-3} g_2 \cdot g_3 \dot{g}_2^{\sigma-1}$$

$$g_5^{\mu} g_2 g_5^2 \dot{g}_2^{\sigma} = g_5^{\mu-3} \cdot g_3^2 \dot{g}_2^{\sigma-1}$$

$$g_5^{\mu} g_2 g_5^3 \dot{g}_2^{\sigma} = g_5^{\mu-2} \cdot g_3 \dot{g}_2^{\sigma-1}$$

$$g_5^{\mu} g_2 g_5^4 \dot{g}_2^{\sigma} = g_5^{\mu-2} g_2 \cdot g_3^2 \dot{g}_2^{\sigma+1}$$

with each element of G permuting the left cosets

$$g \cdot c_q H = c_{q'} H. \tag{10}$$

In this manner any coset space G/H provides an embedding of G into the symmetric group $S(n)$ of all permutation of n objects. By a well-known theorem all orbits of any group action are in one-to-one correspondence to corresponding coset spaces G/H where $\mathbb{S}$ is the stability group of the orbit.

Let us now introduce the set $[G/H]_p^n$ ($o < p < n$, p fixed) which denotes the set of all partitionings of $[G/H]$ into two subsets of p and $n - p$ elements respectively

$$[G/H]_p^n \equiv \{(c_{\pi(1)} \cdots c_{\pi(p)})(c_{\pi(p+1)} \cdots c_{\pi(n)}) \quad \text{for all} \quad \pi \in \mathbb{S}_n\}. \tag{11}$$

The above group action generates an action on $[G/H]_p^n$ which can be used to classify $[G/H]_p^n$ into orbits under G. This is done by choosing a representative partition from $[G/H]_p^n$ and determining under G the stability group $\mathbb{S}_p^n$ which permits only the elements within each subset. Clearly $\mathbb{S}_p^n$ has the form $\mathbb{S}_p^n = G \cap [S(p) \times S(n-p)]$. Application of the coset representatives from $G/\mathbb{S}_p^n$ then generates an orbit of $|G|/|\mathbb{S}_p^n|$ $(p, n-p)$ partitions with $[G/H]_p^n$. For fixed n and p we have the sum rule

$$\sum_b |G|/|\mathbb{S}_p^n(b)| = \binom{n}{p} \tag{12}$$

where the different orbits are denoted by an additional label b. As there exists a complementarity between $[G/H]_p^n$ and $[G/H]_{n-p}^n$, their stability groups must be isomorphic, $\mathbb{S}_{n-p}^n = \mathbb{S}_p^n$, and the orbit analysis is similar. The orbit analysis is also well-determined once a presentation of the group elements is given and the coset representatives chosen. In Haase *et al.* (1987), we have given the complete analysis for the group-subgroups $\mathcal{I}/\mathcal{D}_5$, $\mathcal{I}/\mathcal{D}_3$, $\mathcal{I}/\mathcal{D}_2$. We present here the more simple analysis for $\mathcal{I}/\mathcal{I}$ in Table VI.

Table VI. Orbit representatives and stability groups for $[\mathfrak{I}/\mathfrak{J}]_p^5$.*

$(p, n-p)$	Orbit Representative	S_p^n	$\lvert\mathfrak{I}\rvert/\lvert S_p^n\rvert$
0 5	(–) (0 1 2 3 4)	$\mathfrak{I}$	1
1 4	(0) (1 2 3 4)	$\mathfrak{C}_5$	5
2 3	(01) (2 3 4)	$\mathfrak{D}_5$	10

*The integers labelling the orbit representative is just the indexing of the coset representatives which in this case $[\mathfrak{I}/\mathfrak{J}]$ is given by the power of the generator g_5, since we take $c_q = g_5^q$.

3 Representation Theory

Although much can be done with an abstract group through its generators and abstract definition, one needs to have some realization of the group such as a matrix representation. The entries of the matrices may be over the integers, rational, real or complex numbers. In this section, we present various techniques by which we can establish representations of G, in particular those of the icosahedral group. We follow Brown *et al.* (1978) in part.

As a preliminary we give some definitions in order to establish some classification of all the representation of G over the various fields $\mathbb{F} = \{\mathbb{Z}, \mathbb{Q}, \mathbb{R}, \mathbb{C}\}$. By representation, $\gamma(G)$, we mean a set of matrices $\gamma(G) = \{\gamma(g)$ for all $g \in G$ which is a homomorphism from G into a set of matrices satisfying $\gamma(g_1)\gamma(g_2) = \gamma(g)$ if $g_1 g_2 = g$. If $\gamma(G)$ and $\gamma'(G)$ are two representations then

(i) $\gamma'(G)$ is $\mathbb{F}$-equivalent to $\gamma(G)$ if there exists matrices V and V^{-1} over $\mathbb{F}$ such that $\gamma'(g) = V\gamma(g)V^{-1}$ for all $g \in G$;
(ii) $\gamma(G)$ is $\mathbb{F}$-reducible if $\gamma'(G)$ through $\mathbb{F}$-equivalence has form

$$\gamma'(g) = \begin{pmatrix} \gamma_1(g) & C(g) \\ 0 & \gamma_2(g) \end{pmatrix} \quad \text{for all} \quad g \in G \tag{13}$$

and $\gamma_1(G)$ and $\gamma_2(G)$ are two representations of smaller dimension;
(iii) $\gamma(G)$ is $\mathbb{F}$-decomposable if in (ii) $C(g) = 0$ for all g;
(iv) $\gamma(G)$ is $\mathbb{F}$-fully-reducible if there exists irreducible representations $\gamma^i(G)$ such that by an $\mathbb{F}$-equivalence $\gamma'(G)$ has the form

$$\gamma'(g) = \bigoplus_i \mathbb{I}_{m_i} \times \gamma^i(g) \quad \text{for all} \quad g \in G \tag{14}$$

where m_i is the multiplicity of the irreducible representation $\gamma^i(G)$ in $\gamma(G)$ and $\mathbb{I}_{m_i}$, the $m_i \times m_i$ unit matrix.

Clearly $\mathbb{F}$-fully reducible $\Rightarrow$ $\mathbb{F}$-decomposable $\Rightarrow$ $\mathbb{F}$-reducible. However the reverse is only true for $\mathbb{F} = \{\mathbb{Q}, \mathbb{R}, \mathbb{C}\}$. Moreover it is only over these fields that the irreducible representation (or for short, irreps) of an $\mathbb{F}$-fully reducible representation are unique up to $\mathbb{F}$-equivalence. This is not true for irreps of a $\mathbb{Z}$-fully reducible representation.

From the embedding of fields $\mathbb{Z}$ in $\mathbb{Q}$, $\mathbb{Q}$ in $\mathbb{R}$, $\mathbb{R}$ in $\mathbb{C}$, one also has that:

$$\begin{aligned}&\mathbb{Z}\text{-reducible} \Rightarrow \mathbb{Q}\text{-reducible} \Rightarrow \mathbb{R}\text{-reducible} \Rightarrow \mathbb{C}\text{-reducible and}\\ &\mathbb{Z}\text{-irreducible} \Leftarrow \mathbb{Q}\text{-irreducible} \Leftarrow \mathbb{R}\text{-irreducible} \Leftarrow \mathbb{C}\text{-irreducible.}\end{aligned}$$

But there are the two additional results:

$$\mathbb{Z}\text{-reducible} \Leftarrow \mathbb{Q}\text{-reducible and } \mathbb{Z}\text{-irreducible} \Rightarrow \mathbb{Q}\text{-irreducible.}$$

Thus any representation can be built up from a number of irreducible ones, and as a consequence, the study of irreps of a group, and the related character theory, assumes a major role. The irrep theory of the groups considered here is well-known. But we present for convenience tables of character results of $\mathcal{I}$ and its subgroups, (see Tables VII–XII) and also to establish our notation for labelling irreps and the relation to other commonly used notations. We follow Butler (1981) in this respect where the labelling is developed from the rather natural embedding of these point groups into the rotation group SO_3. This continuous group is the smallest such group containing $\mathcal{I}$ and $\mathcal{O}$. The reduction from SO_3 to the point group corresponds for a physical system to a breaking of isotropic symmetry in 3-space to the smaller point symmetry. The role of the SO_3 group is to classify the various physical tensors such as the elastic tensor, dielectric tensor, stress tensor, as

Table VII. The icosahedral group irrep labels and irrep characters.

		Irreps	[5]	[41]	[32]	$[31^2_+]$	$[31^2_-]$	$A(5)$	Partition Notations
			0	3	2	1	$\tilde{1}$		Butler's Notation
Class	No.								
$C(e)$	1		1	4	5	3	3		
$C(g_5)$	12		1	-1	0	τ	$1-\tau$		
$C(g_5^2)$	12		1	-1	0	$1-\tau$	τ		
$C(g_3)$	20		1	$+1$	-1	0	0		
$C(g_2)$	15		1	0	1	-1	-1		

$\tau = \frac{1}{2}(\sqrt{5}+1)$ $\quad \tau - 1 = \frac{1}{2}(\sqrt{5}-1) = 1/\tau$

Table VIII. The tetrahedral group irrep labels and irrep characters.

		Irreps	[4]	[31]	$[2^2_+]$	$[2^2_-]$	$A(4)$	Partition Notation
			Γ_1	Γ_4	Γ_2	Γ_3		Bethe's Notation
			A_1	T	E_1	E_2		Mulliken's Notation
Class	No.		0	1	2	−2		Butler's Notation
$C(e)$	1		1	3	1	1		
$C(g_3)$	4		1	0	ω	ω^2		
$C(g_2^{-1})$	4		1	0	ω^2	ω		
$C(g_2)$	3		1	−1	1	1		

$\omega = \exp(2\pi i/3)$

some irrep of SO_3. How these tensors behave under the point group is given by branching rules, or "selection rules." In order to provide quantitative results, the matrix elements of the tensor operators need to be known and this is given by the Wigner–Eckart theorem. These group theory techniques have been described fully in Butler (1981). One can find in this book tables of branching rules for all group-subgroup chains of O_3 and evaluation of $3jm$ $6j$ and $9j$ symbols which are required for the application of the Wigner–Eckart theorem, transformations from $SO_3 > G > \cdots$ basic kets to the $|JM\rangle$ kets of $SO_3 > SO_2$ have been given up to $J = 8$ where G includes also the icosahedral group. Transformations between various point group chains have also been calculated. For a discussion on the tensor algebra of the icosahedral group see also McLellan (1961) and Cesare and del Duca (1987). We do not pursue this topic further as our purpose is to construct a point group action on a lattice which involves integral representations.

Table IX. The dihedral group $\mathfrak{D}_5$ irrep labels and irrep characters.

		Irreps	A_1	A_2	E_1	E_2	Mulliken's Notation
Class	No.		0	$\tilde{0}$	1	2	Butler's Notation
$C(e)$	1		1	1	2	2	
$C(g_5)$	2		1	1	$\tau - 1$	$-\tau$	
$C(g_5^2)$	2		1	1	$-\tau$	$\tau - 1$	
$C(g_2)$	5		1	−1	0	0	

Table X. The dihedral group $\mathfrak{D}_3$ irrep labels and irrep characters.

		Irreps	[3]	[21]	[1^3]	$S(3)$	Partition Notation
			Γ_1	Γ_2	Γ_3		Bethe's Notation
			A_1	A_2	E		Mulliken's Notation
Class	No.		0	0	1		Butler's Notation
$C(e)$	1		1	1	2		
$C(g_3)$	2		1	1	−1		
$C(g_2')$	3		1	−1	0		

However, the method used in constructing irreps of G symmetry-adapted to the group-subgroup chain $SO_3 > G$ is Kronecker products, or more descriptively coupling. Given two representations of G, say, $\gamma_1(G)$ and $\gamma_2(G)$, and these may be irreducible or reducible, then the coupling $\gamma_1(G) \times \gamma_2(G)$ generates in general a reducible representation of dimension $|\gamma_1| \times |\gamma_2|$. The reduction into irreducibles is performed by an invertible matrix $V(\gamma_1\gamma_2)$ whose elements $V(\gamma_1\gamma_2)^{\Gamma\gamma i}_{i_1 i_2}$ are called coupling coefficients. In the case when $\gamma_1(G)$ and $\gamma_2(G)$ are irreducibles of some point group of SO_3 the coefficients can be obtained from the $3jm$ tables in Butler (1981). As an example which we will be using later, we consider the Kronecker product of $3(\mathcal{I})$ with itself. The irrep content (and dimensionalities) is

$$3 \times 3 \downarrow \{0 + 2 + 3\} + [1 + \tilde{1}] \tag{15}$$

$$4 \quad 4 \quad 1 \quad 5 \quad 4 \quad 3 \quad 3$$

Table XI. The dihedral group $\mathfrak{D}_2$ irrep labels and irrep characters.

		Irreps	Γ_1	Γ_3	Γ_2	Γ_4	Bethe's Notation
			A_1	B_1	B_2	B_3	Mulliken's Notation
Class	No.		0	$\tilde{0}$	1	$\tilde{1}$	Butler's Notation
$C(e)$	1		1	1	1	1	
$C(g_2)$	1		1	1	−1	−1	
$C(g_2')$	1		1	−1	1	−1	
$C(g_2'g_2)$	1		1	−1	−1	1	

Table XII. Subduction of irreps of the icosahedral groups.

	$\mathfrak{I}$:	0	3	2	1	$\tilde{1}$
$\mathfrak{I}$:	0	1	1	0	0	0
	1	0	1	1	1	1
	2	0	0	1	0	0
	−2	0	0	1	0	0
$\mathfrak{D}_5$:	0	1	0	1	0	0
	$\tilde{0}$	0	0	0	1	1
	1	0	1	1	1	0
	2	0	1	1	0	1
$\mathfrak{D}_3$:	0	1	1	1	0	0
	$\tilde{0}$	0	1	0	1	1
	1	0	1	2	1	1
$\mathfrak{D}_2$:	0	1	1	2	0	0
	$\tilde{0}$	0	1	1	1	1
	1	0	1	1	1	1
	$\tilde{1}$	0	1	1	1	1

where the curly and square sets of brackets separate the symmetric and antisymmetric parts of the products. The coupling matrix which reduces any matrix representation over $\mathbb{R}$ of $3(\mathfrak{I})$ given in an $\mathfrak{I} > \mathfrak{D}_5 > \mathfrak{C}_5 > \mathfrak{C}_1$ basis is given in Table XIII. The matrix was composed from the various $3jm$ symbols of $\mathfrak{I} > \mathfrak{D}_5$ which are tabulated in Butler (1981). One can see by inspection that it is orthogonal.

We have already obtained a representation of G using the group action on $[G/H]$. The group action determines a homomorphism from the abstract group into a set of $n \times n$ permutation matrices—containing only ones and zeroes—acting on $[G/H]$. This representation is a faithful representation called the permutation representation of G by H. We shall denote it as $[G/H](g)$ with elements given by

$$[G/H](g)_q^{q'} \equiv \delta(c_{q'}^{-1} g c_q \in H). \tag{16}$$

For simplicity of notation we will use the permutation form for a permutation matrix

$$[G/H](g) = \begin{pmatrix} 1 & \cdots & q & \cdots & n \\ \pi(1) & \cdots & \pi(q) & \cdots & \pi(n) \end{pmatrix}. \tag{17}$$

One notes that the representation is well-determined once a presentation of the abstract group and subgroup is known and the coset representatives

Table XIII. $V(3 \times 3)$ for $\mathfrak{I} > \mathfrak{D}_5 > \mathfrak{C}_5 > \mathfrak{C}_1$.

			1×1				1×2				2×1				2×2			
	$\mathfrak{D}_5$	$\mathfrak{D}_5$	1.1	1−1	−11	−1−1	1.2	1−2	−12	−1−2	21	2−1	−21	−2−1	22	2−2	−22	−2−2
	$\mathfrak{C}_5$	$\mathfrak{C}_5$																
		$\mathfrak{C}_5$	2	0	0	−2	−2	−1	+1	+2	−2	−1	−1	+2	−2	−1	1	2
$\mathfrak{I}$	$\mathfrak{D}_5$	$\mathfrak{C}_5$																
0	0	0	$\frac{1}{2}$			$\frac{1}{2}$									$\frac{1}{2}$			$\frac{1}{2}$
2	0	0	$-\frac{1}{2}$			$-\frac{1}{2}$									$\frac{1}{2}$			$\frac{1}{2}$
	1	1					$-\sqrt{\frac{1}{12}}$			$-\sqrt{\frac{1}{12}}$	$-\sqrt{\frac{1}{12}}$			$-\sqrt{\frac{1}{12}}$		$\sqrt{\frac{1}{3}}$	$\sqrt{\frac{1}{3}}$	
		−1						$-\sqrt{\frac{1}{12}}$	$\sqrt{\frac{1}{12}}$			$\sqrt{\frac{1}{12}}$	$-\sqrt{\frac{1}{12}}$		$\sqrt{\frac{1}{3}}$			$-\sqrt{\frac{1}{3}}$
	2	2		$-\sqrt{\frac{1}{3}}$	$-\sqrt{\frac{1}{3}}$			$-\sqrt{\frac{1}{12}}$	$-\sqrt{\frac{1}{12}}$			$\sqrt{\frac{1}{12}}$	$\sqrt{\frac{1}{12}}$					
		−2	$-\sqrt{\frac{1}{3}}$			$\sqrt{\frac{1}{3}}$	$-\sqrt{\frac{1}{12}}$			$\sqrt{\frac{1}{12}}$	$\sqrt{\frac{1}{12}}$			$-\sqrt{\frac{1}{12}}$				
3	1	1					$-\sqrt{\frac{1}{6}}$			$-\sqrt{\frac{1}{6}}$	$-\sqrt{\frac{1}{6}}$			$-\sqrt{\frac{1}{6}}$		$-\sqrt{\frac{1}{6}}$	$-\sqrt{\frac{1}{6}}$	
		−1						$-\sqrt{\frac{1}{6}}$	$\sqrt{\frac{1}{6}}$			$\sqrt{\frac{1}{6}}$	$-\sqrt{\frac{1}{6}}$		$-\sqrt{\frac{1}{6}}$			$+\sqrt{\frac{1}{6}}$
	2	2		$-\sqrt{\frac{1}{6}}$	$-\sqrt{\frac{1}{6}}$			$\sqrt{\frac{1}{6}}$	$\sqrt{\frac{1}{6}}$			$-\sqrt{\frac{1}{6}}$	$-\sqrt{\frac{1}{6}}$					
		−2	$-\sqrt{\frac{1}{6}}$			$\sqrt{\frac{1}{6}}$	$+\sqrt{\frac{1}{6}}$			$-\sqrt{\frac{1}{6}}$	$-\sqrt{\frac{1}{6}}$			$\sqrt{\frac{1}{6}}$				
1	$\tilde{0}$	0		$-\frac{1}{2}$	$+\frac{1}{2}$											$\frac{1}{2}$	$-\frac{1}{2}$	
	1	1					$-\frac{1}{2}$			$-\frac{1}{2}$	$\frac{1}{2}$			$\frac{1}{2}$		0	0	
		−1						$-\frac{1}{2}$	$\frac{1}{2}$			$-\frac{1}{2}$	$\frac{1}{2}$		0			0
$\tilde{1}$	$\tilde{0}$	0		$-\frac{1}{2}$	$+\frac{1}{2}$											$-\frac{1}{2}$	$-\frac{1}{2}$	
	2	2		0	0			$-\frac{1}{2}$	$-\frac{1}{2}$			$-\frac{1}{2}$	$-\frac{1}{2}$					
		−2	0			0	$-\frac{1}{2}$			$\frac{1}{2}$	$-\frac{1}{2}$			$\frac{1}{2}$				

chosen. In the case when H is the identity group E, the representation is known as the regular representation.

The permutation representation is a representation over the integers and so the group can be considered as a subgroup of $GL(n, \mathbb{Z})$—the set of all $n \times n$ matrices with integer entries and determinant ± 1. Another property is that the matrices are orthogonal,

$$[G/H](g)^{-1} = ([G/H](g))^T. \tag{18}$$

Thus the group can be embedded in $O(n, \mathbb{Z})$—the set of orthogonal $n \times n$ matrices. A restriction to the field $\{-1, 0, +1\}$ gives a finite group of order $2^n n!$ which is isomorphic to the hyperoctahedral group $\Omega(n)$—the symmetry group of the n-dimensional Cartesian frame (see Section 7). Over the more restricted field $\{0, 1\}$ we have the subgroup of order $n!$ which is isomorphic to the symmetric group $S(n)$. Thus for any permutation representation $[G/H](g)$ there is this hierarchy of group–subgroup embeddings $GL(n, \mathbb{Z}) > O(n, \mathbb{Z}) > \Omega(n) > S(n) > G > H$.

We present in Table XIV the permutation matrices for $\mathfrak{I} > \mathfrak{I}$, $\mathfrak{I} > \mathfrak{D}_5$, $\mathfrak{I} > \mathfrak{D}_3$ and $\mathfrak{I} > \mathfrak{D}_2$. We give only the explicit result for the generators of the dihedral subgroups, the others can be obtained from the presentation of the abstract group in Table I.

The permutation representation is a fundamental element in the construction of other representations as noted by Frobenius. The construction gives the induced representation whose matrix elements are given as

$$\eta \uparrow (g)_{qj}^{q'j'} \equiv [G/H](g)_q^{q'} \times \eta(c_{q'}^{-1} g c_q)_j^{j'} \tag{19}$$

where $\eta(H)$ is a representation of the subgroup H of dimension $|\eta|$. The induced representation $\eta \uparrow (G)$ has dimension $(|G|/|H|) \times |\eta|$. Naturally when the representation of H is the identity $0(H)$, the induced representation $0 \uparrow (G)$ reduces to the permutation representation $[G/H](g)$. The representation $\eta(H)$ need not be irreducible although this is almost always taken to be the case. One important theorem of induced representations that confirms this decision is:

Theorem: *The induced representation $\eta \uparrow (G)$ of a reducible representation $\eta(H)$ is equivalent to the direct sum of the induced representation $\eta_i \uparrow (G)$ of the constituent irreps $\eta_i(H)$* of *$\eta(H)$. That is*

$$\eta \uparrow (G) \simeq \bigoplus_i \mathbb{I}_{m_i} \times \eta_i \uparrow (G)$$
$$\text{where} \quad \eta(H) \simeq \bigoplus_i \mathbb{I}_{m_i} \times \eta_i(H). \tag{20}$$

Table XIV. Permutation representation of the generators of the icosahedral group.*

$[G/H](g)_q^{q'} = \delta(c_{q'}^{-1} g c_q \in H)$

	g_5	g_2	g_3	$\dot{g}_2$
$[\mathfrak{I}/\mathfrak{I}]$	$\begin{pmatrix} 0 & 1 & 2 & 3 & 4 \\ 1 & 2 & 3 & 4 & 0 \end{pmatrix}$	$\begin{pmatrix} 0 & 1 & 2 & 3 & 4 \\ 0 & 3 & 4 & 1 & 2 \end{pmatrix}$	$\begin{pmatrix} 0 & 1 & 2 & 3 & 4 \\ 3 & 1 & 0 & 2 & 4 \end{pmatrix}$	$\begin{pmatrix} 0 & 1 & 2 & 3 & 4 \\ 0 & 4 & 3 & 2 & 1 \end{pmatrix}$
$[\mathfrak{I}/\mathfrak{D}_5]$	$\left(\begin{array}{ccccc\|c} 0 & 1 & 2 & 3 & 4 & \dot{0} \\ 1 & 2 & 3 & 4 & 0 & \dot{0} \end{array}\right)$	$\left(\begin{array}{ccccc\|c} 0 & 1 & 2 & 3 & 4 & \dot{0} \\ \dot{0} & 1 & 3 & 2 & 4 & 0 \end{array}\right)$	$\left(\begin{array}{ccccc\|c} 0 & 1 & 2 & 3 & 4 & \dot{0} \\ 4 & 0 & 3 & \dot{0} & 1 & 2 \end{array}\right)$	$\left(\begin{array}{ccccc\|c} 0 & 1 & 2 & 3 & 4 & \dot{0} \\ 0 & 4 & 3 & 2 & 1 & \dot{0} \end{array}\right)$
$[\mathfrak{I}/\mathfrak{D}_3]$	$\left(\begin{array}{ccccc\|} 0 & 1 & 2 & 3 & 4 & \\ 1 & 2 & 3 & 4 & 0 & \end{array}\right.$	$\left(\begin{array}{ccccc\|} 0 & 1 & 2 & 3 & 4 & \\ \dot{0} & \dot{2} & 2 & 3 & \dot{3} & \end{array}\right.$	$\left(\begin{array}{ccccc\|} 0 & 1 & 2 & 3 & 4 & \\ 0 & 4 & \dot{4} & \dot{2} & \dot{0} & \end{array}\right.$	$\left(\begin{array}{ccccc\|} 0 & 1 & 2 & 3 & 4 & \\ 0 & 4 & 3 & 2 & 1 & \end{array}\right.$
	$\left.\begin{array}{ccccc} \dot{0} & \dot{1} & \dot{2} & \dot{3} & \dot{4} \\ \dot{1} & \dot{2} & \dot{3} & \dot{4} & \dot{0} \end{array}\right)$	$\left.\begin{array}{ccccc} \dot{0} & \dot{1} & \dot{2} & \dot{3} & \dot{4} \\ 0 & \dot{4} & 1 & 4 & \dot{1} \end{array}\right)$	$\left.\begin{array}{ccccc} \dot{0} & \dot{1} & \dot{2} & \dot{3} & \dot{4} \\ 1 & 3 & \dot{1} & 2 & \dot{3} \end{array}\right)$	$\left.\begin{array}{ccccc} \dot{0} & \dot{1} & \dot{2} & \dot{3} & \dot{4} \\ \dot{0} & \dot{4} & \dot{3} & \dot{2} & \dot{1} \end{array}\right)$
$[\mathfrak{I}/\mathfrak{D}_2]$	$\left(\begin{array}{ccccc\|} 0 & 1 & 2 & 3 & 4 & \\ 1 & 2 & 3 & 4 & 0 & \end{array}\right.$	$\left(\begin{array}{ccccc\|} 0 & 1 & 2 & 3 & 4 & \\ 0 & \dot{1} & \ddot{3} & \ddot{0} & \dot{0} & \end{array}\right.$	$\left(\begin{array}{ccccc\|} 0 & 1 & 2 & 3 & 4 & \\ \ddot{2} & \ddot{0} & \dot{3} & 2 & \dot{2} & \end{array}\right.$	$\left(\begin{array}{ccccc\|} 0 & 1 & 2 & 3 & 4 & \\ 0 & 4 & 3 & 2 & 1 & \end{array}\right.$
	$\left.\begin{array}{ccccc} \dot{0} & \dot{1} & \dot{2} & \dot{3} & \dot{4} \\ \dot{1} & \dot{2} & \dot{3} & \dot{4} & \dot{0} \end{array}\right\|$	$\left.\begin{array}{ccccc} \dot{0} & \dot{1} & \dot{2} & \dot{3} & \dot{4} \\ 4 & 1 & \ddot{1} & \dot{3} & \ddot{2} \end{array}\right\|$	$\left.\begin{array}{ccccc} \dot{0} & \dot{1} & \dot{2} & \dot{3} & \dot{4} \\ \ddot{4} & \dot{0} & \ddot{3} & 3 & 1 \end{array}\right\|$	$\left.\begin{array}{ccccc} \dot{0} & \dot{1} & \dot{2} & \dot{3} & \dot{4} \\ \dot{1} & \dot{0} & \dot{4} & \dot{3} & \dot{2} \end{array}\right\|$
	$\left.\begin{array}{ccccc} \ddot{0} & \ddot{1} & \ddot{2} & \ddot{3} & \ddot{4} \\ \ddot{1} & \ddot{2} & \ddot{3} & \ddot{4} & \ddot{0} \end{array}\right)$	$\left.\begin{array}{ccccc} \ddot{0} & \ddot{1} & \ddot{2} & \ddot{3} & \ddot{4} \\ 3 & \dot{2} & \dot{4} & 2 & \ddot{4} \end{array}\right)$	$\left.\begin{array}{ccccc} \ddot{0} & \ddot{1} & \ddot{2} & \ddot{3} & \ddot{4} \\ \dot{4} & 0 & \ddot{1} & 4 & \dot{1} \end{array}\right)$	$\left.\begin{array}{ccccc} \ddot{0} & \ddot{1} & \ddot{2} & \ddot{3} & \ddot{4} \\ \ddot{3} & \ddot{2} & \ddot{1} & \ddot{0} & \ddot{4} \end{array}\right)$

* The g_3 generator is that of the $\mathfrak{D}_3$ subgroup and not of $\mathfrak{I}$ which is ${}^{\mathfrak{I}}g_3 \leftrightarrow g_5^{-1} g_3 g_5$. The permutation forms of $[\mathfrak{I}/\mathfrak{D}_3]$ and $[\mathfrak{I}/\mathfrak{D}_2]$ have been broken up into two and three lines respectively so as to condense the presentation of the table. They should be read colinearly, i.e. (1st line ‖ 2nd line) for $[\mathfrak{I}/\mathfrak{D}_3]$ and (1st line ‖ 2nd line ‖ 3rd line) for $[\mathfrak{I}/\mathfrak{D}_2]$. The coset representatives are basically grouped into sets of five according to Table II in which q runs from 0 to 4. The second and third sets are distinguished by a dot and two dots respectively. The correspondence to Haase *et al.* 1987 is simply $q \to q + 1, \dot{q} \to q + 6, \ddot{q} \to \ddot{q} + 11$ but note that changes of generators and coset representatives have been made.

A point to observe is that if $\eta(H)$ consists of matrices with entries from a field $\mathbb{F}$ then the induced representation is also over $\mathbb{F}$. This is important when constructing integer representations by induction.

To define a vector space for the induced representation we formally define the product

$$|\eta \uparrow qj\rangle \equiv |q\rangle|\eta j\rangle \quad \text{for} \quad q = 1 \cdots n, j = 1 \cdots |\eta| \tag{21}$$

with the orthonormality condition

$$\langle \eta \uparrow q'j' \,|\, \eta \uparrow qj\rangle = \delta_q^{q'} \delta_j^{j'} \tag{22}$$

and the group action

$$O_g|\eta \uparrow qj\rangle = \sum_{q'j'} |\eta \uparrow q'j'\rangle \eta \uparrow (g)_{qj}^{q'j'}. \tag{23}$$

As a representation space of G, the space spanned by $\{|\eta\uparrow qj\rangle\}$ decomposes into irrep spaces of G labelled by $\gamma(G)$

$$|\eta\uparrow qj\rangle = \sum_{a\gamma i} |\eta\uparrow a\gamma i\rangle m(\eta\uparrow)^{a\gamma i}_{qj}. \tag{24}$$

Here a indexes the multiplicity of γ in $\eta\uparrow$, denoted $|\eta\uparrow\colon \gamma|$. In the case when $\eta(H)$ is irreducible, their multiplicity is linked by the Frobenius reciprocity to the subduction of $\eta(H)$ in $\gamma(G)$, that is

$$|\gamma\colon \eta| = |\eta\uparrow\colon \gamma|. \tag{25}$$

The reciprocity allows one to elicit most of the properties of induction from those of subduction. The branching rules for $\mathfrak{I} > \mathfrak{I}$, $\mathfrak{I} > \mathfrak{D}_n$, $n = 2, 3, 5$ are found in Table XII.

The induction coefficient $m(\eta\uparrow)^{a\gamma i}_{qj}$ is an element of an invertible matrix indexed by $(a\gamma i)$ and (qj). They transform the old basis into a new basis $\{|\eta\uparrow a\gamma i\rangle\}$ in which the group action has block diagonal form

$$O_g|\eta\uparrow a\gamma i\rangle = |\eta\uparrow a\gamma i'\rangle\gamma(g)^{i'}_{i}, \tag{26}$$

we have chosen the irreps $\gamma(G)$ to be independent of the multiplicity label.

We determine the induction coefficients $m(\eta\uparrow)^{a\gamma i}_{qj}$ by character projection techniques. Let

$$P(\gamma) \equiv (|\gamma|/|G|) \sum_{g} \chi^{\gamma}(g^{-1})O_g \tag{27}$$

with the property

$$O_g P(\gamma) = P(\gamma)O_g \tag{28}$$

and

$$P(\gamma)P(\gamma') = \delta^{\gamma}_{\gamma'} P(\gamma). \tag{29}$$

The action of these projection operators on the basis vectors $|\eta\uparrow qj\rangle$ is to generate a set of $|\eta| \times |G|/|H|$ dependent vectors in a $|\gamma|$-dimension subspace of the space labelled by $\eta\uparrow$.

$$P(\gamma)|\eta\uparrow qj\rangle = |\eta\uparrow q'j'\rangle P(\eta\uparrow, \gamma)^{q'j'}_{qj} \tag{30}$$

with scalar products

$$\langle\eta\uparrow q'j'|P(\gamma') \cdot P(\gamma)|\eta\uparrow qj\rangle = \delta^{\gamma'}_{\gamma}\langle\eta\uparrow q'j'|P(\gamma)|\eta\uparrow qj\rangle. \tag{31}$$

In the special case when $\gamma' = \gamma$, $q' = q$, $j' = j$, we have

$$\langle\eta\uparrow qj|P(\gamma) \cdot P(\gamma)|\eta\uparrow qj\rangle = \left|\frac{G}{H}\right| \left|\frac{\eta}{\gamma}\right|. \tag{32}$$

By a Gram-Schmidt orthogonalisation procedure we may define a $|\gamma|$ dimensional basis for each subspace, denoted $\{|\eta\uparrow a\gamma i\rangle\}$—these will be some normalized linear combination of the $P(\gamma)|\eta\uparrow qj\rangle$. The scalar product of these two sets defines a matrix which fully reduces the induced representation, that is

$$\langle\eta\uparrow a\gamma i|P(\gamma')|\eta\uparrow qj\rangle = \delta_{\gamma}^{\gamma'} m(\eta\uparrow)_{qj}^{a\gamma i}. \tag{33}$$

Note that the action of the projection operators $|\eta\uparrow a\gamma i\rangle$ is

$$P(\gamma')|\eta\uparrow a\gamma i\rangle = |\eta\uparrow a\gamma i\rangle\, \delta_{\gamma}^{\gamma'}. \tag{34}$$

Let us consider some examples. We begin with the now-familiar Penrose tiling in $\mathbb{E}^2$ but putting it in the terminology given above. Its orientation order is characterized by the action of the cyclic group $\mathcal{C}_5$ generated by g_5. It has only one subgroup, the identity group $\mathcal{E} = \mathcal{C}_1$. Hence we need only the regular-representation in which the representation of g_5 is of the form

$$0(\mathcal{C}_1\uparrow\mathcal{C}_5)(g_5) = [\mathcal{C}_5/\mathcal{C}_1](g_5) = \begin{pmatrix} 0 & 0 & 0 & 0 & 1 \\ 1 & 0 & 0 & 0 & 0 \\ 0 & 1 & 0 & 0 & 0 \\ 0 & 0 & 1 & 0 & 0 \\ 0 & 0 & 0 & 1 & 0 \end{pmatrix}. \tag{35}$$

It is clearly and element of the group Ω_5 and S_5, and hence we have the subgroup relation $\Omega_5 > S_5 > \mathcal{C}_5$. The irrep content of $0\uparrow$ under $\mathbb{R}$-equivalence is obtained from Butler (1981),

$$0\uparrow \simeq 0 + 1 + 2 \tag{36}$$

where 0 is one-dimensional, 1 and 2 two-dimensional. We can choose in our induced representation space a basis $\{|0\uparrow a\gamma i\rangle a = 0, \gamma = 0, 1, 2\}$ such that $0\uparrow(g_5)$ is in block diagonal form, The matrix $m(0\uparrow)$ is of the form ($\tau = \frac{1}{2}(\sqrt{5} + 1)$)

$$m(0\uparrow) = \operatorname{diag}\left(\sqrt{\frac{2}{10}}, \sqrt{\frac{1}{10}}, \sqrt{\frac{3-\tau}{10}}, \sqrt{\frac{1}{10}}, \sqrt{\frac{3-\tau}{10}}\right)$$

$$\times \begin{pmatrix} 1 & 1 & 1 & 1 & 1 \\ 2 & \frac{1}{\tau} & -\tau & -\tau & \frac{1}{\tau} \\ 0 & \tau & 1 & -1 & -\tau \\ 2 & -\tau & \frac{1}{\tau} & \frac{1}{\tau} & -\tau \\ 0 & 1 & -\tau & \tau & -\tau \end{pmatrix}. \tag{37}$$

Under $\mathbb{R}$-equivalence, we then have for $0\uparrow(g_5)$

$$m(0\uparrow)0\uparrow(g_5)m(0\uparrow)^{-1} = 0(g_5) \oplus 1(g_5) \oplus 2(g_5) \tag{38}$$

where

$$0(g_5) = +1, \quad 1(g_5) = \tfrac{1}{2}\begin{pmatrix} \dfrac{1}{\tau} & -\sqrt{\tau+2} \\ \sqrt{\tau+2} & \dfrac{1}{\tau} \end{pmatrix},$$

$$2(g_5) = \tfrac{1}{2}\begin{pmatrix} -\tau & -\sqrt{3-\tau} \\ \sqrt{3-\tau} & -\tau \end{pmatrix}$$

are irrep matrices of the generator $g_5 \in \mathcal{C}_5$ over $\mathbb{R}$. The integer representation is transformed into real representations. However we could have chosen a basis—this is in fact the Jacobi basis—which $m(0\uparrow)$ takes the form in $GL(m, \mathbb{Z})$

$$m(0\uparrow) = \begin{pmatrix} 1 & 1 & 1 & 1 & 1 \\ 4 & -1 & -1 & -1 & -1 \\ 0 & 3 & -1 & -1 & -1 \\ 0 & 0 & 2 & -1 & -1 \\ 0 & 0 & 0 & 1 & -1 \end{pmatrix} \tag{39}$$

whose inverse is in $GL(n, \mathbb{Q})$ – $m(0\uparrow)^{-1} = m(0\uparrow)^T \operatorname{diag}(\frac{1}{5}, \frac{1}{20}, \frac{1}{12}, \frac{1}{6}, \frac{1}{2})$. Therefore we actually have a $\mathbb{Q}$-reduction of $0\uparrow(g_5)$, however only into a one- and four-dimensional block-diagonal form

$$m(0\uparrow)\,0\uparrow(g_5)m(0\uparrow)^{-1} = \begin{pmatrix} 1 & 0 & 0 & 0 & 0 \\ 0 & -\frac{1}{4} & -\frac{5}{12} & -\frac{5}{6} & -\frac{5}{2} \\ 0 & \frac{3}{4} & -\frac{1}{12} & -\frac{1}{6} & -\frac{1}{2} \\ 0 & 0 & \frac{2}{3} & -\frac{1}{6} & -\frac{1}{2} \\ 0 & 0 & 0 & \frac{1}{2} & -\frac{1}{2} \end{pmatrix}. \tag{40}$$

We have also a second $\mathbb{Q}$-equivalence which actually reduces Eq. (35) into integer form. Let $M(0\uparrow)$ be

$$m(0\uparrow) = \begin{pmatrix} 1 & 1 & 1 & 1 & 1 \\ -1 & 1 & 0 & 0 & 0 \\ -1 & 0 & 1 & 0 & 0 \\ -1 & 0 & 0 & 1 & 0 \\ -1 & 0 & 0 & 0 & 1 \end{pmatrix} \quad m(0\uparrow)^{-1} = \tfrac{1}{5}\begin{pmatrix} 1 & -1 & -1 & -1 & -1 \\ 1 & 4 & -1 & -1 & -1 \\ 1 & -1 & 4 & -1 & -1 \\ 1 & -1 & -1 & 4 & -1 \\ 1 & -1 & -1 & -1 & 4 \end{pmatrix} \tag{41}$$

then

$$m(0\uparrow)0\uparrow(g_5)m(0\uparrow)^{-1} = \begin{pmatrix} 1 & 0 & 0 & 0 & 0 \\ 0 & 0 & 0 & 0 & -1 \\ 0 & 1 & 0 & 0 & -1 \\ 0 & 0 & 1 & 0 & -1 \\ 0 & 0 & 0 & 1 & -1 \end{pmatrix}. \tag{42}$$

One cannot by $\mathbb{Q}$-equivalence reduce the matrix further. The significance of these forms will be seen when we consider the next section on space groups. We wish to pursue the extension to the group-subgroup chain $\mathcal{I} > \mathfrak{I}$. The regular representation $0(\mathfrak{I}\uparrow\mathcal{I})$ is also five-dimensional. Therefore similar arguments apply as for the previous $\mathcal{C}_5 > \mathcal{C}_1$ example. Indeed the matrices of Eqs. (35) and (37) can also be used. The generators of $\mathcal{I}$ have the permutational form given in Table XIII. Under $\mathbb{R}$-equivalence, the g_5-generator transforms identically into the form given by Eq. (38), however we combine the two two-dimensional representations. The reason will become apparent shortly. We have (remembering $0\uparrow \equiv 0(\mathfrak{I}\uparrow\mathcal{I})$

$$m(0\uparrow)0\uparrow(g_5)m(0\uparrow)^{-1} = 0(g_5) \oplus 3(g_5) \tag{43}$$

according to the reduction given in Table XII. The $\dot{g}_2$-generator takes a diagonal form (trivially a $0 \oplus 1 \oplus 2$ block form)

$$m(0\uparrow)0\uparrow(\dot{g}_2)m(0\uparrow)^{-1} = 0(\dot{g}_2) + 3(\dot{g}_2) \tag{44}$$

$$\text{where} \quad 0(\dot{g}_2) = +1, \quad 3(\dot{g}_2) = \text{diag}(1, -1, 1, -1).$$

What is not in the same $0 \oplus 1 \oplus 2$ block-form is the g_2-generator

$$m(0\uparrow)0\uparrow(g_2)m(0\uparrow)^{-1} = 0(g_2) \oplus 3(g_2) \tag{45}$$

$$\text{where} \quad 0(g_2) = +1 \quad \text{and} \quad 3(g_2) = \begin{pmatrix} 0 & 0 & 1 & 0 \\ 0 & \frac{4}{5} & 0 & -\frac{1}{5} \\ 1 & 0 & 0 & 0 \\ 0 & -\frac{1}{5} & 0 & -\frac{4}{5} \end{pmatrix}$$

and thus any other group elements containing g_2 in its product (see Table II). Hence we have an $\mathbb{R}$-reduction which reduces the regular representation of $[\mathcal{I}/\mathfrak{I}]$ into the irreps 0 and 3 of $\mathcal{I}$, and in addition reduces the matrix representation of the $\mathfrak{D}_5$ subgroup generated by g_5 and $\dot{g}_2$ into irreducibles over $\mathbb{R}$.

Under the $\mathbb{Q}$-equivalence matrix of Eq. (39) the g_5-generator transforms

identically to that in Eq. (40). The $\dot{g}_2$-generator has the form

$$m(0\uparrow)0\uparrow(\dot{g}_2)m(0\uparrow)^{-1} = \begin{pmatrix} 1 & 0 & 0 & 0 & 0 \\ 0 & 1 & 0 & 0 & 0 \\ 0 & 0 & -\frac{1}{3} & -\frac{2}{3} & -2 \\ 0 & 0 & -\frac{1}{3} & -\frac{2}{3} & 1 \\ 0 & 0 & -\frac{1}{3} & \frac{1}{3} & 0 \end{pmatrix} \tag{46}$$

while that of the g_2-generator has the similar form

$$m(0\uparrow)0\uparrow(g_2)m(0\uparrow)^{-1} = \begin{pmatrix} 1 & 0 & 0 & 0 & 0 \\ 0 & 1 & 0 & 0 & 0 \\ 0 & 0 & -\frac{1}{3} & -\frac{2}{3} & 2 \\ 0 & 0 & -\frac{1}{3} & -\frac{2}{3} & -1 \\ 0 & 0 & \frac{1}{3} & -\frac{1}{3} & 0 \end{pmatrix}. \tag{47}$$

As an icosahedral representation it has $\mathbb{Q}$-irreps of one and four dimensions, but in addition since the g_3-generator of the tetrahedral group has also the same block form as g_2 and $\dot{g}_2$, i.e. with ${}^3g_3 = g_5{}^{\mathfrak{I}}g_3g_5^{-1}$

$$m(0\uparrow)0\uparrow({}^3g_3)m(0\uparrow)^{-1} = \begin{pmatrix} 1 & 0 & 0 & 0 & 0 \\ 0 & 1 & 0 & 0 & 0 \\ 0 & 0 & -\frac{1}{3} & -\frac{2}{3} & 2 \\ 0 & 0 & -\frac{1}{3} & \frac{5}{6} & \frac{1}{2} \\ 0 & 0 & -\frac{1}{3} & -\frac{1}{6} & -\frac{1}{2} \end{pmatrix}. \tag{48a}$$

The tetrahedral subgroup is represented in this basis by a twice repeated identity irrep and a three dimension $\mathbb{Q}$-irrep.

The generators g_2 and $\dot{g}_2$ are invariant under $\mathbb{Q}$-equivalence by the matrix of Eq. (41), which thus gives us a particularly simple four-dimensional integral representation of $\mathfrak{I}$

$$3(g_5) = \begin{pmatrix} 0 & 0 & 0 & -1 \\ 1 & 0 & 0 & -1 \\ 0 & 1 & 0 & -1 \\ 0 & 0 & 1 & -1 \end{pmatrix} \quad 3(g_2) = \begin{pmatrix} 0 & 0 & 1 & 0 \\ 0 & 0 & 0 & 1 \\ 1 & 0 & 0 & 0 \\ 0 & 1 & 0 & 0 \end{pmatrix}$$

$$3(\dot{g}_2) = \begin{pmatrix} 0 & 0 & 0 & 1 \\ 0 & 0 & 1 & 0 \\ 0 & 1 & 0 & 0 \\ 1 & 0 & 0 & 0 \end{pmatrix}. \tag{48b}$$

In Haase *et al.* (1987) we have constructed and reduced the three induced representations of $[\mathfrak{I}/\mathfrak{D}_n]$ with $m = 5, 3, 2$. We had chosen the nontrivial

one-dimensional irrep $\tilde{0}(\mathfrak{D}_m)$ of each dihedral subgroup, and induced a $n = 30/m$ dimensional representation of $\mathfrak{I}$. As seen from Table XII, each contains in its reduced form the two inequivalent three-dimensional irreps 1 and $\tilde{1}$, which feature in the description of the quasilattices in $\mathbb{E}^3$. We delay a discussion on this point until the next section. However, we present in Table XV the reducing matrix for each of these based on the permutation representations given in Table XIV. It is important to note that in the case of the six-dimensional induced representation $\tilde{0}(\mathfrak{D}_5 \uparrow \mathfrak{I})$ there exists no $\mathbb{Q}$-equivalence matrix which decomposes this representation.

Table XV. Reducing matrices of various icosahedral representations.

$m(\tilde{0}\uparrow)$ of $\tilde{0}(D_5 \uparrow I)$:

$\mathbb{R}$-equivalence $\quad m(\tilde{0}\uparrow)\tilde{0}\uparrow(g)m(\tilde{0}\uparrow)^{-1} = 1(g) \oplus \tilde{1}(g)$

$$m(\tilde{0}\uparrow) = \frac{3-\tau}{10}\begin{pmatrix} 0 & -\tau & -1 & 1 & \tau & 0 \\ 1 & 0 & -\tau & -\tau & 0 & 1 \\ -\tau & -1 & 0 & 0 & -1 & \tau \\ 0 & 1 & -\tau & \tau & -1 & 0 \\ -\tau & 0 & -1 & -1 & 0 & \tau \\ 1 & -\tau & 0 & 0 & -\tau & 1 \end{pmatrix}$$

$$1(g_5) = \tfrac{1}{2}\begin{pmatrix} 1/\tau & -\tau & 1 \\ \tau & 1 & 1/\tau \\ -1 & 1/\tau & \tau \end{pmatrix} \qquad 1(g_2) = \begin{pmatrix} -1 & 0 & 0 \\ 0 & 1 & 0 \\ 0 & 0 & -1 \end{pmatrix}$$

$$\tilde{1}(g_5) = \tfrac{1}{2}\begin{pmatrix} -\tau & -1/\tau & 1 \\ 1/\tau & 1 & \tau \\ -1 & \tau & -1/\tau \end{pmatrix} \qquad \tilde{1}(g_2) = \begin{pmatrix} -1 & 0 & 0 \\ 0 & 1 & 0 \\ 0 & 0 & -1 \end{pmatrix}$$

$m(\tilde{0}\uparrow)$ of $\tilde{0}(D_3 \uparrow I)$:

$\mathbb{R}$-equivalence $\quad m(\tilde{0}\uparrow)\tilde{0}\uparrow(g)m(\tilde{0}\uparrow)^{-1} = 1(g) \oplus \tilde{1}(g) \oplus 3(g)$

$$m(\tilde{0}\uparrow) = \sqrt{\tfrac{1}{10}}\begin{pmatrix} 0 & -1 & -1/\tau & 1/\tau & 1 & 0 & -\tau & -1 & 1 & \tau \\ \tau & 1 & 0 & 0 & 1 & \tau & 1/\tau & -1 & -1 & 1/\tau \\ 1/\tau & 1 & \tau & \tau & 1 & -1/\tau & 0 & 1 & 1 & 0 \\ 0 & -1 & \tau & -\tau & 1 & 0 & 1/\tau & -1 & 1 & -1/\tau \\ 1/\tau & -1 & 0 & 0 & -1 & 1/\tau & \tau & 1 & 1 & \tau \\ -\tau & 1 & -1/\tau & -1/\tau & 1 & \tau & 0 & 1 & 1 & 0 \\ 1 & 1/\tau & 0 & 0 & -\tau & 1 & -1 & -1/\tau & \tau & -1 \\ 1 & -\tau & 0 & 0 & 1/\tau & 1 & -1 & \tau & -1/\tau & -1 \\ 1 & 1 & 0 & -2 & 0 & -1 & -1 & 1 & 0 & 1 \\ 1 & 0 & -2 & 0 & 1 & -1 & 1 & 0 & 1 & -1 \end{pmatrix}$$

Table XV continued overleaf

Table XV—*continued.*

$1(g)$ and $\tilde{1}(g)$ as above

$$3(g_5) = \tfrac{1}{2}\begin{pmatrix} -1 & 1/\tau & \tau & 0 \\ -\tau & -1 & -1/\tau & 0 \\ 0 & 0 & 0 & 1 \\ -1/\tau & \tau & -1 & 0 \end{pmatrix} \qquad 3(g_2) = \begin{pmatrix} 1 & 0 & 0 & 0 \\ 0 & 1 & 0 & 0 \\ 0 & 0 & -1 & 0 \\ 0 & 0 & 0 & -1 \end{pmatrix}$$

$\mathbb{R}$-equivalence $\quad m(\tilde{0}\uparrow)\tilde{0}\uparrow(g)m(\tilde{0}\uparrow)^{-1} = [1 \oplus \tilde{1}](g) \oplus 3(g)$

$$m(\tilde{0}\uparrow) = \tfrac{1}{2}\begin{pmatrix} 1 & 0 & 0 & 0 & 1 & 1 & 0 & -1 & 0 & 0 \\ 1 & 1 & 0 & 0 & 0 & 1 & 1 & 0 & -1 & 0 \\ 0 & 1 & 1 & 0 & 0 & 0 & 1 & 1 & 0 & -1 \\ 0 & 0 & 1 & 1 & 0 & -1 & 0 & 1 & 1 & 0 \\ 0 & 0 & 0 & 1 & 1 & 0 & -1 & 0 & 1 & 1 \\ 1 & 1 & 1 & 1 & 1 & 0 & 0 & 0 & 0 & 0 \\ -1 & 1 & 0 & 0 & 0 & -1 & 1 & -1 & 0 & 1 \\ -1 & 0 & 1 & 0 & 0 & 0 & 0 & 0 & -1 & 1 \\ -1 & 0 & 0 & 1 & 0 & 0 & 1 & -1 & 0 & 0 \\ -1 & 0 & 0 & 0 & 1 & -1 & 1 & 0 & -1 & 1 \end{pmatrix}$$

$[1 \oplus 1](g_5)$ and $3(g_5)$ as in Eqs. (42) and (48b) respectively

4 Space Group Concepts

The basic concepts of space groups, in particular to those in higher than three dimensions, can be found in more detail in Koster (1957), Brown *et al.* (1978), Schwarzenberger (1980), Michel and Mozrzymas (1985). We give a brief summary here.

Our structures are described in an n-dimensional Euclidean space $\mathbb{E}^n$ with an associated vector space V^n with vectors $\mathbf{x}$ which can be defined with respect to an origin, a point in $\mathbb{E}^n$, and an orthonormal set of vectors $\mathbf{e}_1 \cdots \mathbf{e}_n$ called an orthonormal basis of V^n. We write

$$\mathbf{x} = \sum \mathbf{e}_i x_i \tag{49}$$

where $(x_1, \ldots, x_n)$ is the coordinate vector of $\mathbf{x}$. An affine mapping of V^n into itself is the pair $(F, \mathbf{t})$ with F an $n \times n$ matrix and $\mathbf{t} \in V^n$. The image of $\mathbf{x}$ under $(F, \mathbf{t})$ is

$$\mathbf{x} \to (F, \mathbf{t})\mathbf{x} = F\mathbf{x} + \mathbf{t}. \tag{50}$$

The unit element is then $(\mathbb{1}, \mathbf{0})$.

The composition law of two such operators is

$$(F_1, \mathbf{t}_1)(F_2, \mathbf{t}_2) = (F_1F_2, \mathbf{t}_1 + F_1\mathbf{t}_2). \tag{51}$$

By a discrete structure in $\mathbb{E}^n$ we mean a subset of $\mathbb{E}^n$ consisting of infinitely many discrete points homogeneously distributed with neighboring points at least some minimum distance away. This structure is called crystallographic if there exist affine mappings $(F, \mathbf{t})$ that

(i) map the structure into itself,
(ii) are isometric, hence $F \in O(n, \mathbb{R})$, and
(iii) contain n linearly independent translation vectors with magnitude larger than or equal to some fixed real number. The appearance of translation vectors implies an infinite periodic extension of the crystallographic structure (CS).

The set of mappings leaving CS invariant forms a group called the space group S of CS. Two immediate properties of the space group are apparent:

(i) all pure translational elements of form $(F, \mathbf{t})$ which leave CS invariant form a normal invariant subgroup called the translation subgroup T of CS, and
(ii) all pure isometric elements $(F, \mathbf{0})$ which leave CS invariant form a finite discrete subgroup called the point group P of CS.

The factor group S/T is a discrete subset of S which contains P as a subgroup. Its elements are of the form $(F, \mathbf{t}_F)$ where each F has a corresponding translation vector $\mathbf{t}_F \notin T$, although it may be $\mathbf{0}$. The composition law of S/T is closed only under modular T. In the case, $S/T = P$, S is called symmorphic otherwise asymmorphic.

The image under T of a vector $\mathbf{x} \in$ CS yields a subset called the lattice L of CS. The crystallographic restriction implies that there exists a set of n vectors $\{\mathbf{b}_1, \ldots, \mathbf{b}_n\}$ spanning V^n, called the lattice basis such that any element of T can be written as an integral linear combination of the lattice basis

$$\mathbf{t} = \sum \mathbf{b}_i \tilde{t}_i \qquad \tilde{t}_i \in Z. \tag{52}$$

Under $(F, \mathbf{t}_F)$ of S/T any vector of the lattice, say $\mathbf{x} + \mathbf{t}$, yields a vector in CS

$$(F, \mathbf{t}_F)(\mathbf{x} + \mathbf{t}) = F\mathbf{x} + F\mathbf{t} + \mathbf{t}_F = (F, \mathbf{t}_F + F\mathbf{t}) \cdot \mathbf{x}. \tag{53}$$

The vector $F\mathbf{t}$ is a pure translation vector which can be written in terms of the lattice basis as

$$F\mathbf{t} = F(\sum \mathbf{b}_i \tilde{t}_i) = \sum (F\mathbf{b}_i)\tilde{t}_i = \sum_{j,i} \mathbf{b}_j (F_{ji}\tilde{t}_i). \tag{54}$$

That is to say, the isometric mapping acts on the pure translation coordinates with respect to the lattice basis as a matrix transformation

$$\tilde{t}_j \to \sum_i \tilde{F}_{ji} \tilde{t}_i \tag{55}$$

where $\tilde{F}$ belongs to the group $GL(n, \mathbb{Z})$. Expressing the lattice basis in terms of the orthogonal basis

$$\mathbf{b}_i = \sum \mathbf{e}_j b_{ji} \qquad i = 1, \ldots, n, \qquad B = (b_{ij}) \tag{56}$$

the crystallographic restriction gives

$$\begin{aligned} B\tilde{F}B^{-1} &= F \in O(n, \mathbb{R}) \\ B^{-1}FB &= \tilde{F} \in GL(n, \mathbb{Z}). \end{aligned} \tag{57}$$

Consider now an isometric transformation of the coordinate basis of V^n:

$$\mathbf{e}_i' = \sum \mathbf{e}_j V_{ji} \qquad V \in O(n, \mathbb{R}). \tag{58}$$

The elements of S transform under the equivalence map as

$$(V, \mathbf{0})(F, \mathbf{t})(V, \mathbf{0})^{-1} = (VFV^{-1}, V\mathbf{t}) = (F', \mathbf{t}') \tag{59}$$

and changes the description of the lattice basis

$$b_{ji} \to b_{ji}' = V_{jk}^{-1} b_{ki}. \tag{60}$$

However the description of $\mathbf{t}$ in terms of the lattice basis remains unchanged, as well as the integer matrix $\tilde{F}$. If V also reduces the matrices F into the form

$$VFV^{-1} = F_1 \oplus F_2 \tag{61}$$

where $F_1 \in O(n_1, \mathbb{R})$ $F_2 \in O(n_2, \mathbb{R})$ $(n_1 + n_2 = n)$ then S decomposes into two space subgroups S_1 and S_2 acting on subspaces V^{n_1} and V^{n_2} respectively. We write $S_1 \oplus S_2$.

The nature of the space subgroups S_1 and S_2 depends on S/T. These subgroups may contain subtranslational elements—the subgroups are sometimes then called subperiodic crystallographic groups—or they may not in which case they are called crystallographic point group. The icosahedral space groups display this behaviour very clearly. In the last section we have constructed various representations which are orthogonal representations although taking integral form. We have also found reducing matrices both over $\mathbb{R}$ and $\mathbb{Q}$ which decompose these representations. The property that a space subgroup contains translational elements can be expressed as follows (see Lu and Birman, 1987; note that they take a more expansive meaning of the term lattice):

(i) If the space group is $\mathbb{Q}$-decomposable into $S_1 \oplus S_2$, the lattices generated by the subtranslational elements of the subspaces V^{n_1}, V^{n_2} are periodic.
(ii) If the space group is $\mathbb{R}$-decomposable but $\mathbb{Q}$-indecomposable, the lattices of the subspaces are aperiodic.

From these statements we see that the five-dimensional $0(\mathfrak{I}\uparrow\mathfrak{I})$ is $\mathbb{Q}$-decomposable into one- and four-dimensional subspaces and therefore supports periodic sublattices. If we restrict our attention to the subgroup $\mathfrak{D}_5 < \mathfrak{I}$ the four-dimensional subspace is further $\mathbb{R}$-decomposable into two-dimensional subspaces but is not $\mathbb{Q}$-decomposable. The two-dimensional subspaces support the Penrose quasilattice (Penrose, 1979). The six-dimensional representation $\tilde{0}(\mathfrak{D}_5\uparrow\mathfrak{I})$ exhibits the same property of the four-dimensional case of $\mathfrak{D}_5$. There does not exist a $\mathbb{Q}$-equivalence that reduces the isometric component of S. The $\mathbb{R}$-equivalence given in Table XV decomposes the space group into two point subgroups. The sublattices in three-dimensions support no translational symmetry as demonstrated by Kramer and Neri (1984). All the other higher dimensional representations constructed in Section 3 are seen to be both $\mathbb{Q}$- and $\mathbb{R}$-decomposable. The $\mathbb{Q}$-equivalence in these cases yields a six-dimensional subspace which by similar arguments to the above Kramer–Neri example is $\mathbb{Q}$-irreducible.

Instead of transforming the coordinate basis we consider a change of lattice basis

$$\mathbf{b}_i' = \mathbf{b}_j M_{ji}.$$

The coordinates of the pure translations with respect to the new lattice basis is

$$\tilde{t}_i \to \tilde{t}_i' = M_{ij}^{-1}\tilde{t}_j$$

and the integral matrix F transforms into

$$\tilde{F} \to \tilde{F}' = M^{-1}\tilde{F}M.$$

If $\tilde{t}_i'$ is to be integer, M^{-1} must have integer entries although M^{-1} need not be in $GL(n, \mathbb{Z})$. Also if $\tilde{F}'$ is to be integral, M is at most in $GL(n, \mathbb{Q})$.

The icosahedral induced representations of Section 3 provide illustration of this point. The integral representations can be thought of as acting on a hypercubic lattice in V^n. The reducing matrices over $\mathbb{Q}$ in Table XV give a redescription of the lattice in terms of a second lattice basis. In the case of $0(\mathfrak{I}\uparrow\mathfrak{I})$ and $\tilde{0}(\mathfrak{D}_3\uparrow\mathfrak{I})$, the $\mathbb{Q}$-equivalence yields in addition a reduction of the integral representation into two integral subrepresentations, the former into one- and four-dimensional $\mathbb{Z}$-irreps and the latter into six- and four-dimensional $\mathbb{Z}$-irreps. The $\mathbb{Z}$-irrep content of $\tilde{0}(\mathfrak{D}_2\uparrow\mathfrak{I})$ are of six-, five- and

four-dimensions although the reducing matrix has not been given. The three different six-dimensional integral representations provided by $\tilde{0}(\mathfrak{D}_5\uparrow\mathfrak{I})$, $\tilde{0}(\mathfrak{D}_3\uparrow\mathfrak{I})$ and $\tilde{0}(\mathfrak{D}_2\uparrow\mathfrak{I})$ correspond to the simple, faced-centred and body-centred cubic lattices that have been given particular attention in the literature (see Rokhsar and Mermin, 1987).

In these examples one can see the interplay between the appearance of rational and irrational numbers on the one hand, and the periodicity and non-periodicity of the lattice on the other. For example the only matrix which can reduce the five-fold generator of $\tilde{0}(\mathfrak{D}_5\uparrow\mathfrak{I})$ contains irrational number τ, the three-dimensional $\mathbb{R}$-irrep of g_5 takes an irrational form

$$\begin{pmatrix} \tau/2 & \sqrt{2-\tau} & 0 \\ -\sqrt{2-\tau} & \tau/2 & 0 \\ 0 & 0 & 1 \end{pmatrix} \tag{62}$$

which acts on the integral components of $\mathbf{t} \in T$ giving

$$\begin{pmatrix} \frac{1}{2}\tau t_1 + \sqrt{2-\tau}\, t_2 \\ -\sqrt{2-\tau}\, t_1 + \frac{1}{2}\tau t_2 \\ t_3 \end{pmatrix}$$

The irrational components cannot be put into integral form and hence three-dimensional translational symmetry cannot be compatible with icosahedral or other point groups containing five-fold symmetry.

5 Stars and Polytopes

So far we have constructed various representations of the icosahedral point group and space groups, emphasizing in particular induced representations of high dimensions and reducing them into irreps under $\mathbb{R}$- and $\mathbb{Q}$-equivalence transformations. It is natural to expect that if the representation spaces are real Euclidean spaces and contain a three-dimensional subspace, then this allows for a geometric and crystallographic analysis. This analysis will be taken up in this section beginning with a definition of stars and their properties, and the construction and classification of polytopes from these stars. The geometric concepts are to be found in Coxeter (1963); the discussion follows Haase *et al.* (1987).

Definition: An n-star in $\mathbb{E}^m$ with $n > m$ is a set of n vectors

$$\mathbb{S} \equiv \{\mathbf{s}_a \in \mathbb{E}^m \quad a = 1, \ldots, n\} \tag{63}$$

such that there is a subset of m vectors spanning $\mathbb{E}^m$.

Definition: An n-line system associated with this star is the collection of n-lines, each line given by

$$\mathbf{l}_a \equiv \tfrac{1}{2}\mathbf{s}_a\sigma_a \qquad -1 \le \sigma_a \le +1 \qquad a = 1, \ldots, n. \tag{64}$$

The n-line system has a common endpoint, the origin. We can associate a polytope with each line system.

Definition: The polytope $\mathcal{K}(n)$ in $\mathbb{E}^m$ associated with the n-line system is the convex set of points

$$\mathcal{K}(n) \equiv \left\{\mathbf{x} \,|\, \mathbf{x} = \frac{1}{2}\sum_{a=1}^{n} \mathbf{s}_a\sigma_a \quad -1 \le \sigma_b \le +1 \quad b = 1, \ldots, n\right\}. \tag{65}$$

The vector sum leads to a set of points not necessarily distinct which lie on the surface or inside the polytope. The edges are translations of the n-lines into various extremal positions. The vertices are obtained by considering a plane through the origin in any general direction. The vector sum of those $\mathbf{s}_a$ lying to one side of the plane is the vector leading to a vertex of $\mathcal{K}(n)$. In general the polytope will be a convex shape displaying the same symmetry as its n-line system. The above definition of the n-line system already imposes central symmetry which is inherited by $\mathcal{K}(n)$. In general polytopes are bounded by parallel-sided $2q$-gons. This can be seen from the polytope $\mathcal{K}(n)$ in $\mathbb{E}^2$. This is a polygon with $\binom{n}{1} = n$ pairs of parallel edges. For each vector $\mathbf{s}_a$, the edges are

$$\mathcal{F}_{\pm}(a) \equiv \{\mathbf{x} \,|\, \mathbf{x} = \pm\mathbf{y}(a) + \tfrac{1}{2}\mathbf{s}_a\sigma_a, \quad -1 \le \sigma_b \le +1\} \tag{66}$$

where $\mathbf{y}(a) \equiv \frac{1}{2}\sum_{b=1}^{n} \text{sign}\,[\det(\mathbf{s}_a\,\mathbf{s}_b)]\mathbf{s}_b$.

In $\mathbb{E}^3$, the polytope $\mathcal{K}(n)$ is a polyhedron with pairs of parallel polygon faces. For any plane defined by coplanar vectors $\{\mathbf{s}_{a_1}, \ldots, \mathbf{s}_{a_q}\}$ there are two faces

$$\mathcal{F}_{\pm}(a_1 \cdots a_q) \equiv \left\{\mathbf{x} \,|\, \mathbf{x} = \pm\mathbf{y}(a_1 \cdots a_q) + \frac{1}{2}\sum_{i=1}^{n} \mathbf{s}_{a_i}\sigma_{a_i} \quad -1 \le \sigma_b \le +1\right\} \tag{67}$$

where $\mathbf{y}(a_1 \cdots a_q) = \frac{1}{2}\sum_{b=1}^{n} \text{sign}\,[\det(\mathbf{s}_{a_1}\mathbf{s}_{a_2}\mathbf{s}_b)]\mathbf{s}_b$. The numbers of different planes gives the number of pairs of faces. If f_q is the number of different $2q$-gon faces, then these satisfy the Fedorov expression

$$\binom{n}{2} = \frac{1}{2}\sum_{q}\binom{q}{2}f_q. \tag{68}$$

Examples in $\mathbb{E}^3$ can be obtained by taking as n-line systems lines joining opposite vertices of the following polyhedra:

star S	polytope $\mathcal{HC}(n)$:
octahedron	cube
cube	rhombic dodecahedron
icosahedron	triacontrahedron
dodecahedron	rhombic enneacontrahedron
icosidodecahedron	truncated icosidodecahedron

Hadwiger (1940) has shown under which circumstances $\mathcal{S}$ in $\mathbb{E}^m$ can be considered as a projection from the Cartesian frame—a star in $\mathbb{E}^n$ of n orthonormal unit vectors

$$\mathcal{S}_n^+ \equiv \{\mathbf{e}_a \in \mathbb{E}^n \mid \mathbf{e}_a \cdot \mathbf{e}_b = \delta_{ab} \quad a, b = 1, \ldots, n\}. \tag{69}$$

For any given star, one defines the linear operator

$$P \equiv \sum_{a=1}^{n} \mathbf{s}_a \mathbf{s}_a^T \tag{70}$$

which is geometrically a projection operator. The theorem states: The star $\mathcal{S} \in \mathbb{E}^m$ is an orthogonal projection from $\mathcal{S}_n^+ \in \mathbb{E}^n$ if an only if $P\mathbf{x} = \lambda\mathbf{x}$ for all $\mathbf{x} \in \mathbb{E}^m$ where λ is a real number constant for all vectors $\mathbf{x}$. Coxeter proves for symmetric line systems: The line system in $\mathbb{E}^3$ having octahedral or icosahedral symmetry is an orthogonal projection from the line system of $\mathcal{S}_n^+$. Specific examples in $\mathbb{E}^3$, where the line systems are diagonal connecting vertices of certain polyhedra, are tabulated below.

Line systems in $\mathbb{E}^3$ as projections from line systems of $\mathcal{S}_n^+$

octahedron	$\mathcal{S}_3^+$
cube	$\mathcal{S}_4^+$
cuboctahedron	$\mathcal{S}_6^+$
icosahedron	$\mathcal{S}_6^+$
rhombic dodecahedron	$\mathcal{S}_7^+$
pentagonal dodecahedron	$\mathcal{S}_{10}^+$
icosidodecahedron	$\mathcal{S}_{15}^+$
triacontrahedron	$\mathcal{S}_{16}^+$

Hence to combine the above results, we have the following interconnections:

$$\begin{array}{ccc} \mathcal{S}_n^+ \in \mathbb{E}^n & \longrightarrow & \mathcal{HC}^+(n) \in \mathbb{E}^n \\ \downarrow \text{projection} & & \downarrow \text{projection} \\ \mathcal{S} \in \mathbb{E}^m & \longrightarrow & \mathcal{HC}(m) \in \mathbb{E}^m \end{array}$$

where $\mathcal{HC}^+(n)$ is easily recognised as the hypercube in $\mathbb{E}^n$. It can be shown

that any octahedrally or icosahedrally symmetric polyhedron in $\mathbb{E}^3$ is a projection of a hypercube in some $\mathbb{E}^n$.

Various other polytopes can be constructed from an n-line system. Instead of taking all n-lines, one partitions the system into two—called a p-line and $(n-p)$-line subsystem. Treating these separately in the same manner as its parent n-line system, one can construct polytopes $\mathcal{K}(n, p)$ and $\mathcal{K}(n, n-p)$. If the parent n-line system has a symmetry group, G say, we can use the orbit analysis of $[G/H]_p^n$, where H is the stability group of one line, to classify in a group theoretical manner all p-line subsystems and hence the corresponding polytopes $\mathcal{K}(n, p) \mid < p < n$ and their geometric features. This analysis was performed in Haase *et al.* (1987) for the cases $\mathcal{S}_6^+$, $\mathcal{S}_{10}^+$ and $\mathcal{S}_{15}^+$ icosahedrally projected in $\mathbb{E}^3$. The orbit analysis of $[\mathcal{I}/\mathcal{T}]_p^5$ in Table V indicates that in $\mathbb{E}^4$ we have two polytopes, classifications (01234) and (1234), with one type of three-dimensional boundary, (234), and one rhombus face type (01).

The construction $\mathcal{K}(n, p)$ can be thought of in a different way. By removing all edges from $\mathcal{K}(n)$ not parallel to one of the p-lines contained in the chosen p-line subsystem, and then collapsing together all remaining disjoint sections of $\mathcal{K}(n)$, one forms the polytope $\mathcal{K}(n, p)$ corresponding to the p-line subsystem. One can perform this for all the $\sum_{p=1}^{n} \binom{n}{p}$ possible ways of selecting p-line subsystem. Repetition of polytopes exists if a symmetry group appears for the n-line system. Resolution of these repetitions is given by the aforementioned orbit analysis.

The symmetry group of the n-line system of $\mathcal{S}_n^+$ and the hypercube in $\mathbb{E}^n$ is the hyperoctahedral group $\Omega(n)$. As we have seen in the earlier sections, it features prominently when we constructed integral induced representations. To conclude this section we combine the various geometric results with the earlier algebraic results. The procedure can be summarized as follows:

(i) One finds for a group G an integer representation of order n either by induction, subduction or coupling (or even a mixture of these methods). If the representation is of permutational form (one non-zero entry in each row and column) it may be embedded in the hyperoctahedral group $\Omega(n)$.
(ii) The basis vectors in $\mathbb{E}^n$ form the star $\mathcal{S}_n^+$ which under character projection by G determines a star $\mathcal{S} \in \mathbb{E}^m$, and its associated n-line system.
(iii) An orbit analysis of the n-line system classifies all subsystems and hence all polytopes constructed from the inequivalent p-line subsystems.

The procedure has been illustrated in Haase *et al.* (1987) for $\tilde{0}(\mathcal{D}_q \uparrow \mathcal{I})$ $q = 5, 3, 2$. The representation space is of dimension $60/2q$, and the projected subspace belongs to the three-dimensional irrep $1(\mathcal{I})$. The largest

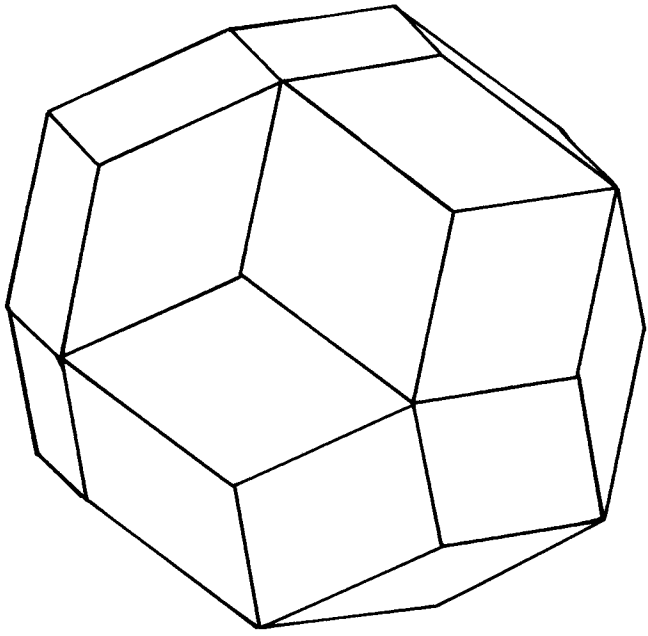

Figure 5. Triacontrahedron (32, 60, 30).

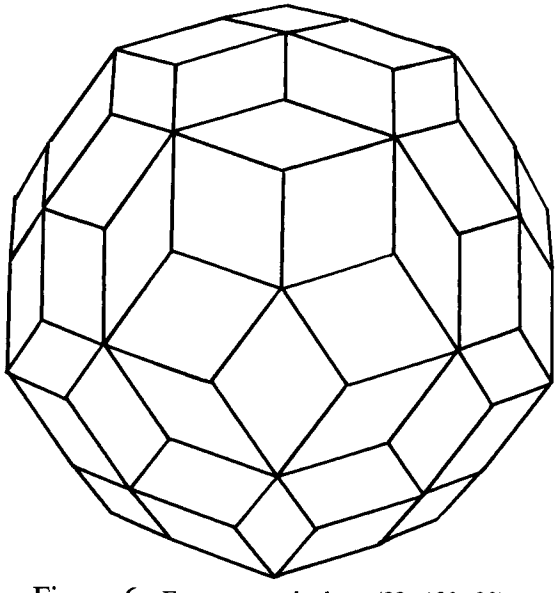

Figure 6. Enneacontrahedron (92, 180, 90).

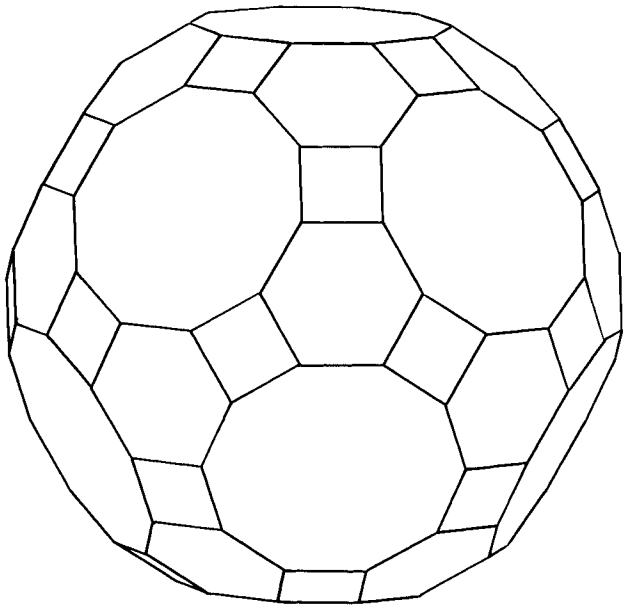

Figure 7. Truncated icosidodecadron (120, 180, 62).

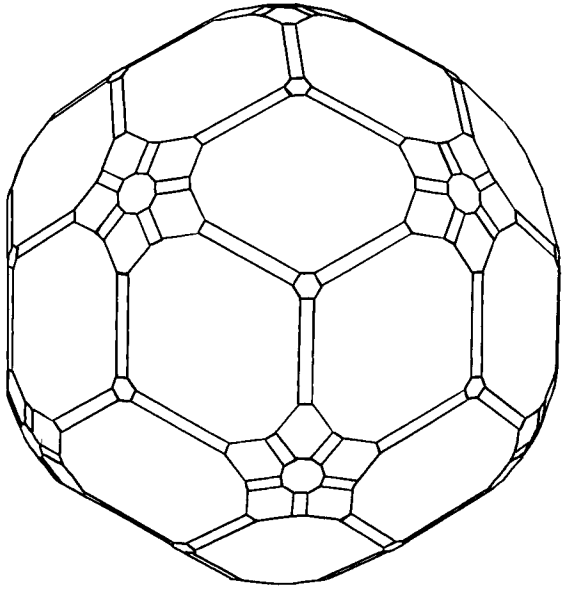

Figure 8. Polyhedron (476, 720, 242).

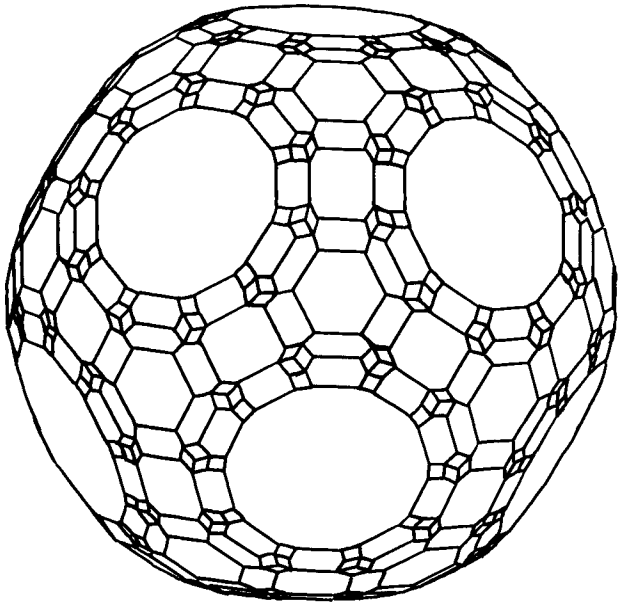

Figure 9. Polyhedron (960, 1740, 782).

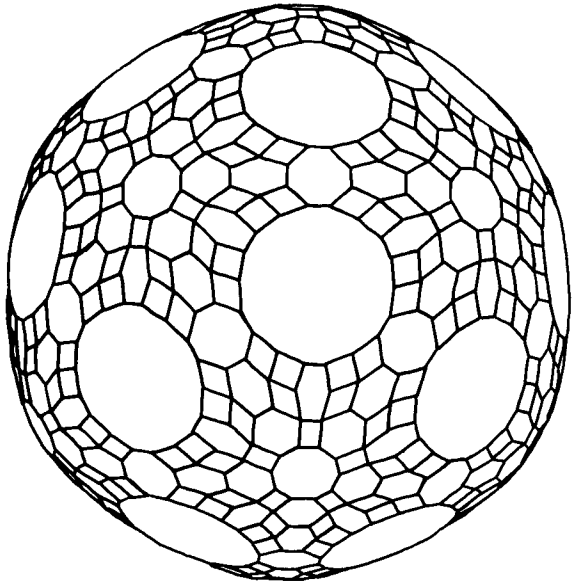

Figure 10. Polyhedron (1200, 1980, 782).

polyhedra displaying the icosahedral group symmetry are given in Figs. 5, 6 and 7. In addition we give polyhedra displaying more complex faceting see Figs. 8–10. These were obtained by anti-symmetrized couplings of the induced representations $\tilde{0}(\mathfrak{D}_q \uparrow \mathfrak{I})$ $q = 5, 3, 2$. They are projections of the hypercube in $\mathbb{E}^n$ with $n = 45$, 105 and 20.

With the observed triacontrahedral shapes of the $Al_6Li\,Cu_3$ quasicrystal grains and the dodecahedral shapes in the *i*-phase of Al-Mn-Si, the phenomenon of facet formation and growth among these quasicrystal structures is of particular interest. It is usually thought that translational order gives rise to facets. However this feature is lacking in quasicrystals. The growth facets and equilibrium shapes of crystals are usually obtained by the Wulff construction which is the polyhedra bounded by the faces of lowest free surface energy. The largest growth facets are those with smallest growth rates. An analysis on quasicrystalline equilibrium shapes has been given by Ho *et al.* (1987). The polyhedral equilibrium shapes correspond to those obtained here as projections.

6 Cells and Quasilattices

In this section we describe a method which allows one to obtain from a periodic lattice Y in $\mathbb{E}^n$ a non-periodic quasilattice in $\mathbb{E}^m$, $m < n$. This construction applies in particular to the icosahedral quasilattice in $\mathbb{E}^3$ obtained from the hypercubic lattice Y in $\mathbb{E}^6$.

The method is based on dualization and intersection in $\mathbb{E}^n$. Its geometric content can be seen from the example of the square lattice Y of edge length l in $\mathbb{E}^2$. Its square cells are bounded by edges and vertices. Define a dual lattice Y^* in $\mathbb{E}^2$ whose cell centers are located at the vertices of Y. The cells and cell boundaries appear as local dual pairs formed from a cell and a vertex, two edges, or a vertex and a cell from Y and Y^* respectively. Dual boundaries have complementary dimension, intersect in a single point $\mathbf{q}$ and are spanned, with respect to this point, by mutually orthogonal (sets of) vectors. Let $\mathbb{E}_1^\perp$ be a line in $\mathbb{E}^2$ of slope $\tan\alpha$ and $\mathbb{E}_2^\perp$ its orthogonal complement. The line intersects with edges of Y, and one can mark the edges of Y^* dual to these intersected edges. These dual edges form a continuous sequence of lines, compare Fig. 11. Moreover, the projections of these dual edges to the intersecting line form a tiling of this line into segments of length $\cos\alpha$ and $\sin\alpha$ respectively.

The tiling property can be seen in Fig. 11, but it is by no means obvious from the prescription given. A geometric proof can be given by the construction of epicells, compare Kramer (1987c): For each dual pair of edges, construct a new cell of dimension 2, called an epicell and centered at $\mathbf{q}$, with the property that its orthogonal projections to $\mathbb{E}_2^\perp$ and $\mathbb{E}_1^\perp$ coincides with the

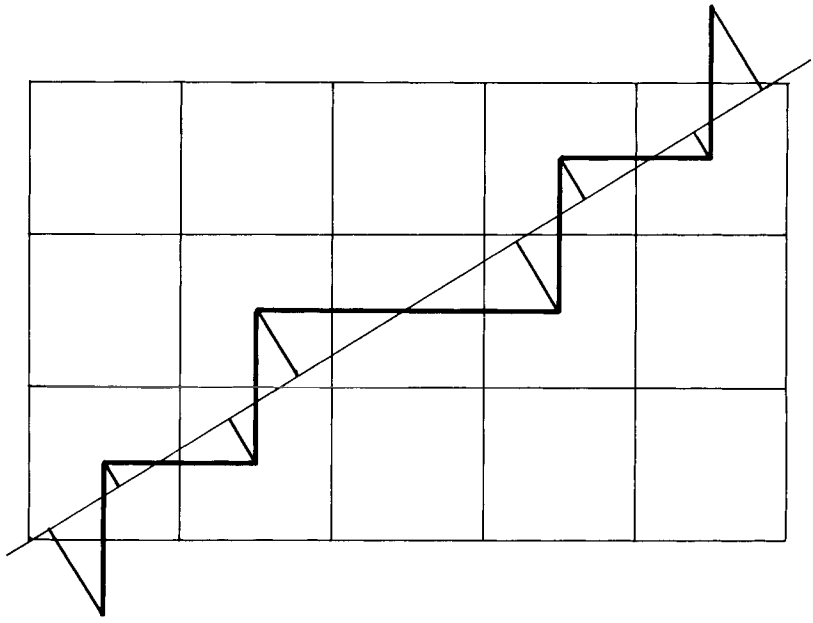

Figure 11. The method of dualization and intersection. The square lattice Y in the plane intersects with a line of slope $\tan \alpha$. If the line intersects with an edge from a cell of Y, the edge from the dual lattice Y* is marked as a heavy line. The dual edges form a continuous line, and their projections to the intersecting line form a non-periodic tiling with tiles of length $\sin \alpha$ and $\cos \alpha$.

corresponding projections of the edges from Y and Y^* respectively. As shown in Fig. 12, there are two types of epicells which are squares of edge length $\cos \alpha$ or $\sin \alpha$, each with two boundaries parallel to $\mathbb{E}_2^1$ and two boundaries parallel to $\mathbb{E}_1^1$. Two different squares can be used to replace the former unit cell of Y, and so the translated copies of these two representatives tile $\mathbb{E}^2$ periodically. If now the line $\mathbb{E}_1^1$ intersects with the new cells, the intersections clearly must form a tiling with tiles of length $\cos \alpha$ and $\sin \alpha$ respectively. For irrational $\tan \alpha$, this tiling is non-periodic.

To treat the hypercubic lattice Y in $\mathbb{E}^6$ in the same manner, we use algebraic expressions for the boundaries. The epicell construction is described in Section 9. Here we consider the pairs of dual boundaries of dimension $p = 3$ and located at the point $\mathbf{q}$ in $\mathbb{E}^6$.

6.1 Definition: For the hypercubic lattice Y spanned by $\mathbf{b}_1, \ldots, \mathbf{b}_6$ and its dual Y^*, let $l \to r(l)$ be a permutation of $1, \ldots, 6$, $\varepsilon = \pm 1$ and define the

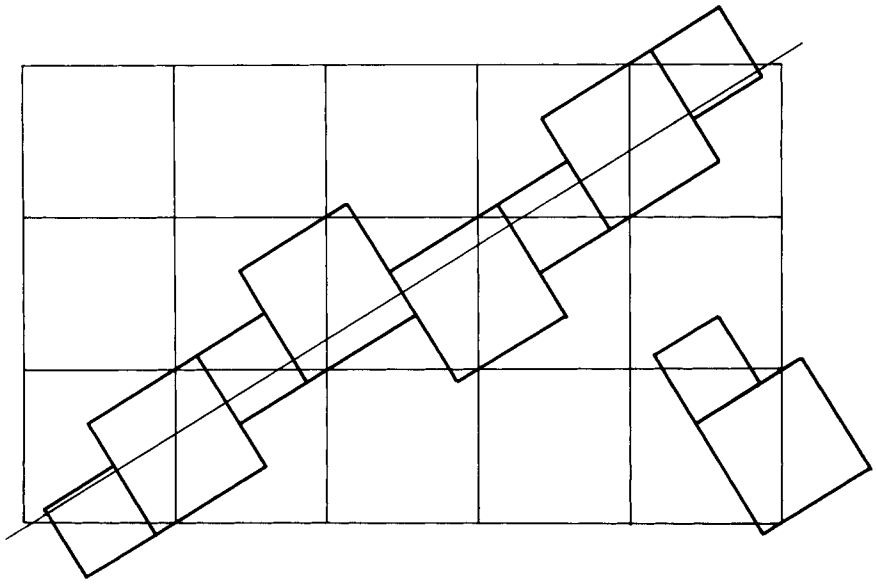

Figure 12. The method of epicells. The square unit cell of the lattice Y is replaced by two squares, called epicells, of edge length $\sin\alpha$ and $\cos\alpha$ respectively. This replacement is illustrated in the lower right-hand part. The boundaries of the epicells are parallel or perpendicular to the intersecting line. The sequence of intersections of the line with the periodic tiling provided by the epicells yields a non-periodic tiling of the line which is identical with the one obtained by dualization and intersection.

pair of dual 3-boundaries

$$h(3;\mathbf{q}) = \left\{\mathbf{y} \mid \mathbf{y}\frac{1}{2}\sum_{i=1}^{3}\lambda_{r(i)}\varepsilon_{r(i)}\mathbf{b}_{r(i)} + \frac{1}{2}\sum_{j=4}^{6}\varepsilon_{r(j)}\mathbf{b}_{r(j)} + \sum_{l=1}^{6} n_{r(l)}\varepsilon_{r(l)}\mathbf{b}_{r(l)}\right\} \tag{71}$$

$$h^*(3;q) = \left\{\mathbf{y} \mid \mathbf{y} = \frac{1}{2}\sum_{j=1}^{4}(1+\lambda_{r(j)})\varepsilon_{r(j)}\mathbf{b}_{r(j)} + \sum_{l=1}^{6} n_{r(l)}\varepsilon_{r(l)}\mathbf{b}_{r(l)}\right\},$$

$$-1 < \lambda_1 \leq 1, \qquad n_{r(l)} \in Z. \tag{72}$$

The points of $h(3;\mathbf{q})$ can be characterized by the inequalities

$$h(3;\mathbf{q})\colon \mathbf{y}\cdot\varepsilon_{r(j)}\mathbf{b}_{r(j)} = \tfrac{1}{2}(2n_{r(j)}+1), \qquad j = 4,5,6$$

$$\tfrac{1}{2}(2n_i - 1) < \mathbf{y}\cdot\varepsilon_{r(i)}\mathbf{b}_{r(i)} \leq \tfrac{1}{2}(2n_{r(i)}+1), \qquad i = 1,2,3. \tag{73}$$

Now decompose $\mathbb{E}^6$ as

$$\mathbb{E}^6 \to \mathbb{E}_1^3 + \mathbb{E}_2^3, \qquad \mathbb{E}_1^3 \perp \mathbb{E}_2^3 \tag{74}$$

into subspaces which carry the irreducible representations $[31_+^2]$ and $[31_-^2]$ of $\mathfrak{I}$. The subscripts 1 and 2 are used to denote the orthogonal projections to these two subspaces. Let $\mathbf{c}_2$ denote a fixed vector from $\mathbb{E}_2^3$ and consider the points

$$\mathbf{y} = \mathbf{c}_2 + \mathbf{x}_1 . \tag{75}$$

Define

$$\gamma_{r(l)} = \mathbf{c}_2 \cdot \mathbf{b}_{r(l)2} . \tag{76}$$

Then the condition that $\mathbf{y}$ be a point of $h(3; \mathbf{q})$ takes the form

$$\begin{aligned} \mathbf{x}_1 \cdot \varepsilon_{r(j)} \mathbf{b}_{r(j)1} + \gamma_{r(j)} &= \tfrac{1}{2}(2n_{r(j)} + 1), \qquad j = 4, 5, 6 \\ \tfrac{1}{2}(2n_i - 1) &< \mathbf{x}_1 \cdot \varepsilon_{r(i)} \mathbf{b}_{r(i)1} + \gamma_{r(i)} < \tfrac{1}{2}(2n_{r(i)} + 1), \\ i &= 1, 2, 3. \end{aligned} \tag{77}$$

These equations in $\mathbb{E}_1^3$ have an interpretation in terms of a 6-grid with the constants $\gamma_{r(i)}$ being shift parameters: The first three equations require that the point $\mathbf{x}_1$ is on the intersection of three planes which are perpendicular to $\varepsilon_{r(j)} \mathbf{b}_{r(j)1}, j = 4, 5, 6$; the last three equations require that $\mathbf{x}_1$ be between parallel planes which are perpendicular to $\varepsilon_{r(i)} \mathbf{b}_{r(i)1}$, $i = 1, 2, 3$.

If we follow now the dualization-and-intersection-method in $\mathbb{E}^6$, we construct, in case $\mathbf{y} = \mathbf{c}_2 + \mathbf{x}_1$ intersects with $h(3; \mathbf{q})$, the dual boundary $h^*(3; \mathbf{q})$ and project it to the subspace $\mathbb{E}_1^3$. This projection has the points

$$\mathbf{y}_1 = \frac{1}{2} \sum_{j=4}^{6} (1 + \lambda_{r(j)}) \varepsilon_{r(j)} \mathbf{b}_{r(j)1} + \sum_{l=1}^{6} n_{r(l)} \varepsilon_{r(l)} \mathbf{b}_{r(l)1} . \tag{78}$$

Clearly this projection is a rhombohedron spanned by the vectors $\varepsilon_{r(j)} \mathbf{b}_{r(j)1}$, $j = 4, 5, 6$, and it is precisely the rhombohedron which would result from the dualization in $\mathbb{E}_1^3$ of the 6-grid described in Kramer and Neri (1984) and in Kramer (1985, 1986b). Note however that this dualization lacks all the metrical properties associated with dualization in the space $\mathbb{E}^6$ and based on Y and Y^*.

6.2 Proposition: *The dualization and intersection in $\mathbb{E}^6$ based on pairs of dual boundaries $h(3; \mathbf{q})$ and $h^*(3; \mathbf{q})$ from Y and Y^* yields the same equations as the dualization method in $\mathbb{E}_1^3$.*

Note that the equations given in $\mathbb{E}_1^3$ provide a constructive way for generating a quasilattice. The equations for $j = 4, 5, 6$ determine a unique

vector $\mathbf{x}_1$ for any set of integers $n_{r(4)}$, $n_{r(5)}$, $n_{r(6)}$. With this value of $\mathbf{x}_1$, the numbers $n_{r(1)}$, $n_{r(2)}$, $n_{r(3)}$ may be determined from the equations with $i = 1, 2, 3$. This fixes a rhombohedral cell spanned by the vectors $\varepsilon_{r(j)}\mathbf{b}_{r(j)1}$, $j = 4, 5, 6$. Variation of the integers $n_{r(j)}$ yields all rhombohedral cells of this shape in parallel positions. In the next step one chooses a new permutation $l \to r(l)$ and generates a new type of rhombohedra in parallel positions. This process is repeated with the thick and the thin rhombohedral cell each in 10 possible orientations, corresponding to the 10 cosets $\mathfrak{I}/\mathfrak{D}_3$. Here, the subgroup $\mathfrak{D}_3$ is the stability group of the three basis vectors defining the rhombohedron.

The icosahedral quasilattice has a layer structure which is illustrated in Fig. 13. Infinite parallel layers occur in positions perpendicular to the six vectors which form the edges of the quasilattice. If the vertex points are projected along the rotation axes of order 5, 3 and 2, one obtains the patterns given in Figs. 14–16. These patterns may be compared with the experimental results from transmission electron microscopy, compare Urban *et al.* (1986).

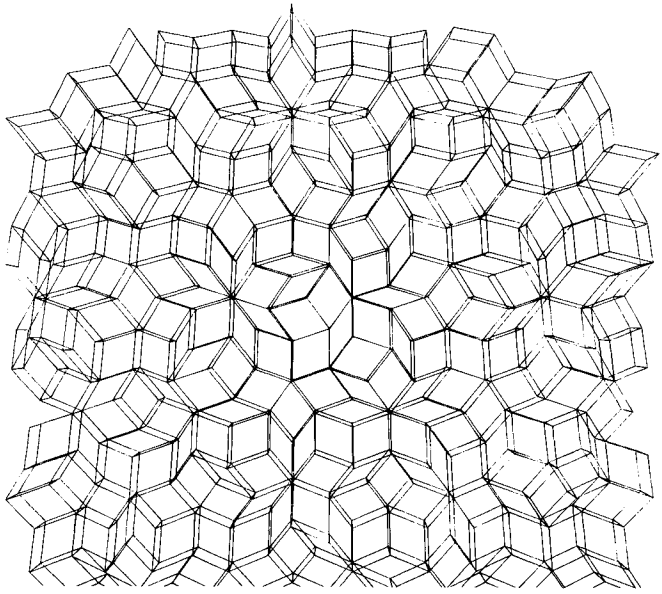

Figure 13. Layer structure of the icosahedral quasilattice. Rhombohedra with four edges perpendicular to a fixed face of the dodecahedron form six systems of infinite parallel layers in the quasilattice. Shown is a single such layer in a central projection.

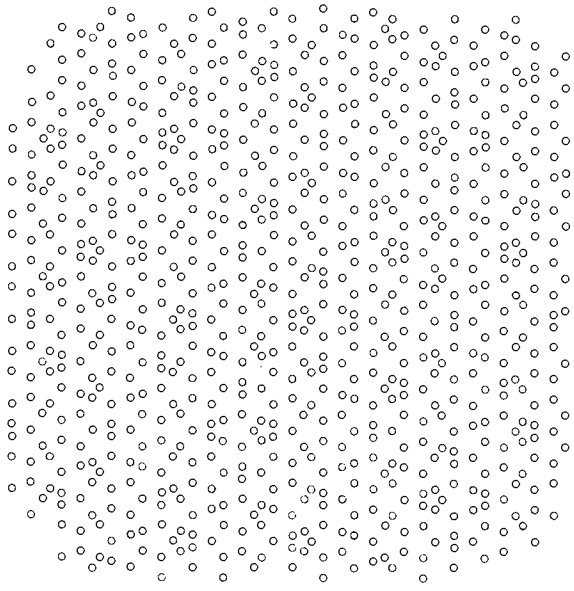

Figure 14. Orthogonal projection along a five-fold axis of the vertex points of the quasilattice into a plane.

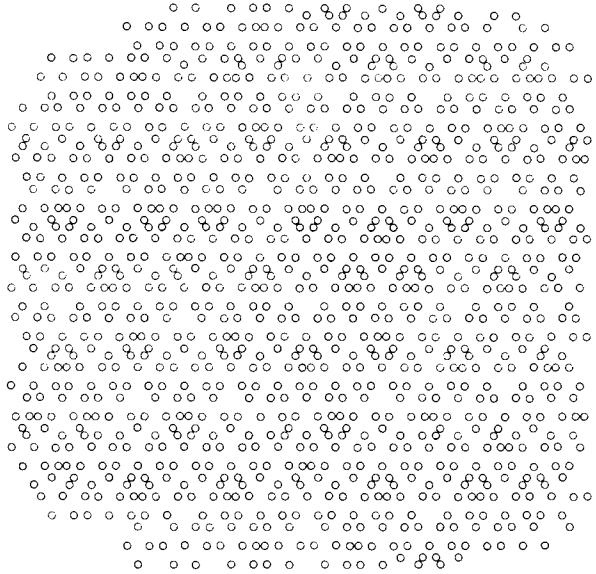

Figure 15. Orthogonal projection along a three-fold axis of the vertex points of the quasilattice into a plane.

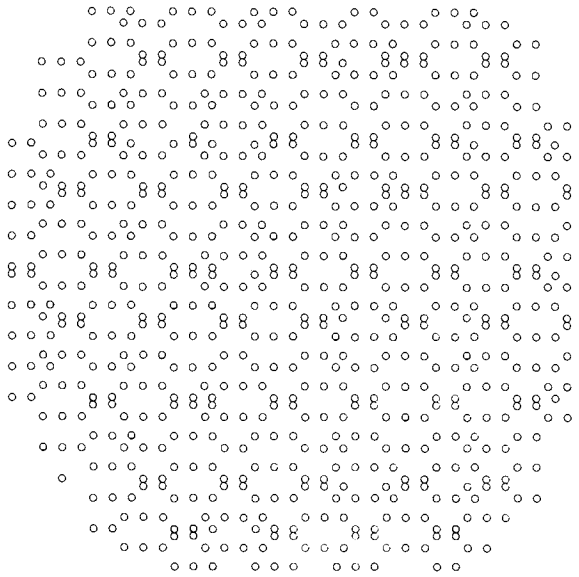

Figure 16. Orthogonal projection along a two-fold axis of the vertex points of the quasilattice into a plane.

7 Continuous and Subgroup Relations for the Cubic and Icosahedral Groups

The relation between the periodic cubic phases and the non-periodic icosahedral phase has been stressed by several authors, compare Audier and Guyot (1986). In Kramer (1987a) it was shown that there is a relation between the cubic F-lattice and the icosahedral quasilattice through a continuous rotation in $\mathbb{E}^6$. In the present section all three cubic lattices P, I and F are considered and related by continuous rotations in $\mathbb{E}^7$. We shall use the hyperoctahedral group $\Omega(n)$ described in Section 8.

We start with the cubic lattice I. Its well-known Wigner–Seitz cell is determined by 7 vectors which fall under the cubic point group $\Omega(3) \sim \mathcal{O}_h$ into two orbits of 4 and 3 vectors respectively. Application of a criterium due to Hadwiger (1940) shows that this star can be obtained as the projection of a basis for the hypercubic lattice in $\mathbb{E}^7$. An explicit basis of this lattice is formed by the column vectors of the matrix Q^I given in Table XVII. The projections corresponding to rows 1, 2, 3 and 4, 5, 6 respectively determine in $\mathbb{E}^3$ the two orbits of 4 and 3 vectors mentioned before.

Now we relate the matrix Q^I to the point groups: consider the irreducible representations 1^-, $\tilde{1}^-$ and 0^- of $\Omega(3)$ in integer form, Table XVI, and

Table XVI. Generators and representations of the cubic subgroups $\Omega^P(3)$, $\Omega^I(3)$ and $\Omega^F(3)$ of the hyperoctahedral group $\Omega(7)$. The subgroup $\mathcal{C}_{3v}$ is generated by g_3 and h_2.

g	$\Omega^P(g)$									$\Omega^I(3)$	$\Omega^F(3)$
	1^-			$\bar{1}^-$			0^-				
g_3	0	0	1	0	0	1	1			$\begin{vmatrix}1&2&3&4&5&6&7\\2&3&1&5&6&4&7\end{vmatrix}$	$\begin{vmatrix}1&2&3&4&5&6&7\\2&3&1&5&6&4&7\end{vmatrix}$
	1	0	0	1	0	0					
	0	1	0	0	1	0					
h_2	0	1	0	0	−1	0	1			$\begin{vmatrix}1&2&3&4&5&6&7\\2&1&3&\bar{5}&\bar{4}&\bar{6}&7\end{vmatrix}$	$\begin{vmatrix}1&2&3&4&5&6&7\\2&1&3&\bar{5}&\bar{4}&\bar{6}&7\end{vmatrix}$
	1	0	0	−1	0	0					
	0	0	1	0	0	−1					
$g_2'g_2$	−1	0	0	−1	0	0	1			$\begin{vmatrix}1&2&3&4&5&6&7\\2&1&7&\bar{4}&\bar{5}&6&3\end{vmatrix}$	$\begin{vmatrix}1&2&3&4&5&6&7\\4&\bar{5}&\bar{3}&1&\bar{2}&\bar{6}&7\end{vmatrix}$
	0	−1	0	0	−1	0					
	0	0	1	0	0	1					
g_2	−1	0	0	−1	0	0	1			$\begin{vmatrix}1&2&3&4&5&6&7\\3&7&1&\bar{4}&5&\bar{6}&2\end{vmatrix}$	$\begin{vmatrix}1&2&3&4&5&6&7\\\bar{4}&\bar{2}&6&\bar{1}&\bar{5}&3&7\end{vmatrix}$
	0	1	0	0	1	0					
	0	0	−1	0	0	−1					
i_2	−1	0	0	−1	0	0	−1			$\begin{vmatrix}1&2&3&4&5&6&7\\\bar{1}&\bar{2}&\bar{3}&\bar{4}&\bar{5}&\bar{6}&\bar{7}\end{vmatrix}$	$\begin{vmatrix}1&2&3&4&5&6&7\\\bar{1}&\bar{2}&\bar{3}&\bar{4}&\bar{5}&\bar{6}&\bar{7}\end{vmatrix}$
	0	−1	0	0	−1	0					
	0	0	−1	0	0	−1					

Table XVII. Schur operators related to the cubic lattice I.

$$Q^I = \tfrac{1}{2}\begin{vmatrix} \bar{1} & 1 & 1 & & & \bar{1} \\ 1 & \bar{1} & 1 & & & \bar{1} \\ 1 & 1 & \bar{1} & & & \bar{1} \\ & & & 1 & & \\ & & & & 1 & \\ & & & & & 1 \\ 1 & 1 & 1 & & & 1 \end{vmatrix} \qquad S^I(\gamma) = \begin{vmatrix} \bar{1} & & & & & & \\ & \bar{1} & & & & & \\ & & \bar{c} & & & & \bar{s} \\ & & & 1 & & & \\ & & & & 1 & & \\ & & & & & 1 & \\ & & s & & & & \bar{c} \end{vmatrix}$$

$$R^I(\gamma) = \begin{vmatrix} -\frac{1}{3}(2+c) & \frac{1}{3}(1-c) & \frac{1}{3}(1-c) & 0 & 0 & 0 & -\sqrt{\frac{1}{3}}s \\ \frac{1}{3}(1-c) & -\frac{1}{3}(2+c) & \frac{1}{3}(1-c) & 0 & 0 & 0 & -\sqrt{\frac{1}{3}}s \\ \frac{1}{3}(1-c) & \frac{1}{3}(1-c) & -\frac{1}{3}(2+c) & 0 & 0 & 0 & -\sqrt{\frac{1}{3}}s \\ 0 & 0 & 0 & 1 & 0 & 0 & 0 \\ 0 & 0 & 0 & 0 & 1 & 0 & 0 \\ 0 & 0 & 0 & 0 & 0 & 1 & 0 \\ \sqrt{\frac{1}{3}}s & \sqrt{\frac{1}{3}}s & \sqrt{\frac{1}{3}}s & 0 & 0 & 0 & -c \end{vmatrix}$$

$c = \cos\gamma$, $s = \sin\gamma$.

combine them into the representation

$$\gamma^P = 1^- \oplus \tilde{1}^- \oplus 0^- . \tag{79}$$

Since the diagonal blocks of γ^P have the form of signed permutation matrices, one obtains the subgroup relation

$$\Omega^P(3) < \Omega(3) \times \Omega(3) \times \Omega(1) < \Omega(7). \tag{80}$$

The symbol $\Omega^P(3)$ denotes the cubic group associated with the lattice P and with the representation γ^P. The subgroups in $\Omega(3) \times \Omega(3) \times \Omega(1)$ act on the indices 1, 2, 3; 4, 5, 6; 7 respectively.

Now let γ^P act on Q^I from the left. Since the columns of Q^I form orbits under $\Omega(3)$, there exists a representation γ^I of $\Omega(3)$ such that

$$\gamma^P Q^I = Q^I \gamma^I. \tag{81}$$

We write this relation in terms of groups as

$$\Omega^P(3) Q^I = Q^I \Omega^I(3). \tag{82}$$

The representation γ^I consists of signed permutation matrices and moreover has a block form in view of the two orbits. Therefore one finds

$$\Omega^I(3) < \Omega(4) \times \Omega(3) < \Omega(7) \tag{83}$$

where $\Omega(4)$ and $\Omega(3)$ act on the indices 1, 2, 3, 7 and 4, 5, 6 for the columns of Q^I. It is easy to verify that the groups $\Omega^P(3)$ and $\Omega^I(3)$ share the subgroup $\mathcal{C}_{3v}$, compare Table XVI.

7.1 Proposition: *The cubic groups associated with the cubic lattices P and I are Q-equivalent subgroups of* $\Omega(7)$ *related through the subgroups*

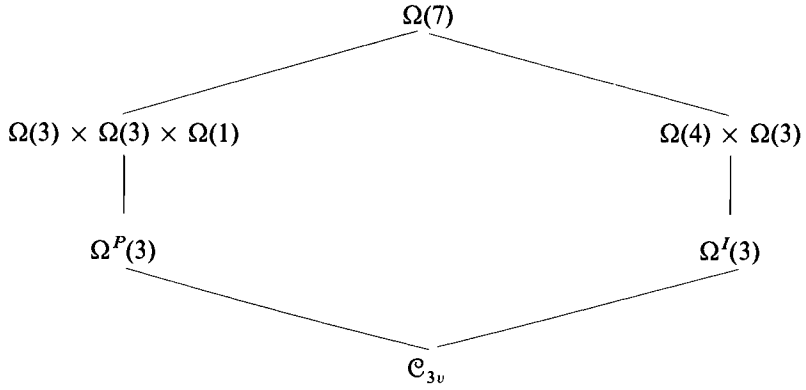

(84)

To obtain the full set of operators which commute with the representation γ^P restricted to the subgroup $\mathcal{C}_{3v}$, we employ the concept of Schur operators. First of all we bring this representation to reduced orthogonal form with the help of the matrix

$$M = J \oplus J' \oplus 1 \tag{85}$$

where J and J' are the 3×3 matrices

$$J = \sqrt{\tfrac{1}{6}} \begin{vmatrix} \sqrt{3} & -\sqrt{3} & 0 \\ 1 & 1 & -2 \\ \sqrt{2} & \sqrt{2} & \sqrt{2} \end{vmatrix} \qquad J' = \sqrt{\tfrac{1}{6}} \begin{vmatrix} -1 & -1 & 2 \\ \sqrt{3} & -\sqrt{3} & 0 \\ \sqrt{2} & \sqrt{2} & \sqrt{2} \end{vmatrix} \tag{86}$$

and where for $h \in \mathcal{C}_{3v}$

$$M\gamma^P M^{-1} = ([21] \oplus [3]) \oplus ([21] \oplus [1^3]) \oplus [3] \tag{87}$$

in a notation of partitions for $\mathcal{C}_{3v} \sim \mathcal{S}(3)$. Applications of Schur's lemma to this representation shows that the most general orthogonal matrix S commuting with it can have two one-parameter rotations associated with the pairs of [21] and [3] irreducible representations, and possible reflections within the irreducible subspaces. For fixed S, the operator which commutes with $\gamma^P \downarrow \mathcal{C}_{3v}$ is then given by

$$R = M^{-1} S M. \tag{88}$$

This general result applies in particular to Q^I, and we get:

Table XVIII. Schur operators related to the cubic lattice F.

$$Q^F = \tfrac{1}{2}\begin{vmatrix} & 1 & 1 & & 1 & \bar{1} & \\ 1 & & 1 & \bar{1} & & 1 & \\ 1 & 1 & & 1 & \bar{1} & & \\ & \bar{1} & 1 & & \bar{1} & \bar{1} & \\ 1 & & \bar{1} & \bar{1} & & \bar{1} & \\ 1 & 1 & & \bar{1} & \bar{1} & & \\ & & & & & & 1 \end{vmatrix} \qquad S^F(\alpha) = \begin{vmatrix} c & & & \bar{s} & & & \\ & c & & & \bar{s} & & \\ & & 1 & & & & \\ \bar{s} & & & \bar{c} & & & \\ & \bar{s} & & & \bar{c} & & \\ & & & & & \bar{1} & \\ & & & & & & 1 \end{vmatrix}$$

$$R^F(\alpha) = \begin{vmatrix} \frac{1}{3}(2c+1) & -\frac{1}{3}(c-1) & -\frac{1}{3}(c-1) & 0 & \sqrt{\frac{1}{3}}s & -\sqrt{\frac{1}{3}}s & 0 \\ -\frac{1}{3}(c-1) & \frac{1}{3}(2c+1) & -\frac{1}{3}(c-1) & -\sqrt{\frac{1}{3}}s & 0 & \sqrt{\frac{1}{3}}s & 0 \\ -\frac{1}{3}(c-1) & -\frac{1}{3}(c-1) & \frac{1}{3}(2c+1) & \sqrt{\frac{1}{3}}s & -\sqrt{\frac{1}{3}}s & 0 & 0 \\ 0 & -\sqrt{\frac{1}{3}}s & \sqrt{\frac{1}{3}}s & -\frac{1}{3}(2c+1) & \frac{1}{3}(c-1) & \frac{1}{3}(c-1) & 0 \\ \sqrt{\frac{1}{3}}s & 0 & -\sqrt{\frac{1}{3}}s & \frac{1}{3}(c-1) & -\frac{1}{3}(2c+1) & \frac{1}{3}(c-1) & 0 \\ -\sqrt{\frac{1}{3}}s & \sqrt{\frac{1}{3}}s & 0 & \frac{1}{3}(c-1) & \frac{1}{3}(c-1) & -\frac{1}{3}(2c+1) & 0 \\ 0 & 0 & 0 & 0 & 0 & 0 & 1 \end{vmatrix}$$

$c = \cos\alpha, s = \sin\alpha$.

7.2 Proposition: *The matrix Q^I is obtained from the one-parameter family of rotations*

$$R^I(\gamma) = M^{-1}S^I(\gamma)M, \qquad 0 \le \gamma < 2\pi \tag{89}$$

as

$$Q^I = R^I\left(\frac{2\pi}{3}\right) \tag{90}$$

with $S^I(\gamma)$ given in Table XVII.

Next we extend the analysis to the face-centered lattice F. Here we augment the 6×6 matrix M given in Kramer (1987a) into a 7×7 matrix Q^F given in Table 18 such that

$$\gamma^P Q^F = Q^F \gamma^F \tag{91}$$

which in terms of the groups implies

$$\Omega^P(3)Q^F = Q^F\Omega^F(3). \tag{92}$$

The representation γ^F of $\Omega(3)$ has the form of a subgroup of $\Omega(6) \times \Omega(1)$ and hence of $\Omega(7)$. Again one finds that Q^F commutes with the representation subduced to the subgroup $\mathcal{C}_{3v}$.

7.3 Proposition: *The cubic groups associated with the cubic lattices P and F are Q-equivalent subgroups of* $\Omega(7)$ *related by*

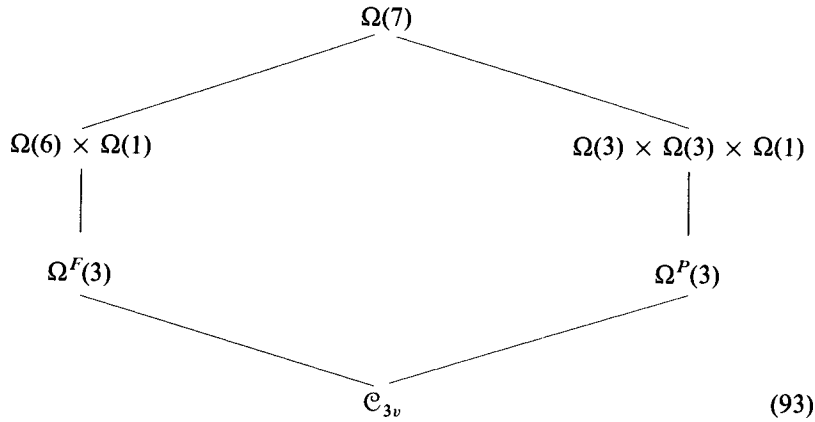

(93)

Since the explicit reduction with respect to $\mathcal{C}_{3v}$ *is the same as before, the matrix* Q^F *must be related to a Schur operator.*

7.4 Proposition: *The matrix* Q^F *is obtained from the one-parameter family of rotations*

$$R^F(\alpha) = M^{-1}S^F(\alpha)M \qquad 0 \leq \alpha < 2\pi \tag{94}$$

as

$$Q^F = R^F\left(\frac{2\pi}{3}\right) \tag{95}$$

with $S^F(\alpha)$ *given in Table XVIII.*

From the point of view of quasilattices in $\mathbb{E}^3$ obtained by projection, the orthogonal matrices $R^I(\gamma)$, $R^F(\alpha)$ given in Tables XVII, XVIII may be considered as bases of the hypercubic lattice in $\mathbb{E}^7$ whose projections to $\mathbb{E}^3$ are obtained from the rows 1, 2, 3 of these matrices. All quasilattices obtained in this fashion display the point symmetry $\mathcal{C}_{3v}$. To find the higher point symmetry $\Omega(3)$, the parameters γ, α must be chosen with the particular values given above.

The parameters γ, α allow one to discuss the relation between different cubic lattices and the icosahedral quasilattice from a dynamical point of view, for example by considering the energy of the lattice as a function of these parameters. The connection to the icosahedral quasilattice follows from the continuous rotation given in Kramer (1987a). This rotation connects the cubic lattice F with the icosahedral quasilattice through a rotation

angle β in a subspace $\mathbb{E}^6$ of the present space $\mathbb{E}^7$. The full subgroup relations are summarized in the following diagram:

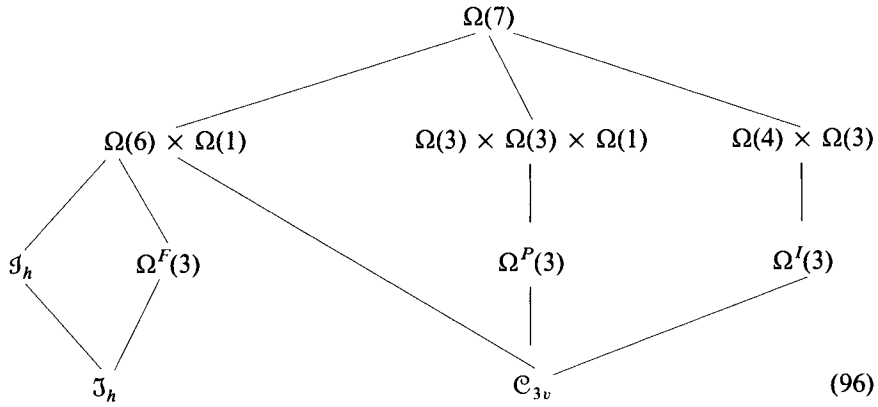

(96)

The vectors associated with the lattices I, F and with the icosahedral quasilattice are given in Fig. 17.

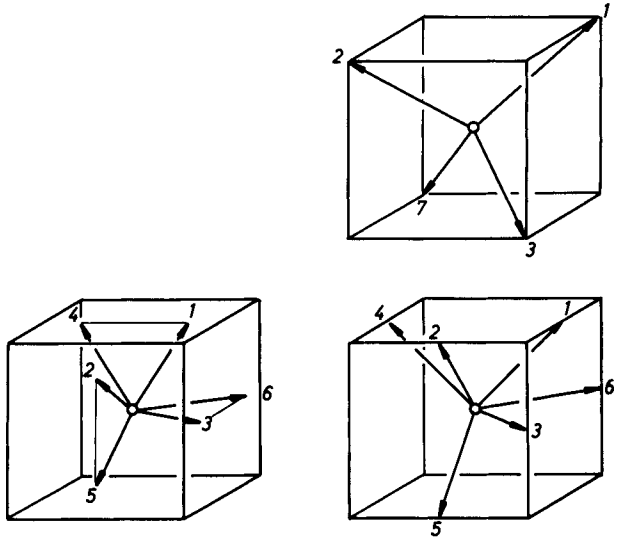

Figure 17. The vectors associated with the cubic and icosahedral (quasi-) lattices. Top: Vectors 1, 2, 3 and 7 for the body-centered lattice I, corresponding to the top columns of the matrix $\mathbf{Q}^I$ given in Table II. Bottom, right: Vectors 1, ..., 6 for the face-centered lattice F, corresponding to the top columns of the matrix $\mathbf{Q}^F$ given in Table III. Bottom, left: Vectors 1, ..., 6 for the icosahedral quasilattice. These vectors point to the vertices of an icosahedron embedded into the cube.

8 The Hyperoctahedral Group and Its Representations

Let $R(n)$ denote the group generated by all $n \times n$ real diagonal reflection matrices,

$$R(n) = \{\varepsilon \mid \varepsilon_{ij} = \varepsilon_i \delta_{ij},\ i,j = 1, \ldots, n\} \tag{97}$$

and associate with the symmetric group $S(n)$ the representation by permutation matrices,

$$S(n) = \{d(p) \mid d_{ij}(p) = \delta_{ip(j)},\ i,j = 1, \ldots, n\}. \tag{98}$$

A permutation $p \in S(n)$ induces an automorphism σ_p of $R(n)$ through

$$\sigma_p : \varepsilon \to d(p)\varepsilon\, d^{-1}(p). \tag{99}$$

8.1 Definition: The hyperoctahedral group is the semidirect product

$$\Omega(n) = \{(\varepsilon, p) \mid (\varepsilon_1, p_1)(\varepsilon_2, p_2) = (\varepsilon_1 \sigma_{p_1}(\varepsilon_2), p_1 p_2)\} \tag{100}$$

and has the defining representation

$$\gamma(\varepsilon, p) = \{\varepsilon_i d_{ij}(p),\ i,j = 1, \ldots, n\}. \tag{101}$$

As a short-hand notation for elements of $\Omega(n)$ we shall use a two-row symbol

$$(\varepsilon, p) \to \begin{bmatrix} 1 & \cdots & n \\ \varepsilon_1 p(1) & \cdots & \varepsilon_n p(n) \end{bmatrix} \tag{102}$$

and moreover we shall indicate the value $\varepsilon_i = -1$ by $\varepsilon_i p(i) \to \overline{p(i)}$.

The hyperoctahedral group (compare Coxeter and Moser (1965)), is the holohedry group of the hypercubic lattice in $\mathbb{E}^n$ and plays a fundamental role in the theory of quasilattices (compare Kramer (1986b)). For its representation theory we refer to Baake (1984). Since $\Omega(n)$ is a semidirect product with invariant subgroup $R(n)$, the representation theory of $\Omega(n)$ is essentially determined from the *IR* of $R(n)$ and $S(n)$.

8.2 Proposition: *The irreducible representations of $R(n)$ fall into classes characterized by two integers (n_1, n_0), $n_1 + n_0 = n$. A representative of a class is given by*

$$\gamma^{(n_1, n_0)}(\varepsilon) = (\varepsilon_1 \cdots \varepsilon_{n_1})^1 (\varepsilon_{n_1+1} \cdots \varepsilon_n)^0; \tag{103}$$

all other IR of the same class are obtained by an index permutation of the n matrix elements ε_i.

To obtain the IR of $\Omega(n)$, we apply the induction technique for semi-direct product groups as described for example by Coleman (1968). First we use the automorphism σ of $R(n)$ from $S(n)$ to generate the orbit

$$\sigma: \gamma^{(n_1, n_0)}(\varepsilon) \to \gamma^{(n_1, n_0)}(\sigma(\varepsilon)). \tag{104}$$

Clearly this orbit covers precisely all *IR* of $R(n)$ characterized by the integers (n_1, n_0). The stability subgroup H of $S(n)$ which fulfills

$$\sigma_H: \gamma^{(n_1, n_0)}(\sigma_H(\varepsilon)) = \gamma^{(n_1, n_0)}(\varepsilon) \tag{105}$$

is given by

$$H = S(n_1) \times S(n_0) < S(n). \tag{106}$$

Now we choose an *IR* of H. Using the standard description of *IR* of $S(n)$ by partitions, these *IR* are of the form

$$\gamma^{f_1 \times f_0}(H) = \gamma^{f_1}(S(n_1)) \times \gamma^{f_0}(S(n_0)) \tag{107}$$

where f_1, f_0 are partitions of n_1, n_0 respectively. The representations of the little group $R(n) \times (S(n_1) \times S(n_0))$ take the form

$$\gamma^{(n_1, n_0) f_1 \times f_0}(\varepsilon h) = \gamma^{(n_1, n_0)}(\varepsilon) \gamma^{f_1 \times f_0}(h). \tag{108}$$

Now the *IR* are fully described by:

8.3 Proposition: *The IR of* $\Omega(n)$ *are labeled by two non-negative integers* (n_1, n_0), $n_1 + n_0 = n$ *and by a pair of partitions* f_1, f_0 *for the groups* $S(n_1)$, $S(n_0)$. *They are given by inducing a representation of* $\Omega(n)$ *from the representation* $\gamma^{(n_1, n_0) f_1 \times f_0}$ *of the little group. If*

$$c_j, j = 1, \ldots, |S(n)|/(|S(n_1)| \cdot |S(n_0)|) \tag{109}$$

denotes coset representatives of $S(n_1) \times S(n_0)$ *in* $S(n)$, *then*

$$\gamma_{ij}^{(n_1, n_0) f_1 \times f_0}(\varepsilon, p) = \gamma^{(n_1, n_0)}(\sigma_{c_i^{-1}}(\varepsilon)) \gamma^{f_1 \times f_0}(h) \delta(c_i^{-1} p c_j, h \in (S(n_1) \times S(n_0))). \tag{110}$$

For $n_1 = 0$ *or* $n_0 = 0$, *the groups* $S(n_1)$ *or* $S(n_0)$ *are to be replaced by the identity.*

A particular role is played by the one-dimensional IR

$$\gamma^{(n, 0)[n]}(\varepsilon, p) = \varepsilon_1 \cdots \varepsilon_n. \tag{111}$$

8.4 Proposition: *Let* k *denote the permutation*

$$k = \begin{bmatrix} 1 & \cdots & n_1 & n_1 + 1 & \cdots & n \\ n_1 + 1 & \cdots & n_1 & & \cdots & n_1 \end{bmatrix} \tag{112}$$

so that

$$k(S(n_1) \times S(n_0))k^{-1} = S(n_0) \times S(n_1). \tag{113}$$

Then

$$\gamma^{(n_1, n_0)f_1 \times f_0}(\varepsilon, p) = \gamma^{(n, 0)[n]}(\varepsilon, p)\gamma^{(n_0, n_1)f_0 \times f_1}(k(\varepsilon, p)k^{-1}). \tag{114}$$

In labeling cosets of $S(n_1) \times S(n_0) < S(n)$ *we may use the standard set of coset representatives*

$$c_i = c_i(j), \quad j = 1, \ldots, n, \tag{115}$$

defined by the restrictions

$$c_i(1) < \cdots < c_i(n_1), \quad c_i(n_1 + 1) < \cdots < c_i(n). \tag{116}$$

This choice yields

8.5 Proposition: *The defining representation of* $\Omega(n)$ *is*

$$\gamma^{(1, n-)[1] \times [n-1]}(\varepsilon, p) \tag{117}$$

with matrix elements

$$\gamma^{(1, n-1)[1] \times [n-1]}(\varepsilon, p) = \varepsilon_i \, \delta_{ip(j)}. \tag{118}$$

Proof: The standard coset representatives for $S(1) \times S(n-1) < S(n)$ may be chosen as

$$c_j = \begin{bmatrix} 1 & 2 & \cdots & n \\ j & \cdot & \cdots & \cdot \end{bmatrix} \qquad j = 1, \ldots, n \tag{119}$$

so that

$$pc_j = c_{p(j)}h \tag{120}$$

and

$$\sigma_{p^{-1}}(\varepsilon) = \{\varepsilon_{p(j)} \, \delta_{ij}\}. \tag{121}$$

Then one obtains the matrix elements given in the Def. 8.1.

We note a particular property of the hyperoctahedral groups for one-dimensional $IR\gamma^{f_1 \times f_0}$ of $S(n_1) \times S(n_0)$: in this case the dimension of the *IR* is

$$\dim = \ell = \binom{n}{n_1}, \tag{122}$$

and all matrices have the form of signed $\ell \times \ell$ permutation matrices. This leads to

Table XIX. Irreducible representations of $\Omega(6)$. The dimension for given (n_1, n_0) is dim $= |f_1||f_0|6!/(n_1!\, n_0!)$. For $n_1 < n_0$, the partitions f_1, f_0 are interchanged and the symmetry given before Prop. 8.5 applies.

(n_1, n_0)	$6!/(n_1!\, n_0!)$	$f_1^{\lvert f_1\rvert}$						$f_0^{\lvert f_0\rvert}$	
(6,0)	1	$[6]^1$ $[1^6]^1$	$[51]^5$ $[21^4]^5$	$[42]^9$ $[2^21^2]^9$	$[41^2]^{10}$ $[31^3]^{10}$	$[3^2]^5$ $[2^3]^5$	$[321]^{16}$		
(5,1)	6	$[5]^1$ $[1^5]^1$	$[41]^4$ $[21^3]^4$	$[32]^5$ $[2^21]^5$	$[31^2]^6$			$[1]^1$	
(4,2)	15	$[4]^1$ $[1^4]^1$	$[31]^3$ $[21^2]^3$	$[2^2]^2$				$[2]^1$ $[11]^1$	
(3,3)	20	$[3]^1$ $[1^3]^1$	$[21]^2$					$[3]^1$ $[1^3]^1$	$[21]^2$

8.6 Proposition: *Any IR* $\gamma^{(n_1, n_0)f_1 \times f_0}$ *of* $\Omega(n)$ *with*

$$f_1 \times f_0 = [n_1] \times [n_0], [1^{n_1}] \times [n_0], [n_1] \times [1^{n_0}], [1^{n_1}] \times [1^{n_0}] \quad (123)$$

yields a group/subgroup embedding

$$\Omega(n) < \Omega(\ell), \qquad \ell = \binom{n}{n_1} \quad (124)$$

through

$$\gamma^{(n_1, n_0)f_1 \times f_0}(\Omega(n)) < \Omega(\ell). \quad (125)$$

In Table XIX we give all the IR of the hyperoctahedral group $\Omega(6)$ as an example. This group will be used in what follows.

Now we turn to relations between the hyperoctahedral groups and the icosahedral group $\mathfrak{I}$. In particular there is an embedding

$$\mathfrak{I} < \Omega(6) \quad (126)$$

given first in Kramer and Neri (1984) and obtained by induction from the dihedral group $\mathfrak{D}_5$ in Haase *et al.* (1987). Of particular interest is the subduction to $\mathfrak{I}$ for representations of $\Omega(6)$ other than the defining representation. This subduction can be obtained by use of the characters of the representations. In Table XX we give subduction results for a number of *IR* of $\Omega(6)$ of low dimension. Note that the *IR* of $\Omega(6)$ chosen are characterized by one-dimensional representations of the subgroup $S(n_1) \times S(n_0)$, and so the general result of Prop. 8.6 applies. For the cases of interest it yields the embeddings

$$n_1 = 2 : \mathfrak{I} < \Omega(6) < \Omega(15) \quad (127)$$

$$n_1 = 3 : \mathfrak{I} < \Omega(6) < \Omega(20) \quad (128)$$

Table XX. Some subductions from irreps of $\Omega(6)$ to irreps of $\mathfrak{I}$.

		$\Omega(6) \rightarrow$ (2,4)	[2] [4] $[1^2]$ $[1^4]$	$[1^2]$ [4] [2] $[1^4]$	(3,3)	[3] [3] $[1^3]$ $[1^3]$	$[1^3]$ [3] [3] $[1^3]$
$\mathfrak{I}$	[5]		1	0		0	2
$\downarrow$	[41]		1	1		2	2
	[32]		2	1		0	2
	$[31^2_+]$		0	1		2	0
	$[31^2_-]$		0	1		2	0

which at the same time are embeddings of $\mathfrak{I}$ into these hyperoctahedral groups. In Haase *et al.* (1987), we constructed, by induction from dihedral groups, embeddings of the icosahedral group into $\Omega(15)$ and $\Omega(10)$. This poses the question if there are relations between these very different constructions. The result for $n = 15$ is the following:

8.7 Proposition: *The induced IR of* $\Omega(6)$ *for* $(n_1, n_0) = (2, 4)$ *when subduced to* $\mathfrak{I}$ *are Z-equivalent to representations of* $\mathfrak{I}$ *induced from the IR* 0 *and* $\tilde{0}$ *of* $\mathfrak{D}_2$. *The embeddings of* $\mathfrak{I}$ *are conjugate in* $\Omega(15)$.

Proof: First of all we make use of the fact that the little group in the construction of *IR* of $\Omega(6)$ given in Prop. 8.3 may be replaced by a conjugate subgroup of $\Omega(6)$. We can find a conjugation such that

$$q(R(6) \times S(2) \times S(4))q^{-1} > \mathfrak{D}_2 \tag{129}$$

and find the subductions for all representations of the little group. Next we observe that the 15 cosets of the little group are associated with all pairs of numbers from 1, ..., 6. The same holds true for the 15 cosets of $\mathfrak{I}/\mathfrak{D}_2$ considered within $\Omega(6)$, and then it is easy to see that the coset generators of the new little group can be chosen as the generators of $\mathfrak{I}/\mathfrak{D}_2$. The corresponding induced representations of $\mathfrak{I}$ must then coincide. Comparing now the original standard form of the *IR* of $\Omega(6)$, the conjugation by q yields an equivalence of the representations. Since q is an element of $\Omega(6)$ and is represented by an element of $\Omega(15)$, this equivalence has the properties claimed. For the *IR* of the form $(n_1, n_0) = (3, 3)$ we get similar results.

8.8 Proposition: *The induced IR of* $\Omega(6)$ *for* $(n_1, n_0) = (3, 3)$ *when subduced to* $\mathfrak{I}$ *are Z-conjugate to representations of* $\mathfrak{I}$ *induced from the IR* 0 *and* $\tilde{0}$ *of* $\mathfrak{D}_3$. *The embeddings are conjugate in* $\Omega(20)$.

Proof: Again there is a conjugate little group with the subgroup $\mathfrak{D}_3$. The 10 cosets $\mathfrak{I}/\mathfrak{D}_3$ determine only half of the cosets of $\Omega(6)$ with respect to the

Table XXI. Equivalence of representations subduced from irreps of $\Omega(6)$ and induced from irreps of dihedral groups $\mathfrak{D}_m$.

$(n_1, n_0)f_1f_0 \downarrow \mathfrak{I}$			$\eta \uparrow \mathfrak{I}$	$\mathfrak{D}_m$
(2, 4)	$[1^2]$	[4]	$\tilde{0}$	$\mathfrak{D}_2$
	[2]	$[1^4]$	$\tilde{0}$	
	[2]	[4]	0	
	$[1^2]$	$[1^4]$	0	
(3, 3)	[3]	[3]	$2 \times \tilde{0}$	$\mathfrak{D}_3$
	$[1^3]$	$[1^3]$	$2 \times \tilde{0}$	
	[3]	$[1^3]$	2×0	
	$[1^3]$	[3]	2×0	

new little group, but it is easy to find a second set of 10 representatives for a conjugate form of $\mathfrak{I}$ with the same subgroup $\mathfrak{D}_3$. Then the construction proceeds as before.

Note that the subduction results for *IR* of $\Omega(6)$ which were derived independently in Table XX are in line with the results of Table XXI.

9 The Hypercubic Lattice in $\mathbb{E}^6$, Its Metrical Dual, and Its Epicells

In this section we shall rearrange the cells of the hypercubic lattice in a way which yields, upon intersection with $\mathbb{E}^3$, a non-periodic quasilattice whose cells are the two types of rhombohedra described for the first time by Kowalewski (1938). The analysis employs notions of the space group action on $\mathbb{E}^6$ and some basic concepts from algebraic topology.

The hypercubic space group is the semidirect product $T \wedge \Omega(6)$ where the translation group is

$$T = \left\{ \mathbf{b} \mid \mathbf{b} = \sum_{i=1}^{6} n_i \mathbf{b}_i, \mathbf{b}_j \cdot \mathbf{b}_k = \delta_{jk}, j, k = 1, \ldots, 6 \right\}. \tag{130}$$

For $\Omega(6)$ we shall use the notation $\Omega(6) = \{(\varepsilon, r)\}$. Introduce geometric objects in $\mathbb{E}^6$ with the help of the hypercubic unit cell and its boundaries of dimension $p = 0, \ldots, 5$, called p-boundaries:

9.1 Definition: The hypercubic unit cell in $\mathbb{E}^6$ is the hypercube

$$h(6) = \left\{ \mathbf{y} \mid \mathbf{y} = \frac{1}{2} \sum_{i=1}^{6} \lambda_i \mathbf{b}_i \right\} \tag{131}$$

with the p-boundaries

$$h(p; g) = \left\{ \mathbf{y} \mid \mathbf{y} = \frac{1}{2} \sum_{i=1}^{p} \lambda_{r(i)} \varepsilon_{r(i)} \mathbf{b}_{r(i)} + \frac{1}{2} \sum_{j=p+1}^{6} \varepsilon_{r(j)} \mathbf{b}_{r(j)} \right\} \tag{132}$$

where g denotes an element of $\Omega(6)$ and where all λ range over $-1 \leq \lambda \leq 1$.

9.2 Definition: The geometric object obtained by the action of T on all p-boundaries is called the complex Y.

9.3 Definition: For any $h(p; g)$ construct a dual $(6 - p)$-boundary as $h^*(0) = 0$,

$$h^*(6 - p; g) = \left\{ \mathbf{y} \mid \mathbf{y} = \frac{1}{2} \sum_{j=p+1}^{6} \lambda_{r(j)} \varepsilon_{r(j)} \mathbf{b}_{r(j)} + \frac{1}{2} \sum_{j=p+1}^{6} \varepsilon_{r(j)} \mathbf{b}_{r(j)} \right\}$$
$$p = 1, \ldots, 5. \tag{133}$$

9.4 Definition: The geometric object obtained by the action of T on all dual boundaries is called the complex Y^*.

The structure of Y and Y^* can be described in terms of notions from algebraic topology (compare Munkres (1984)):

9.5 Definition: An n-dimensional Euclidean cell complex is a collection K of convex polytopes in $\mathbb{E}^n$ such that

(1) every face of a polytope from K is in K,
(2) the intersection of any two polytopes is a face of each of them.

9.6 Definition: The p-skeleton $K^{(p)}$ of an Euclidean cell complex K in $\mathbb{E}^n$ is the subcomplex of all faces with dimensions $s, s \leq p < n$.

9.7 Proposition: *The complexes Y and Y^* defined above are Euclidean cell complexes in $\mathbb{E}^6$.*

In algebraic topology, there are several notions of duality. We shall need the following one:

9.8 Definition: Two Euclidean cell complexes K, K^* are called the metrical dual to each other if all faces of complementary dimension can be grouped into local pairs $h(p)$, $h^*(n - p)$ such that

(1) $h(p)$ and $h^*(n-p)$ intersect in a single point q,
(2) with respect to q, $h(p)$ and $h^*(n-p)$ are spanned by mutually orthogonal sets of vectors.

This definition is non-empty as we shall show.

9.9 Proposition: *The Euclidean cell complexes Y and Y^* are the metrical dual of one another and both have the full hypercubic space-group symmetry.*

Proof: We start with pairs of boundaries of the hypercube containing the origin. For a pair as given in Defs. 9.1 and 9.3, the point $\mathbf{q}$ is given by

$$\mathbf{q} = \frac{1}{2} \sum_{j=p+1}^{6} \varepsilon_{r(j)} \mathbf{b}_{r(j)} \tag{134}$$

and the orthogonality condition is fulfilled since the sets of vectors $\mathbf{b}_{r(i)}$, $i = 1, \ldots, p$ and $\mathbf{b}_{r(j)}$, $j = p+1, \ldots, 6$ are orthogonal to each other. To prove the result globally for Y and Y^*, note that all pairs of boundaries in $\mathbb{E}^n$ are obtained from the action of the translation group T which preserves the local conditions (1) and (2). Finally the complexes Y and Y^* both display the full hypercubic space group symmetry.

Now we turn to the splitting of $\mathbb{E}^6$ under the action of the icosahedral subgroup $\mathcal{I} < \Omega(6)$. The irreducible representations $[31_+^2]$ and $[31_-^2]$ determine two subspaces $\mathbb{E}_1^3$ and $\mathbb{E}_2^3$.

9.10 Definition: The projection of all vectors and polytopes to the subspaces $\mathbb{E}_1^3$ and $\mathbb{E}_2^3$ will be denoted by the subscripts 1 and 2 respectively, e.g.

$$\mathbf{y} = \mathbf{y}_1 + \mathbf{y}_2, \ \mathbf{y}_1 \perp \mathbf{y}_2, \ \mathbf{y}_1 \in \mathbb{E}_1^3, \ \mathbf{y}_2 \in \mathbb{E}_2^3. \tag{135}$$

The next concept to be introduced involves six-dimensional polytopes in $\mathbb{E}^6$, called epicell, which are built from the boundaries $h(3;)$ and $h^*(3;)$ of Y and Y^* respectively. Here we denote the boundaries by elements $g = (\varepsilon, r)$.

9.11 Definition: Let $h(3; g)$ and $h^*(3; g)$ be a local pair of dual boundaries, and consider their projections $h_1^*(3; g)$ and $h_2(3; g)$ to $\mathbb{E}_1^3$ and $\mathbb{E}_2^3$ respectively. The corresponding epicell is the six-dimensional polytope

$$kl(3+3; g) = \{\mathbf{x} \mid \mathbf{x} = \mathbf{x}_1 + \mathbf{x}_2, \ \mathbf{x}_1 \in h_1^*(3; g), \ \mathbf{x}_2 \in h_2(3; g)\} \tag{136}$$

or in explicit form

$$\mathbf{x} = \frac{1}{2}\sum_{j=4}^{6}(\varepsilon_{r(j)}\mathbf{b}_{r(j)} + \frac{1}{2}\sum_{j=4}^{6}(\lambda_{r(j)}\varepsilon_{r(j)}\mathbf{b}_{r(j)})_1 + \frac{1}{2}\sum_{i=1}^{3}(\lambda_{r(i)}\varepsilon_{r(i)}\mathbf{b}_{r(i)})_2. \quad (137)$$

The projections $h_1^*(3; g)$ and $h_2(3; g)$ are called the 1- and 2-chart of the epicell. This definition applies to all pairs of 3-boundaries associated with the hypercube, and it can be extended by the action of T to all pairs of 3-boundaries from Y and Y^*.

To discuss the local properties of the epicells we first classify the 3-boundaries associated with the first hypercube $h(6)$ under the action of the space group. We refer to Kramer (1986b) for the point group symmetry and to Kramer (1988a) for the space group symmetry.

At the center of each 3-boundary, the space group $T \wedge \Omega(6)$ generates a subgroup conjugate to $S(3) \times \Omega(3)$, Kramer (1986). If $\Omega(6)$ is restricted to $\mathcal{I}$, this local point group reduces to $\mathfrak{D}_3$. In both cases it follows that the points belonging to a 3-boundary must carry this local point symmetry group. The total number of 3-boundary of the first hypercube is 160. All 8 3-boundaries whose center is a linear combination of three fixed basis vectors can be related by translations from T. It follows that the 160 3-boundaries fall into 20 subsets not related by translations from T. For the space group $T \wedge \mathcal{I}$, the 20 representatives of the subsets can be generated by application of coset representatives from $\mathcal{I}/\mathfrak{D}_3$, compare Kramer (1988a). This reduces the 3-boundaries under the space group action to two representatives As all other hypercubic cells are obtained by translation, this is a complete classification of all 3-boundaries.

The 3-boundaries are 3-dimensional polytopes in $\mathbb{E}^6$ and intersect at most in boundaries of lower dimension. The epicells are six-dimensional polytopes, and their intersection properties are much more complicated. The proofs are given in Kramer (1988a):

9.12 Definition: The two representative epicells are given by

$$kl_\alpha : \mathbf{y} = \tfrac{1}{2}(-\mathbf{b}_4 - \mathbf{b}_5 + \mathbf{b}_2) + \tfrac{1}{2}(-\lambda_4\mathbf{b}_4 - \lambda_5\mathbf{b}_5 + \lambda_2\mathbf{b}_2)_1 + \tfrac{1}{2}(\lambda_1\mathbf{b}_1 + \lambda_3\mathbf{b}_3 + \lambda_6\mathbf{b}_6)_2 \quad (138)$$

$$kl_\beta : \mathbf{y} = \tfrac{1}{2}(\mathbf{b}_1 + \mathbf{b}_3 + \mathbf{b}_6) + \tfrac{1}{2}(\lambda_1\mathbf{b}_1 + \lambda_3\mathbf{b}_3 + \lambda_6\mathbf{b}_6)_1 + \tfrac{1}{2}(-\lambda_4\mathbf{b}_4 + \lambda_5\mathbf{b}_5 + \lambda_2\mathbf{b}_2)_2. \quad (139)$$

The 20 epicells obtained by the action of the coset representatives from $\mathcal{I}/\mathfrak{D}_3$ are called the representative set.

9.13 Proposition: *The two representative epicells have the local point symmetry* $\mathfrak{D}_3$ *with respect to their centers.*

Proof. The epicells are defined through their 1- and 2-charts. The local point symmetry of these charts results from the local point symmetry of $h(3;)$ and $h^*(3;)$ and is compatible with the projection to $\mathbb{E}_1^3$ and $\mathbb{E}_2^3$ respectively.

9.14 Proposition: *The representative set of 20 epicells has no intersections of dimension 6 and forms a new fundamental domain in* $\mathbb{E}^6$ *under the translation group T. The action of this group determines a periodic space filling of* $\mathbb{E}^6$.

This key result on the epicells has important implications for the intersection of the subspace $\mathbb{E}_1^3$ with the hypercubic lattice. Instead of the cell complex Y, we may choose the pattern formed from the epicells as an equivalent description in $\mathbb{E}^6$. Note that this new pattern is not a Euclidean cell complex since the second property of Def. 9.5 is lacking. The epicells are not in face-to-face position, and in Kramer (1988a) it is shown that a given 5-boundary of an epicell is shared by the 5-boundaries of 3 other epicells.

9.15 Proposition: *The intersection of a subspace* $\mathbb{E}_1^3$ *with the periodic space filling by epicells is a non-periodic space filling built from two types of rhombohedral cells, each in 10 different possible orientations.*

Proof: The boundaries of an epicell are parallel or perpendicular to the subspace $\mathbb{E}_1^3$. If the epicell intersects with a fixed subspace $\mathbb{E}_1^3$, this intersection is the 1-chart of this epicell. These 1-charts occur in the form of two types of rhombohedra in 10 possible orientations.

The two types of rhombohedra were discussed by Kowalewski (1938) in relation to Kepler's triacontahedron and by Mackay (1982) as a generalization of the Penrose tiles to $\mathbb{E}^3$. Kramer and Neri (1984) constructed the first infinite quasilattice from these tiles by the dualization method. The quasilattice now appears from the epicell construction as a simple consequence of the intersection with the six-dimensional periodic epicell tiling, and all proofs on the nonperiodic tiling properties result from the space group theory of the original lattice Y in $\mathbb{E}^6$.

We now apply this space group theory to a description of boundaries of the epicells. In the 1- and 2-charts, consider those boundaries whose 2-chart remains a 3-boundary $h_2(3;\tilde{g})$ while in their 1-chart we restrict the points to the faces, edges or vertices of $h_1^*(3;\tilde{g})$ respectively. These boundaries occur in the intersection with $\mathbb{E}_1^3$ as faces, edges or vertices of the rhombohedral

cells. What we are going to describe are not these boundaries for individual epicells. Instead we describe the union of all these boundaries from the full representative set of 20 epicells.

9.16 Proposition: *The union of epicell boundaries of dimension* $p + 3$, $p = 0, 1, 2$, *for the representative set are represented by polytopes of dimension* $p + 3$ *given by the new epicells*

$$kl(p + 3; g) = \{\mathbf{y} \mid \mathbf{y} = \mathbf{y}_1 + \mathbf{y}_2,\ \mathbf{y}_1 \in h_1^*(p; g),\ \mathbf{y}_2 \in \mathbf{h}_2(6 - p; g)\}. \quad (140)$$

For $p = 0, 1, 2$, *these polytopes have the point symmetry groups* $\mathfrak{I}$, $\mathfrak{D}_5$ *and* $\mathfrak{D}_2$ *with respect to their center. The full set of representatives is obtained by starting with* $g = e, \ell_\gamma, \ell_\delta$, *compare Table XXII, and then acting with coset representatives from* $\mathfrak{I}/\mathfrak{D}_5$ *for* $p = 1$, *from* $\mathfrak{I}/\mathfrak{D}_2$ *for* $p = 2$.

The family of polytopes $h_2(6 - p; g)$, $p = 0, 1, 2$, are the well-known zonohedra which are described by Coxeter (1963) and in the present

Table XXII. The representative epicell polytopes $kl(p + 3; g)$ describe the epicells and the union of their boundaries. Their 1-charts for $p = 2, 1, 0$ represent the faces, edges and vertices of the rhombohedral quasicrystal cells in $\mathbb{E}_1^3$. The stability groups are indicated as H.

$p = 3$: $kl(3 + 3; 1_\alpha)$	$H = \mathfrak{D}_3$
$h_1^*(3; 1_\alpha) = \frac{1}{2}(-(1 + \lambda_4)\mathbf{b}_4 - (1 + \lambda_5)\mathbf{b}_5 + (1 + \lambda_2)\mathbf{b}_2)_1$	
$h_2(3; 1_\alpha) = \frac{1}{2}(-\mathbf{b}_4 - \mathbf{b}_5 + \mathbf{b}_2)_2 + \frac{1}{2}(\lambda_1\mathbf{b}_1 + \lambda_3\mathbf{b}_3 + \lambda_6\mathbf{b}_6)_2$	
$kl(3 + 3; 1_\beta)$	
$h_1^*(3; 1_\beta) = \frac{1}{2}((1 + \lambda_1)\mathbf{b}_1 + (1 + \lambda_3)\mathbf{b}_3 + (1 + \lambda_6)\mathbf{b}_6)_1$	
$h_2(3; 1_\beta) = \frac{1}{2}(\mathbf{b}_1 + \mathbf{b}_3 + \mathbf{b}_6)_2 + \frac{1}{2}(-\lambda_4\mathbf{b}_4 - \lambda_5\mathbf{b}_5 + \lambda_2\mathbf{b}_2)_2$	
$p = 2$: $kl(2 + 3; 1_\delta)$	$H = \mathfrak{D}_2$
$h_1^*(2; 1_\delta) = \frac{1}{2}((1 + \lambda_3)\mathbf{b}_3 + (1 + \lambda_6)\mathbf{b}_6)_1$	
$h_2(4; 1_\delta) = \frac{1}{2}(\lambda_1\mathbf{b}_1 - \lambda_5\mathbf{b}_5 + \lambda_2\mathbf{b}_2 + \lambda_4\mathbf{b}_4)_2 + \frac{1}{2}(\mathbf{b}_3 + \mathbf{b}_6)_2$	
$p = 1$: $kl(1 + 3; 1_\gamma)$	$H = \mathfrak{D}_5$
$h_1^*(1; 1_\gamma) = \frac{1}{2}((1 + \lambda_1)\mathbf{b}_1)_1$	
$h_2(5; 1_\gamma) = \frac{1}{2}(\mathbf{b}_1)_1 + \frac{1}{2}(\lambda_3\mathbf{b}_3 + \lambda_6\mathbf{b}_6 - \lambda_4\mathbf{b}_4 - \lambda_5\mathbf{b}_5 + \lambda_2\mathbf{b}_2)_2$	
$p = 0$: $kl(0 + 3; e)$	$H = \mathfrak{I}$
$h_1^*(0; e) = O$	
$h_2(6; e) = \frac{1}{2}\left(\sum_{i=1}^{6} \lambda_i\mathbf{b}_i\right)_2$	

quasilattice frame by Haase *et al.* (1987); except for the fact that we need them here in the perpendicular space $\mathbb{E}_2^0$.

The view of the quasilattice emerging from this analysis is the following: The faces, edges and vertices of the rhombohedral cells in $\mathbb{E}_1^3$ represent points from the intersection of $\mathbb{E}_1^3$ with the union of boundaries of dimension 5, 4, 3 of the representative set of epicells. In particular the case $p = 0$ describes in $\mathbb{E}_1^3$ the quasilattice with a single point-like atom at each vertex. In $\mathbb{E}^6$ the corresponding union of epicell boundaries has the dimension 3.

10 Quasicrystal Models and Their Fourier Transform

The epicell concept yields a geometric interpretation of the non-periodic quasilattice in terms of polytopes associated with the lattice Y in $\mathbb{E}^6$. In the present section we consider a restricted model for the atomic density which is suggested, but not enforced by the epicell concept.

Consider a density f in $\mathbb{E}^6$ which respects the symmetry of the space group $T \wedge \mathfrak{I}$. The density obtained in the subspace $\mathbb{E}_1^3$ is then given by the values of f supported on the points of this subspace. The density f is obtained from the values prescribed on the unit hypercube which forms a fundamental domain under the translation group $\mathfrak{T}$. Since the set of 20 representative epicells forms a second fundamental domain, the density f can be prescribed on the points of these 20 polytopes. Suppose now that two translated copies of a fixed epicell intersect with the chosen subspace $\mathbb{E}_1^3$. As this intersection occurs in the two epicells with a different value of $\mathbf{x}_2 - \mathbf{q}$, where $\mathbf{q}$ is the center of the epicell, the density in general takes different values on the two epicells. We say that the density f is not stable on the tiles.

There is a possible restriction of f which does lead to a density stable on the tiles, and this restriction will be called a quasicrystal model:

10.1 Definition: In the quasicrystal model associated with the lattice Y in $\mathbb{E}^6$ and with the intersecting subspace $\mathbb{E}_1^3$, the density is prescribed on each epicell with the restriction

$$f(\mathbf{x}_1, \mathbf{x}_2) = f(\mathbf{x}_1) \quad \text{independent of} \quad \mathbf{x}_2 . \tag{141}$$

Moreover, $f(\mathbf{x}_1)$ must have the correct point symmetry.

This definition has the consequence that, whenever the chosen subspace $\mathbb{E}_1^3$ hits an epicell, the intersection supports a stable density characteristic for the epicell. We extend the restriction given in Def. 10.1 to the epicell boundaries described in Prop. 9.16.

Now we proceed to the Fourier theory of the quasicrystal. Let T^{R} denote the lattice reciprocal to Y with vectors $\mathbf{k}^{\mathrm{R}}$, split the $\mathbf{k}$-space $\mathbb{E}^6$ into subspaces $\mathbb{E}_1^3$ and $\mathbb{E}_2^3$ in correspondence to the position space, and denote the projections of the reciprocal lattice vectors to these subspaces by the subscripts 1 and 2 respectively.

To describe the restriction of the density f to the subspace $\mathbb{E}_1^3$, it proves useful to introduce the cut function

$$v(\mathbf{x}_1, \mathbf{x}_2) = \delta^3(\mathbf{x}_2 - \mathbf{c}_2). \tag{142}$$

The vector $\mathbf{c}_2$ fixes the position of the intersection with respect to the subspace $\mathbb{E}_2^3$. By use of the convolution theorem applied to the product of the periodic function with v, one obtains

10.2 Proposition: *The Fourier transform for the intersection of the subspace $\mathbb{E}_1^3$ with the lattice Y has the form*

$$\tilde{f}(\mathbf{k}_1) = \sum_{k^{\mathrm{R}} \in T^{\mathrm{R}}} \delta^3(\mathbf{k}_1 - \mathbf{k}_1^{\mathrm{R}}) \exp(i\mathbf{k}_2^{\mathrm{R}} \cdot \mathbf{c}_2) a(\mathbf{k}_1^{\mathrm{R}}, \mathbf{k}_2^{\mathrm{R}}) \tag{143}$$

where the Fourier coefficients a are given by

$$a(\mathbf{k}_1^{\mathrm{R}}, \mathbf{k}_2^{\mathrm{R}}) = \int_{FD} d^3x_1\, d^3x_2 f(x_1, x_2) \exp(-i(\mathbf{k}_1^{\mathrm{R}} \cdot x_1 + \mathbf{k}_2^{\mathrm{R}} \cdot x_2)). \tag{144}$$

In the quasicrystal model described in Def. 10.1, the periodic density f is restricted by $f(\mathbf{x}_1, \mathbf{x}_2) \to f(\mathbf{x}_1)$. This leads to a factorization of the Fourier coefficients into a kinematical part and a part depending of $f(\mathbf{x}_1)$.

10.3 Definition: The auxiliary functions d are given by the integrals

$$\begin{aligned} d(\mathbf{k}_1, \mathbf{k}_2; g) &= \int_{h_1^*(p;g)} d^3x_1 f(\mathbf{x}_1) \exp(-i\mathbf{k}_1 \cdot \mathbf{x}_1) \\ &= \int_{h_2(6-p;g)} d^3x_2 \exp(-i\mathbf{k}_2 \cdot \mathbf{x}_2) \end{aligned} \tag{145}$$

where $p = 3$ for the epicells $kl(3 + 3; g)$ and $p = 0, 1, 2$ for the union of their boundaries, and where g is taken from a coset with respect to an appropriate stability group.

10.4 Proposition: *The Fourier transform for the quasicrystal model with the space group $T \wedge \mathfrak{I}$ and with the fundamental domain described by the representative set of epicells has the form given in Table XXIII. The epicells contribute to $p = 3$, the union of their boundaries to $p = 0, 1, 2$ respectively.*

Table XXIII. Fourier coefficients for the epicells, $p = 3$, and for the union of epicell boundaries, $p = 2, 1, 0$ corresponding to face, edge and vertex positions of the rhombohedral cells. The functions d are integrals given in Def. 10.3 over the charts of the epicells given in Table XXI.

$p = 3$;

$$a(\mathbf{k}_1^R, \mathbf{k}_2^R) = \sum_{c_i \in \mathcal{I}/\mathfrak{D}_3} (d(\mathbf{k}_1^R, \mathbf{k}_2^R; c_i 1_\alpha) + d(\mathbf{k}_1^R, \mathbf{k}_2^R; c_i 1_\beta))$$

$p = 2$:

$$a(\mathbf{k}_1^R, \mathbf{k}_2^R) = \sum_{c_i \in \mathcal{I}/\mathfrak{D}_2} d(\mathbf{k}_1^R, \mathbf{k}_2^R; c_i 1_\delta)$$

$p = 1$:

$$a(\mathbf{k}_1^R, \mathbf{k}_2^R) = \sum_{c_i \in \mathcal{I}/\mathfrak{D}_5} d(\mathbf{k}_1^R, \mathbf{k}_2^R; c_i 1_\gamma)$$

$p = 0$:

$$a(\mathbf{k}_1^R, \mathbf{k}_2^R) = d(\mathbf{k}_1^R, \mathbf{k}_2^R; e)$$

Proof: All epicell polytopes in $\mathbb{E}^6$ under consideration are described by a 1-chart and a 2-chart. In the quasicrystal model with the restricted density, the integration over an epicell polytope separates into a factor in the 1-chart which involves the density $f(\mathbf{x}_1)$, and into a factor in the 2-chart which is the characteristic function of a polytope in $\mathbb{E}_2^3$. The integration extends over the full new fundamental domain provided by the epicells and by the union of their boundaries. This integration can be reduced to a sum over the cosets of a point group which is the stability group of the corresponding epicell polytopes. The stability groups for $p = 3, 2, 1, 0$ are $\mathfrak{D}_3$, $\mathfrak{D}_2$, $\mathfrak{D}_5$ and $\mathcal{I}$ respectively. For a different approach to the Fourier transform compare Rohksar *et al.* (1987).

Acknowledgments

One of us (RWH) would like to thank the Alexander-von-Humboldt-Stiftung for the award of a research fellowship. This work was also supported by the Deutsche Forschungsgemeinschaft. Technical assistance in the preparation of the figures by L. Kramer is gratefully acknowledged.

References

Audier, M. and Guyot, P. (1986). Al_4Mn quasicrystal atomic structures, diffraction data and Penrose tiling. *Phil. Mag.* **B53**, L43–L51.

Baake, M. (1984). Structure and representations of the hyperoctahedral group. *J. Math. Phys.* **25**, 3171–3182.

Bak, P. (1985). Phenomenological theory of icosahedral incommensurate ("quasi-periodic") order in Mn-Al alloys. *Phys. Rev. Lett.* **54**, 1517–1519.

Bak, P. (1986). Icosahedral crystals: where are the atoms? *Phys. Rev. Lett.* **56**, 861–864.

Brown, H., Bülow, R., Neubüser, J., Wondratschek, H. and Zassenhaus, H. (1978). *Crystallographic Groups of Four-dimensional Space*. Wiley, New York.

Butler, P. (1981). *Point Group Symmetry Application: Methods and Tables*. Plenum Press, New York.

Cesare, S. and Del Duca, V. (1987). Tensor algebra for the icosahedral group. *Riv. Nuov. Cim.* **10**, 24–33.

Coleman, A. J. (1968). *Induced and subduced representations. In Group Theory and Its Applications* (Loebl, E. M. ed.). Academic Press, New York.

Coxeter, H. S. M. (1963). *Regular Polytopes*. 2nd ed. Macmillan, New York.

Coxeter, H. S. M. and Moser, W. O. (1965). *Generators and Relations for Discrete Groups*. 2nd ed. Springer, New York.

De Bruijn, N. G. (1981). Algebraic theory of Penrose's non-periodic tilings of the plane I, II. *Proc. Konig. Ned. Akad. Weten.* **A84**, 39–66.

Dubost, B., Lang, J.-M., Tanaka, M., Sainfort, P. and Audier, M. (1986). Large AlCuLi single quasicrystals with triacontahedral solidification morphology. *Nature* **324**, 48–50.

Duneau, M. and Katz, A. (1985). Quasiperiodic patterns. *Phys. Rev. Lett.* **54**, 2688–2691.

Elser, V. (1986). The diffraction pattern of projected structures. *Acta Cryst.* **A42**, 36–43.

Elser, V. (1987). The growth of quasicrystals. In *Proc. XV. Int. Coll. on Group Theor. Meth. in Physics, Philadelphia 1986* (Gilmore, R. ed.) World Scientific, Singapore, 162–183.

Elser, V. and Henley, C. L. (1985). Crystal and quasicrystal structures in Al-Mn-Si alloys. *Phys. Rev. Lett.* **55**, 2883–2886.

Frank, F. C. and Kasper, J. S. (1958). Complex alloy structures regarded as sphere packings. I. Definitions and basic principles. *Acta Cryst.* **11**, 184–190.

Frank, F. C. and Kasper, J. S. (1959). Complex alloy structures regarded as sphere packings. II. Analysis and classification of representative structures. *Acta Cryst.* **12**, 483–499.

Garg, A. and Levine, D. (1987). Faceting and roughening in quasicrystals. *Phys. Rev. Lett.* **59**, 1683–1686.

Goshen, S. Y. and Birman, J. L. (1987). Tensorial properties distinguishing icosahedral symmetry from cubic or isotropic SO(3) symmetry. In *Proc. XV. Int. Coll. Group Theor. Meth. in Physics, Philadelphia 1986* (Gilmore, R., ed.) World Scientific, Singapore, 278–281.

Gähler, F. and Rhyner, J. (1985). Equivalence of the generalised grid and projection methods for the construction of quasiperiodic tilings. *J. Phys. A: Gen. Phys.* **19**, 267–277.

Haase, R. W., Kramer, P., Kramer, L. and Lalvani, H. (1987). Polyhedra of three quasilattices associated with the icosahedral group. *Acta Cryst.* **A43**, 574–587.

Hadwiger, H. (1940). Über ausgezeichnete Vektorsterne und Reguläre Polytope. *Comm. Math. Helvetici* **13**, 90–107.

Hamermesh, M. (1962). *Group Theory and its Application*. Addison-Wesley, Reading.

Ho, T. L., Jaszczak, J. A., Li, Y. H. and Saam, W. F. (1987). Faceting in bond-oriented glasses and quasicrystals. *Phys. Rev. Lett.* **59**, 1116–1119.

Janssen, T. (1985). Crystallography of quasicrystals. *Acta Cryst.* **A42**, 261–271.

Jarić, M. V. (1986). Diffraction from quasicrystals: Geometric structure factor. *Phys. Rev.* **B34**, 4685–4698.

Katz, A. and Duneau, M. (1986). Quasiperiodic patterns and icosahedral symmetry. *J. Physique* **47**, 181–196.

Koster, G. F. (1957). *Space Groups and Their Representations*. Academic Press, New York.

Klein, F. (1913). Lectures on the Icosahedron. Translation by G. G. Morris, London. From *Vorlesungen über das Ikosaeder und die Auflösung der Gleichungen fünften Grades*, (1884) Leipzig.

Kowalewski, G. (1938). *Der Keplersche Körper und andere Bauspiele*. Koehlers Antiquarium, Leipzig.

Kramer, P. (1982). Non-periodic central space filling with icosahedral symmetry using copes of seven elementary cells. *Acta Cryst.* **A38**, 257–264.

Kramer, P. and Neri, R. (1984). On periodic and non-periodic space fillings of E(m) obtained by projection. *Acta Cryst.* **A40**, 580–587.

Kramer, P. (1985). On the theory of a non-periodic quasilattice associated with the icosahedral group. *Z. Naturf.* **40a**, 775–788.

Kramer, P. and Kramer, L. (1985). Diffraction and layer structure of a quasilattice. *Z. Naturf.* **40a**, 1162–1163.

Kramer, P. (1986a). Quasilattices in E(3) and their projection from lattices in E(n). *J. de Physique Coll.* **C3**, 75–81.

Kramer, P. (1986b). On the theory of a non-periodic quasilattice associated with the icosahedral group II. *Z. Naturf.* **41a**, 897–911.

Kramer, P. (1987a). Continuous rotation from cubic to icosahedral order. *Acta Cryst.* **A43**, 486–489.

Kramer, P. (1987b). Das Pentagramma macht Dir Pein? Violation of periodic symmetry in quasicrystals. In *Proc. XV. Int. Coll. on Group Theor. Meth. in Physics, Philadelphia 1986* (Gilmore, R., ed.) World Scientific, Singapore, 146–161.

Kramer P. (1987c). Atomic order in quasicrystals is supported by several unit cells. *Mod. Phys. Lett.* **B1**, 7–18.

Kramer, P. (1987d). Non-periodic translational order in quasicrystals with stable atomic density on several cells. *Int. J. Mod. Phys.* **B1**, 145–166.

Kramer, P. (1988a). Space-group theory for a non-periodic icosahedral quasilattice. *J. Math. Phys.* **29**, 516–524.

Kramer, P. (1988b). Quasicrystals: From periodic to non-periodic order in solids. In *Fractals, Quasicrystals, Chaos, Knots and Algebraic Quantum Mechanics* (Ammann, A. and Cederbaum, L. S., Gans, W., eds.) Kluwer Dordrecht, 73–91.

Kramer, P. and Mackay, A. L. (1985). Crystallography: Some answers but more questions. *Nature* **316**, 17–18.

Levine, D. and Steinhardt, P. J. (1984). Quasicrystals: a new class of ordered structures. *Phys. Rev. Lett.* **53**, 2477–2480.

Litvin, D. B., Kopsky, V. and Birman, J. L. (1987). Symmetry and phase transitions in decagonal quasicrystals. In *Proc. XV. Int. Coll. Group Theor. Meth. in Physics, Philadelphia 1986* (Gilmore, R., ed.) World Scientific, Singapore, 282–287.

Lu, J. P. and Birman, J. L. (1987). Symmetry of quasiperiodic lattices and decomposability of crystallographic point groups. In *Proc. XV. Int. Coll. Group Theor. Meth. in Physics, Philadelphia 1986* (Gilmore, R., ed.) World Scientific, Singapore, 270–277.

Mackay, A. L. (1982). Crystallography and the Penrose pattern. *Physica* **114A**, 609–613.

Mackay, A. L. (1986). What has the Penrose tiling got to do with the icosahedral phase? Geometrical aspects of the icosahedral quasicrystal problem. *J. Microscopy* **146**, 233–243.

Mackay, A. L. (1987). A bibliography of quasicrystals. *Int. J. of Rapid Solidification* **2**, S1–S41.

McLellan, A. G. (1961). Eigenfunctions for integer and half-odd integer values of J symmetrized according to the icosahedral group and the group C_{3v}. *J. Chem. Phys.* **34**, 1350–1359.

Michel, L. and Mozrzymas, J. (1985). Inst. Hautes Etudes Scientifiques, Workshop on Mathematical Crystallography, preprint, August 1985.

Munkres, J. R. (1984). *Elements of Algebraic Topology*. Addison-Wesley, Menlo Park.

Penrose, R. (1974). The role of aesthetics in pure and applied mathematical research. *Bull. Inst. Math. Appl.* **10**, 266–271.

Rokhsar, D. S., Mermin, N. D. and Wright, D. C. (1987). Rudimentary quasicrystallography: the icosahedral and decagonal reciprocal lattices. *Phys. Rev.* **B35**, 4587–4594.

Schwarzenberger, R. L. E. (1980). *N-dimensional Crystallography*. Pitman, San Francisco.

Shechtman, D., Blech, I., Gratias, D. and Cahn, J. W. (1984). Metallic phase with long-range orientational order and no translational symmetry. *Phys. Rev. Lett.* **53**, 1951–1953.

Steinhardt, P. J. (1987). Transition states in quasicrystals. Preprint.

Stephens, P. W. and Goldman, A. I. (1986). Sharp diffraction maxima from an icosahedral glass. *Phys. Rev. Lett.* **56**, 1168–1171.

Urban, K., Kramer, P. and Wilkens, M. (1986). Quasikristalle. *Phys. Blätter* **42**, 373–378.

Widom, M. (1988). Microscopic model of a 2-D quasicrystal forming binary alloy. Preprint.

Chapter 4

Some Local Properties of the Three-Dimensional Penrose Tilings

ANDRÉ KATZ

Centre de Physique Théorique de l'Ecole Polytechnique
Palaiseau, France

Contents

1 Introduction 147
2 The Projection Method 149
2.1 A Low-Dimensional Model 149
2.2 The Three-Dimensional Penrose Tilings 152
3 The Local Isomorphism Property 157
3.1 The Low-Dimensional Case 157
3.2 The Three-Dimensional Case 160
4 Classification of Local Packings 162
4.1 The Existence Domains of the Tiles 162
4.2 The Local Environments in the Penrose Tilings 164
5 The Cut Description and the Oblique Tiling 169
6 Matching Rules for the 3-DPT 173
6.1 Decorations of the Facets and of the Tiles 176
6.2 Outline of the Proof 178
References 182

1 Introduction

This chapter deals with the local properties of the three-dimensional Penrose tilings. We first explain the global construction of these tilings

APERIODICITY AND ORDER 2
Introduction to the
Mathematics of Quasicrystals

Copyright © 1989 by Academic Press, Inc.
All rights of reproduction in any form reserved.
ISBN 0-12-040602-0

through the so-called "projection method", starting with a simple low-dimensional model. As is well known (Katz and Duneau, 1986; Elser, 1986), such a construction yields in a straightforward way the main global properties of the three-dimensional Penrose tilings, namely their icosahedral symmetry and their quasiperiodicity, but we do not discuss these questions here. They are discussed in Chapter 3 of this volume and in Chapter 4 of the preceeding volume.

The first local property which we describe is the "local isomorphism property" (Gardner, 1977), which, roughly speaking, asserts that the "large" infinity of different Penrose tilings share the same set of bounded parts, so that they are essentially indistinguishable from each other. The next topic is to show how one can classify the local patterns in the tilings, and as an example we construct the 24 packings of tiles around a common vertex, without entering into too many technicalities. Then we establish the relation between the projection method, which is limited to the construction of tilings, and the more general "cut method", which is in fact the general way of constructing quasiperiodic sets of points. We briefly describe the theory of the "oblique tiling", a periodic tiling of the six-dimensional space whose sections yield the Penrose tilings. This oblique tiling provides a simple proof of the projection construction and appears as a natural generalization of the cut method when one is interested not only in quasiperiodic sets of points, but also of higher dimensional objects. The last section deals with the problem of the "matching rules": The question is to find local constraints on the packing, such that any tiling fulfilling these constraints is a quasiperiodic Penrose tiling. We show that such matching rules exist for the three-dimensional case as in the two-dimensional one, but the theory is of a very different nature and does not involve any reference to the self-similarity properties of the tilings.

Before beginning discussing our subject, it is worthwhile to emphasize that the relationship between quasiperiodic sets of points and quasiperiodic tilings is not at all the same as in the periodic case. As is well known, one can attach a periodic tiling to any periodic distribution of points in such a way that the theories of both objects are essentially the same. This relation, which accounts for the relevance of periodic tilings in classical crystallography, is no longer true in the quasiperiodic case. Consider for instance the modulated crystals: they are quasiperiodic sets of atoms, but since they present infinitely many different non-isometric local structures, it is impossible to associate to them a tiling, which by definition involves only a finite number of different tiles.

As a consequence, one should not consider that the icosahedral quasiperiodic tilings (of which the Penrose tilings are the best known examples) play any universal role with respect to the quasicrystals, and for

instance, the Ammann rhombohedra which build the Penrose tilings need not have anything to do with "unit cells" for the quasicrystals. On the contrary, the Penrose tilings should be assigned a more modest role as very useful tools to understand a rather involved geometry.

2 The Projection Method

2.1 A Low-Dimensional Model

To explain the projection method, let us first deal with the simplest case, which consists of tiling a straight line through the projection of a set of selected edges of the square lattice of the plane.

Consider (Fig. 1) the plane $\mathbb{R}^2$ equipped with the square lattice $\mathbb{Z}^2$, and draw in this plane the line **E** to be tiled. Now, define a strip by shifting along this line **E** the unit square of the lattice. This "thickens" the line in such a way that there is exactly enough room between the boundaries of the strip to insert a unit square of the lattice. Observe that the upper boundary of the strip is obtained from the lower one through the translation by a diagonal of the square, the choice of which depends on the orientation of the straight line: for a positive slope, the diagonal involved goes from the lower right

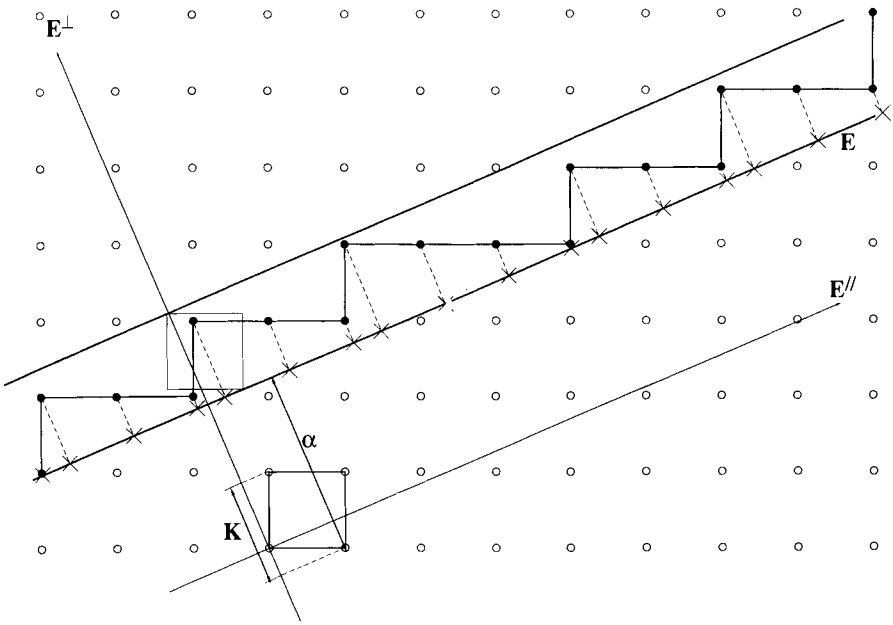

Figure 1. The low-dimensional model of the projection method.

corner to the upper left, and for a negative slope, one has to make the other choice (if the line is either horizontal or vertical, then the two choices are equivalent, but we shall not be interested in such special cases).

Now, the claim is that for almost all choices of the initial line **E**, there exists a unique continuous zig-zag line, made up of edges of the square lattice, which goes exactly through all the vertices of the lattice falling inside the strip. Then we obtain the tiling of the line **E** through the orthogonal projection of the broken line onto **E**: this yields a tiling with two kinds of tiles, which are the projections of the two kinds of edges (horizontal and vertical) of the square lattice.

The positions of the line **E** which are forbidden are those for which **E** intersects the lattice. In fact, if there is a lattice point on one boundary of the strip, there is also a lattice point on the other boundary, and these two points belong to the same square as the extremities of one of its diagonals, so that there are two ways for the broken line to turn around this square, which creates an ambiguity.

The claim may be proved in a formal way (see the oblique lattice below) but in this simple case one may content oneself with the following remarks:

(1) Observe first that for almost all positions of the initial line, the boundaries of the strip do not intersect the lattice, and let us restrict ourselves to such a "generic" situation. Now, when attempting to construct a zig-zag line going through all the vertices falling inside the strip, one could encounter two types of obstructions: the zig-zag line could either bifurcate (with more than two first neighbors of a vertex falling inside the strip) or terminate (with fewer than two such neighbors). But it is clear that none of these obstructions can arise with our special choice for the width of the strip: it is narrow enough to forbid any bifurcation, since no lattice square has its four vertices inside the strip, and large enough to avoid any interruption of the zig-zag line, since each time a diagonal of a lattice square falls inside the strip then so does one of the two remaining vertices of this square.

Although this low dimensional example may look rather trivial, it is sufficient to understand the main features of this class of tilings. As a first important property, let us now show that whenever the slope of the line **E** is irrational, the tiling resulting from this construction is non-periodic. In fact, it is clear that if the slope is a rational number p/q, then the translation of vector (q, p) preserves both the lattice and the strip and thus maps the broken line onto itself. In such a case, we get a periodic tiling with a unit cell made of p projections of the vertical edge and q projections of the horizontal one (and this unit cell is the minimal one if the integers p and q are co-prime). On the other hand, it is always true that the ratio of the relative abundance of the two types of tiles is well defined and is equal to the slope of **E**. But since this ratio is certainly rational for a periodic tiling, we

see that for any irrational slope we get a non-periodic tiling. Moreover, observe that to each sequence of rational numbers converging to a given irrational slope, this construction associates a sequence of periodic tilings whose cells become larger and larger and whose vertices converge point-wise to the vertices of the non-periodic tiling defined through the irrational slope, in such a way that these non-periodic tilings appear as "interpolations" between periodic ones.

(2) The second property which is worthwhile mentioning here is that for a given irrational slope the previous construction yields infinitely many different tilings, which correspond to all the possible positions of the strip with respect to the square lattice. It is natural to classify these positions by the projection of the line $\mathbf{E}$ onto the orthogonal line, denoted $\mathbf{E}^{\perp}$, going through the origin. Observe now that two tilings are equivalent through a translation if and only if there exists a lattice translation in the plane which maps the corresponding strips onto each other, and then the translation which relates the two tilings is simply the projection on $\mathbf{E}$ of this lattice vector. In other words, two tilings are equivalent if and only if the projections of the corresponding lines $\mathbf{E}$ onto $\mathbf{E}^{\perp}$ differ by the projection on $\mathbf{E}^{\perp}$ of a lattice vector. But the projection of the lattice is a countable set, and when taking the quotient of the whole line $\mathbf{E}^{\perp}$ by this countable set, one obtains an uncountable set of different tilings (recall that, in order to avoid possible ambiguities in the construction, we require the line $\mathbf{E}$ not to contain any lattice point. This constraint removes only a countable number of positions, and does not alter the previous conclusion).

As we shall see below, this "large" infinity of different tilings corresponding to a given irrational slope share in fact the same set of finite subsets: this is the local isomorphism property and means that all the local properties of these tilings are the same or, in other words, that they are indistinguishable from a local point of view. For the moment, let us only point out what happens when one moves the strip along $\mathbf{E}^{\perp}$: each time a vertex goes out of the strip, another one enters into it, and these two points are the two vertices of the diagonal of some square in the lattice. Then the broken line "jumps" from one way of turning around this square to the other one, and in the tiling of $\mathbf{E}$, this jump corresponds to the exchange of two tiles of different kinds: a sequence long-short is replaced by a sequence short-long, or vice-versa. This is the only elementary transformation in these tilings, but since the slope is irrational, such elementary changes occur infinitely many times for any finite translation of the strip along $\mathbf{E}^{\perp}$, and this is sufficient to generate infinitely many different tilings.

Before turning to the construction of the three-dimensional Penrose tilings, let us introduce some notations: to conform with a well-established notation, we shall denote $\mathbf{E}^{\parallel}$ the vector subspace parallel to the tiled space

$\mathbf{E}$, and we define the two projections $\pi^{\parallel}$ and $\pi^{\perp}$ as the orthogonal projections on $\mathbf{E}^{\parallel}$ and $\mathbf{E}^{\perp}$ respectively. Let $\mathbf{K}$ be the projection of the unit square onto $\mathbf{E}^{\perp}$, and for any α in $\mathbf{E}^{\perp}$, let $\mathbf{K}_{\alpha}$ denote the translated $\mathbf{K} + \alpha$. Then for almost all α the boundary $\partial\mathbf{K}_{\alpha}$ does not intersect $\pi^{\perp}(\mathbb{Z}^2)$ and in these "non-ambiguous" cases the projection construction can be rephrased in the following form: To obtain the vertices of the non-periodic tiling, take all the vertices in $\mathbb{Z}^2$ whose projections on $\mathbf{E}^{\perp}$ fall inside $\mathbf{K}_{\alpha}$, and project them on $\mathbf{E}^{\parallel}$. Such a formulation is clearly equivalent to the previous one and is useful for the description of the 3-dimensional Penrose tilings, for which we have to consider a six-dimensional hypercubic lattice and we cannot draw a global picture analogous to Fig. 1.

2.2 *The Three-Dimensional Penrose Tilings*

Apart from going to higher dimensions, which does not raise any conceptual problem, the new features which we have to incorporate in the construction concern the icosahedral symmetry of the three-dimensional Penrose tilings. Let us first make precise the notion of symmetry involved here.

For periodic lattices, the symmetry point group is defined as the largest subgroup of the rotation group such that the lattice coincides with its image under any operation in this point group up to a translation. This translation depends of course on the center of rotation, whose choice is arbitrary. For the non-periodic lattices discussed here, we have to slightly modify this definition to take into account the fact that the projection method yields an infinite number of different structures which are locally (that is, in any bounded region) indistinguishable from each other. The natural definition in this new context is then to require the images of the tiling under the point group to be equivalent to it or, more precisely, to require that the strips which define these images differ only by some translations in the high dimensional space from the strip which defines the initial tiling.

As one can see, this definition differs from the classical one only through the meaning of the translation: in the periodic case, one considers only translations belonging to the tiled space (no higher dimensional space is involved!). In our construction, we allow any translation of the higher dimensional space: its component parallel to the tiled space $\mathbf{E}^{\parallel}$ is an ordinary translation of the tiling, and the orthogonal component (belonging to $\mathbf{E}^{\perp}$) transforms it in an equivalent one.

Now, it is clear that we have to consider the point group as a subgroup of the rotations of the higher dimensional space, so that the symmetry of

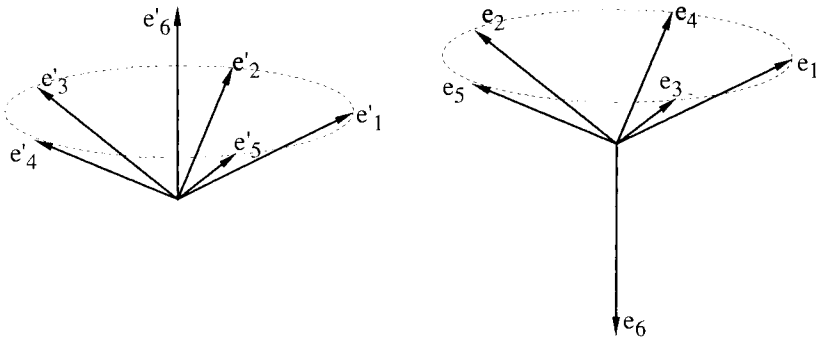

Figure 2. The orientations of six icosahedral vectors $\mathbf{e}'_i$ in $\mathbf{E}^\perp$ and $\mathbf{e}_i$ in $\mathbf{E}^\parallel$. There is an unique orientation of $\mathbf{E}^\perp$ and $\mathbf{E}^\parallel$ in $\mathbb{R}^6$ such that these vectors are the projections of the canonical basis of $\mathbb{R}^6$.

the tiling will result from three independent symmetry requirements:

- The high dimensional periodic lattice must be invariant under the icosahedral group, that is, the icosahedral group must be represented as a subgroup of the point group of the high dimensional lattice.
- The directions of the two orthogonal subspaces $\mathbf{E}^\parallel$ and $\mathbf{E}^\perp$ must be invariant under this action of the icosahedral group.
- And finally, the "window" $\mathbf{K}$ must also be invariant under the icosahedral group up to a translation, which means that its shape must exhibit the icosahedral symmetry.

The simplest implementation of these constraints makes use of the six-dimensional simple hypercubic lattice, and the projection construction results in the three-dimensional Penrose tilings. Consider the six-dimensional Euclidean space $\mathbb{R}^6$ together with its canonical orthonormal basis $\{\boldsymbol{\varepsilon}_i, i = 1 \cdots 6\}$. Then the simple hypercubic lattice is defined as the set of all linear combinations of the basis vector with integer coefficients. We define a linear representation of the icosahedral group in $\mathbb{R}^6$ as follows: consider in the ordinary space a regular icosahedron with a five-fold vertical axis and the six vectors joining the origin and six vertices such that these vectors point upward; we label these vectors such that $\mathbf{e}'_6$ is the vertical vector, $\mathbf{e}'_1$ is arbitrary, the angle between $\mathbf{e}'_i$ and $\mathbf{e}'_{i+1}$ is acute and the orientation of the triplet $(\mathbf{e}'_1, \mathbf{e}'_2, \mathbf{e}'_6)$ is direct (see Fig. 2). Then the linear representation is defined in $\mathbb{R}^6$ by the condition that it permutes the vectors $\boldsymbol{\varepsilon}_i$ in the same way that the ordinary action of the icosahedral group in $\mathbb{R}^3$ permutes the six vectors $\mathbf{e}'_i$ which we have just defined. One obtains the following matrices for the five-fold rotation g with axis $\mathbf{e}'_6$ and for the three-fold

rotation h with axis $\mathbf{e}'_4 + \mathbf{e}'_5 + \mathbf{e}'_6$:

$$g = \begin{bmatrix} 0 & 0 & 0 & 0 & 1 & 0 \\ 1 & 0 & 0 & 0 & 0 & 0 \\ 0 & 1 & 0 & 0 & 0 & 0 \\ 0 & 0 & 1 & 0 & 0 & 0 \\ 0 & 0 & 0 & 1 & 0 & 0 \\ 0 & 0 & 0 & 0 & 0 & 1 \end{bmatrix} \quad \text{and} \quad h = \begin{bmatrix} 0 & -1 & 0 & 0 & 0 & 0 \\ 0 & 0 & -1 & 0 & 0 & 0 \\ 1 & 0 & 0 & 0 & 0 & 0 \\ 0 & 0 & 0 & 0 & 0 & 1 \\ 0 & 0 & 0 & 1 & 0 & 0 \\ 0 & 0 & 0 & 0 & 1 & 0 \end{bmatrix}$$

Since the action on $\mathbb{R}^6$ is by (signed) permutations of the basis vectors, it is immediate that the whole hypercubic lattice is invariant under this representation, and our first symmetry requirement is thus fulfilled.

The next step is to look for the invariant subspaces in $\mathbb{R}^6$. As is well known from group theory, the icosahedral group has two non equivalent irreducible representations of dimension 3, and when decomposing the six-dimensional action defined above into irreducible representations by the standard method, one precisely finds these two representations. The relation between them is simply the following: if we realize both representations in the same three-dimensional space, then a rotation of $2\pi/3$ in one representation is a rotation of $-2\pi/3$ around the same axis for the other, and a rotation of $2\pi/5$ in one is a rotation of $\pm 4\pi/5$ around the same axis in the other. Observe that since these representations are non equivalent, the decomposition is unique and the orientations of the corresponding three-dimensional invariant subspaces are completely determined: these two three-dimensional subspaces are to be our $\mathbf{E}^{\parallel}$ and $\mathbf{E}^{\perp}$, as required by our second symmetry condition.

To distinguish between $\mathbf{E}^{\parallel}$ and $\mathbf{E}^{\perp}$, let us choose $\mathbf{E}^{\perp}$ as the subspace on which the orthogonal projections of the basis vectors $\boldsymbol{\varepsilon}_i$ are in the same relative position as the vectors $\mathbf{e}'_i$, which from now on will be identified with these projections. Then it is easy to verify that the projections $\mathbf{e}_i$ of the vectors $\boldsymbol{\varepsilon}_i$ on the other invariant subspace $\mathbf{E}^{\parallel}$ are in the relative position depicted on Fig. 2: the rule is simply that two vectors whose projections on $\mathbf{E}^{\parallel}$ form an acute angle have projections on $\mathbf{E}^{\perp}$ which form an obtuse angle, and vice-versa.

With this information, it is straightforward to compute the projectors $\pi^{\parallel}$ and $\pi^{\perp}$ on $\mathbf{E}^{\parallel}$ and $\mathbf{E}^{\perp}$ respectively. They are given by:

$$\pi^{\parallel} = \frac{1}{2\sqrt{5}} \begin{bmatrix} \sqrt{5} & 1 & -1 & -1 & 1 & 1 \\ 1 & \sqrt{5} & 1 & -1 & -1 & 1 \\ -1 & 1 & \sqrt{5} & 1 & -1 & 1 \\ -1 & -1 & 1 & \sqrt{5} & 1 & 1 \\ 1 & -1 & -1 & 1 & \sqrt{5} & 1 \\ 1 & 1 & 1 & 1 & 1 & \sqrt{5} \end{bmatrix}$$

and

$$\pi^{\perp} = \frac{1}{2\sqrt{5}} \begin{bmatrix} \sqrt{5} & -1 & 1 & 1 & -1 & -1 \\ -1 & \sqrt{5} & -1 & 1 & 1 & -1 \\ 1 & -1 & \sqrt{5} & -1 & 1 & -1 \\ 1 & 1 & -1 & \sqrt{5} & -1 & -1 \\ -1 & 1 & 1 & -1 & \sqrt{5} & -1 \\ -1 & -1 & -1 & -1 & -1 & \sqrt{5} \end{bmatrix}$$

Finally, let us specify the "window" in $\mathbf{E}^{\perp}$: it is the projection of the unit hypercube in $\mathbb{R}^6$. Since the hypercube is the convex envelope of its vertices $\sum_{i=1}^{6} \eta_i \varepsilon_i$, where the 64 vertices correspond to all the possible combinations of $\eta = 0$ or 1, and since the projection is linear, we find that the window $\mathbf{K}$ is the convex envelope of the 64 points $\sum_{i=1}^{6} \eta_i \mathbf{e}_i'$, with the same values of η_i. It is easy to see that only 32 of these 64 points fall on the convex envelope, in such a way that $\mathbf{K}$ is a polyhedron with 30 identical rhombic facets, 60 edges and 32 vertices, which is denoted the rhombic triacontahedron (Fig. 3).

The rhombic triacontahedron presents the full icosahedral symmetry, and thus fits our last symmetry requirement. In fact, its 32 vertices fall into two orbits under the action of the icosahedral group: 12 vertices form a

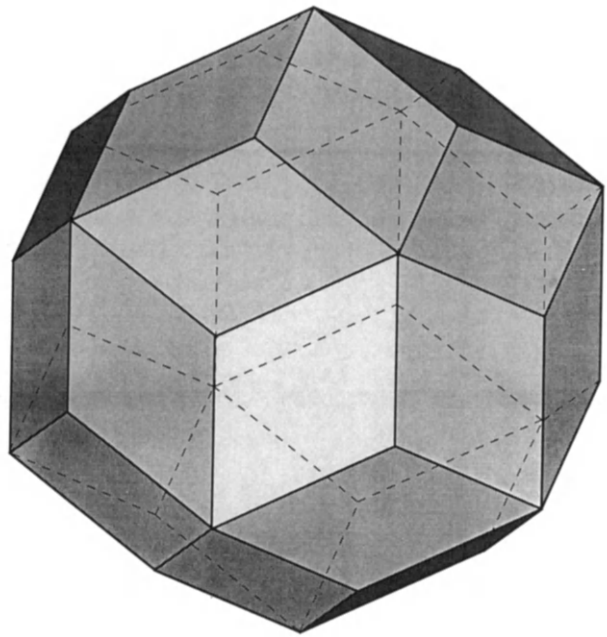

Figure 3. The rhombic triacontahedron.

regular icosahedron, and the 20 others a regular dodecahedron. Five rhombic facets are adjacent to each "icosahedral" vertex through an acute angle, and three come on each "dodecahedral" vertex with an obtuse angle.

Now, the construction of the three-dimensional Penrose tilings runs exactly as in the one-dimensional model: for any translation α in $\mathbf{E}^\perp$ such that the boundary $\partial\mathbf{K}_\alpha$ does not intersect the set $\pi^\perp(\mathbb{Z}^6)$, select all the vertices in $\mathbb{Z}^6$ whose projections on $\mathbf{E}^\perp$ fall inside $\mathbf{K}_\alpha$ and project them on $\mathbf{E}^\parallel$.

It is easy to verify that the set of forbidden α's, which was the projection of the lattice in the low dimensional example, is now the union of 15 dense families of planes, each family containing all the planes parallel to a symmetry plane of the icosahedral group, which intersect the projection $\pi^\perp(\mathbb{Z}^6)$. Since these planes are the projections of crystalline four-dimensional planes in $\mathbb{R}^6$, each of them contains infinitely many points of $\pi^\perp(\mathbb{Z}^6)$. Observe that this union is of measure zero, which means that almost all translations α are permitted. However, these planes completely disconnect $\mathbf{E}^\perp$: any continuous path in $\mathbf{E}^\perp$ crosses infinitely many such planes. In fact, we shall see that the elementary transformations of the tilings occur at these crossings, in such a way that this union of planes is a kind of "bifurcation locus".

Let us describe the resulting structure: the key point is that all the vertices of $\mathbb{Z}^6$ which fall inside the strip $\pi^{\perp\,-1}(\mathbf{F}_\alpha)$ are on a "corrugated" three-dimensional surface made of three-dimensional facets of hypercubes, which plays exactly the same role as the broken line in the previous example. We thus get after projection of this surface onto $\mathbf{E}^\parallel$ a tiling of $\mathbf{E}^\parallel$ by means of the projections of the three-dimensional facets of the hypercubic lattice, and we have now to examine these tiles.

Since these tiles are the projections of three-dimensional Euclidean cubes, we know *a priori* that they are parallelohedra. However, we get in fact rhombohedra on account of the icosahedral symmetry.

Let us first study the shapes of the two-dimensional facets which build the boundaries of our tiles: the six-dimensional hypercubic lattice has $\binom{6}{2} = 15$ different directions of two-dimensional facets. However, it is easy to see that they all belong to the same orbit of the icosahedral group. Consider for instance the geometry in $\mathbf{E}^\parallel$ as depicted in Fig. 2: the 15 directions of facets are spanned by all the pairs of vectors $\mathbf{e}_i$. Beyond the obvious five-fold symmetry around $\mathbf{e}_6$, one sees immediately that the facet $\{\mathbf{e}_1, \mathbf{e}_6\}$ corresponds to the facet $\{\mathbf{e}_1, \mathbf{e}_2\}$ through a five-fold rotation around $\mathbf{e}_1$, and slightly less immediately that the facet $\{\mathbf{e}_1, \mathbf{e}_2\}$ corresponds to the facet $\{\mathbf{e}_1, \mathbf{e}_3\}$ through the five-fold rotation around $\mathbf{e}_4$ which maps $\mathbf{e}_1$ on $-\mathbf{e}_3$ and $\mathbf{e}_2$ on $\mathbf{e}_1$. Thus we have the same shape realized in 15 different orientations, and it is a rhomb with angles $\text{Acos}(1/\sqrt{5}) = \text{Atan}(2) \approx 63° 26'$ and $\pi - \text{Atan}(2)$. In the same way, one can see that the $\binom{6}{3} = 20$ directions of three-dimensional facets fall into two orbits under the icosahedral group,

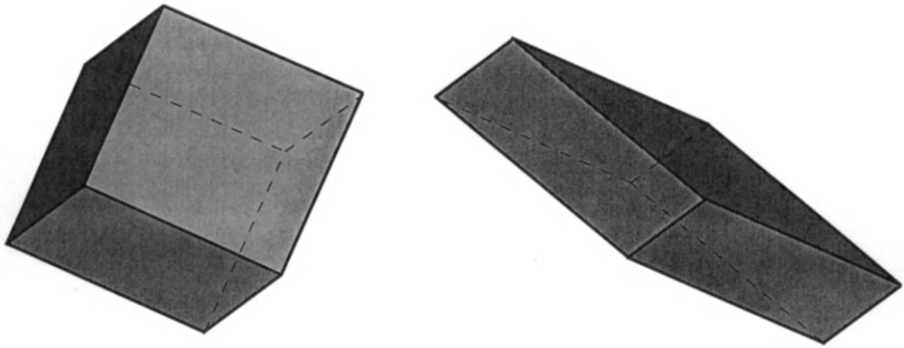

Figure 4. The two Ammann rhombohedra.

corresponding to two different shapes, each of them being realized in ten different orientations. Not surprisingly, these two tiles are the only two rhombohedra one can build with only one rhomb. They are known as Ammann rhombohedra (Mackay, 1982) and are depicted on Fig. 4: the thick one presents three rhombs joining together on the three-fold axis through their acute angle, and the flat one is built in the other way, with three obtuse angles around the three-fold axis.

Finally, the three-dimensional Penrose tilings are packings face-to-face of Ammann rhombohedra. Of course, only a small number of all the configurations which are possible from a combinatorial point of view are actually realized in this tilings: this is closely related to the long range order exhibited by these structures, namely their quasiperiodicity. Deferring the classification of the local packings to a subsequent section, we shall now enter into more details about the local isomorphism property.

3 The Local Isomorphism Property

The local isomorphism is a two-fold property: the first part is that *any finite packing of tiles which appears in a given tiling, appears infinitely many times in the same tiling with a well-defined frequency*. The second part asserts that *any finite packing of tiles which appears in a given tiling, appears in all the tilings*.

As will be made clear below, the first part is true for any tiling obtained by the projection method, while the second depends on some geometrical features of the construction.

3.1 The Low-Dimensional Case

To explain these properties, let us return to the low-dimensional model of Fig. 1. We want to show that any finite patch of tiles which appears

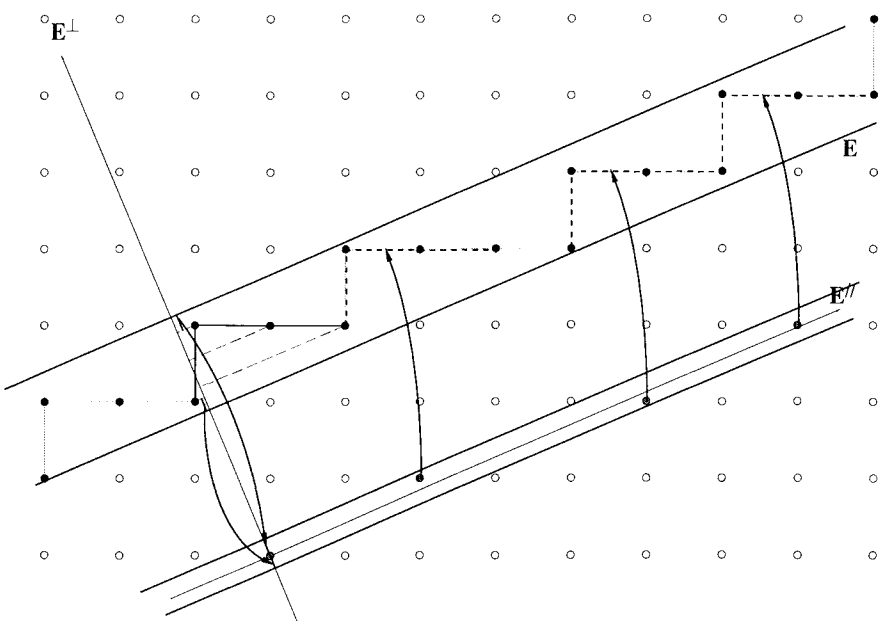

Figure 5. The construction of the auxiliary strip and an illustration of the local isomorphism property for the low dimensional model.

somewhere in the tiling is repeated infinitely many times. For this, let us pick such a finite sequence in $\mathbf{E}^{\parallel}$ and "lift" it as a piece of the zig-zag line. Since the boundaries of the strip are assumed not to contain any point of the lattice, it is clear that the projection on $\mathbf{E}^{\perp}$ of this piece of the zig-zag line does not touch the boundaries of the window $\mathbf{K}_{\alpha}$: there is some room left on each side, and this is the key of the property.

In fact, let us define an auxiliary strip whose thickness is equal to this space left around the projection: more technically, consider in $\mathbf{E}^{\perp}$ the set of translations which keep the projection of the finite piece of zig-zag line inside the window $\mathbf{K}_{\alpha}$. In this low-dimensional example, this set of translations is simply a segment of the line $\mathbf{E}^{\perp}$ which contains the origin. Now, consider the auxiliary strip for which this segment is the window. On account of the irrationality of the slope, this auxiliary strip certainly contains infinitely many lattice points. For each of these points, the translation which maps the origin onto it is a lattice translation "almost parallel" to $\mathbf{E}^{\parallel}$, and which by construction maps our finite piece of zig-zag line inside the main strip. But there is only one zig-zag line contained in this strip, so that the image of the finite piece through such a translation is another identical finite piece of the same zig-zag line, which yields upon projection

on $\mathbf{E}^{\parallel}$ a copy of our initial patch of tiles (Fig. 5). This proves the first part of the local isomorphism property in this low-dimensional case.

It can be shown that the set of translations falling in the auxiliary strip (or its projection on $\mathbf{E}^{\parallel}$), which is of course non-periodic on account of the irrationality of the orientation, is nevertheless distributed with a well-defined density: in fact, this set of translations is, as the tiling itself, a relatively dense quasiperiodic set. Since the density of these translations is nothing else but the frequency with which the given finite sequence is repeated, we conclude that this frequency is also well-defined.

Let us now make a few remarks about the relation between the length of the finite sequence and the frequency of its repetitions: it is clear that the density of translations is inversely proportional to the width of the auxiliary strip, so that the question is equivalent to the following: how fast does the projection on $\mathbf{E}^{\perp}$ of a finite piece of the zig-zag line approaches the end points of the window $\mathbf{K}_{\alpha}$ when length of the piece grows?

The answer is given by the classical theory of approximation in arithmetic, and depends on arithmetical properties of the slope. If this slope is an algebraic number (that is, a zero of a polynomial with integer coefficients) it can be shown, as a consequence of Roth's theorem, that for almost all sequences the mean distance between two successive copies of the sequence is proportional to its length: this corresponds to the fact that algebraic numbers are not very well approximated by rational numbers. On the contrary, if the slope is very well approximated by rational numbers, for instance, if it is a Liouville number, then the mean distance between copies of a sequence can grow faster than any power of the length of that sequence.

Finally, it is interesting to examine what happens when the slope of $\mathbf{E}^{\parallel}$ becomes a rational number: then the tiling is periodic and for large enough finite sequences, the associated set of translations is simply the set of periods. This is easily observed in our framework: for a rational slope, the projection of the lattice on $\mathbf{E}^{\perp}$ is a discrete set. It may happen that for a short sequence of tiles, the window of the auxiliary strip is large enough to contain more than one point of this set. But for longer sequences the origin is the only such point. Then the set of translations corresponds to the set of lattice vectors which project on the origin through $\pi^{\perp}$, and this intersection of $\mathbf{E}^{\parallel}$ with $\mathbb{Z}^2$ is precisely the set of periods.

Let us now come to the second part of the local isomorphism property, and show that any finite patch of tiles which appears in one tiling appears in all the family. We now have to consider two parallel strips corresponding to two tilings. As in the previous case, we pick a finite sequence in one tiling, lift it in the zig-zag line and project the finite piece of the line onto $\mathbf{E}^{\perp}$. We now construct an auxiliary strip by looking for all the translations in

$\mathbf{E}^{\perp}$ which map this projection into the window corresponding to the other tiling. Of course, what we obtain is merely the translation of the auxiliary strip of the previous case by the vector which maps the first strip onto the other, so that for an irrational slope (and a uniformly *dense* projection of the lattice), there are infinitely many lattice translations inside the auxiliary strip, which entails the conclusion.

However, observe that the argument now breaks down in the special case of a rational slope; in fact, it may happen that the translated window of the auxiliary strip does not contain any point of the *discrete* projection of the lattice on $\mathbf{E}^{\perp}$, in such a way that the set of translations is empty. We shall need this remark later for the definition of the local isomorphism classes.

3.2 The Three-Dimensional Case

Let us now turn to the three-dimensional Penrose tilings. In fact, there is almost nothing to change in the previous discussion.

Observe first that we are in a "completely irrational" case: this means that the two projections of the hypercubic lattice $\mathbb{Z}^6$ on $\mathbf{E}^{\parallel}$ and $\mathbf{E}^{\perp}$ are both dense and homogeneous. Then consider a tiling defined by the associated rhombic triacontahedron $\mathbf{K}_{\alpha}$, pick any finite patch of tiles in it, lift them as a set of three-dimensional facets of the hypercubic lattice, and project these facets on $\mathbf{E}^{\perp}$. As in the previous model, and since we restrict to the cases where no points of $\pi^{\perp}(\mathbb{Z}^6)$ fall on the boundary of the triacontahedron, this projection does not touch the boundary. We define an auxiliary strip whose window is the set of translations which keep the projection inside the triacontahedron $\mathbf{K}_{\alpha}$, and it is clear that any lattice translation that falls inside the auxiliary strip maps the set of three-dimensional facets onto a piece of the three-dimensional "corrugated surface" in such a way that the projection on $\mathbf{E}^{\parallel}$ of this lattice translation maps our finite patch of tiles onto a copy of it. Observe that by construction the window of the auxiliary strip is a convex polyhedron, and that any facet of this polyhedron is parallel to one of the facets of the triacontahedron.

Due to the homogeneity of $\pi^{\perp}(\mathbb{Z}^6)$, the density of copies of a given finite patch is simply proportional to the volume of the corresponding auxiliary window. However, the precise distribution of these copies depends on the shape of the window, which in turn depends on the shape of the patch. Loosely speaking, if the patch is very elongated in one direction in $\mathbf{E}^{\parallel}$, then the auxiliary window will be very flat in the corresponding direction in $\mathbf{E}^{\perp}$, resulting in very sparse copies in the direction of elongation of the patch.

This shows that any finite set of tiles which appears one time in a given tiling, appears infinitely many times. Now, the same argument shows that this finite set of tiles appears also in every three-dimensional Penrose tiling:

we have only to consider, instead of the set of translations which keep the previous projection inside the triacontahedron $\mathbf{K}_\alpha$, the set of translations which map it inside any other allowed triacontahedron $\mathbf{K}_\beta$. Once again, the homogeneity of $\pi^\perp(\mathbb{Z}^6)$ insures that we will find infinitely many lattice translations in the auxiliary strip defined by this new window.

To conclude the considerations relative to the notion of local isomorphism, let us observe the following: in the general projection method, the non-periodicity of the tilings results of the orientation of $\mathbf{E}^\parallel$ being irrational (expressed by the condition $\mathbf{E}^\parallel \cap \mathbb{Z}^n = \{0\}$) and the second part of the local isomorphism property results of the projection of $\mathbb{Z}^n$ on $\mathbf{E}^\perp$ being homogeneous and dense. For the low-dimensional example, this is of course the same condition, but this is not the case in general: even when $\mathbf{E}^\parallel \cap \mathbb{Z}^n = \{0\}$, one may find a sublattice in $\mathbf{E}^\perp \cap \mathbb{Z}^n$. In such a situation, $\mathbf{E}^\perp$ splits into the product of two subspaces, the projection of $\mathbb{Z}^n$ being homogeneous and dense on one component and a discrete periodic lattice on the other. Accordingly, the argument for the second part of the local isomorphism property works only when the translation mapping on each other the windows of the two strips involved is parallel to the "dense" component, and otherwise, breaks down. Then the set of all the tilings falls into classes, known as "local isomorphism classes" (Levine, 1986), each class containing a set of tilings sharing the same set of finite subsets. It is easy to see that the family of local isomorphism classes is parametrized by the points of the unit cell of the sublattice on which projects $\mathbb{Z}^n$ in the "discrete" component.

Moreover, we have in this general case to redefine the symmetry of the structure in the following "final" form: an operation is a symmetry of a tiling if and only if the image up to a translation is a tiling belonging to the same local isomorphism class.

However, this does not happen for the three-dimensional Penrose tilings, for which $\mathbf{E}^\perp$ and $\mathbf{E}^\parallel$ play equivalent roles. In other words, we have only one local isomorphism class in this case, and one cannot distinguish between all these tilings on the basis of any local property, so that for physical purposes one should generally think of all the class as a single object. Let us sketch how this idea can be made mathematically rigorous: take arbitrarily any two tilings in the same local isomorphism class, and select an arbitrary vertex as the origin in each of them. Since the choices are arbitrary, the two tilings do not in general coincide on any neighborhood of their origin. However, one can show that there exist infinite sequences of translations which bring in coincidence larger and larger regions of the first one with larger and larger identical neighborhoods of the origin in the second one, in such a way that the sequence of translated copies of the first tiling converges point-wise to the second one. Loosely speaking, one can

consider these sequences of translations as a way of handling "infinite" translations, and conclude that the "fine" distinctions between the infinity of different tilings are rubbed out as soon as one allows "infinite" translations in the definition of their equivalence.

4 Classification of Local Packings

In the previous section, we have shown the existence of a set of translations which map any finite part of the tiling onto a copy of it. We shall now compute explicitly these sets when the finite part under consideration contains only one tile, and examine the more complex situations where the finite parts are all the possible arrangements of tiles around a common vertex.

4.1 The Existence Domains of the Tiles

To begin with, consider a single edge, and let us find all the points in the tiling which are the origins of such an edge. Let $\mathbf{K}_\alpha$ be the triacontahedron defining the tiling, and $\mathbf{e}_1$ the edge: in order to find an edge $\mathbf{e}_1$ attached to the point x in the tiling, we must have both x and $x + \mathbf{e}_1$ in this tiling. If ξ is the unique vertex of $\mathbb{Z}^6$ such that $\pi^{\parallel}(\xi) = x$, then both ξ and $\xi + \varepsilon_1$ must belong to the strip, which means that the two projections "on the other side" $x' = \pi^{\perp}(\xi)$ and $x' + \mathbf{e}'_1 = \pi^{\perp}(\xi + \varepsilon_1)$ must fall simultaneously in $\mathbf{K}_\alpha$. It is immediate that the set of such x' is the intersection of $\mathbf{K}_\alpha$ with the translated $\mathbf{K}_\alpha - \mathbf{e}'_1$. Due to the very geometry of the triacontahedron, this intersection is simply the parallelohedron spanned by the five other vectors $\mathbf{e}'_i$, $i = 2 \cdots 6$. It is named rhombic icosahedron since it has twenty facets which are the same rhombs found in the triacontahedron and is easily seen to be the projection through $\pi^{\perp}$ of a five-dimensional facet of the hypercube.

We shall call this icosahedron the "existence domain" of the edge: each point falling in it corresponds to the origin of an edge $\mathbf{e}_1$ in the tiling. Observe that we could as well consider the "existence domain" of the extremities of the edge: it is the intersection of $\mathbf{K}_\alpha$ with $\mathbf{K}_\alpha + \mathbf{e}'_1$, and is readily seen to be another rhombic icosahedron, which corresponds to the previous through a translation of vector $\mathbf{e}'_1$. Of course, the points in the intersection of these two existence domains correspond to vertices in the tiling which are both the origin and the extremity of an edge parallel to $\mathbf{e}_1$.

This notion of existence domain is simply a reinterpretation of the set of translations associated to the auxiliary strips of the previous section: these sets were "relative" translations with respect to a given copy of the local pattern. We consider now "absolute" sets of translations, with respect to the origin. Of course, both sets share the same geometry and the same volume.

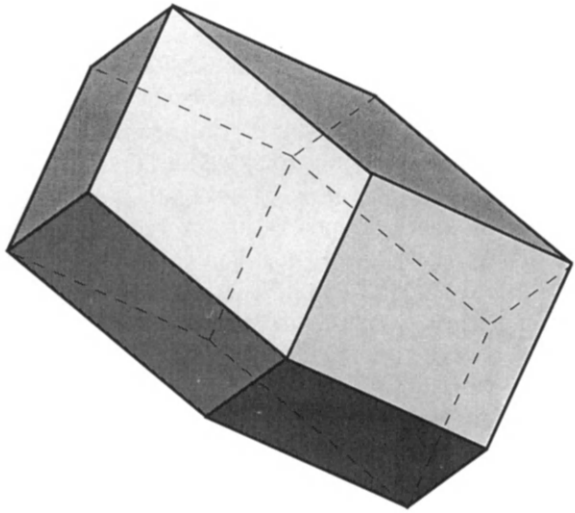

Figure 6. The rhombic dodecahedron, a projection of a four-dimensional facet of the hypercube and the existence of the rhomb which build the boundary of the Ammann tiles.

Now, if we make this analysis for all the directions of edges, we find 12 rhombic icosahedra in our triacontahedron. They cover completely (and several times) the triacontahedron, and this corresponds to the fact that any vertex in the tiling is the origin or the extremity of at least one edge (and in fact several ones).

One can work out the same classification for the facets and the tiles themselves: consider for instance the facet spanned by $\{\mathbf{e}_1, \mathbf{e}_2\}$: a vertex x in the tiling is attached to such a facet if and only if both x and $x + \mathbf{e}_2$ are the origins of an edge $\mathbf{e}_1$. Then the corresponding existence domain is the intersection of the icosahedron corresponding to the edge $\mathbf{e}_1$ and its translation through the vector $-\mathbf{e}_2'$. Since this translation belongs to the set of vectors which span the icosahedron, the geometry is again very simple: the intersection is the parallelohedron spanned by the four remaining vectors $\mathbf{e}_i'$, $i = 3 \cdots 6$. It is a rhombic dodecahedron with twelve facets and can be considered as the projection on $\mathbf{E}^\perp$ of a four-dimensional facet of the hypercube (Fig. 6).

One can find 60 such rhombic dodecahedra in the triacontahedron, corresponding to the four vertices of each of the fifteen directions of two-dimensional facets. As previously, they cover the whole triacontahedron, and they intersect on subsets corresponding to points simultaneously attached to each of the relevant facets.

Finally, let us make the same construction for the tiles: in order for a

rhombohedron $\{\mathbf{e}_1, \mathbf{e}_2, \mathbf{e}_3\}$ to be attached to the point x, one must have a facet $\{\mathbf{e}_1, \mathbf{e}_2\}$ attached to the two points x and $x + \mathbf{e}_3$. The corresponding x' in $\mathbf{E}^\perp$ are found in the intersection of the dodecahedron $\{\mathbf{e}'_3, \mathbf{e}'_4, \mathbf{e}'_5, \mathbf{e}'_6\}$ and its translation through $-\mathbf{e}'_3$. The resulting polyhedron is simply the rhombohedron $\{\mathbf{e}_4, \mathbf{e}_5, \mathbf{e}_6\}$, so that we can conclude that the existence domains of the Ammann rhombohedra are other rhombohedra. More precisely, it is easy to see that the existence domain of a rhombohedron $\{\mathbf{e}_i, \mathbf{e}_j, \mathbf{e}_k\}$ is the rhombohedron $\{\mathbf{e}'_l, \mathbf{e}'_m, \mathbf{e}'_n\}$, where (i, j, k, l, m, n) is a permutation of $(1 \cdots 6)$. Each of these existence domains sits in the triacontahedron in eight different positions according to the vertex considered as the origin of the corresponding tile, and they tile the triacontahedron in many different ways (in fact, one can show that there are 120 tilings of the triacontahedron by the rhombohedra, and that these tilings have no symmery, in such a way that they correspond to only one orbit under the icosahedral group).

Observe that the existence domain of a tile of a given type (prolate or oblate) is a rhombohedron of the same type. This leads us to a non-trivial conclusion concerning the relative abundance of the two types of tiles: as explained in the previous section, the homogeneity of the projection $\pi^\perp(\mathbb{Z}^6)$, which results from the irrationality of the orientations, implies that the frequency, with which is found any given pattern, is proportional to the volume of its existence domain. Since, as one can easily compute, the ratio of the volumes of the two kinds of rhombohedra is the golden mean $\tau = (\sqrt{5} + 1)/2 = 1.618\ldots$, one can conclude that the prolate rhombohedra are τ times more abundant in any three-dimensional Penrose tiling than the oblate ones.

Our next step will be to describe how one can work out the complete classification of the possible local environments of each vertex in the tiling.

4.2 *The Local Environments in the Penrose Tilings*

As mentioned earlier, a vertex x is simultaneously attached to two patterns if and only if the corresponding point x', which is the projection on $\mathbf{E}^\perp$ of the vertex of $\mathbb{Z}^6$ "above" x, falls in the intersection of the associated existence domains. In particular, we can find the list of tiles attached to any vertex x by looking for all the existence domains of tiles in which the corresponding x' falls in the triacontahedron. In fact, the intersections of these $8 \times 20 = 160$ rhombohedra yield a cellular decomposition of the triacontahedron in which each cell corresponds to a local environment whose frequency in the tiling is proportional to the volume of the cell.

However, the study of this cellular decomposition is not very simple.

Observe that each existence domain of tile is the projection on $\mathbf{E}^{\perp}$ of a three-dimensional facet belonging to the boundary of the six-dimensional hypercube, so that the boundaries of the cells are made of the projections of the $16 \times 15 = 240$ two-dimensional facets of the hypercube, and the situation is difficult to visualize directly.

A possible way to work out this study is the following: one can produce with a computer a set of drawings of the traces of these 240 rhombs on a family of planes orthogonal to a five-fold axis of the triacontahedron. These drawings are used to identify the vertices of the cells (which are either a vertex of a rhomb, the intersection of two edges, of an edge and a rhomb or of three rhombs) and one can then compute analytically their coordinates. Finally, one can decompose the cells into tetrahedra and compute their volumes exactly.

Of course, on account of the icosahedral symmetry, it is sufficient to make this study inside a fundamental domain of the icosahedral group, which is a cone centered on the center of the triacontahedron and bounded by three planes intersecting pair-wise on a two-fold, three-fold and five-fold axis (the trace on the triacontahedron of the fundamental domain is a quarter of a facet).

Using this crude method, one finds that there exist only twenty four local environments in the three-dimensional Penrose tilings.

Rather than describing precisely each of these environments, let us explain how one can generate the whole set step by step. The idea is to examine what happens when one crosses a boundary between two cells.

The departure point is the cell closest to the boundary of the triacontahedron. It is the intersection of all the existence domains of rhombohedra which contain in their boundaries the same facet of the triacontahedron. Given the two vectors which span the facet, there are four choices for a third vector, so that this cell is the intersection of four existence domains of rhombohedra and thus corresponds to an environment made of four tiles, whose construction is straightforward: consider for instance the facet $\alpha + \{\mathbf{e}'_1, \mathbf{e}'_2\}$ of the triacontahedron translated at $\alpha \in \mathbf{E}^{\perp}$. The points close enough to this facet fall in the intersection of the four existence domains $\alpha + \{\mathbf{e}'_1, \mathbf{e}'_2, \mathbf{e}'_3\}$, $\alpha + \{\mathbf{e}'_1, \mathbf{e}'_2, \mathbf{e}'_4\}$, $\alpha + \{\mathbf{e}'_1, \mathbf{e}'_2, \mathbf{e}'_5\}$ and $\alpha + \{\mathbf{e}'_1, \mathbf{e}'_2, \mathbf{e}'_6\}$. This means that around the corresponding points in $\mathbf{E}^{\parallel}$, we find the four tiles spanned by $\{\mathbf{e}_4, \mathbf{e}_5, \mathbf{e}_6\}$, $\{\mathbf{e}_3, \mathbf{e}_5, \mathbf{e}_6\}$, $\{\mathbf{e}_3, \mathbf{e}_4, \mathbf{e}_6\}$ and $\{\mathbf{e}_3, \mathbf{e}_4, \mathbf{e}_5\}$. This packing is easily seen to form a rhombic dodecahedron. This simplest environment is realized in 30 configurations, corresponding to the 30 facets of the triacontahedron, and since there are only 15 different orientations of dodecahedra, we see that each of them is tiled in two different ways, corresponding to a pair of parallel opposite facets in the triacontahedron. These two tilings are related by a symmetry with respect to the symmetry

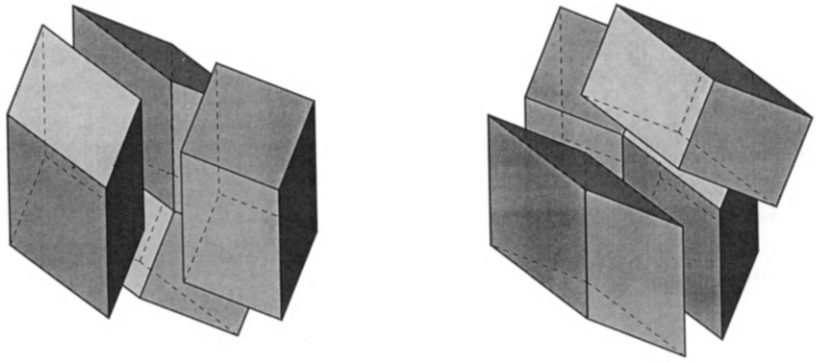

Figure 7. The two tilings of the rhombic dodecahedron by means of two prolate and two oblate rhombohedra.

plane orthogonal to the long diagonal of the rhombic dodecahedron (Fig. 7).

These environments play a special role because their existence domains covers completely the boundary of the triacontahedron, so that when one moves the triacontahedron in $\mathbf{E}^{\perp}$ to generate infinitely many different tilings, the vertices which appear in or vanish from the tiling (that is, whose images in $\mathbf{E}^{\perp}$ enter into or leave the moving triacontahedron) are generically surrounded by this special environment (there are two other environments whose existence domains touch the boundary, but the contact is by an edge or a vertex, so that they generically do not intervene in the present considerations). Moreover, for each point leaving the triacontahedron through a given facet, there is another point entering through the opposite facet, and these two points differ by the sum of four vectors $\mathbf{e}_i'$, which maps on each other the two opposite facets. It is easy to see that the image in $\mathbf{E}^{\parallel}$ of such a sum of four vectors is the small translation which maps on each other the two possible positions of the internal vertex of a tiled rhombic dodecahedron.

In other words, the generic local process which transforms a Penrose tiling into another is simply the "jump" of the internal point of a dodecahedron from one position to the only other one, accompanied by the reflection of the surrounding four tiles. This is sufficient to generate the whole family of Penrose tilings, since the non-generic transformations can be analyzed as a succession of such "jumps", involving neighboring dodecahedra. Observe the complete analogy with the low-dimensional model discussed above.

Let us now examine what happens when one crosses a cell boundary inside the triacontahedron. As mentioned above, such a boundary is a piece

of a two-dimensional facet and is thus attached to four existence domains of tile. In the previous case, these four existence domains were of course on the same side of their common facet, but this is no longer the case for the internal facets, for which one finds either one domain on one side and three on the other, or two domains on each side. This controls the way in which some tiles in the first environment are substituted by others when one enters into the domain of the second environment by crossing the boundary: in the first case, one leaves the domain of one tile to enter at the same time into the domains of three other tiles (or the converse). Similarly, in the second case, one finds the substitution of a pair of tiles by another pair.

Here is a simple argument which exhibits precisely these substitutions: recall that the only elementary change in the tiling is the "jump" of the internal point of a dodecahedron together with the reflection of its tiling. Such a jump does not change the type of environment of the internal point but does affect the types of environment of the vertices of the tiling which are on the boundary of the dodecahedron in which the jump occurs, and we get in this way all the elementary substitutions. To describe them, we have only to look at the packing of four tiles which build the dodecahedron and the effect on it of the symmetry with respect to the plane orthogonal to the long diagonal (Fig. 7). Observe first that the 14 vertices of the dodecahedron fall in four classes of orbits under this symmetry: four vertices fall in the plane and are invariant, the "tips" along the long diagonal are exchanged, and the other vertices fall in two pairs of equivalent orbits of two points. For each class of orbits, we have only to read the effect of the symmetry on the picture. The results are depicted in Fig. 8: for the "tips", the substitution exchanges a pair of oblate rhombohedra and a pair of prolate ones. The vertices in the symmetry plane give the only other type of substitution $2 \leftrightarrow 2$, with a pair oblate-prolate replaced by another pair oblate-prolate symmetric with respect to the symmetry plane. There are two kinds of substitution $1 \leftrightarrow 3$, corresponding to the remaining classes of orbits: in the first one, an oblate rhombohedron is exchanged with a triplet prolate-prolate-oblate, and in the second, a prolate one is exchanged with a triplet oblate-oblate-prolate, as shown on the figure.

This concludes the description of the method which allows to construct the 24 environments. Of course, not all the possible combinations of these elementary substitutions occur, but only those prescribed by the cellular decomposition of the triacontahedron. At each step, that is, for a given boundary of a cell corresponding to a known environment, one has to identify the quadruplet of rhombohedra involved in the substitution, then identify the substitution and perform it .... The situation is made more difficult by the fact that it happens that two rhombs (of which are made the boundaries of the cells) overlap in the triacontahedron, so that one has to perform

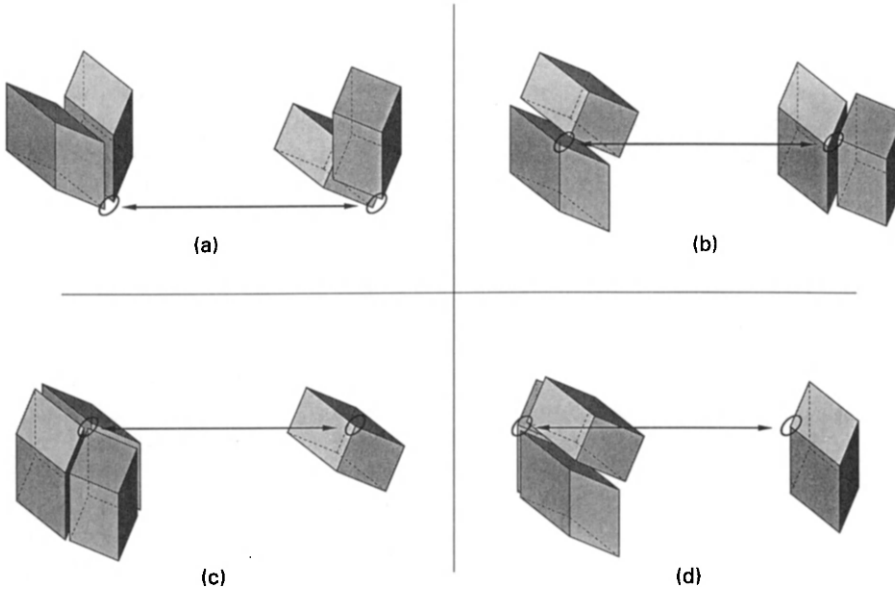

Figure 8. The four elementary substitutions of tiles which generate the whole set of local environments of vertices in the three-dimensional Penrose tilings.

two substitutions at the same time (such overlappings, which correspond to "flat cells" of zero volume, play a key role in the existence of matching rules for the three-dimensional Penrose tilings, as explained below).

The same method of classification of local environments may of course be applied to other problems. For instance, one can look for the possible sets of edges attached to each vertices. This amounts to study of the cellular decomposition of the triacontahedron induced by its intersections with twelve other triacontahedra translated by $\pm \mathbf{e}_i'$. Up to the icosahedral symmetry, there are 16 such sets, and the corresponding cells (which are of course exact unions of cells of the previous classification) are not simpler to construct.

Finally, let us give some numerical results: there is a fraction $\tau^{-3} \approx 0.236\ldots$ of all the vertices which are surrounded by the simplest environment of four tiles. The vertices which are surrounded by a symmetric star of twelve edges correspond to a union of cells whose shape is a small triacontahedron, concentric to the triacontahedron which defines the tiling and homothetic with a ratio τ^{-2}, so that the relative abundance of these vertices is $\tau^{-6} \approx 0.056\ldots$. In this last set, the vertices surrounded by a whole star of 12 thick rhombohedra correspond to the central cell of the triacontahedron. It is again a triacontahedron, homothetic of the main one with a ratio τ^{-3}, and thus the fraction of such vertices is $\tau^{-9} \approx 0.013\ldots$. This cell plays a

special role with respect to the self-similarity properties of these tilings: one can show that the vertices surrounded by such a star of 12 thick rhombohedra are the vertices a new Penrose tiling "inflated" with a ratio τ^3, which means that the tiles of this "inflated" tiling are homothetic of the previous ones with this ratio. Then the short diagonal of the inflated thin tile coincide with the long diagonal of the previous thick tile, in such a way that the two vertices of this inflated short diagonal correspond in the old tiling to vertices surrounded by two interpenetrating stars of 12 thick rhombohedra which share a rhombohedron (however, it is important to observe that there are infinitely many ways to extract an "inflated" tiling with the same ratio τ^3, out of a given one: namely, by selecting the vertices which fall in a small triacontahedron, homothetic with the ratio τ^{-3}, *whatever the position of this small triacontahedron inside the main one.* This is in sharp contrast with the two-dimensional Penrose tilings for which there is a *unique* inflation of ratio τ).

5 The Cut Description and the Oblique Tiling

We shall now establish the relation between the projection method which is discussed here and the more general "cut description" of any quasiperiodic set of points (Bak, 1986).

Let us return once again to the low-dimensional model of Fig. 1. One can devise several variants of the strip construction. For instance, it is clearly equivalent to select those points which fall inside our strip and to select one vertex (the upper left in this case) for each square in the lattice which intersects the line $\mathbf{E}$: this is a possible approach of the so-called "grid method" (De Bruijn, 1981). In another variant, one can build directly the vertices of the tiling of $\mathbf{E}$ as the intersections with $\mathbf{E}$ of a suitable set of line segments periodically distributed in the plane.

In fact, consider the projection $\mathbf{K}$ of the unit square onto the line $\mathbf{E}^\perp$: it is a line segment attached to the origin. Now, let us attach a copy of $-\mathbf{K}$ (the inversion of $\mathbf{K}$ through the origin) to each vertex of the lattice. We obtain in this way the lattice of line segments depicted in Fig. 9, and one immediately sees that the intersections of these segments with $\mathbf{E}$ are nothing else but the vertices of the non periodic tiling built on $\mathbf{E}$ with the strip method.

This conclusion remains true in higher dimensions. Here is a simple argument which is dimension-independent: consider a lattice point p and project it on $\mathbf{E}^\parallel$ and $\mathbf{E}^\perp$. It falls inside the strip if its projection on $\mathbf{E}^\perp$ falls inside $\mathbf{K}_\alpha$, that is can be written $\alpha + \zeta$, where α is the translation of the strip and $\zeta \in \mathbf{K}$. But this equality can be read $p - \zeta \in \mathbf{E}^\parallel + \alpha$, which precisely

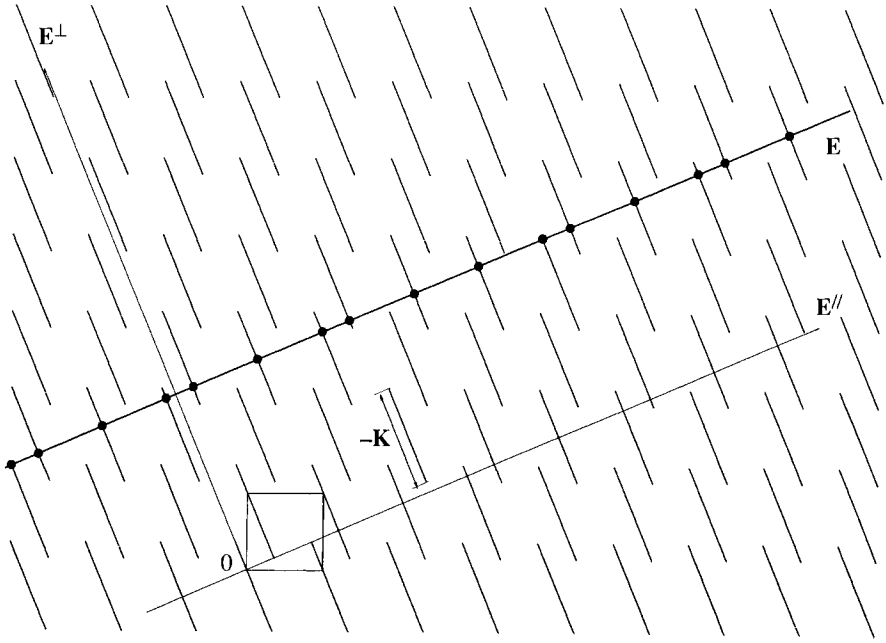

Figure 9. The cut method in the low-dimensional model.

expresses the intersection of the cut $\mathbf{E}^{\parallel} + \alpha$ with the copy of $-\mathbf{K}$ translated at the point p, and this intersection is the projection of p onto $\mathbf{E}^{\parallel}$.

This is the "cut method". As shown above, it contains the projection construction of our non-periodic tilings as a special case but is a more general way for constructing quasiperiodic sets of points: the idea is that one does not destroy the quasiperiodicity (which depends only on the periodicity in the high-dimensional space and on the cut being a plane), if one replaces $-\mathbf{K}$ by more general "atomic surfaces" which need not to be contained in a plane parallel to $\mathbf{E}^{\perp}$. Notice the analogy with the classical theory of modulated crystals of Janner and Janssen, which appears as a special case of this cut construction where $\mathbf{E}^{\perp}$ is one-dimensional and the "atomic surfaces" connect to each other to form continuous lines.

Until now, we have considered as granted that the projection construction actually yields tilings. This is clearly the case for the low-dimensional model, but it would be better to have a dimension-independent argument. Such a general argument is provided by the construction of the so-called "oblique tiling".

The idea is the following: consider any tiling of $\mathbb{R}^n$ and any plane cut

through this tiling. Each time the cut is generic, that is, intersects transversely the boundaries of the tiles, the traces of the tiles on the cut make up a covering of the cut, without overlaps or holes. But this covering is not a tiling in general, since there is no reason for the traces of the tiles to belong to a finite set of shapes. For instance, consider a cut with an irrational slope through the standard square tiling of the plane: since there is no minimal distance between the vertices of the tiling and the cut, there is no minimal length for the segments of the induced covering of the cut, and this entails that there are infinitely many different lengths in this covering.

However, it is possible to adapt the shape of the tiles of tiling of $\mathbb{R}^n$ to the orientation of the cut in order to obtain only a finite number of shapes in the generic cuts: the trick is to make the boundaries of the tiles parallel to either the cut $\mathbf{E}^{\parallel}$ or its orthogonal $\mathbf{E}^{\perp}$. The construction of such an oblique tiling is as follows. Since it is recursive, one can explain it for the plane without restricting the generality (Fig. 10).

Let us start with the unit square, spanned by the canonical basis $(\boldsymbol{\varepsilon}_1, \boldsymbol{\varepsilon}_2)$. We define $\mathbf{e}_i = \pi^{\parallel}(\boldsymbol{\varepsilon}_i)$ and $\mathbf{e}'_i = \pi^{\perp}(\boldsymbol{\varepsilon}_i)$ for $i = 1, 2$. Observe that $\boldsymbol{\varepsilon}_i \wedge \boldsymbol{\varepsilon}_2 = \mathbf{e}_1 \wedge \boldsymbol{\varepsilon}_2 + \mathbf{e}'_1 \wedge \boldsymbol{\varepsilon}_2 = 1$ (this is the area of the unit square), and that the two exterior products $\mathbf{e}_1 \wedge \boldsymbol{\varepsilon}_2$ and $\mathbf{e}'_1 \wedge \boldsymbol{\varepsilon}_2$ are both positive. This means that the two parallelograms spanned by $\{\mathbf{e}_1\ \boldsymbol{\varepsilon}_2\}$ and $\{\mathbf{e}'_1, \boldsymbol{\varepsilon}_2\}$ do not overlap, so that the union $\{\mathbf{e}'_1, \boldsymbol{\varepsilon}_2\} \cup (\mathbf{e}'_1 + \{\mathbf{e}_1, \boldsymbol{\varepsilon}_2\})$ is still a unit cell for the lattice $\mathbb{Z}^2$, as depicted on the second part of Fig. 10. Now, let us proceed to the same decomposition for the vector $\boldsymbol{\varepsilon}_2$ and each parallelogram. For the same reasons, we get a new unit cell of $\mathbb{Z}^2$ made of four subcells spanned by $\{\mathbf{e}'_1, \mathbf{e}_2\}$, $\{\mathbf{e}'_1, \mathbf{e}'_2\}$, $\{\mathbf{e}_1, \mathbf{e}_2\}$ and $\{\mathbf{e}_1, \mathbf{e}'_2\}$. But the two subcells spanned by $\{\mathbf{e}'_1, \mathbf{e}'_2\}$ and $\{\mathbf{e}_1, \mathbf{e}_2\}$ are flat and give a null contribution, so that we obtain finally only two subcells whose union is a fundamental domain of $\mathbb{Z}^2$ (last part of Fig. 10). The corresponding tiling of the plane (Fig. 11) is the oblique tiling.

Observe that whatever the order of the decomposition, the resulting tiling is the same. Since each tile is the product of the projection of a basis vector on $\mathbf{E}^{\parallel}$ by the projection of the other on $\mathbf{E}^{\perp}$, it is clear that any cut parallel to $\mathbf{E}^{\parallel}$ which does not intersect the lattice inherits a tiling by means of the two projections $\mathbf{e}_1$ and $\mathbf{e}_2$, which is again our non-periodic tiling: in fact, the subset of the boundary of the tiles of the oblique tiling which is parallel to $\mathbf{E}^{\perp}$ is by construction the same as the set of "atomic surfaces" of the cut description.

Due to its recursive character, the same argument works in any dimension. For the three-dimensional Penrose tilings, it runs as follows: start with the unit hypercube spanned by $\{\boldsymbol{\varepsilon}_1, \boldsymbol{\varepsilon}_2, \boldsymbol{\varepsilon}_3, \boldsymbol{\varepsilon}_4, \boldsymbol{\varepsilon}_5, \boldsymbol{\varepsilon}_6\}$, decompose $\boldsymbol{\varepsilon}_1$ as $\mathbf{e}_1 + \mathbf{e}'_1$ in $\mathbf{E}^{\parallel}$ and $\mathbf{E}^{\perp}$ to obtain a new cell made of the two parallelohedra $\{\mathbf{e}_1, \boldsymbol{\varepsilon}_2, \boldsymbol{\varepsilon}_3, \boldsymbol{\varepsilon}_4, \boldsymbol{\varepsilon}_5, \boldsymbol{\varepsilon}_6\}$ and $\{\mathbf{e}'_1, \boldsymbol{\varepsilon}_2, \boldsymbol{\varepsilon}_3, \boldsymbol{\varepsilon}_4, \boldsymbol{\varepsilon}_5, \boldsymbol{\varepsilon}_6\}$, and iterate the process. Since the property of getting a cell of $\mathbb{Z}^6$ is preserved at each step,

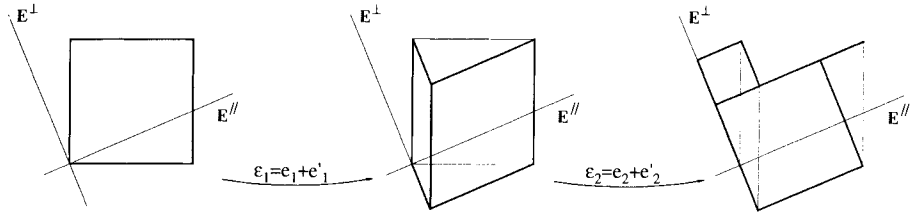

Figure 10. The construction of the unit cell of the oblique tiling of the plane in the low-dimensional model.

we end with a final cell which is *a priori* the union of 64 subcells. However, only those which are spanned by three vectors in $\mathbf{E}^{\parallel}$ and three vectors in $\mathbf{E}^{\perp}$ have a non-zero volume, so that the cell of the oblique tiling is in fact the union of 20 subcells, each of which being the product of a rhombohedron in $\mathbf{E}^{\parallel}$ by its existence domain in $\mathbf{E}^{\perp}$, in such a way that any cut parallel to $\mathbf{E}^{\parallel}$ which does not intersect the lattice $\mathbb{Z}^6$ inherits the three-dimensional Penrose tiling.

Beyond providing a satisfactory proof of the fact that the projection method actually yields tilings, the notion of oblique tiling is to be under-

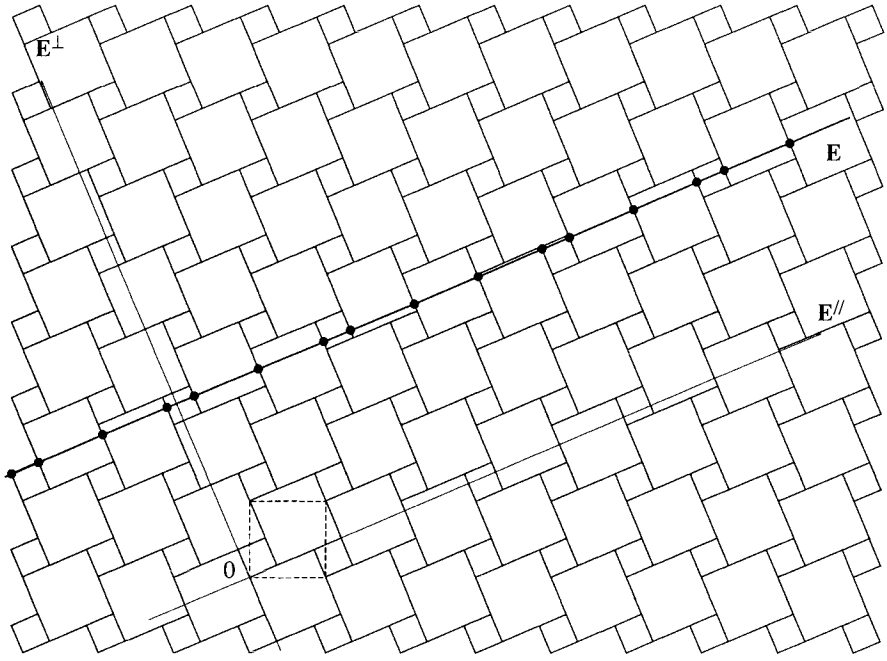

Figure 11. The oblique tiling of the plane.

stood as a generalization of the cut method in the following sense: the cut method is a way of selecting points (zero-dimensional objects) by intersection between the cut and the atomic surfaces. Sections of the oblique tilings, on the other hand, select either points, edges, facets, or the entire tiles.

Observe that the "atomic surfaces" of the cut method, which are triacontahedra attached to each vertex of $\mathbb{Z}^6$, appear in the construction of the oblique tiling as one of the two lowest dimensional flat cells, spanned by the 6 projections $\mathbf{e}_i'$. More generally, consider the 44 flat cells: due to the symmetric roles played by $\mathbf{E}^{\parallel}$ and $\mathbf{E}^{\perp}$ in the construction, they fall in two sets of 22 cells which are parallel either to $\mathbf{E}^{\parallel}$ or $\mathbf{E}^{\perp}$. Let us focus on this last set: Besides the three-dimensional triacontahedron, it contains six four-dimensional cells which are the products of an edge in $\mathbf{E}^{\parallel}$ by its existence domain in $\mathbf{E}^{\perp}$ (a rhombic icosahedron). The generic intersection between such a four-dimensional cell and a three-dimensional cut is a one-dimensional object which yields an edge of the tiling, just as the zero-dimensional intersection of the cut with the atomic surface is a vertex. Similarly, the fifteen remaining flat cells are five-dimensional products of a facet in $\mathbf{E}^{\parallel}$ by its existence domain in $\mathbf{E}^{\perp}$, and their two-dimensional intersections with the cut yield the facets of the tilings.

6 Matching Rules for the 3-DPT

Up to now, we have considered only global methods to construct our tilings. In fact, such global methods are required to prove global properties, the main of which being the quasiperiodicity, and have played an important role in the understanding of the diffraction patterns of the quasicrystals. However, while providing us with useful examples of structures exhibiting both sharp Bragg peaks and icosahedral symmetry, these global methods do not by themselves shed any light on the origin of the quasicrystalline ordering or on the onset of the icosahedral symmetry rather than any crystalline one.

Although this last question is clearly not a problem of pure geometry, it is interesting to look for the existence of local constraints on the packing of the tiles, which could force the resulting tilings to be quasiperiodic Penrose tilings, just as the simple rule of packing cubes face to face results in a periodic tiling. Such "matching rules" are well-known for the two-dimensional Penrose tilings. They consist in a set of decorations of the edges of the two Penrose rhombs, which can of course be realized in several ways, such that any tiling in which any pair of adjacent tiles shares the same decoration on their common edge is a quasiperiodic Penrose tiling.

In the two-dimensional case, the matching rules are derived using the strong self-similarity properties of the Penrose tilings of the plane, namely the *unique* inflation and deflation, which govern all the properties of these

tilings. We shall show here that similar matching rules exist for the three-dimensional case. However, the theory explained below does not depend on self-similarity considerations.

Observe first that the very possibility for the existence of such rules, depends in an essential way on the fact that the triacontahedron is not a generic projection of the six-dimensional hypercube.

More precisely, consider a generic projection of the six-dimensional hypercubic lattice on a three-dimensional subspace: then the kernel of the projection is a three-dimensional subspace which intersects any lattice subspace in a generic position. This means that the dimension of this intersection is 0 for one- two- or three-dimensional lattice subspaces, and $m - 3$ for an m-dimensional subspace, $m > 3$.

However, this is not the case for the projection $\pi^{\perp}$ involved in the three-dimensional Penrose tiling. In fact, we have as a consequence of the icosahedral symmetry a set of relations of the type: $\mathbf{e}'_1 - \mathbf{e}'_4$ parallel to $\mathbf{e}'_3 - \mathbf{e}'_2$, which can be written:

$$(\mathbf{e}'_1 - \mathbf{e}'_4) \wedge (\mathbf{e}'_3 - \mathbf{e}'_2) = 0$$

By application of the icosahedral group, we obtain fifteen such relations. Each of them means that the corresponding two-dimensional lattice subspaces spanned by pairs of vectors of the type $\{(\boldsymbol{\varepsilon}_1 - \boldsymbol{\varepsilon}_4), (\boldsymbol{\varepsilon}_3 - \boldsymbol{\varepsilon}_2)\}$ intersects the kernel $\mathbf{E}^{\parallel} = (\pi^{\perp})^{-1}(0)$ along a one-dimensional subspace (which is not a lattice subspace!), and this is not generic.

Observe that the symmetry implies a maximal non-genericity in the sense that any perturbation of the projection direction breaks at least one of these relations. In other words, these relations force the icosahedral symmetry.

In a previous section, we have defined the existence domains of the local environments of the vertices in the tiling: the boundaries of these cells are the projections on $\mathbf{E}^{\perp}$ of all the two-dimensional facets of the hypercube. As a consequence of the above relations, one can see that many of these projections overlap in $\mathbf{K}$, yielding "flattened" cells of zero volume which correspond to local packings which do not appear in the icosahedrally symmetric tilings but would appear in any tiling defined through a "tilted" $\mathbf{E}^{\parallel}$. Intuitively, one can hope that by setting rules which forbid these packings, one can force altogether the symmetry and the quasiperiodicity of the permitted tilings, and this is precisely what we are going to do.

On the other hand, the form of the rules we are looking for is simply the matching of decorations of the boundaries of the tiles, which are the two-dimensional facets. Their existence domains are rhombic dodecahedra, and we have one dodecahedron in $\mathbf{K}$ for each vertex of the facet. We are thus led to examine more precisely these rhombic dodecahedra: they present three orthogonal symmetry planes, two of which intersect on the long diagonal of

the dodecahedron. Consider the eight sectors in which these three planes partition the dodecahedron (Fig. 12). We define the matching rules by setting a different decoration in each of these eight sectors and we shall show that this is sufficient to force the symmetry and the quasiperiodicity of all the tilings with matching decorations.

It is natural to ask for a further condition of symmetry for the decoration, which is simply that the set of decorated tiles of each type should be the same for the ten different orientations of the tiles. This will yield constraints, not only on the relation between the decoration of tiles of different orientations, but also on the symmetry of the decoration of each tile.

In fact, to each symmetry operation in $\mathbf{E}^{\parallel}$ is attached an operation in $\mathbf{E}^{\perp}$: they are the images of the same operation in the "abstract" icosahedral group under its two representations acting respectively in $\mathbf{E}^{\parallel}$ and $\mathbf{E}^{\perp}$. Now, observe that it may happen that two sectors of dodecahedra in $\mathbf{K}$ are related in two different ways: first, through a symmetry operation, and second, as being attached to different vertices of the same direction of facet. In this situation, the two decorations derived for the second sector from the decoration of the first must coincide, and this appears as a symmetry constraint on the decoration of the facet itself.

We shall now establish these decorations.

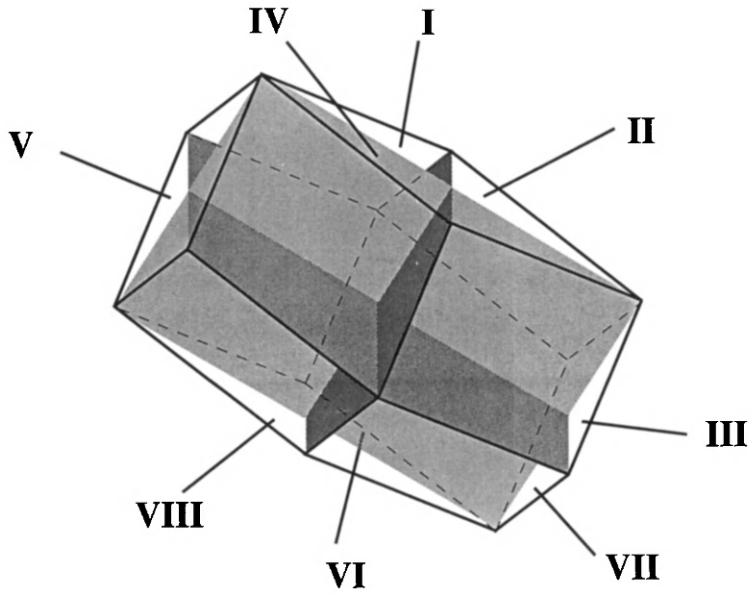

Figure 12. The eight sectors of the rhombic dodecahedron defined by its three symmetry planes.

6.1 *Decorations of the Facets and of the Tiles*

We have sixty dodecahedra to decorate: one for each vertex of the fifteen directions of facets. Of course, the decoration of dodecahedra corresponding to different vertices of the same facet are to be the same. Let us focus on the symmetry considerations. First, we ask the decorations of dodecahedra corresponding to different orientations to be mapped on each other by the icosahedral group, so that we have only one dodecahedron to decorate. Second, since the icosahedral group is generated by reflections, we have only to look at the symmetry planes to determine the symmetry of the decoration itself. Consider for instance the dodecahedron $\{\mathbf{e}_2', \mathbf{e}_3', \mathbf{e}_4', \mathbf{e}_5'\}$ (corresponding to the facet $\{\mathbf{e}_1, \mathbf{e}_6\}$ and the symmetry with respect to the plane $\{\mathbf{e}_2', \mathbf{e}_5'\}$. It exchanges the quadruplet of sectors (I, IV, VIII, V) respectively with (II, III, VII, VI). It is easy to see that this symmetry is related in $\mathbf{E}^{\parallel}$ to the symmetry with respect to the short diagonal of the facet, and this controls the relation between the sectors of the pairs (I, II), (IV, III), (VIII, VII) and (V, VI). Now consider the symmetry plane $\{\mathbf{e}_3', \mathbf{e}_4'\}$. It maps the dodecahedron on an other which corresponds to the same facet attached to the opposite vertex, while the related operation in $\mathbf{E}^{\parallel}$ is the symmetry

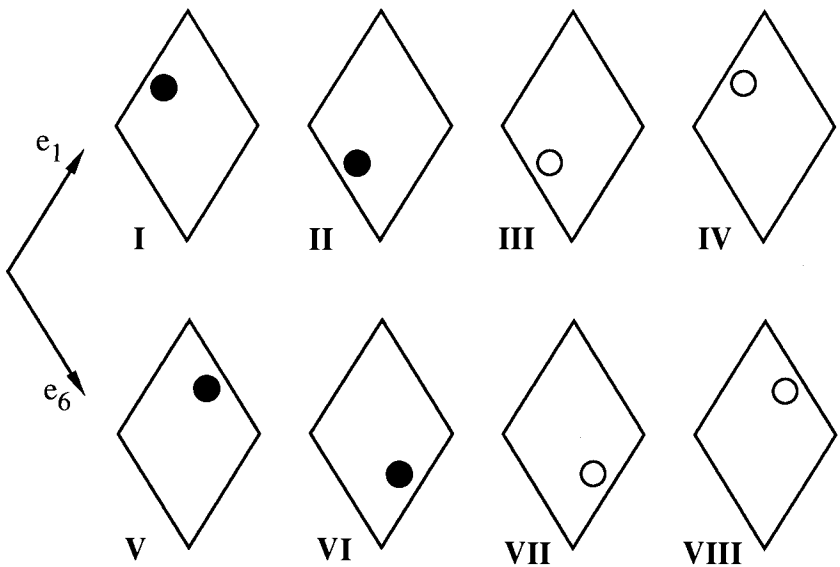

Figure 13. The decoration of the facets associated to the eight sectors of the rhombic dodecahedron.

with respect to the long diagonal of the facet. Now, this operation exchanges the quadruplet of sectors (I, II, III, IV) respectively with (V, VI, VII, VIII), and this controls the relation between the decoration of sectors of the pairs (I, V), (II, VI), (III, VII) and (IV, VIII). Finally, the symmetry plane $\{\mathbf{e}'_1, \mathbf{e}'_6\}$ exchanges the quadruplet of sectors (I, II, VI, V) respectively with (IV, III, VII, VIII), while exchanging in $\mathbf{E}^{\parallel}$ the two sides of the facet $\{\mathbf{e}_1, \mathbf{e}_6\}$. Thus we see that we have only one independent decoration of the facet, which in view of the symmetries involved can be chosen as a marking of one quadrant of the rhomb, different on the two sides of the facet (we choose a white disk on a side and a black one on the other; Fig. 13). Then the rule is to match a white disk with a black one, in order to get the same decorated facet in the two matching rhombohedra.

We have now to examine what are the decorated tiles obtained through this procedure. Consider the tiling defined by the triacontahedron $\mathbf{K}_\alpha$ and the direction of rhombohedron spanned by $\{\mathbf{e}_1, \mathbf{e}_m, \mathbf{e}_n\}$. Then, the existence domain of these rhombohedra is the rhombohedron $\alpha + \{\mathbf{e}'_i, \mathbf{e}'_j, \mathbf{e}'_k\}$, where (i, j, k, l, m, n) is a permutation of $(1, \ldots, 6)$, and we have to examine how this domain is partitioned in subdomains by the partitions of the dodecahedra attached to each of its facets.

Observe first that one of the planes in each of the dodecahedron corresponding to the three facets $\alpha + \{\mathbf{e}'_i, \mathbf{e}'_j\}$ overlaps with the boundary of the rhombohedron, so that we get only six planes for these facets. For the opposite facets $\alpha + \mathbf{e}'_k + \{\mathbf{e}'_i, \mathbf{e}'_j\}$, we have to consider the corresponding dodecahedron translated by $-\mathbf{e}'_k$, and we see that only the plane orthogonal to the long diagonal cuts our existence domain, yielding three other planes. One has to verify that these nine planes divide each thick rhombohedron into forty two subdomains and each thin rhombohedron in twenty four subdomains.

One can construct the decorated tile corresponding to each of these subdomains by inspecting in which sector of the relevant dodecahedron falls the origin of each facet, and one is helped in this rather involved task by symmetry considerations. When looking at the decorated tiles which are actually different, one observes that there are only fourteen of them for the thick rhombohedron, and eight for the thin one. Four of them are depicted on Fig. 14 for each type, and the whole set is generated through the following procedure.

For the thin rhombohedron, take the reflection of each of the depicted ones in any of its symmetry planes, and inverse at the same time the color of all the circles. One gets in this way the eight decorated thin tiles. For the thick one, there are two steps. First take the inverse of each of the depicted rhombohedra with respect to its center, inverting the color of all the circles. There are now eight tiles. Second, take the reflection of each of them in

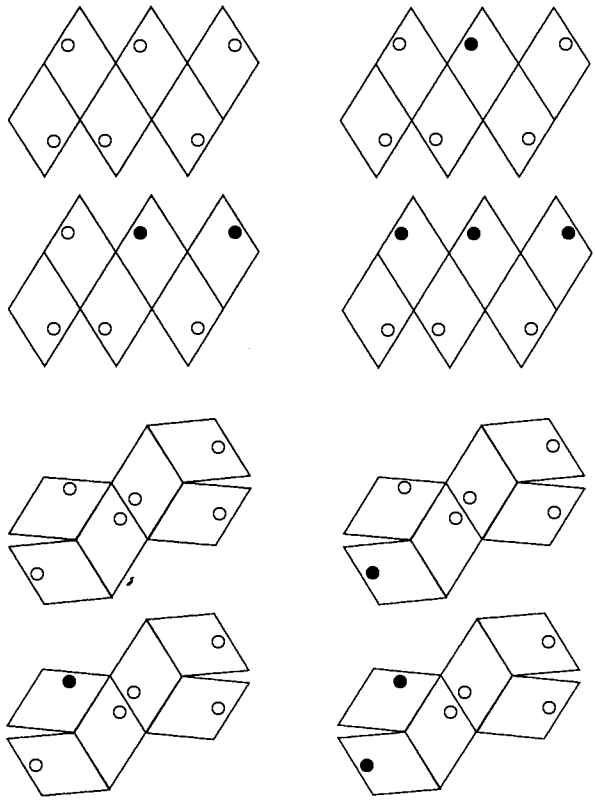

Figure 14. Four prolate and four oblate decorated Ammann tiles which generate the whole set.

any of its symmetry planes, without changing the circles. Two out of the eight are invariant through this last operation, so that one gets finally fourteen different decorated thick rhombohedra.

6.2 *Outline of the Proof*

We claim that any tiling with matching decorations is a quasiperiodic Penrose tiling. Without reproducing here a complete proof (Katz, 1988), which involves rather technical tools from algebraic topology, we shall try to give a flavor of how it works.

Let us first return to the cut description of the tilings: up to now, we have used plane cuts, but we need a generalization of this point of view. Observe that in the previous description the cut plays a double role. On one hand, it works as a means of selecting vertices or tiles, and on the other, it is the

space on which the tiling is actually built. We shall now distinguish between those two roles. Let us fix once and for all $\mathbf{E}^{\parallel}$ as the space on which the tiling is built by projection of vertices of $\mathbb{Z}^6$ through $\pi^{\parallel}$. Now one can use three-dimensional surfaces more general than planes to select the vertices to be projected.

As previously, the vertices selected are those whose attached triacontahedron $-\mathbf{K}$ is intersected by the cut. Since we are now accepting as a cut any continuous (without boundary) three-dimensional surface, we have to make more precise this notion: observe first that in a six-dimensional space the intersection of two three-dimensional manifolds is generically a discrete set of points. There are two possible orientations at each point (loosely speaking, the cut is either "entering into" or "going out from" the triacontahedron) so that each intersection point bears a sign ± 1, and we choose the orientations such that for a plane cut, which intersects at most once any triacontahedron, this sign is positive. Then one defines the intersection index between the cut and any triacontahedron as the sum of these signs for all the intersections of the cut with this triacontahedron. We shall only consider situations in which the intersection index is 0 or $+1$, this last case corresponding to the selected points.

On the other hand, this notion is interesting only if the intersection index is continuous with respect to continuous deformations of the cut. To achieve this, we must require that the intersection never falls on the boundary of the triacontahedron. That is, rather to consider as a possible cut any three-dimensional surfaces in $\mathbb{R}^6$, we allow only cuts entirely contained in the complement $\mathbb{R}^6 - \{\bigcup_{\xi \in \mathbb{Z}^6} \xi - \partial\mathbf{K}\}$ of the boundaries of all the atomic surfaces. Observe that this constraint plays exactly the same role that the genericity constraint which we have required on the plane cuts in order to remove any ambiguity in the tiling.

Moreover, observe that defining this "forbidden set" does not restrict the set of points which can be selected in this way. In fact, one can show (using elementary homology theory) that for any given set of vertices in $\mathbb{R}^6$ there exists a family of cuts (an homology class) which selects only this set.

This is the first idea of the proof. The second one is that, in order to restrict this generality and pick out the cuts which select only whole tiles, we have to enlarge this "forbidden set." This leads to the following reinterpretation of the oblique tiling.

The boundaries of the subcells of the oblique tiling are made of three-dimensional parallelohedra which from their very construction fall in two different types. The first type is made of products of a rhombohedron in $\mathbf{E}^{\parallel}$ by the facets of the boundary of its existence domain in $\mathbf{E}^{\perp}$, and one can say that they are "parallel to $\mathbf{E}^{\parallel}$". Conversely, the second type is made of products of facets of a tile in $\mathbf{E}^{\parallel}$ by its existence domain in $\mathbf{E}^{\perp}$: these are

"parallel to $\mathbf{E}^{\perp}$". As already mentioned (see Figs. 10 and 11), the traces of this last type on the set of planes parallel to $\mathbf{E}^{\perp}$ and going through each vertex of $\mathbb{Z}^6$ glue together to form the atomic surfaces of the cut description. We are now interested in the first type, which we are to consider as an enlarged "forbidden set".

In fact, one can prove rigorously that any cut which does not intersect these boundaries "parallel to $\mathbf{E}^{\parallel}$" selects only whole tiles. This can be seen on Fig. 11, although some topological "low dimension artifacts" lead paradoxically to a more difficult situation in this case. Observe nevertheless that any wavy line running roughly in the direction of $\mathbf{E}^{\parallel}$ without crossing any boundary parallel to $\mathbf{E}^{\parallel}$ selects only whole tiles: the line is "locally channeled" between the boundaries and forced to go out of each subcell it has entered through an atomic surface corresponding to the end point of a tile.

However, this channeling is only local, since there is a choice each time the line leaves a subcell corresponding to the long tile. The next cell may correspond either to a long or a short tile, in such a way that the line can "drift" far from a straight line, and the resulting tiling is not quasiperiodic.

The situation is similar for the three-dimensional Penrose tilings (in fact, it is simpler from a mathematical point of view). The main point is that any continuous three-dimensional surface which does not intersect the boundaries "parallel to $\mathbf{E}^{\parallel}$" selects only whole tiles (this is the "local channeling") but any set of tiles can be selected in this way (no global ordering is implied). As we shall see, this is the point which changes drastically when one takes the matching rules into account.

Our third step is to associate an oblique tiling to the non periodic tilings involving matching decorated tiles. This is an easy task since this new oblique tiling is only a refinement of the previous one. One has to dissect the previous subcells into forty-two (for the cell corresponding to the thick rhombohedron) or twenty-four (for the thin one) in order to obtain the new subcells which are the product of a tile in $\mathbf{E}^{\parallel}$ by the subdomain of existence of its decoration in $\mathbf{E}^{\perp}$. Then the matching condition is automatically fulfilled, since each facet is in fact selected only one time. Since there are more subcells, there are more boundaries, and if one defines as the new "forbidden set" the enlarged set of boundaries "parallel to $\mathbf{E}^{\parallel}$", one can verify as previously that any smooth cut which does not intersect this enlarged forbidden set selects only whole decorated tiles, and this property corresponds again to a "local channeling".

The key point of the proof is to show that it does appear now a kind of "global channeling". Qualitatively, the idea is the following.

As explained earlier, the components of the boundaries which are "parallel to $\mathbf{E}^{\perp}$" glue together along $\mathbf{E}^{\perp}$ to form the atomic surface attached to each vertex of the high-dimensional lattice. Observe now that the situation

is quite similar for the components "parallel to $\mathbf{E}^{\parallel}$": they glue together to form a connected patch of five-dimensional objects attached to each vertex of the lattice. However, before we express the matching rules through the new oblique tiling, these patches essentially do not interact: that is, although two patches associated to neighboring vertices may touch each other, they form only finite "islands" and there are no infinite connected sets of such patches. This is precisely why the cut may turn around these boundaries to reach any subcell of the oblique tiling, and thus why the single condition of packing the tiles face to face does not result in any global ordering.

Now, when we express our matching rules by enlarging the "forbidden set" as explained above, this is no longer true. The new contributions to the "forbidden set" coming from the boundaries of the subdomains of existence of the decorated tiles happen to build sufficiently many "bridges" between the previous patches to yield infinite connected sets in a way which limits severely the possible cuts.

Of course, the geometry in six dimensions is far richer than in two, so that it is difficult to give a low-dimensional model of the real situation. Nevertheless, it is interesting to remark the following: in the two-dimensional picture of Fig. 11, and without any matching rules, the "patches" are the line segments parallel to $\mathbf{E}^{\parallel}$ which go through each vertex of $\mathbb{Z}^2$. Now let us enlarge these segments to mimic the effects of expressing some matching rules. Observe that the only topological change which may take place in this context is the connection between two segments, and this can occur only if the slope of $\mathbf{E}^{\parallel}$ is a rational number. So we can conclude that the kind of rules we are dealing with exists in the low-dimensional model only for *periodic* tilings, and the effect of such matching rules is to disconnect the plane in a countable number of strips which correspond to a finite number of tilings.

The geometry involved in the six-dimensional space for the Penrose tilings is far more tricky. It is clearly impossible for the extended forbidden set to disconnect $\mathbb{R}^6$ into a set of "tubes", for this set would be countable and we know that there is an uncountable infinity of different Penrose tilings. On the contrary, our "forbidden set" is to be considered as a "net", whose four-dimensional "strands" intersect on zero- and two-dimensional "nodes". The meshes of such a net are sufficient to lock in a three-dimensional cut.

More technically, one can show that the five-dimensional polyhedra which build up the forbidden set sit along a family of four-dimensional planes, which are parallel to the 15 directions of symmetry planes of the icosahedral group. These planes are completely covered by the polyhedra in such a way that, as far as only the topology is concerned, one can "retract"

the complicated polyhedra onto the planes and forget about them. Then one can compute exactly the relevant homology group of the complement in $\mathbb{R}^6$ of the system of planes, and show that in each class of this group, there is a unique three-dimensional plane, which is of course parallel to $\mathbf{E}^{\parallel}$. This entails the conclusion that any tiling by the Ammann rhombohedra with matching decorations is a quasiperiodic Penrose tiling.

As a conclusion, let us make two remarks. The first one is that in the course of the proof, one has never to assume that the cuts are topological three-dimensional planes, that is, surfaces which can be continuously deformed onto a plane. The conclusion is that any cut (without boundary) compatible with the rules is of this type. Technically, it is a tremendous simplification to be able to conclude on the basis of homology considerations, without entering the far more complicated computations of homotopy groups.

This leads us to the second remark: We cannot assert that these rules are not too strong, i.e., that it is not possible to weaken them and reduce the number of different decorated tiles while keeping the same conclusion.

For instance, one could try to get rid of one of the symmetry planes in the decomposition of the rhombic dodecahedron, namely to forget about the difference between the two sides of the facets, or between black and white dots (this is the only case which deserves consideration, since getting rid of any one of the other planes leads to rules which are trivially compatible with periodic tilings). Such a simplification results in only two different decorated rhombohedra for each shape, so that it is worthwhile to discuss whether this simpler decoration is sufficient to define matching rules forcing quasiperiodicity.

However, a careful examination of the forbidden set corresponding to these weak rules shows that the four-dimensional planes discussed above are no longer completely covered by it, and the discusssion is whether the holes which appear are large enough (this is of course a matter of shape, not of size) for a cut to "escape" through them, in which case the weak rules are not sufficient. Such questions seem to be very difficult.

References

Bak, P. (1986). *Phys. Rev. Lett.* **56** 861.
De Bruijn, N. G. (1981). *Nederl. Akad. Wetensh. Proc. Ser. A* **43**, 39–66.
Elser, V. (1986). *Acta Crys.* **A42**, 36.
Gardner, M. (1977). *Sci. Am.* **236**, n° 1, 110.
Katz, A. (1988). *Comm. Math. Phys.* **118**, 263.
Katz, A. and Duneau, M. (1986). *J. Phys. France* **47**, 181.
Levine, D. (1986). *J. Phys. France* **47** C3, 125.
Mackay, A. L. (1982). *Physica* **114A**, 66.

Chapter 5

Defects in Quasicrystals

J. BOHSUNG and H.-R. TREBIN

Institut für Theoretische und Angewandte Physik der Universität Stuttgart
Stuttgart
Federal Republic of Germany

Contents

1 Introduction 184
2 The Perfect Quasicrystal 186
2.1 Some Aspects of Quasiperiodic Structures in the Density Wave Approach 186
2.2 An Example for a Microscopic Model: The Pentagonal Quasiperiodic Pattern 188
2.3 Comparison of Continuum and Microscopic Model 189
3 Defects in Quasicrystals 189
3.1 Introduction 189
3.2 Construction of Topological Defects 190
3.3 Defects in the Continuum Approach 201
3.4 The Topological Classification of Defects in Quasicrystals 205
3.5 Line Singularities in Icosahedral Quasicrystals 212
3.6 A Speculative Remark 213
4 The Motion of Dislocations in Quasicrystals 213
4.1 Introduction 213
4.2 Construction of a Dislocation Dipole 214
4.3 Creation and Motion of Mistakes 214
5 Conclusion 218
References 219

APERIODICITY AND ORDER 2
Introduction to the
Mathematics of Quasicrystals

Copyright © 1989 by Academic Press, Inc.
All rights of reproduction in any form reserved.
ISBN 0-12-040602-0

1 Introduction

As a rule, order is accompanied or even reveals itself by defects. Penrose patterns carry long-range translational and orientational order. Therefore one expects also typical structural defects to exist. In the search for defects of quasiperiodic systems it is helpful first to remember their periodic counterparts.

The classical structural defects in periodic crystals are dislocations, disclinations, dispirations, stacking faults, and twin boundaries (Nabarro, 1979; Friedel, 1981; Harris, 1970). Of these, dislocations may be found in any system of periodic translational symmetry, like the pattern of the fingerprints or the coat of zebras. The points, where dislocations pierce the surface of a crystal, can be made visible by etching techniques. Dislocations mediate plastic flow, catalyze crystal growth, and strongly influence all transport processes, in particular electric resistance. In two-dimensional hexagonal crystals, bound pairs of dislocations and anti-dislocations are present at any finite temperature and destroy the long-range translational order (Halperin and Nelson, 1978). Only quasi-long-range order of algebraically decaying Debye-Waller correlation functions can persist. At higher temperatures the pairs unbind and destroy the translational order, leaving, however, quasi-long-range bond-orientational order ("hexatic phase"; for most recent observation in liquid-crystal films, see Cheng *et al.*, 1987).

Disclinations in crystals perturb the alignment of lattice directions. Since disclinations carry a very high strain energy, they are seen in extremely soft crystals only, like the flux-line lattices of superconductors (Träuble and Essmann, 1968). It has been an important insight, that a disclination-antidisclination pair ("dipole") is equivalent to a dislocation. When these dipoles, abundant in the hexatic phase, are freed at high temperatures to isolated disclinations, the bond-orientational symmetry also breaks down, and the two-dimensional crystal becomes fluid.

In the tetrahedrally close-packed (Frank–Kasper) phases of metallic alloys, where most atoms gather to clusters in the form of icosahedra, there are lines, along which the icosahedra are widened by insertions of tetrahedral wedges (Shoemaker, 1988). The lines, which arrange into lattices of space-group symmetry, are interpreted as wedge-disclinations in a medium of bond-orientational order, which is a generalization of a nematic liquid crystal (Sadoc, 1983). Amorphous metals are viewed as irregular entanglement of disclination lines, whose crossing is inhibited by topological obstruction (Nelson, 1983; Widom, 1988).

Whereas dislocations are characterized by pure translational elements of the crystal space group—the Burgers vectors, and disclinations by rotational elements, the dispirations are associated with screw axes or mirror

glides, operations which appear only in nonsymmorphic space groups. Stacking faults are mismatches of crystal planes, frequently generated by splitting a dislocation into two of fractional Burgers vector and moving them apart. Finally, twin boundaries are interfaces between differently oriented crystals and are comprised of many dislocations. Icosahedral twinning of cubic crystallites is one controversial explanation of the non-crystallographic symmetries in material like shechtmanite (Shechtman *et al.*, 1984; Pauling, 1987).

There are several incentives to identify the analogues of dislocations and disclinations in quasicrystals. Penrose patterns are two-dimensional systems, and according to phase space counting fluctuations of the atomic displacements are so strong that exact long-range order is reduced to quasi-long-range order just as in periodic crystals (Levine *et al.*, 1985). What are the defects involved in the process? Are there purely translatory structural defects ("dislocations") and rotatory ("disclinations"), and are dipoles of the latter equivalent to the former? Is the motion of dislocations as simple (namely along glide planes) as in crystals, so that after unbinding of the dipoles these singularities move as free gas molecules? Does proliferation of dislocations in a quasi-periodic icosahedral phase induce the "icosahedratic" phase? Are disclinations the elementary excitations in pentagonal and icosahedral quasicrystals, which mediate the loss of long-range bond orientational order in transitions to the amorphous or fluid state?

On the way to an answer of these questions, we make use of the fact that the long range positional order of quasicrystals arises by projecting vertices of hypercubic lattices onto lower dimensional subspaces. The necessity of higher dimensions is motivated in Section 2 both in a continuum model and a microscopic model. In Section 3, dislocations and disclinations are constructed via the Volterra process in the hypercubic lattices. Suitable projection proves, that the singularities are not only accompanied by deformations in real space ("phonon strain"), but also by deformations in phase space ("phason strain"). In the microscopic model the phason strain manifests itself in the form of exceptional vertices, called mistakes (Lu and Birman, 1986). Thus disclinations and dislocations are accompanied by clouds of mistakes and become "dressed" like polarons. Also in Section 3 methods of algebraic topology are applied to the classification of singularities in quasiperiodic systems. It is ascertained that disclination dipoles are equivalent to single dislocations. Finally, dislocation motion is demonstrated by the example of a dislocation dipole, whose constituents slowly move apart.

Thus, the article is a contribution to the analysis of defects in quasicrystals and their kinetics. Before we treat the defected state, we remind of some properties of the perfect system.

2 The Perfect Quasicrystal

To construct quasicrystals, a variety of methods has been developed in the past. These can be divided into continuum approaches (see, for example, Kalugin *et al.*, 1985; Levin *et al.*, 1985; Jarić 1985; Bak, 1985; Troian and Mermin, 1985) and microscopic models (Penrose, 1974; de Bruijn, 1981; Kramer and Neri, 1984; Duneau and Katz, 1985; Katz and Duneau, 1986), both of which we are going to review briefly.

2.1 Some Aspects of Quasiperiodic Structures in the Density Wave Approach

Landau's theory of phase transitions answers the question, into which ordered phases an isotropic liquid (described by a constant mass density ρ_0) may condense below a critical temperature T_c (Landau and Lifshitz, 1980). During the condensation process the translational symmetry of the liquid phase is broken by an inhomogeneous mass density $\rho(\mathbf{r})$ which is superposed to ρ_0 and transforms like an irreducible representation of the symmetry group of the liquid phase.

These irreducible representations are labeled by wave vectors $\mathbf{K} \in R^d$ (d is the dimension of the space considered).

$$\rho(\mathbf{r}) = \sum_{\mathbf{K} \in R^d} \rho_{\mathbf{K}} e^{i\mathbf{K}\cdot\mathbf{r}} + cc. \tag{1}$$

The Landau free energy of the ordered phase is expanded into powers of $\rho_{\mathbf{K}}$:

$$F(P, T, \rho_{\mathbf{K}}) = F_0 + \tfrac{1}{2} \sum_{\mathbf{K}} A|\rho_{\mathbf{K}}|^2 + B \sum_{\mathbf{K}_1 + \mathbf{K}_2 + \mathbf{K}_3 = \mathbf{0}} \rho_{\mathbf{K}_1}\rho_{\mathbf{K}_2}\rho_{\mathbf{K}_3} + C \sum_{\mathbf{K}_1 + \cdots + \mathbf{K}_4 = \mathbf{0}} \rho_{\mathbf{K}_1}\rho_{\mathbf{K}_2}\rho_{\mathbf{K}_3}\rho_{\mathbf{K}_4} + \cdots \tag{2}$$

In the minimization process of F, the coefficients $A, B, C, \ldots$ pick out special wave vectors: A selects a shell $\mathbf{K} = \text{const}$, $B, C, \ldots$ select discrete sets of elements out of this shell. The choice of $B, C, \ldots$ fixes the stable structures.

2.1.1 Two-Dimensional Pentagonal Structures. If the fifth-order term dominates the expansion (2), in two dimensions the ground state mass density $\rho(\mathbf{r})$ is composed of five plane waves, whose wave vectors form an equilateral pentagon:

$$\rho(\mathbf{r}) = \sum_{i=1}^{5} \rho_{\mathbf{K}_i} e^{i\mathbf{K}_i\cdot\mathbf{r}} + \cdots \tag{3}$$

where $\sum_{i=1}^{5} \mathbf{K}_i = \mathbf{0}$ and the ellipses denote higher harmonics (see for example Bak, 1985). The density $\rho(\mathbf{r})$ is nonperiodic but nonetheless ordered.

To unveil the symmetry of this structure, one maps the five two-dimensional wave vectors $\mathbf{K}_i$ onto orthogonal vectors $\mathbf{K}_i^{(5)}$ of a five-dimensional space R^5 and formally establishes a five-dimensional density (Bak, 1985; Sachdev and Nelson, 1985):

$$\rho^{(5)}(\mathbf{x}) = \sum_{i=1}^{5} \rho_{\mathbf{K}_i} e^{i\mathbf{K}_i^{(5)} \cdot \mathbf{x}}, \qquad \mathbf{x} \in R^5. \tag{4}$$

This density represents a simple cubic structure in R^5.

We can reproduce $\rho(\mathbf{r})$, if we restrict $\rho^{(5)}(\mathbf{x})$ to a special plane P, spanned by two orthonormal vectors $\mathbf{z}_1, \mathbf{z}_2 \in R^5$:

$$\rho^{(5)}(\mathbf{x} \in P) = \sum_{i=1}^{5} \rho_{\mathbf{K}_i} e^{i\{\xi_1(\mathbf{K}_i^{(5)} \cdot \mathbf{z}_1) + \xi_2(\mathbf{K}_i^{(5)} \cdot \mathbf{z}_2)\}}. \tag{5}$$

Equation (5) is equivalent to Eq. (3), if we choose ξ_1, ξ_2 as the components of $\mathbf{r} \in R^2$ and $\mathbf{K}_i^{(5)} \cdot \mathbf{z}_{1,2}$ as the components K_{i1}, K_{i2} of $\mathbf{K}_i$.

We are now interested in those translations of $\rho^{(5)}(\mathbf{x})$ in R^5 which leave the Landau free energy of the corresponding two-dimensional system invariant. For a shift of $\rho^{(5)}$ by a vector $\gamma \in R^5$ we obtain:

$$\tilde{\rho}^{(5)}(\mathbf{x}) = \rho^{(5)}(\mathbf{x} + \gamma) = \sum \rho_{\mathbf{K}_i} e^{i(\mathbf{K}_i^{(5)} \cdot \mathbf{x} + \mathbf{K}_i^{(5)} \cdot \gamma)}. \tag{6}$$

From Eq. (6) it is seen, that the phases ϕ_i of $\rho_{\mathbf{K}_i} = |\rho_{\mathbf{K}_i}| e^{i\phi_i}$ may be interpreted as translational degrees of freedom in R^5: if we choose the origin of R^5 such that $\rho_{\mathbf{K}_i}$ is real when $\gamma = \mathbf{0}$, then

$$\phi_i = \mathbf{K}_i \cdot \gamma. \tag{7}$$

Inserting the complex coefficients $\rho_{\mathbf{K}_i}$ into the free energy expansion (2) one observes, that F only depends on the sum

$$\Gamma = \sum_{i=1}^{5} \phi_i = \sum_{i=1}^{5} \mathbf{K}_i \cdot \gamma, \tag{8}$$

which is the component of γ along the diagonal $\Delta = \sum_{i=1}^{5} \mathbf{K}_i^{(5)}$ in R^5.

Hence, the free energy is invariant under all translations in the four-dimensional subspace R^4 orthogonal to the subspace Δ spanned by Δ. R^4 consists of two mutually orthogonal two-dimensional planes: the physical plane P, whose vectors $\mathbf{u}$ represent pure in-plane translations of $\rho(\mathbf{r})$, and the "phase" plane $P_\perp$, whose vectors $\mathbf{v}$ cause phase shifts of the density waves without influencing the energy of ρ.

Thus, R^5 divides into three orthogonal subspaces:

$$R^5 = P \oplus P_\perp \oplus \Delta. \tag{9}$$

The four translational degrees of freedom of P and $P_\perp$, if position dependent, correspond to four hydrodynamic modes $\mathbf{u}(\mathbf{r})$ and $\mathbf{v}(\mathbf{r})$.

The two "phonon-like" excitations $\mathbf{u}(\mathbf{r})$ are equivalent to the displacive modes of usual periodic structures. The additional excitations $\mathbf{v}(\mathbf{r})$ are the analog of the "phasons" in incommensurate crystals. These modes appear because four of the five wave vectors $\mathbf{K}_i$ are linearly independent in the field of rational numbers (see for example Kalugin *et al.*, 1985).

2.1.2 Three-Dimensional Icosahedral Structures. A mass density $\rho(\mathbf{r})$ of icosahedral symmetry requires six density waves of wave vectors pointing to the corners of an icosahedron. This structure becomes stable by contributions of the sixth- and tenth-order term in the free energy expansion (2) (Bak, 1985).

Because all six wave vectors are rationally linearly independent, the icosahedral structures carry six hydrodynamic modes. Each may be interpreted as a translation in a six-dimensional space. The three shifts in physical space cause phonon-modes, the three degrees of freedom in the orthogonal space correspond to phasons.

2.2 *An Example for a Microscopic Model: The Pentagonal Quasiperiodic Pattern*

For the construction of microscopic models of quasicrystals in arbitary dimensions the projection formalism is very popular (Duneau and Katz, 1985). To obtain two-dimensional pentagonal quasiperiodic patterns, we start from a five-dimensional hypercubic lattice L_γ in R^5, which is shifted by a vector $\gamma \in R^5$:

$$L_\gamma = Z^5 - \gamma. \tag{10}$$

In R^5 a two-dimensional tiling plane P is embedded in such a way, that it remains invariant under the group C_5 of all cyclic permutations of the five canonical basis vectors $\mathbf{e}_i$ $(i = 1, \ldots, 5)$ of R^5.

Aside from P, C_5 leaves two other subspaces of R^5 invariant:

- the one-dimensional space Δ spanned by $\mathbf{\Delta} = \sum_{i=1}^{5} \mathbf{e}_i$,
- another two-dimensional space $P_\perp$.

P, $P_\perp$ and Δ are mutually orthogonal, i.e. R^5 falls into three C_5-invariant subspaces as in Eq. (9).

From the lattice L_γ we select a special set of points inside a strip S, which is cut out of L_γ by moving the five-dimensional unit cube W^5 along the tiling plane P:

$$S = \{\mathbf{x} \in R^5 | \mathbf{x} = \mathbf{x}_T + W^5; \quad \mathbf{x}_T \in P\}. \tag{11}$$

The tiling arises, if all those lattice points and two-faces, which belong to the five-dimensional hypercubes inside S, are projected onto P.

The choice of the shift vector γ affects the tiling in three ways:

- Variations of γ in P lead to pure translations of the lattice.
- Variations of γ in $P_\perp$ preserve the local isomorphism (LI-)class (Katz and Duneau, 1986) i.e. any finite section of one tiling is found in every other tiling of the same LI-class, however, without global congruence in general.
- Variations of γ within Δ result in tilings of different LI-classes. The special class, where γ is orthogonal to $\mathbf{\Delta}$, is named after R. Penrose.

Quasicrystals of one and the same LI-class have identical physical properties, in particular the same free energy and diffraction spectrum, because up to all scales they contain identical sections.

2.3 *Comparison of Continuum and Microscopic Model*

The pentagonal structures of the continuum model (Section 2.1.1) and the microscopic approach (Section 2.2) display remarkable similarities:

- Both structures hide the symmetry of a five-dimensional simple cubic lattice.
- The shift vector γ of the microscopic model corresponds to the phases in the density wave picture:
  The "phonon"-variable $\mathbf{u}$ is equivalent to the projection of γ onto P. The "phason"-variable $\mathbf{v}$ corresponds to the projection of γ onto $P_\perp$. The phase shifts associated with a variation of $\mathbf{v}$ in the density wave picture are analogous to special rearrangements of rhombuses in the microscopic picture, such that the LI-class remains unchanged.
- Shifts of γ in Δ lead to patterns of different LI-classes, in the continuum model they produce structures $\rho(\mathbf{r})$ of differing free energy.

3 Defects in Quasicrystals

3.1 *Introduction*

In this chapter we illuminate some features of topological defects in quasicrystals.

- Section 3.2 is devoted to topological point defects like dislocations or disclinations in two-dimensional quasicrystals. We remind of analogous defects in periodic crystals and generalize the well-known methods used for their construction.

- In Section 3.3 we define topological defects in the density wave picture and compare their features with those of the microscopic approach.
- In Section 3.4 we analyse topological defects in quasicrystals with the help of homotopy theory.
- Sections 3.5 and 3.6 are addressed to line singularities in icosahedral quasicrystals and to a speculative remark on configurations.

3.2 *Construction of Topological Defects*

3.2.1 Dislocations in Periodic Crystals. If the plastic deformation of a perfect periodic crystal were initiated by parallel displacement of two crystal planes, a force would be necessary of the order of the shear modulus μ. However, in experiment forces smaller by 10^{-4} already cause plastic flow (see, e.g., Friedel, 1967).

This fact is explained by the concept of dislocations. Due to their presence the two planes are sheared by a consecutive motion. To understand this process we discuss dislocations from a microscopic geometric point of view.

The simplest type is the edge dislocation. It arises if an extra half plane is inserted into the crystal lattice (Fig. 1). The defect itself is the line L (or the point L in the case of the two-dimensional example of Fig. 1) where the half plane terminates. In L the lattice is structurally changed whereas outside of L it is only distorted without loosing the topology of the perfect lattice.

The motion of an edge dislocation is demonstrated in Fig. 2. Only a slight replacement of atoms near the defect core is requested to displace the dislocation by one lattice constant (Fig. 2b). After the dislocation has traversed the crystal, it appears as if the two halfs of the crystal have been sheared rigidly (Fig. 2c).

A general construction method for dislocations is the Volterra process (Friedel, 1967). It can also be applied for other types of line defects (like disclinations, see below). The Volterra process consists of the following steps (see Fig. 3):

1. Cut the crystal along an arbitrary surface Σ which is bounded by a line L (Fig. 3a).
2. Separate the two arising lips Σ_1 and Σ_2 by a vector $\mathbf{b}$, the Burgers vector of the dislocation, which has to be a lattice vector (Fig. 3b).
3. Fill the space between Σ_1 and Σ_2 with perfect crystal matter or remove extra matter.
4. Glue the lips together. Because $\mathbf{b}$ is a lattice vector, this process restores the lattice everywhere outside the line L except for continuous deformations (Fig. 3c).

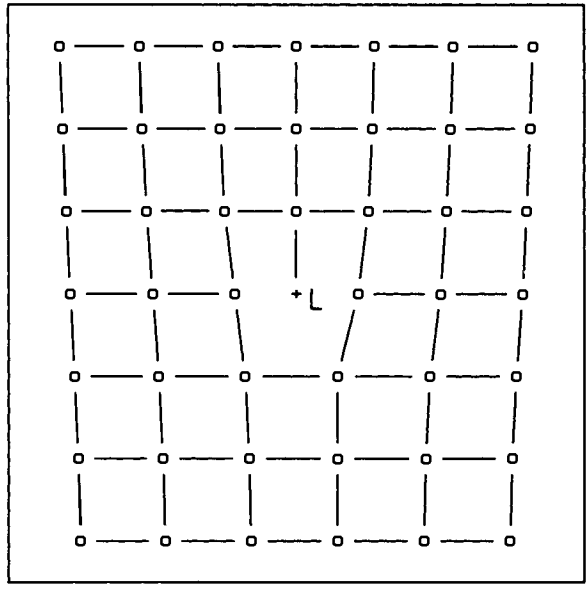

Figure 1. Edge dislocation in a square lattice. An additional row of atoms terminates in the defect core L. At L, the topology of the lattice is changed, outside L the lattice is only distorted.

From the description it becomes clear that the final result is independent of the special choice of Σ. The defect is completely defined by its position L and by the Burgers vector $\mathbf{b}$. Only along L the lattice geometry is essentially disturbed, outside it is just distorted.

3.2.2 Creation of Dislocations in a Two-Dimensional Quasicrystal. In this section we construct a dislocation in a two-dimensional pentagonal

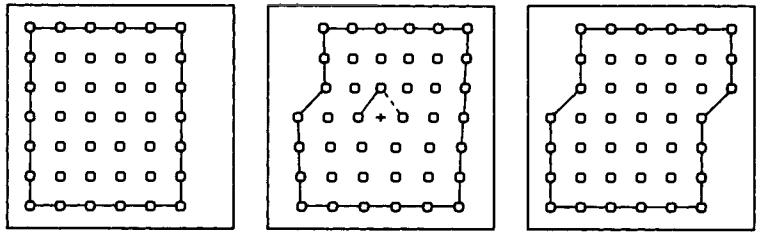

Figure 2. Motion of an edge dislocation. a. Initial state without dislocation. b. Propagating dislocation; only the atoms close to the core jump. c. Final state equivalent to a rigid shear. (The dislocation has traversed the whole crystal.)

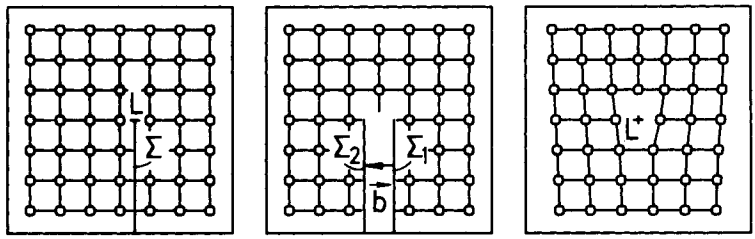

Figure 3. Volterra process for the construction of a dislocation in a square lattice (see text for detailed explanation).

quasicrystal (Bohsung and Trebin, 1987). We proceed as close as possible to the case of periodic crystals.

In the quasicrystalline pattern itself a Volterra process cannot be performed because translational symmetry is absent. We cannot specify any lattice vector linking two equivalent lips of a cut.

In analogy to the crystalline case one could remove a piece of one of the trails which wind through the pattern (see Fig. 4). Indeed the remaining lips match, but along the glue types of vertices originate which do not belong to the original LI-class (these vertices are marked in Fig. 4). The result is not a point singularity, but a linear stacking fault.

Although this attempt is in vain, it guides us in how to proceed, if we analyse the removal of a trail in terms of the five-dimensional hypercubic lattice L.

Every trail in the pattern corresponds uniquely to a four-dimensional canonical hyperplane of L (Gähler and Rhyner, 1985). Therefore, the removal of a trail is equivalent to the removal of a hyperplane in L, i.e. to a Volterra cut in the hypercubic lattice, which generates a dislocation. Only the transfer to the tiling plane is not correct.

To carry out this step properly we have to remember the strip S which is embedded in the hypercubic lattice L_γ with an irrational slope (see Section 2.2). Its presence destroys the original cubic symmetry of the lattice. Therefore, the two now four-dimensional lips Σ_1 and Σ_2 resulting from the Volterra cut are no longer equivalent.

For the following it proves useful to change from the "active" viewpoint of Section 2.2, where the strip is fixed in R^5 and the lattice is translated, to the equivalent "passive" one with fixed lattice L and shifted strip $S_\gamma = \gamma + S$.

Figure 5 illustrates the problem for a three-dimensional cubic lattice with an embedded strip S_γ. The two lips Σ_1 and Σ_2 cut out sections of the strip (they are hatched in Fig. 5). The sections do not touch, when the two lips are

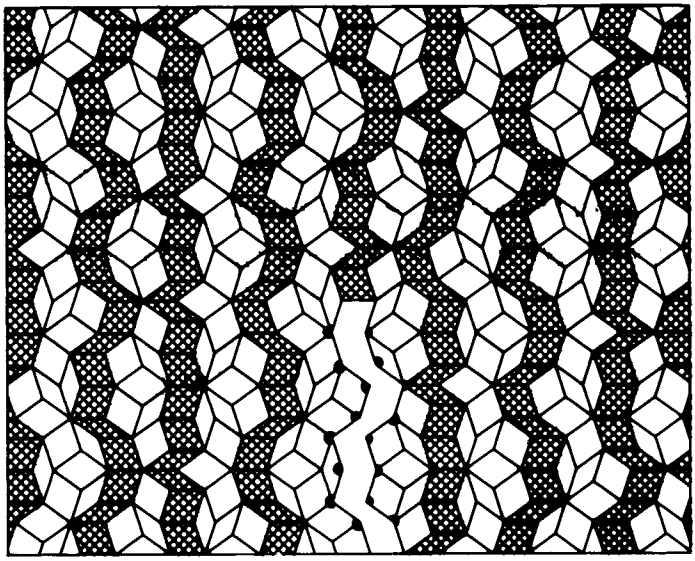

Figure 4. Quasicrystal of the Penrose-LI-class. Some of the trails, which run through the lattice, are hatched. Removing a piece of a trail and glueing the lips together leads to vertices outside the original LI-class (marked by dots).

matched. This is the reason for the appearance of a stacking fault in the pattern of Fig. 4.

How to solve this problem becomes clear in Fig. 6: if the strip which arrives at Σ_2 is bent around the singular line (in the five-dimensional case around the singular three-dimensional space respectively), the two sides of the strip match again. This bending is performed, if the shift vector γ is changed from an initial value γ_{start} at Σ_1 to a vector γ_{end} at Σ_2 and if γ_{end} differs from γ_{start} exactly by the Burgers vector $\mathbf{b}$:

$$\gamma_{\text{end}} = \gamma_{\text{start}} + \mathbf{b}. \tag{12}$$

In the case of our two-dimensional quasicrystal the Burgers vector $\mathbf{b}$ is a lattice vector $\mathbf{b} \in Z^5$.

To prove the necessity of relation (12), we choose the lip Σ_1 orthogonal to $\mathbf{e}_1$:

$$\Sigma_1 = \{\mathbf{x} \in R^5 \mid \mathbf{x} \cdot \mathbf{e}_1 = K_1; K_1 \in Z\}. \tag{13}$$

The second lip Σ_2 arises from the first by action of a translation $\{1, \mathbf{b}\}$[1] onto Σ_1:

$$\Sigma_2 = \{1, \mathbf{b}\}\Sigma_1 = \{\mathbf{x} \in R^5 \mid \mathbf{x} \cdot \mathbf{e}_1 = K_1 + \mathbf{b} \cdot \mathbf{e}_1; K_1 \in Z, \mathbf{b} \in Z^5\}. \tag{14}$$

[1] $\{1, \mathbf{b}\}$ is an element of the space group of the five-dimensional crystal lattice. $\mathbf{b}$ denotes the Burgers vector of the dislocation.

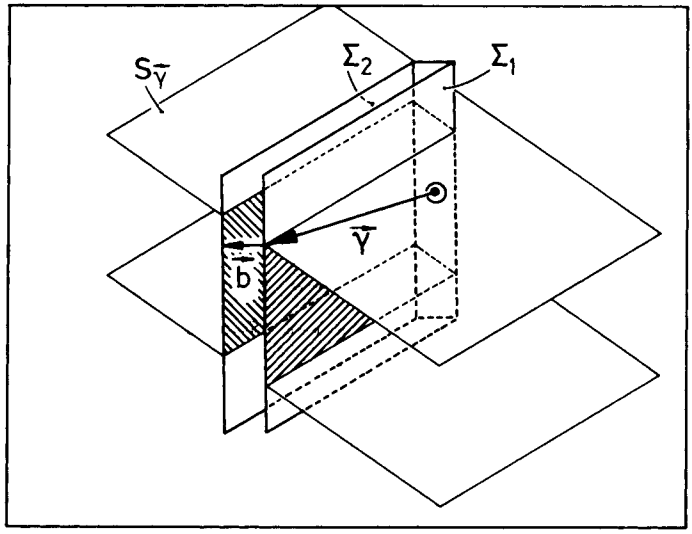

Figure 5. Schematic illustration of a Volterra cut in a three-dimensional cubic lattice with embedded strip S_γ. The two intersections (hatched) of the lips Σ_1 and Σ_2 with S_γ, respectively do not touch after glueing the lips together.

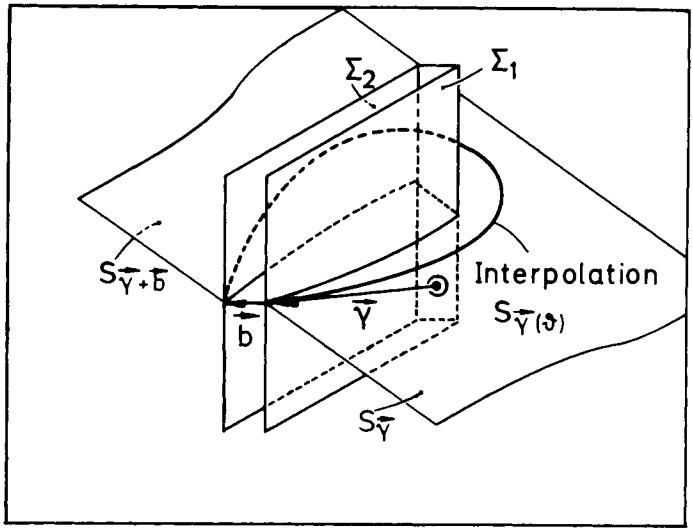

Figure 6. Interpolation between the strips S_γ and $S_{\gamma+b}$ (schematically). For clarity only the top of each strip is depicted.

Apart from the action of $\{1, \mathbf{b}\}$ on the lip Σ_1 we have to study the behaviour of the strip $S_{\gamma_{\text{start}}}$, if it is translated by $\mathbf{b}$ (compare with Eq. (11), the strip is now shifted by a vector γ):

$$S_{\gamma_{\text{end}}} = \{1, \mathbf{b}\} S_{\gamma_{\text{start}}} = \{\mathbf{x} \in R^5 \mid \mathbf{x} = \mathbf{x}_T + \gamma_{\text{start}} + \mathbf{b} + W^5; \mathbf{x}_T \in P\}. \quad (15)$$

The right hand side describes a strip with shift vector $\gamma_{\text{start}} + \mathbf{b}$.

To explicitly construct a dislocation in a two-dimensional quasicrystal, we have to choose an interpolation rule between γ_{start} and γ_{end}. For simplicity we interpolate linearly in the polar angle θ, as we encircle the core of the defect in the tiling plane:

$$\gamma(\theta) = \gamma_{\text{start}} + \frac{\theta}{2\pi} \mathbf{b}. \quad (16)$$

A dislocation with the same interpolation formula but in the frame of the method of Fibonacci grids has already been constructed by Socolar *et al.* (1986).

Our strip in R^5 is now bent due to the varying $\gamma(\theta)$. On the path around the singular point the pattern is composed of many pieces of tilings according to different shift vectors $\gamma(\theta)$. In the selection of these pieces there is still some arbitrariness due to the interpolation and the shift vectors γ involved.

Which pieces are suitable is decided from energetics. We demand all local structures to be energetically degenerate. Why, is explained by a look on a normal cubic crystal with dislocation: the local structure outside the core of the defect is everywhere cubic. In periodic crystals, the environment of the dislocation belongs to *one structure* (for instance a cubic one). The generalization to quasicrystals consists in taking *all the pieces from the same LI-class*. From Section 2.1 we know, that the LI-class is specified by the projection of γ onto $\mathbf{\Delta}$ (i.e. by $\gamma \cdot \mathbf{\Delta}$). So we have to restrict the shift vector $\gamma(\theta)$ in Eq. (16) by the condition:

$$\gamma(\theta) \cdot \mathbf{\Delta} = \text{const.} \quad (17)$$

From Eq. (16) we recognize, that Eq. (17) allows only Burgers vectors orthogonal to $\mathbf{\Delta}$:

$$\mathbf{b} \cdot \mathbf{\Delta} = 0. \quad (18)$$

In Fig. 7a dislocation in a Penrose pattern (i.e. $\gamma \cdot \mathbf{\Delta} = 0$, see Sect. 2.1) of Burgers vector $\mathbf{b} = (-1, 1, 0, 0, 0)$ is presented.

Figure 7a shows the defect before the lips of the four-dimensional hyperplanes have been glued together. Two trails in the pattern are removed according to the two nonzero components of $\mathbf{b}$.

In Fig. 7b the lips are linked, they match perfectly.

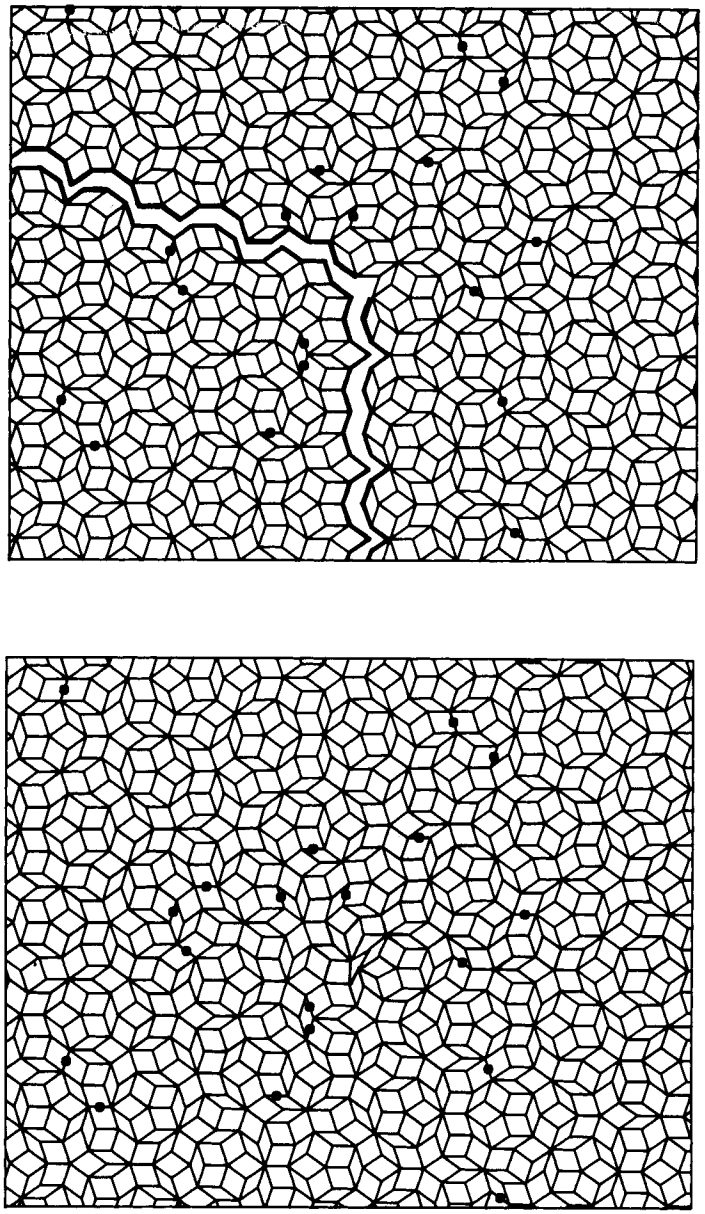

Figure 7. Dislocation in a Penrose pattern with Burgers vector $\mathbf{b} = (-1, 1, 0, 0, 0)$. The dots mark those edges which are bounded by vertices outside the Penrose-LI-class. a. Undistorted state. Two trails are removed according to the two nonzero components of $\mathbf{b}$. b. Final state after glueing the lips together.

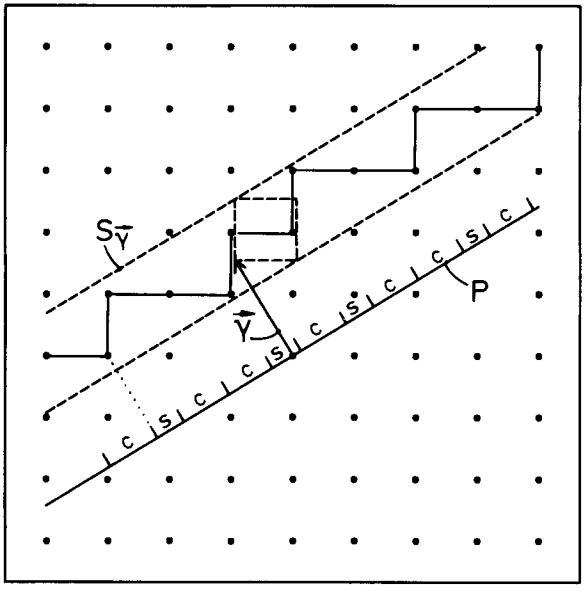

Figure 8. Construction of a one-dimensional quasicrystal by the projection method.

3.2.3 Mistakes. Looking carefully on the defected pattern of Fig. 7 one notices some vertices outside the chosen LI-class, although restriction (17) is valid. In the following we call these exceptional vertices mistakes. Mistakes turn out to be really new and interesting aspects of defects in quasicrystals compared to those in periodic crystals. In this section we illustrate mistakes in a one-dimensional quasicrystal and discuss some of their geometrical properties in two-dimensional quasiperiodic patterns. A deeper understanding of mistakes is gained in Section 3.3 where defects in the microscopic picture are compared with those in the continuum model.

The decisive difference in the construction process of defects in quasicrystals is the bending of the strip, as is demonstrated for the case of a one-dimensional quasicrystal in Fig. 8: a tiling line P is embedded in a square lattice with irrational slope. The lattice points and all one-dimensional faces of the squares inside the strip S_γ are projected onto the tiling line, leading to a sequence of long (c) and short (s) distances. The LI-class depends only on the slope of P and not on the choice of the shift vector γ (Katz and Duneau, 1986).

In Fig. 9 the strip interpolates between S_γ and $S_{\gamma+\varepsilon}$. The tiling line itself pertains its constant slope through the lattice, i.e. the LI-class does not change along it.

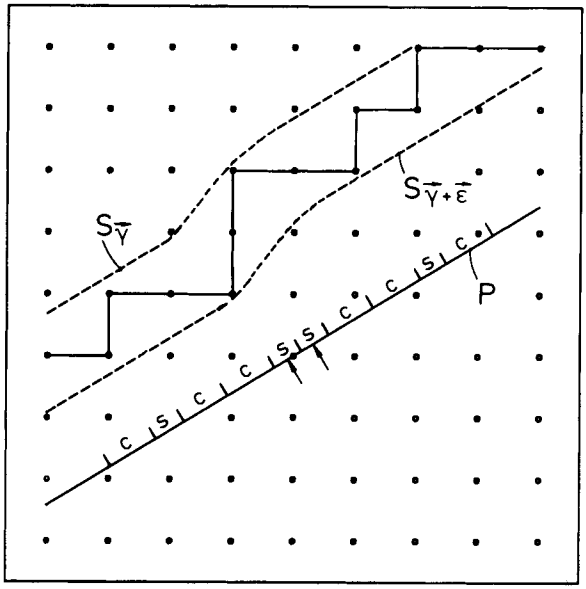

Figure 9. Interpolation between two one-dimensional quasicrystals of different shift vectors. In the transition region two short segments are adjacent (labeled by arrows), a sequence which is not allowed in a perfect quasicrystal of this LI-class.

Where the strip is curved, some sequences occur, which do not belong to the LI-class of the perfect system, for example the two neighbouring short segments in Fig. 9.

We now understand mistakes as points in the pattern, where different locally perfect tilings of one LI-class do not fit. In crystals, all local structures are identical and, therefore, match perfectly.

Mistakes in two-dimensional quasicrystals display another interesting property, which becomes visible, if we mark the trails in the pattern and their boundary lines. The trails jump at a mistake as seen in Fig. 10. These jumps remind of phase shifts and of the phasons occurring in the continuum model (Section 2.1). We discuss this relation in Section 3.3.

3.2.4 Disclinations in Periodic Crystals. A disclination also is constructed by a Volterra process. Now, however, the two lips are related by a lattice rotation instead of a translation. In Fig. 11 a 90°-disclination is shown in a square lattice. Figure 11a presents the undistorted lattice; in Fig. 11b the lips are closed.

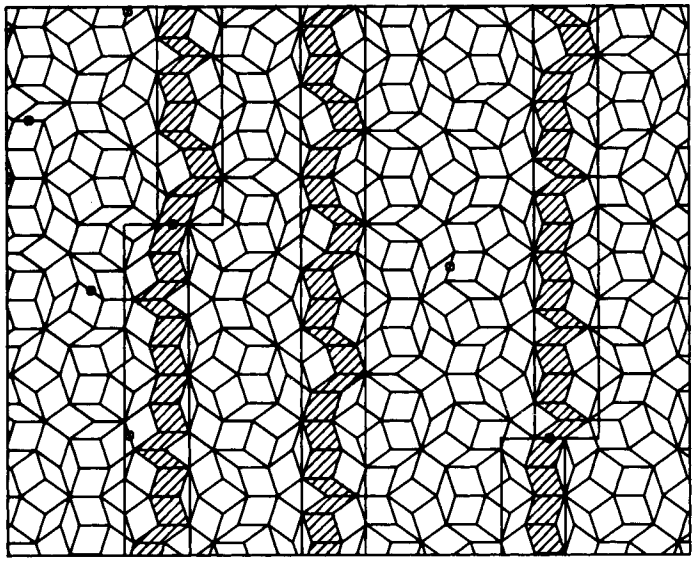

Figure 10. Mistakes cause phase shifts of trails.

3.2.5 Construction of a Disclination in a Two-Dimensional Quasicrystal. As in the case of the dislocation it is generally not possible to construct a disclination by cutting out or adding a sector of the tiling, because there is no global fivefold symmetry (an exception is the highly singular pattern of zero shift vector). Therefore, we again carry out the Volterra process in the five-dimensional hypercubic lattice and bend the strip in a suitable manner.

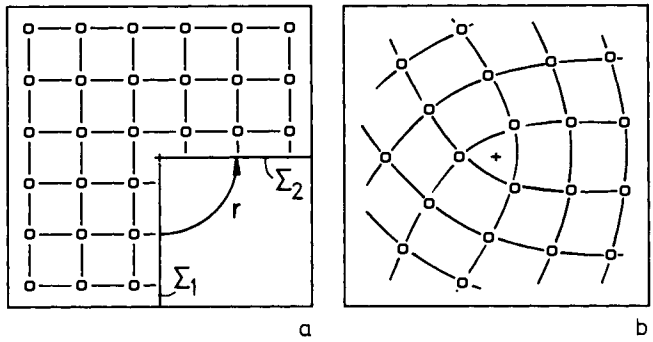

Figure 11. Volterra process for the construction of a 90°-disclination in a square lattice. a. A 90°-sector is removed from the lattice. Lips Σ_1 and Σ_2 are equivalent. b. Final state after glueing the lips together.

In the process we have to choose a group of rotations which map the two lips Σ_1 and Σ_2 onto each other. It seems to be obvious to take all rotations of the full point group[2] of the hypercubic lattice. But as before we have to take care that the resulting pattern contains only local tilings of one LI-class.

The rotations, which leave the LI-class invariant are discussed in Section 3.4, where the defects are classified by topological tools. They are the cyclic permutations of the canonical basis vectors in R^5 yielding the group C_5. This restricted set does not change the orientation between P and Z^5, when the two lips are closed and the lattice is distorted[3].

To transfer the disclination from the hypercubic lattice to the pattern, it is again necessary to bend the strip, so that the intersections of Σ_1 and Σ_2 with the strip match after glueing.

Figure 12 demonstrates how to proceed for a 90°-disclination in a three-dimensional lattice with irrationally embedded strip S_γ.

The two lips match, if the strip at Σ_2 corresponds to a shift vector γ_{end} which is rotated by 90° with respect to γ_{start}.

Hence, to create a disclination in a pentagonal quasicrystal, the shift vector γ_{start} has to be rotated by an element of C_5.

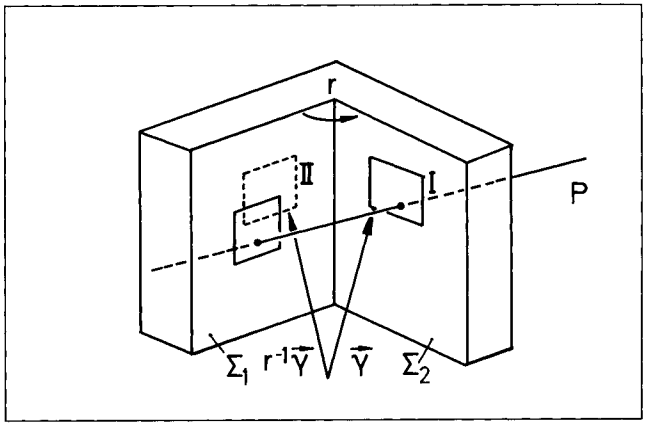

Figure 12. Schematic illustration of a disclination in a cubic lattice with embedded strip S_γ. For clarity the strip itself is not shown, only its intersections with the two lips Σ_1 and Σ_2. Intersection I of the strip S_γ with Σ_1 matches perfectly with intersection II of $S_{r^{-1}\gamma}$ with Σ_2, when the sector is closed.

[2] This group is the hyperoctahedral group $\Omega(5)$ (Kramer and Neri, 1984).

[3] This orientation determines the LI-class of the tiling. If it is changed, even the shapes of the rhombs alter.

For a proof of this statement, choose Σ_1 orthogonal to $\mathbf{e}_1$:

$$\Sigma_1 = \{\mathbf{x} \in R^5 \,|\, \mathbf{x} \cdot \mathbf{e}_1 = K_1; K_1 \in Z\}. \tag{19}$$

Σ_2 arises from Σ_1 by a rotation $\{r, \mathbf{0}\}$, where $r \in C_5$:

$$\Sigma_2 = \{r, \mathbf{0}\}\Sigma_1 = \{\mathbf{x} \in R^5 \,|\, (r^{-1}\mathbf{x}) \cdot \mathbf{e}_1 = K_1; K_1 \in Z\}. \tag{20}$$

The element $\{r, \mathbf{0}\}$ acts on the strip $S_{\gamma_{\text{start}}}$ as follows (cp. Eq. 11):

$$\{r,\mathbf{0}\}S_{\gamma_{\text{start}}} = \{\mathbf{x} \in R^5 \,|\, \mathbf{x} = (r^{-1}\mathbf{x}_T) + (r^{-1}\gamma_{\text{start}}) + W^5; \mathbf{x}_T \in P\}. \tag{21}$$

$r^{-1}\mathbf{x}_T$ is again a vector of P.

The right hand side of Eq. (21) describes a strip with a shift vector $\gamma_{\text{end}} = r^{-1}\gamma_{\text{start}}$.

In Fig. 13, an example for a 72°-disclination in a Penrose pattern is depicted, where we have chosen the following interpolation formula between γ_{start} and γ_{end}:

$$\gamma_i(\theta) = \gamma_{\text{start},i} + \frac{\theta}{8\pi/5} \cdot \{\gamma_{\text{start},i-1} - \gamma_{\text{start},i}\}; \; i = 1, \ldots, 5 \tag{22}$$

γ_i is the i-th component of γ, θ is again the polar angle of the tiling plane. Note, that the strip is bent before the lips are glued together, so $0 \leqslant \theta < 8\pi/5$.

Figure 13a shows the disclination with open sector, in Fig. 13b the sector is closed. As in the case of dislocated quasicrystals, mistakes accompany the singularity.

3.2.6 Dislocations as Disclination Dipoles. The topological classification of defects (see Section 3.4) proves that dislocations of Burgers vector $\mathbf{b}$ correspond to disclination dipoles.

In Fig. 14 this fact is illustrated for a dislocation in a quadratic lattice with Burgers vector $\mathbf{b} = (-2, -2)$. D can be considered as the center of a 90°-disclination (compare with Fig. 11). Point A (the three points have to be identified) marks an antidisclination, i.e. a disclination where a sector of extra matter is added.

Figure 15 presents the analogous case for a dislocation of Burgers vector $\mathbf{b} = (0, -2, 2, 2, -2)$ in a two-dimensional quasicrystal. As in the crystalline case we can identify the two cores D and A of a disclination dipole. For a more detailed investigation see Section 3.4.5.

3.3 Defects in the Continuum Approach

Frequently, it is sufficient to describe the physical properties of topological defects in crystals phenomenologically in terms of elasticity theory.

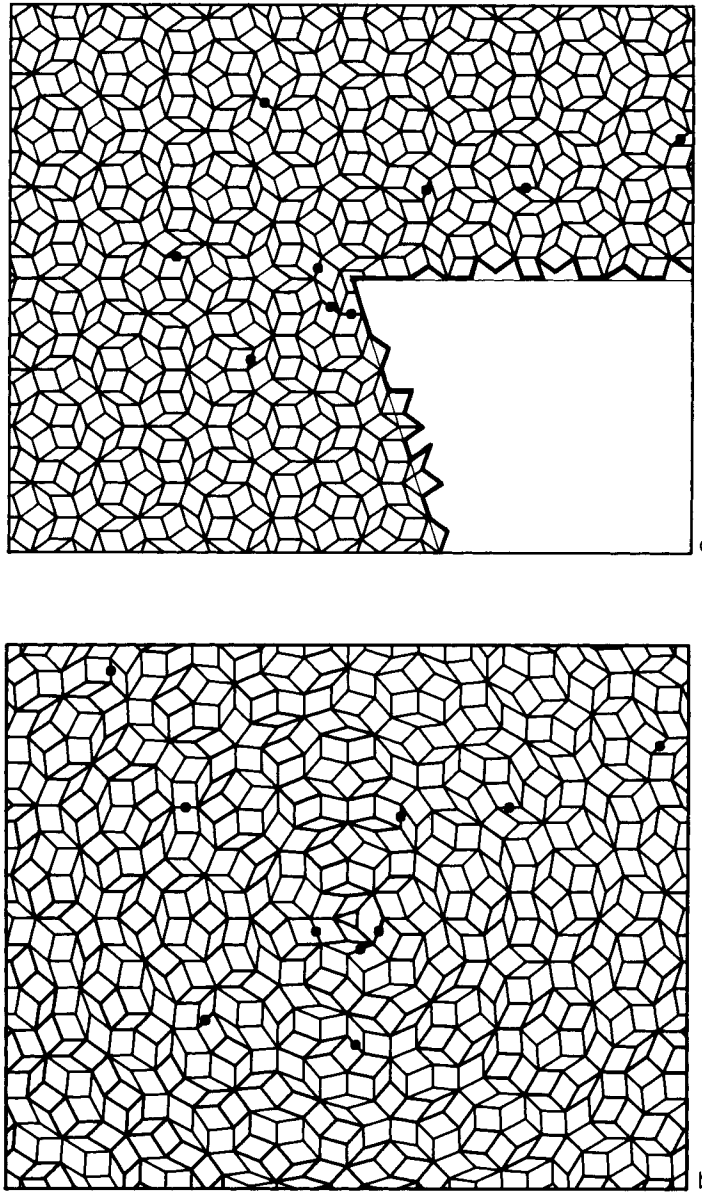

Figure 13. 72°-disclination in a Penrose pattern. As in the case of dislocations, several mistakes are present. a. Undistorted state. The lips match. b. Final state, when the sector is closed.

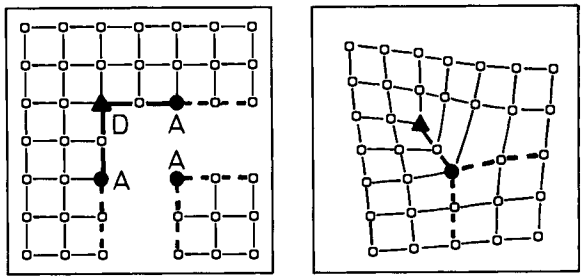

Figure 14. A dislocation of Burgers vector $\mathbf{b} = (-2, -2)$ in a square lattice is equivalent to a disclination dipole. a. Undistorted state. D labels the disclination, the three points A, which have to be identified, mark the antidisclination. b. Final state. Instead of the normal coordination number 4 the disclination is only threefold coordinated whereas the antidisclination has five bonds.

To define a dislocation in this framework, we consider a closed loop C which encircles the dislocation core L. To every point $\mathbf{r}$ of C we ascertain a vector $\mathbf{u}(\mathbf{r})$ describing the displacement relative to the perfect state.

If we sum up all displacements $\mathbf{u}$ on C, the result will not be zero but a Bravais lattice vector of the crystal, denoted Burgers vector (Friedel, 1967):

$$\oint d\mathbf{u} = \oint_C \frac{\partial \mathbf{u}}{\partial s} ds = \mathbf{b} \tag{23}$$

For a disclination the net displacement is given by:

$$\oint d\mathbf{u} = 2 \sin \frac{\Omega}{2} \boldsymbol{\omega} \times \mathbf{r}. \tag{24}$$

Ω is the angle between the two lips Σ_1 and Σ_2, and $\boldsymbol{\omega}$ is the rotation axis. Equations (23) and (24) demonstrate, that the displacement field of a crystal with topological defect is not integrable, i.e. the space is no longer simply connected.

To arrive at all aspects of a topological point defect in a pentagonal quasicrystal, we have to study the corresponding defect in the five-dimensional hypercubic structure $\rho^{(5)}(\mathbf{x})$ (Section 2.1.1). In analogy to the crystalline case the displacement $\gamma(\mathbf{x})$ of every point $\mathbf{x} \in R^5$ is measured relatively to its position in the perfect state on a closed loop around the defect core. As in the microscopic picture (Section 3.2.2) we restrict γ to vectors of $P \oplus P_\perp$.

A dislocation in the density $\rho^{(5)}(\mathbf{x})$ carries a Burgers vector

$$\oint d(\mathbf{u} + \mathbf{v}) = \mathbf{b} \in Z^5. \tag{25}$$

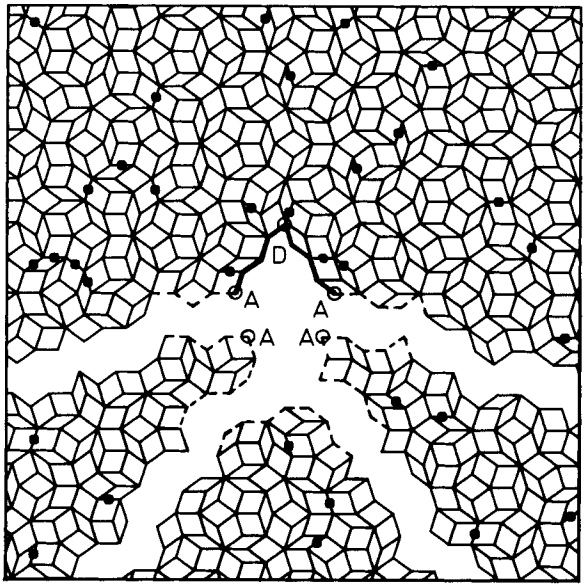

Figure 15. Equivalence between a dislocation of Burgers vector $\mathbf{b} = (0, -2, 2, 2, -2)$ and a 72°-dislocation dipole. The two cores are marked by A (antidisclination, the four points have to be identified) and D (disclination).

Any Burgers vector must have a component in $P_\perp$ due to the irrational slope of P in Z^5 (Levine *et al.*, 1985).

In the strain field about the defect, therefore, both fields $\mathbf{u}(\mathbf{x})$ and $\mathbf{v}(\mathbf{x})$ must participate. Thus every dislocation (and also every disclination) in a quasicrystal is accompanied by a phason strain $\mathbf{v}(\mathbf{r})$ in addition to the usual phonon strain $\mathbf{u}(\mathbf{r})$.

The dynamics of quasicrystals in the density wave model have been described in a hydrodynamic theory of Lubensky *et al.* (1985). Whereas the "in-plane" displacements $\mathbf{u}(\mathbf{r})$ are associated with normal sound modes, the modes coupled with $\mathbf{v}(\mathbf{r})$ are not propagating but rather diffusive.

As analysed by Lubensky *et al.*, (1986), the diffusive character of the phasons which follow dislocations reduces their mobility by up to four orders of magnitude and hence may greatly influence the plastic properties of quasicrystals.

In the microscopic picture, the phason strain is expressed by the occurence of mistakes (see also Socolar *et al.*, 1986). The motion of a dislocation is accompanied by mistakes moving through the quasicrystal by local rearrangements of vertices. In Section 4 the motion of a dislocation dipole and its accompanying mistakes is studied in detail.

3.4 *The Topological Classification of Defects in Quasicrystals*

Methods of algebraic topology have been developed in the last decade to classify defects in ordered media (for a review, see for example Mermin (1979) and Trebin (1982)). In this section, we are going to apply these methods to defects in quasicrystals.

3.4.1 Introductory Remarks. The basic concepts of the topological defect classification are introduced via a simple example, the isotropic planar ferromagnet. At high temperatures, the elementary ferromagnets are disordered; there is no macroscopic magnetization. Below the Curie temperature, the magnets start to align, and the arising order is characterized by a two-dimensional magnetization vector $\mathbf{m}$, which one may draw from the origin of an order parameter space $X = R^2$. The length of $\mathbf{m}$ is determined by temperature, the direction of $\mathbf{m}$, however, by chance (unless an orienting field is present). Also possible would be a magnetization $\tilde{\mathbf{m}}$ of different direction, but identical magnitude. The heads of all allowed magnetization vectors cover a circle S^1, which is denoted reduced order parameter space V. In practice the macroscopic magnetization varies in space due to growth conditions, boundary conditions, or external fields. The system is described by a mapping $R^d \to X$ from d-dimensional physical space (here $d = 2$) into order parameter space. In case of weak variations, the length of the vectors remains constant. The field is then valued not in the full order parameter space X, but only in the reduced one, V. Singularities, or defects, are now points, lines, or walls, where the reduced order parameter is not defined, as in the two examples of Fig. 16. Defects are denoted topologically

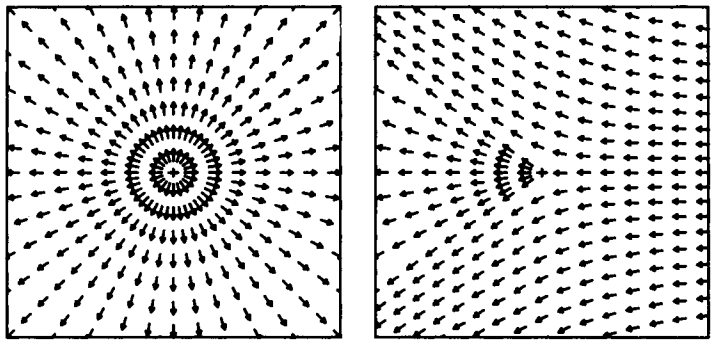

Figure 16. Point defects in a two-dimensional isotropic ferromagnet. a. Topologically stable point defect. b. Topologically unstable point defect.

stable, if they cannot be smoothed out by a change of the field in a small neighborhood of the singular set. Removal of the topologically stable source singularity of Fig. 16a, for example, requires a global rearrangement of the field, which (in an infinite system) costs an infinite amount of energy. The topologically unstable singularity of Fig. 16b can vanish by just local surgery.

In general, there are many types of topologically stable defects, like sinks, sources, crosspoints, or circulations for the planar ferromagnet. To distinguish them and to place them into classes, one can use the following equivalence relation, known as "Kléman–Toulouse" principle (Toulouse and Kléman, 1976): two singularities are equivalent or belong to the same class, if the core of one can be replaced by the core of the other. The locally restricted exchange of cores allows the transformation of one defect into the other by a small amount of energy, whereas for nonequivalent defects the transformation into another type requires an energetically costly global modification of the field. With the Kléman–Toulouse-principle the defect classification has become a problem of how to extend a continuous field over neighbourhoods of singularities, which can be attacked by topological tools.

In case of the planar ferromagnet each point singularity is labelled by an integer—the winding number, which is found in the following way: one encircles the defect along a closed path and draws the vectors, which one meets, from a common origin in order parameter space. This procedure yields a closed loop in the reduced order parameter space $V = S^1$, and the number of times, which the loop winds around the circle S^1, is the label of the singularity. Loops of winding number zero classify the topologically unstable defects. If two defects merge, their winding numbers add. In general, point singularities in the plane and line singularities in three-space are tested by closed contours (these are known as Burgers circuits in crystals). The values of the reduced order parameter along the contour form a loop in V, whose homotopy class (consisting of the loop and all those into which it is continuously deformable) labels the defect. The set of homotopy classes has the structure of the conjugacy classes of a group—the fundamental group $\pi_1(V)$ of the reduced order parameter space V, which expresses connectivity properties of V. If $\pi_1(V)$ is abelian, each conjugacy class contains only a single group element, which directly labels the defect. The unit element corresponds to the unstable singularities, defect merger to the product of group elements or conjugacy classes. In the present example, the fundamental group $\pi_1(V = S^1)$ is the (abelian) group of integers, and its elements correspond to the winding numbers.

Point singularities in the three-space are tested by two-spheres S^2. The reduced order parameters on this sphere form a sphere in V. The singularities

are labelled by the homotopy classes of spheres in V. These again have—in essence—the structure of a group, denoted second homotopy group $\pi_2(V)$. Walls in three space are tested by the zero-sphere S^0, which consists of two points. The labelling set, $\pi_0(V)$, corresponds to the different connected components of V.

The crucial step on the way to the defect classification is to determine the reduced order parameter space V. Frequently a group G is acting transitively on V, which says, that it can transform any element $v \in V$ into any other. In the case of a three-dimensional isotropic ferromagnet, where the reduced order parameter is a three-dimensional vector of fixed length, and $V = S^2$ the two-sphere, this is the group $SO(3)$ of all rotations. Let us choose a representative point in S^2, say the vector $\mathbf{m}_0$ along the z-direction, and another point $\mathbf{m}$, that is obtained from $\mathbf{m}_0$ via a rotation $g \in SO(3)$: $\mathbf{m} = g\mathbf{m}_0$. The set of all rotations turning $\mathbf{m}_0$ into $\mathbf{m}$ is the left coset gH, where H is the symmetry group of $\mathbf{m}_0$, consisting of the rotations about the z-axis: $H = SO(2)$. The points in $SO(3)$ are in continuous one-to-one correspondence with the set G/H of left cosets of H in G, and we can identify the reduced order parameter space with a coset space: $V = G/H$. G is denoted as unbroken symmetry group, because it characterizes the symmetry of the high temperture phase (in our examples the paramagnetic state) and thus also the symmetry of the free energy density; H is denoted broken symmetry group.

3.4.2 Reduced Order Parameter Spaces for Crystals. From the preceding analysis we can immediately derive the reduced order parameter space for periodic three-dimensional crystals. Since crystals not only possess rotational but also translational symmetry, the unbroken symmetry group G is the full Euclidean group $E(3) = O(3) \wedge T^3$, the broken symmetry group H is the space group S, and V is the coset space $E(3)/S$. An element $g \in E(3)$ consists of a translation $\mathbf{t}$ and a rotation r: $g = \{r, \mathbf{t}\}$. To associate an element of V with a point p of the defected crystal, we have to perform two steps: first a fixed perfect reference crystal has to be selected. Second, at p a copy of the perfect crystal is to be adjusted in such a way, that it coincides locally with the distorted crystal structure. If $g \in E(3)$ is the rigid body operation, which translates and rotates the reference crystal into the adjusted one, then the reduced order parameter at p is $gS \in E(3)/S$.

The question may be raised why we have not taken the affine group Aff(3) as unbroken symmetry group, and for H the crystal symmetry S_A in Aff(3). The elements of Aff(3) can dilate, compress, or shear the crystal lattice. Use of $V_A = \text{Aff}(3)/S_A$ leads to new singularities, like "shear type" defects. However, because a uniform crystal, if sheared, enhances its free energy (in contrast to a rigidly rotated one), the additional singularities have

much higher energy: selecting the unbroken symmetry group amounts to selecting the energy range of the defects.

A word of caution must be added: translations and rotations in the mapping $R^3\backslash D \to E(3)/S$, $\mathbf{x} \mapsto g(\mathbf{x}) = \{r(\mathbf{x}), \mathbf{t}(\mathbf{x})\}$ (where D denotes the defect set) are not independent (Mermin, 1979; Trebin, 1982; Kutka, 1985). Similarly, as a general strain tensor is subjected to compatibility conditions in order to be derivable from a displacement field, also compatiblity relations exist between the fields $\mathbf{r}(\mathbf{x})$ and $\mathbf{t}(\mathbf{x})$ which might restrict the topological defect classification for crystals. No influence of these conditions has been found on the classification of dislocations or disclinations (although the classification of pointlike solitons has been affected, see Section 3.6).

3.4.3 The Symmetry of Quasicrystals. For the topological classification of defects in quasicrystals the notion of unbroken and broken symmetry must be applied to an aperiodic system, which in almost all cases also does not possess a point symmetry. The word symmetry is ill defined without the object, upon which a symmetry operation is acting. In the framework of the projection method, the quasicrystalline system consists of hypercubic lattice L_γ, tiling plane P, and strip S. After our discussion of Section 2.2 it is reasonable to apply the symmetry operations to the lattice L_γ within the active view point, leaving P and S fixed.

Let us consider the case of pentagonal quasicrystals. The translation group of the hypercubic lattice we denote by Z^5. Its rotation group is the hyperoctahedral group $\Omega(5)$. Then, with respect to a *lattice point*, the symmetry group H_L of L_γ is the semidirect product

$$H_L = \Omega(5) \wedge Z^5. \tag{26}$$

However, if we consider all operations with respect to the *origin of* R^5 situated in the tiling plane P, we have to conjugate H_L with a translation $\{1, \gamma\}$ by the shift vector γ:

$$H_L^{\text{conj}} = \{1, \gamma\}^{-1}\Omega(5) \wedge Z^5\{1, \gamma\}. \tag{27}$$

Now we can state, that H_L^{conj} is "a symmetry group of the quasicrystalline pattern", in the sense that a tiling projected from L_γ is identical to one projected from $H_L^{\text{conj}} L_\gamma = L_\gamma$. When conjugating a rotation $\{r, \mathbf{0}\} \in H_L$, we obtain $\{r, -\gamma + r\gamma\}$. Thus, the rotations are accompanied by fractional translations, and H_L^{conj} is in a certain sense nonsymmorphic.

3.4.4 Reduced Order Parameter Space of a Quasicrystal. As in the case of periodic crystals, we identify the reduced order parmeter space of a quasicrystal with a coset space $V = G/H$. What is the unbroken symmetry

group G? It must be equal to or a subgroup of $E(5)$[4] and, for singularities in the low energy range, it must be an invariance group of the free energy of quasicrystals. From Section 2.2 we know, that all patterns of one LI-class are energetically degenerate. Therefore, the elements of G have to be able to rotate or translate the lattice L_γ into all those positions which lead to patterns of *one LI-class* but *arbitrary orientations* in the tiling plane, i.e. they have to fulfill the following conditions:

- The vectors $\mathbf{t}$ in the translations $\{1, \mathbf{t}\} \in G$ are elements of the orthogonal complement of Δ in R^5 (i.e. of the four-dimensional space $R^4 = P \oplus P_\perp$), because the shift vectors $(\gamma + \mathbf{t})$ of the translated lattices $\{1, \mathbf{t}\} L_\gamma = L_{\gamma+\mathbf{t}}$ must have the same projection onto $\mathbf{\Delta}$ as γ.
- The rotational part G_{rot} of G must be compatible with the restriction posed to the translations. So, G_{rot} is not the group of all possible proper rotations in R^5 (i.e. $SO(5)$), but is reduced to the direct product of all rotations in R^4 with those in Δ, i.e. to $SO(4)_{R^4} \times 1_\Delta$.
- The group $SO(4)_{R^4} \times 1_\Delta$ contains elements, which change the slope of P with respect to the lattice. These rotations must be excluded, because otherwise even the shape of the tiles is altered. Only such rotations of $SO(4)_{R^4}$ are allowed, which belong to the direct product of the in-plane rotations $r_T \in SO(2)_T$ of P with those in $P_\perp$ (i.e. $r_\perp \in SO(2)_\perp$).

Therefore, we arrive at the result:

$$G_{\text{rot}} = SO(2)_T \times SO(2)_\perp \times 1_\Delta \tag{28}$$

and

$$G = G_{\text{rot}} \wedge R^4. \tag{29}$$

The broken symmetry group H is composed of those elements of H_L^{conj}, which are contained in G:

$$H = G \cap H_L^{\text{conj}} = \{1, \gamma\}^{-1} C_5 \wedge T^* \{1, \gamma\}. \tag{30}$$

As in Section (3.2.5), C_5 denotes the group of cyclic permutations of the basis vectors of Z^5. $T^* \in R^4$ is the subgroup of those discrete translations of Z^5 which have no component along $\mathbf{\Delta}$. An element $\mathbf{t}^* \in T^*$ has the form

$$\mathbf{t}^* = \sum_{i=1}^{4} n_i \mathbf{a}_i;\ n_i \in Z;\ \mathbf{a}_i = \mathbf{e}_5 - \mathbf{e}_i. \tag{31}$$

The reduced order parameter space for pentagonal quasicrystals follows as:

$$V = (G_{\text{rot}} \wedge R^4)/H. \tag{32}$$

[4] Since we are only investigating classes of loops in V, it suffices to restrict attention to one connected part of V. Therefore, G can be chosen as connected, i.e. it contains only the proper rotations of $O(5)$ yielding the group $SO(5)$.

As in the case of normal crystals, every point in V (i.e. every coset of H in G) corresponds to a perfect system, which arises from the reference system (i.e. the lattice L_γ) by the action of any element of the coset and subsequent projection. In contrast to periodic crystals, two perfect quasiperiodic patterns which belong to different points in V may not be matched by a rigid motion. They are only locally isomorphic and not globally. This is a consequence of the fact that in general the action of an element $g \in G$ on L_γ changes the union of two-faces in the strip S and thus also the tiling itself.

3.4.5 Topological Point Defects in Two-Dimensional Quasicrystals. In two-dimensional ordered structures, topological point defects are classified by the first homotopy group $\pi_1(V)$. If the order parameter space V is known, $\pi_1(V)$ can be determined by standard methods (see, e.g., Trebin, 1982).

Since the group H is discrete, $\pi_1(V)$ is isomorphic to the lift $\bar{H}$ of H into the universal covering group $\bar{G}$ of G (Trebin, 1982):

$$\pi_1(V) = \bar{H} = \{1, \gamma\}^{-1} Z \wedge Z^4 \{1, \gamma\}. \tag{33}$$

An element $r \in Z$ labels a rotation of C_5 by $r \cdot 72°$. An element $(n_1, n_2, n_3, n_4) \in Z^4$ marks a translation of the group T^* by the vector $\mathbf{t}^* = \sum_{i=1}^{4} n_i \mathbf{a}_i$.

Dislocations—If we consider only translational displacements in the pattern, it is sufficient to deal with a reduced order parameter space V_{trans}, which only contains the translational parts of the groups G and H:

$$V_{\text{trans}} = R^4/T^*. \tag{34}$$

This order parameter space already has been investigated by Kléman *et al.* (1986).

The dislocations are classified by the homotopy group $\pi_1(V_{\text{trans}}) = Z^4$ (here the conjugation can be omitted, because $\{1, \gamma\}$ commutes with the elements of Z^4). Each element $(n_1, n_2, n_3, n_4) \in Z^4$ corresponds to the Burgers vector $\mathbf{b} = \mathbf{t}^*$. After encircling the core of the defect, the lattice L_γ has become a lattice $L_{\gamma+\mathbf{b}}$.

In the explicit construction of a dislocation (Section 3.2.2) the shift vector γ was linked to the strip and not to the lattice. The advantage of this choice was the possibility to separate the Volterra process into two steps:

- First, only the strip was bent. Therefore, the tiling remains undistorted and only the mistakes occur (see, e.g., Fig. 7a).
- Second, the four-dimensional lips Σ_1 and Σ_2 of the Volterra process were glued together thus distorting the lattice and the tiling (see, e.g., Fig. 7b).

For the defect classification, however, it proves to be more convenient to distort only the lattice. Of course, both viewpoints are equivalent.

Disclinations—A pure disclination corresponds to the conjugation class of an element $\{1, \gamma\}^{-1}\{r, \mathbf{0}\}\{1, \gamma\}$ of the fundamental group (for the analogous case in a periodic lattice, see Trebin (1982)).

To compute this class, we must conjugate the element $\{1, \gamma\}^{-1}\{r, \mathbf{0}\}\{1, \gamma\}$ by any element $\{1, \gamma\}^{-1}\{s, \mathbf{t}^*\}\{1, \gamma\}$ of the group $\pi_1(V)$:

$$\begin{aligned}\{1, \gamma\}^{-1}\{s, \mathbf{t}^*\}\{r, \mathbf{0}\}\{s, \mathbf{t}^*\}^{-1}\{1, \gamma\} &= \{1, \gamma\}^{-1}\{sr, \mathbf{t}^*\}\{s^{-1}, -s^{-1}\mathbf{t}^*\}\{1, \gamma\} \\ &= \{1, \gamma\}^{-1}\{srs^{-1}, \mathbf{t}^* - srs^{-1}\mathbf{t}^*\}\{1, \gamma\} \\ &= \{1, \gamma\}^{-1}\{r, (1 - r)\mathbf{t}^*\}\{1, \gamma\}. \qquad (35)\end{aligned}$$

The last step is justified because the group C_5 is abelian.

From Eq. (35) we conclude that the conjugation class consists of all elements $\{1, \gamma\}^{-1}\{r, T^*_{\text{sub}}\}\{1, \gamma\}$, where T^*_{sub} denotes a subset of the translational group T^*. For a given r, T^*_{sub} is spanned by the vectors $\{(1 - r)(\mathbf{e}_5 - \mathbf{e}_i)\}$; $i = 1, \ldots, 4$. The vector $\mathbf{t}^*$ in Eq. (35) determines the position of the disclination with respect to the origin of R^5, about which the rotations of the reference lattice are performed.

A disclination at the origin of R^5 (i.e. at the origin of the tiling) is described by the element of $\pi_1(V)$:

$$\{1, \gamma\}^{-1}\{r, \mathbf{0}\}\{1, \gamma\} = \{r, \mathbf{0}\}\{1, -r^{-1}\gamma + \gamma\}. \qquad (36)$$

Equation (36) can be interpreted as follows: before glueing the two lips of the Volterra process together (characterized by $\{r, \mathbf{0}\}$), we have to change the shift vector γ_{start} into $\gamma_{\text{end}} = \{1, r^{-1}\gamma_{\text{start}} - \gamma_{\text{start}}\}\gamma_{\text{start}} = r^{-1}\gamma_{\text{start}}$. This is exactly the modification we had performed in Section 3.2.5.

Disclination dipole—A dislocation is topologically equivalent to a disclination dipole. We demonstrate this statement for a disclination placed at the origin of R^5 and its antidisclination placed at $\mathbf{t} \in Z^5$. For simplicity in the following we omit the conjugation by $\{1, \gamma\}$. The disclination is labelled by

$$\{r, \mathbf{0}\}. \qquad (37)$$

The antidisclination is given by conjugation of $\{r^{-1}, \mathbf{0}\}$ with the vector $\mathbf{t}$:

$$\{1, \mathbf{t}\}\{r^{-1}, \mathbf{0}\}\{1, \mathbf{t}\}^{-1} = \{r^{-1}, (1 - r^{-1})\mathbf{t}\}. \qquad (38)$$

The translational vector in the antidisclination is always contained in the sublattice T^*, hence both defects preserve the original LI-class.

In the topological defect classification the combination of defects is described by the group product (Trebin, 1982). Therefore, for the disclination dipole we get:

$$\{r, \mathbf{0}\}\{r^{-1}, (1 - r^{-1})\mathbf{t}\} = \{1, (r - 1)\mathbf{t}\}. \qquad (39)$$

Equation (39) labels a dislocation with Burgers vector $\mathbf{b} = (r - 1)\mathbf{t}$, which is always an element of T^*.

In Section 3.2.6, a dislocation with Burgers vector $\mathbf{b} = (0, -2, 2, 2, -2)$ was shown (Fig. 15). After a slight adjustment [5] of some tiles near the defect centre, the disclination dipole becomes visible. The two cores (marked by D for disclination and A for antidisclination) are separated by the projection of the vector $\mathbf{t} = (0, -2, 0, 2, 0)$ on the tiling plane.

3.5 *Line Singularities in Icosahedral Quasicrystals*

Icosahedral quasicrystals can be constructed by projection from a six-dimensional hypercubic lattice onto a three-dimensional tiling plane (see, e.g., Katz and Duneau, 1986). Because here in contrast to the two-dimensional case all patterns belong to the same LI-class (Levine and Steinhardt, 1986), for the unbroken symmetry group all translations in six-dimensional space are permitted. The rotational part of G must leave the tiling space invariant; hence

$$G = \{SO(3)_T \times SO(3)_\perp\} \wedge R^6. \tag{40}$$

In the sense of Section 3.4.4 we obtain for the broken symmetry group H of an icosahedral quasicrystal (cp. Eq. 30):

$$\begin{aligned} H &= G \cap \{1, \gamma\}^{-1}\{\Omega(6) \wedge Z^6\}\{1, \gamma\} \\ &= \{1, \gamma\}^{-1}\{A(5) \wedge Z^6\}\{1, \gamma\}. \end{aligned} \tag{41}$$

The full point group $\Omega(6)$ of the hypercubic lattice is reduced to the icosahedral group $A(5)$.

To classify line defects in icosahedral quasicrystals, we have to investigate the fundamental group $\pi_1(V)$, where $V = G/H$ is again the reduced order parameter space (see Section 3.4.4). With the help of standard methods of homotopy theory (Trebin, 1982) we arrive at the result:

$$\pi_1(V) = \{1, \gamma\}^{-1}\{\bar{A}(5) \wedge Z^6\}\{1, \gamma\}. \tag{42}$$

$\bar{A}(5)$ denotes the lift of the icosahedral group into $SU(2)$. The fundamental group classifies dislocation and disclination lines; the Volterra process proceeds as in the two-dimensional case.

[5] Only such adjustments are allowed which lead at the most to the creation of mistakes but leave the LI-class otherwise unchanged.

3.6 A Speculative Remark

The topological theory of defects not only classifies singularities but also topological solitons in ordered media. These are nonsingular mappings $R^d \to V$, which, due to fixed boundary conditions, cannot decay to the uniform ground state. For pointlike topological solitons in particular, which also are denoted configurations, the boundary conditions are such that the reduced order parameter is constant far away from a point. Hence the points at infinity all can be identified, and the mapping can be interpreted as going from the d-dimensional sphere S^d to V, since $S^d = R^d \cup \{\infty\}$. Accordingly, the configurations are labelled by elements of the homotopy group $\pi_d(V)$.

The existence of configurations has been discussed for crystals, and it was found that homotopy theory yields wrong results. Due to compatibility conditions (Gunn and Ma, 1980; Trebin, 1983), configurations are not labelled by elements of $\pi_d(E(d)/H)$, where H denotes the crystal space group, but by the connected components ("islands") of the group of diffeomorphisms $\mathfrak{IC}^d$ of the d-sphere S^d, denoted $\pi_0(\mathfrak{IC}^d)$. For dimension $d = 4$, $\pi_0(\mathfrak{IC}^d)$ is still unknown; for $d = 1, 2, 3, 5$ it is trivial, i.e. no stable configurations exist. For $d = 6$ there are 27 stable configurations, since $\pi_0(\mathfrak{IC}^6) = Z_{28}$, the 28-element cyclic group.

Before the discovery of incommensurate systems the dimensionality of crystals was restricted to 3. With the advent of icosahedral quasicrystals dimension 6—where definitely the first stable configurations are existing—is accessible to observation. If we allow the local patterns to move out of their LI-class, and hence the space of degeneracy to extend to $E(6)/\Omega(6) \wedge Z^6$, three-dimensional cross-sections through six-dimensional configurations may show up as particularly deformed icosahedral quasicrystals.

4 The Motion of Dislocations in Quasicrystals

4.1 Introduction

In Section 3.2.1, some properties of dislocations in periodic crystals were listed. The forces necessary to initiate plastic flow are low in a crystal with dislocations. These defects, which mediate a stepwise shear have a high mobility: to shift a dislocation by one lattice constant a, only a few atoms near the defect core have to jump over distances of the order of a; outside the core the lattice remains essentially unchanged (cp. Fig. 2).

In a quasicrystal, a dislocation is accompanied by mistakes (Section 3.2.3). According to the hydrodynamic theory of Lubensky *et al.* (1986), the mobility of dislocations is strongly reduced due to the fact that their motion is coupled to diffusive modes. It is speculated that, therefore, the plasticity limit is drastically increased.

In this section, we investigate how mistakes are created and how they move in a pentagonal quasiperiodic pattern if the two cores of a dislocation dipole are separated.

4.2 Construction of a Dislocation Dipole

A dislocation dipole consists of two dislocations of opposite Burgers vectors. For the construction of such a dipole in a quasicrystal the two cores are placed at points a and $-a$ on the x-axis of the tiling plane. To bend the strip S_γ properly we introduce two angles θ_1 and θ_2 about each core and interpolate the shift vector γ in the following way:

$$\gamma(\theta_1, \theta_2) = \gamma_{\text{start}} + \frac{\theta_1}{2\pi}\mathbf{b} + \frac{\theta_2}{2\pi}(-\mathbf{b}). \tag{43}$$

The two angles θ_1 and θ_2 are related to the polar angle θ by:

$$\cos\theta_1 = \frac{r\cdot\cos\theta - a}{\sqrt{r^2 + a^2 - 2ra\cos\theta}};\ \cos\theta_2 = \frac{r\cdot\cos\theta + a}{\sqrt{r^2 + a^2 + 2ra\cos\theta}}. \tag{44}$$

The resulting dislocation dipole is depicted in Fig. 17. The lips are not closed and the removed trails are visible (cp. Fig. 7a).

4.3 Creation and Motion of Mistakes

If the two cores of the dislocation dipole are close, the quasicrystal outside the centre remains nearly perfect; only a few mistakes occur. When the cores separate, the two defects become more and more isolated dislocations and the number of mistakes increases. This is demonstrated in Fig. 18 for two different distances.

We study the motion process by looking at the marked mistake. From Fig. 18a to Fig. 18b it has walked along the hatched piece of the trail. On its way several vertices in the trail have jumped to new positions. Outside, the structure is unchanged. Generally, only when mistakes are created (for example the two mistakes marked by 1 in Fig. 18b) or along trails where they move is the structure altered. The rest of the pattern remains untouched.

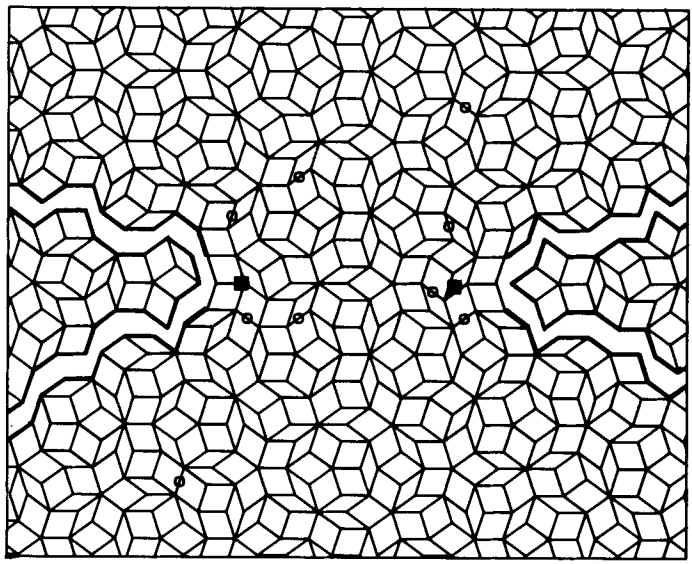

Figure 17. Dislocation dipole in a Penrose pattern of Burgers vector $\mathbf{b} = \pm(0, -1, 0, 0, 1)$. Undistorted state.

The creation and motion process is inquired in detail in Fig. 19, where we have isolated one trail of the defected quasicrystal. In the sequence from Fig. 19a to Fig. 19h the two defect cores (not shown) are separated slowly.

In Fig. 19a no mistake is seen. Fig. 19b demonstrates the creation of a pair of mistakes. It is induced by a jump of the dotted vertex along the arrow of Fig. 19a. The jump can also be interpreted as a flip of the hexagon which contains the dotted vertex.

In the next figures of the sequence, the two mistakes move apart by further jumps of vertices (in Fig. 19d the mistake at the top has left the picture). It is remarkable, that all vertices jump by exactly the same amount.

In summary, the motion of dislocations in quasicrystals is characterized by the following features:

- In contrast to periodic crystals the pattern of a quasicrystal varies outside the core of a moving dislocation. However, the variations are restricted to points where mistakes are created or trails along which they move.
- The creation and motion of mistakes happens by well-defined jumps of vertices. These jumps are the microscopic interpretation of the diffusive modes to which the dislocation motion is coupled in continuum theory (Lubensky *et al.*, 1986).

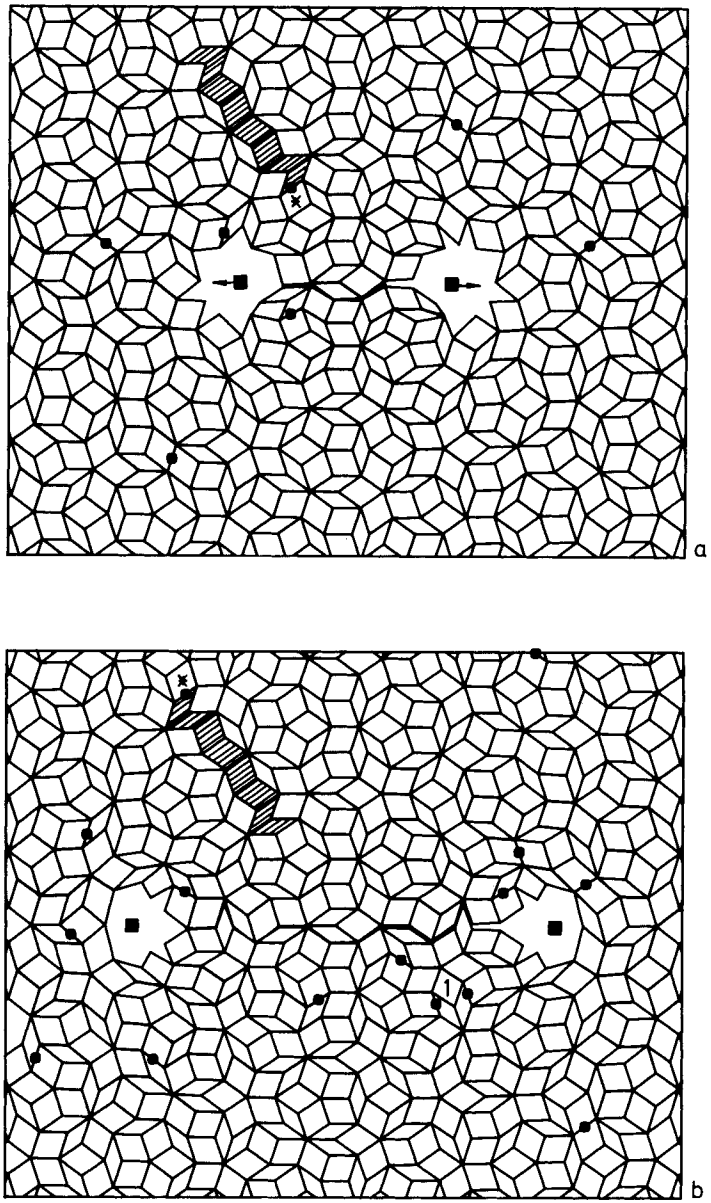

Figure 18. Two dislocation dipoles in a Penrose pattern of different core separation. For details, see text.

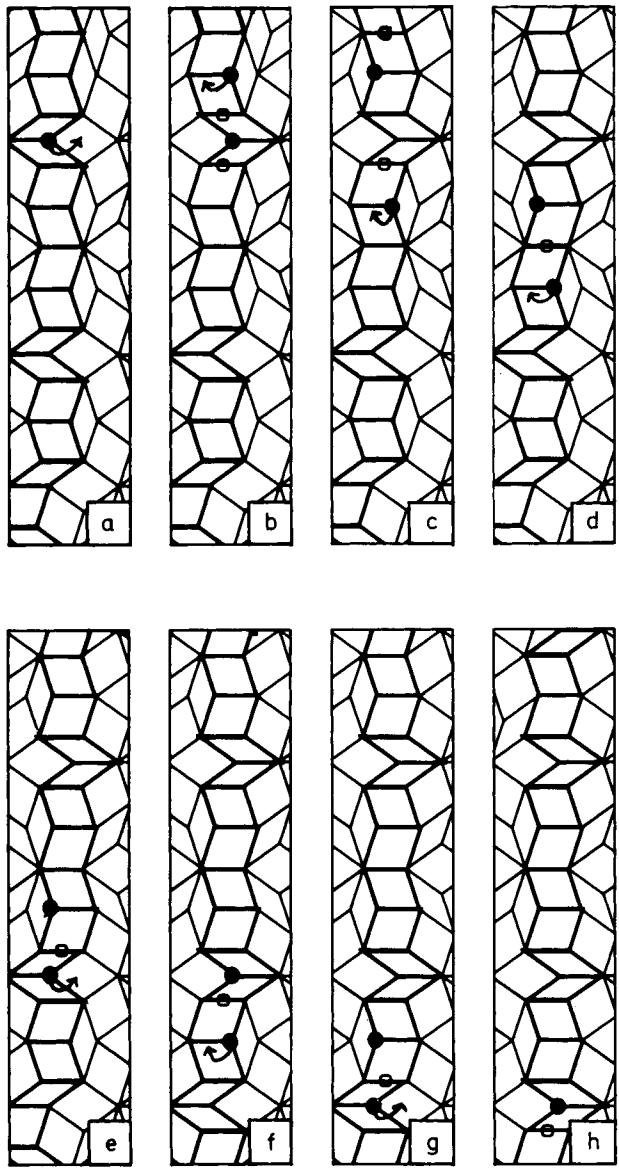

Figure 19. Trail in a quasicrystal, which contains a dislocation dipole. From *a* to *h* the two cores are separated slowly to demonstrate the motion process of a mistake. For details, see text.

5 Conclusion

In the preceding two sections we have constructed topological defects in quasicrystals, which are a generalization of dislocations and disclinations in periodic crystals. In quasicrystals, these singularities always are accompanied by "phason strain", which appears in the form of "mistakes" in the tiling, i.e. by exceptional vertices. At a mistake, the quasicrystal changes from one element of the LI-class to another (see Fig. 9). Thus, mistakes are like kinks of a soliton, regions, where the soliton amplitude moves from one vacuum state to the next. In the language of incommensurate systems, mistakes correspond to discommensurations, which are mismatches in the phase of the modulating incommensurate wave.

At the mistake, the line (or surface in three dimensions), which marks the average position of the trail, performs a discontinuous jump ("jag"). High-resolution transmission electron micrographs along fivefold axes of Al-Mn-quasicrystals display the trails and also reveal mistakes (like in Fig. 1 of Hiraga *et al.* (1985), where a jag is evident in a vertical trail). Also dislocations have been spotted in electron micrographs by counting missing trails along a closed loop (Hiraga and Hirabayashi, 1987).

Urban *et al.* (1985) have reported transitions from the quasicrystalline to the amorphous state of $Al_{86}Mn_{14}$ by electron irradiation. The process was recorded by a series of electron diffraction patterns. These show several of the decagonal stars of sharp diffraction spots gradually developing into rings without change of the radius. The results indicate that the local neighbourhoods of the atoms are preserved while the angular correlations are perturbed. Disclinations as described in this article are candidates for elementary excitations which drive the icosahedral into the amorphous phase. A transition from the glassy to the icosahedral phase was achieved by Poon *et al.* (1985) through annealing, the process, however, was not observed continuously.

We have demonstrated, that a dislocation is equivalent to a disclination dipole. Therefore, in quasicrystals the same mechanisms are present, which in two-dimensional periodic crystals initiate the phase transitions from the crystalline to the hexatic and from the hexatic to the liquid phase, namely stepwise unbinding of disclination quadrupoles (equivalent to dislocation dipoles) into their constituents. According to the kinetics of dislocation and disclination motion, however, it is doubtful whether these processes happen in quasicrystals. The topological defects are surrounded by a cloud of mistakes. They form polaron-type excitations, whose mobility and interaction must be renormalized compared to the case of hexagonal crystals. The mobility is strongly reduced according to the hydrodynamic theories (Lubensky *et al.*, 1986). Because a cloud of mistakes has to be built up in the

successive separation of the disclinations, the binding energy might be so large that the transition temperatures become unreasonably high.

We have seen that the rigid motion characterizing a disclination is composed of a rotation and a fractional translation. Disclinations, therefore, should be more exactly called "dispirations."

Apart from dislocations and disclinations also stacking faults can exist in quasicrystals. They are generated by Volterra cuts just as in the case of dislocations, but without bending of the strip. Twin boundaries, too, can be constructed with the help of many specially arranged dislocations. If we allow local neighbourhoods, which do belong to different LI-classes, then the topological theory predicts many other, highly energetic types of singularities, including sections through six-dimensional pointlike solitons.

References

Bak, P. (1985). Symmetry, stability and elastic properties of icosahedral incommensurate crystals. *Phys. Rev. B* **32**, 5764–5772.

Bohsung, J. and Trebin, H.-R. (1987). Disclinations in quasicrystals. *Phys. Rev. Lett.* **58**, 2277–2280.

de Bruijn, N. G. (1981). Algebraic theory of Penrose's non-periodic tilings of the plane. *Ned. Akad. Weten. Proc. Ser. A* **84**; *Indag. Math. A* **43**, 39–66.

Cheng, M., Ho, J. T., Hui, S. W., Pindak, R. (1987). Electron-diffraction study of free-standing liquid-crystal films. *Phys. Rev. Lett.* **59**, 1112–1115.

Duneau, M. and Katz, A. (1985). Quasiperiodic patterns. *Phys. Rev. Lett.* **54**, 2688–2691.

Friedel, J. (1967). *Dislocations*. Pergamon Press, London.

Friedel, J. (1981). Dislocations and walls in crystals. In *Physics of Defects* (Balian, R., Kléman, M. and Poirier, J.-P., eds.). North Holland Publ. Co., 1–131.

Gähler, F. and Rhyner, J. (1986). Equivalence of the generalized grid and projection methods for the construction of quasiperiodic tilings. *J. Phys. A: Math. Gen.* **19**, 267–277.

Gunn, J. M. F. and Ma, K. B. (1980). On textural defects in crystals. *J. Phys. C* **13**, 963–966.

Halperin, B. I. and Nelson, D. R. (1978). Theory of two-dimensional melting. *Phys. Rev. Lett.* **41**, 121–124.

Harris, W. F. (1970). The dispiration: a distinct new crystal defect of the Weingarten-Volterra type. *Phil. Mag.* **22**, 949–952.

Hiraga, K., Hirabayashi, M., Inoue, A. and Masumoto, T. (1985). Icosahedral quasicrystals of a melt-quenched Al–Mn alloy observed by high-resolution electron microscopy. *Sci. Rep. Inst. Tohokun Univ.* **A32**, 309–314.

Hiraga, K. and Hirabayashi, M. (1987). Dislocations in an Al-Mn-Si icosahedral quasicrystal observed by high-resolution electron microscopy. *Jap. Journ. of Apl. Phys.* **26**, L155–L158.

Jarić, M. V. (1985). Long-range icosahedral orientational order and quasicrystals. *Phys. Rev. Lett.* **55**, 607–610.

Kalugin, P. A., Kitaev, A. and Levitov, L. (1985). $Al_{0.86}Mn_{0.14}$: a six-dimensional crystal. *Pis'ma Zh. Eksp. Teor. Fiz.* **41**, 119–121. *JETP Lett.* **41**, 145–149.

Katz, A. and Duneau, M. (1986). Quasiperiodic patterns and icosahedral symmetry. *J. Phys. (Paris)* **47**, 181–196.

Kléman, M., Gefen, Y. and Pavlovitch, A. (1986). Topological defects in non-Haüyan crystallography: the two-dimensional case. *Europhys. Lett.* **1**, 61–69.

Kramer, P. and Neri, R. (1984). On periodic and non-periodic space-fillings of E^m obtained by projection. *Acta Cryst. A* **40**, 580–587.

Kutka, R. (1985). *Topologische Defektklassifikation mit Nebenbedingungen.* Thesis, University of Regensburg.

Landau, L. D. and Lifshitz, E. M. (1980). *Statistical Physics.* Pergamon Press, London.

Levine, D., Lubensky, T. C., Ostlund, S., Ramaswamy, S., Steinhardt, P. J. and Toner, J. (1985). Elasticity and dislocations in pentagonal and icosahedral quasicrystals. *Phys. Rev. Lett.* **54**, 1520–1523.

Levine, D. and Steinhardt, P. J. (1986). Quasicrystals I: definition and structure. *Phys. Rev. B* **34**, 596–616.

Lu, J. P. and Birman, J. L. (1986). Mistakes in quasilattices. *Phys. Rev. Lett.* **57**, 2701–2705.

Lubensky, T. C., Ramaswamy, S. and Toner, J. (1985). Hydrodynamics of icosahedral quasicrystals. *Phys. Rev. B* **32**, 7444–7452.

Lubensky, T. C., Ramaswamy, S. and Toner, J. (1986). Dislocation motion in quasicrystals and implications for macroscopic properties. *Phys. Rev. B* **33**, 7715–7719.

Mermin, N. D. (1979). The topological theory of defects in ordered media. *Rev. Mod. Phys.* **51**, 591–649.

Nabarro, F. R. (1979). *Dislocations in solids.* North-Holland Publ. Co., Amsterdam.

Nelson, D. R. (1983). Order, frustration, and defects in liquids and glasses. *Phys. Rev. B* **28**, 5515–5535.

Pauling, L. (1987). So-called icosahedral and decagonal quasicrystals are twins of an 820-atom cubic crystal. *Phys. Rev. Lett.* **58**, 365–368.

Penrose, R. (1974). The role of aesthetics in pure and applied mathematical research. *Bull. Inst. Math. Appl.* **10**, 266–271.

Poon, S. J., Drehman, A. J. and Lawless, K. R. (1985). Glassy to icosahedral phase transformation in Pd-U-Si alloys. *Phys. Rev. Lett.* **55**, 2324–2327.

Sachdev, S. and Nelson, R. (1985). Incommensurate icosahedral density waves in rapidly cooled metals. *Phys. Rev. B* **32**, 689–695.

Sadoc, J. F. (1983). Periodic networks of disclination lines: application to metal structures. *J. Phys. Lett. (Paris)* **44**, L707–L715.

Shechtman, P., Gratias, D. and Cahn, J. W. (1984). Metallic phase with long-range orientational order and no translational symmetry. *Phys. Rev. Lett.* **53**, 1951–1954.

Shoemaker, D. P. and Shoemaker, C. B. (1988). Icosahedral coordination in metallic crystals. In *Aperiodicity and Order, Vol. 1* (Jarić, M. V., ed.), Academic Press, 1–57.

Socolar, J. E. S., Lubensky, T. C. and Steinhardt, P. J. (1986). Phonons, phasons, and dislocations in quasicrystals. *Phys. Rev. B* **34**, 3345–3360.

Toulouse, G. and Kléman, M. (1976). Principles of a classification of defects in ordered media. *J. Phys. Lett. (Paris)* **37**, L149–L151.

Träuble, H. and Essmann, U. (1968). Fehler im Flußliniengitter von Supraleitern zweiter Art. *Phys. stat. sol.* **25**, 373–393.

Trebin, H.-R. (1982). The topology of non-uniform media in condensed matter physics. *Adv. Phys.* **31**, 195–254.

Trebin, H.-R. (1983). Configurations in crystals, rod lattices, and lamellar systems. *Phys. Rev. Lett.* **50**, 1381–1384.

Troian, S. and Mermin, N. D. (1985). Mean-field theory of quasicrystalline order. *Phys. Rev. Lett.* **54**, 1524–1527.

Urban, K., Moser, N. and Kronmüller, H. (1985). Phase transitions between the quasicrystalline, crystalline and amorphous phases in Al-14% Mn. *Phys. stat. sol. (a)* **91**, 411–422.

Widom, M. (1988). Short- and long-range icosahedral order in crystals, glass, and quasicrystals. In *Aperiodicity and Order, Vol. 1* (Jarić, M. V., ed.). Academic Press, 59–110.

Index

A

Affine group, 207
Algebraic numbers, 159
Ammann rhombohedra, 148, 157
Ammann tiles, 48
Aperiodicity, 21, 22
Atomic surfaces, 170, 171, 173

B

Bowtie, 71
Burgers vector, 184, 190–196, 201, 203–204, 210, 212, 214

C

Configuration, 213
Continuum model, 185–186, 189, 197–198, 201
Convex, 8
Convex hull, 9
Correct arrangement, 60
Corrugated surface, 160
Crystallographic restriction, 13
Crystallography
  cubic lattices, 123–129
  hypercubic space group, 135–137
  in n dimensions, 83, 117
  lattice, 107–108
  space group theory, 106–110
  subperiodic groups, 108
Cube, 2
Cuboctohedron, 12
Cut construction, 169–173
Cut description, 169
Cut method, 148
Cyclic group
  induced representation of, 101–103
  relation to Penrose pattern, 101

D

Defect, 184–185, 189–191, 195, 201, 203–208, 210–213, 218
  classification, 185, 205–208, 210–213
Deflation, 173
Density wave, 186–188, 203–204
Diffraction
  from quasicrystals, 82–85, 141–143
  epicell construction, 117–123, 135–143
Dirichlet domain, 24
Disclination, 184, 198, 199–204, 211–214, 218–219
  dipole, 201, 203, 211–212, 218
Dislocation, 184, 190–196, 201, 203–204, 210–214, 218–219
  dipole, 214–217

motion of, 190–191, 213–214
Dispiration, 184, 219
Dual lattice, 15
polyhedron, 15
tiling, combinatorial, 16
Dually situated tiling, 17

E

Edge
of a polygon, 7
of a polyhedron, 9
of a tiling, 9
Equivalence
combinatorial, 37
symmetrical, 12
Euclidean group, 207–209
Euler's formula, 23, 24
Existence domains, 162

F

Face of a polyhedron, 8
Fibonacci sequence, 73
Forbidden set, 179
Fundamental group, 206, 211

G

Glide reflection, 11
Golden ratio, 71
Grid method, 169
Group, 85
action of, 85
conjugacy class, 89
coset with respect to subgroup, 89
cubic, 85, 123–129
cyclic, 85
dihedral, 85, 94–97
generator, 85
hyperoctahedral, 130–135
icosahedral, 85, 89, 137
octahedral, 85, 123–129
orbit under, 85
point group, 84
representation, 92–106
rotation group, 93–94
space group, 106–110
stability group, 89–91
tetrahedral, 85, 94

H

Homotopy class, 206–207
Homotopy group, 207, 210
Hydrodynamic modes, 188
Hydrodynamic theory, 204, 214, 218
Hypercubic lattice, 153
boundaries of unit cell, 136
cell complex of, 136
dual cell complex of, 136
epicells of, 137–141
point group of, 130
space group of, 135
Hyperoctahedral group, 98, 113, 130
cubic subgroups, 123–129
icosahedral subgroup, 104–106
irreducible representations, 130–135

I

Icosahedral group
coset representatives, 90
factorization, 90–91
generators, 89
induced representation, 99, 104–106
irreducible representations, 93
permutation representation, 99
quasilattice for, 83, 117–123
layer structure, 121
relation to cubic lattices, 123–129
rhombohedral cells, 83, 135–141
subduction of representation, 96
tensor algebra of, 94
Icosahedral symmetry, 152
Icosahedron, 2
Icosidodecahedron, 12
Incorrect sequence, 76
Inflation, 169, 173
rules, 56
Invariant subspace, 154
Inversion, 11

J

Jester's cap, 56

K

Kite and dart pattern, 54

L

Landau theory, 186
Lattice, 13
Laves net, 39
Legal arrangement, 60
LI-Class, 189, 192, 195, 197–198, 209–210, 213, 218–219
Linear representation, icosahedral group, 153
Liouville numbers, 159
Local isomorphism, 44, 148, 151, 157–162
  classes, 160, 161
Locally legal pattern, 55

M

Matching rules, 54, 148, 173–182
Microscopic model, 185–186, 188–190, 197, 203–204
Mistakes, 55, 185, 197–198, 201–202, 204, 210, 212, 214–215, 217–218
  motion of, 214–215, 217
Multigrid, 29

N

Nonperiodicity, 19

O

Oblate rhombohedron, 164
Oblique tiling, 148, 169–173, 180
Octahedron, 2
Order
  non-periodicity, 82–85, 110, 117–123
  orientational, 83–85, 108–110
  periodicity, 81–85, 108–109, 123–129
Order parameter space, 205
  reduced, 205–208

P

Parallelohedron, 6, 27
Patch of a tiling, 23
Penrose pattern, 83, 101, 184, 189, 195–196
Penrose tiles, 21, 45
  three-dimensional, 47
Periodicity, 18
Phason strain, 185, 188–189, 204, 218
Phonon strain, 185, 188–189, 204
Point group, 12, 85–92, 101–106
Polygon, 7
Polyhedron, 8
Polytope
  cell for quasilattice, 117–123
  morphology of quasicrystal, 117
  star of, 110–117
  with point symmetry, 110–117
Projection construction, 149–157
Projection formalism, 188–189, 197
Projection method, 148
Projection, tilings obtained by, 31
Prolate rhombohedron, 164, 166, 167
Prototile, 9

Q

Quasicrystal, 7
  atomic model, 82–83
  cells of, 83, 117–123
  diffraction properties, 82–83, 141–143
  facet formation, 117
  epicell construction, 117–119
  glass model, 82
  growth, 82, 117
  model, 85, 141–143
  Monte-Carlo simulation, 82
  orientational order, 83–85, 108–110
  quasilattice of, 117–121
  relation to crystal, 123–129
Quasilattice, 84–85
  duality, 117–123, 135–141
  dualization method, 117–121
  icosahedral, 118–123, 135–143
Quasiperiodicity, 21
Quasiperiodic tilings, 148

R

Reflection, 11
Regular solids, 2
Representation of group, 92
  coupling, 95–96
  F-decomposable, 92

F-equivalent, 92
F-fully reducible, 92
F-reducible, 92
induced, 96–106
Kronecker product, 95–96
multiplicity, 100
projection operators, 100–101
reciprocity, 100
regular, 101
Rhombic dodecahedron, 27, 32, 163
Rhombic icosahedron, 162
Rhombic triacontahedron, 155
Rhombus pattern, 54
Rotary inversion, 11
Rotation, 11
screw, 11
Roth's theorem, 159

S

Schur operators, application to quasicrystals, 123–129
Self-similarity, 169
strong, 173
Space group, 106–110
Stacking fault, 185, 192–193, 219
Star
of vectors, 110
polytope construction from, 110–117
Symmetry, 11
five-fold, 13
group, 11
operation, 11
Symmetry group, 11
finite, 12
Symmetry point group, 152

T

Tetrahedron, 2
Three-dimensional Penrose tilings, 147, 152–157
Tile, 7
Tiling, 7
Delaunay, 27
Dirichlet, 24
dissection, 28
edge-to-edge, 9
face-to-face, 9
isogonal, 12
isohedral, 12
isotoxal, 12
k-hedral, 9
monohedral, 9
normal, 9
Penrose, 21, 33, 45
Tilings
combinatorially equivalent, 11
congruent, 10
equal, 11
Transitivity, 12, 17
local criterion for, 35
Translation, 11
Triacontahedron, 33, 155

U

Unit cell, 18

V

Valence, 8
Vertex
of a polygon, 8
of a polyhedron, 8
of a tiling, 9
Vertex figure, 8
Volterra process, 185, 190, 192, 194, 198–199, 210–212

W

Wang tiles, 42, 48
Window, 153, 155
Worm, 63, 64, 72

Z

Zonohedron, 32

Contents of Previous Volume

Volume 1: Introduction to Quasicrystals

1 Icosahedral Coordination in Metallic Crystals
David P. Shoemaker and Clara B. Shoemaker

2 Short- and Long-Range Icosahedral Order in Crystals, Glass, and Quasicrystals
Michael Widom

3 Metallurgy of Quasicrystals
Robert J. Schaefer and Leonid A. Bendersky

4 Quasicrystallography
Per Bak and Alan I. Goldman

5 Stability and Deformations in Quasicrystalline Solids
Ofer Biham, David Mukamel, and S. Shtrikman

6 Symmetry, Elasticity, and Hydrodynamics in Quasiperiodic Structures
T. C. Lubensky